An Assessment of Flywheel Storage for Efficient Provision of Reliable Power for Residential Premises in Islanded Operation

A thesis submitted for the fulfilment of the requirements for the degree

of

Doctor of Philosophy

Department of Mechanical Engineering and Aeronautics

School of Mathematics, Computer Science and Engineering

at

City, University of London

Author: Mustafa Edries Amiryar

London, 2019

Abstract

Energy storage systems (ESS) are key devices for improving power quality, electrical system stability and system efficiency by contributing to the balance of supply and demand. They can enhance the flexibility of electrical systems by mitigating supply intermittency, which has recently become problematic due to the increased penetration of renewable generation. The subject of this thesis is flywheel energy storage system (FESS), a technology that is gathering great interest due to benefits offered over alternative energy storage solutions, including high cycle life, long calendar life, high round-trip efficiency, high power density, operation at high ambient temperatures and low negative environmental impact. This thesis describes the modelling and assessment of small scale energy system incorporating FESS with solar photovoltaic (PV) and a diesel generator for use in islanded residential premises with highly intermittent or non-existent grid infrastructure. In this application, incorporation of FESS is shown to be beneficial in comparison to a system without storage or one with the alternative storage technology, Li-Ion batteries. The thesis begins with a description of flywheel storage systems configured for electrical storage which comprises of a mechanical part; flywheel rotor, bearings and containment, and an electric drive part; motor-generator and associated power electronics. Each of these components is described in the thesis along with the equations and modelling, itself carried out in the MATLAB/Simulink environment. Finally, the flywheel model is combined with a model of an islanded residential power system incorporating a solar PV system with a diesel generator. Such a system would be particularly useful for off-grid applications or those with weak grids as occurs in developing countries.

Acknowledgement

Firstly, I would like to express my sincere gratitude to my enthusiastic supervisor, Professor Keith R. Pullen for his patience and tolerance, motivation, immense knowledge and continuous support in guiding me with his valuable feedback throughout this PhD.

I thank Professor Lambros Ekonomou who has been an inspiration with his great advice and support during early years of PhD. A special mention goes to Dr. Daniel Nankoo who has been a truly dedicated mentor. I thank Daniel wholeheartedly, not only for his academic support, but also for providing me with so many wonderful opportunities.

I am extremely grateful to my father and my MSc supervisor, Prof Anil Pahwa who have been a great inspiration for me to do the PhD in the first place.

I thank my colleague and fellow lab mate, Shahjahan Miah for being an excellent teaching partner with motivating discussions and a great support in MATLAB programming. Many thanks also go to Amir Hosseinpour, a former colleague who have completed his PhD in Supercharging, for his invaluable input given his experience in MATLAB/Simulink.

I am grateful to my beloved mother, my brothers, my sisters and other family members for supporting me spiritually throughout this PhD and my life in general.

Finally, but by no means least, a special thanks to my lovely wife, for her love and support and being by my side while completing the PhD, living every single minute of it, and to my dear son, for his tolerance and understanding, who both have made it possible for me to complete what I started.

Declarations

I grant powers of discretion to the University Librarian to allow this dissertation to be copied in whole or in part without further reference to me. This permission covers only single copies made for study purposes, subject to normal conditions of acknowledgement.

Table of Contents

List of Figures

List of Tables

Abbreviations

AMB	Active magnetic bearing
BLDCM	Brushless DC machine
BRIC	Brazil, Russia, India and China
BTB	Back-to-back
CHB	Cascaded H-bridge
CREST	Centre for Renewable Energy Systems Technology
DFIM	Double fed induction machine
DG	Distributed Generation
DGen	Diesel generator
DoD	Depth of discharge
dq	Direct-quadrature
EMF	Electromagnetic force
ESS	Energy storage systems
FC	Flying capacitor
FCC	Forced commutated cycloconverter
FESS	Flywheel energy storage system
FOC	Field oriented control
GHG	Greenhouse gas emissions
GSC	Grid side converter
HAM	Halbach array machine
HTS	High temperature superconductors
IGBT	Insulated-gate bipolar transistor
IM	Induction machine
I-V	Current-voltage
JET	Joint European Torus
MC	Matrix converter
MG	Motor-generator

MPPT	Maximum power point tracking
NPC	Neutral point clamped
PCC	Point of common coupling
PI	Proportional integral
PM	Permanent magnet
PMB	Passive magnetic bearing
PMDC	Permanent magnet DC
PMSM	Permanent magnet synchronous machine
PV	Photovoltaic
P-V	Power-voltage
PWM	Pulse width modulation
RES	Renewable energy sources
SMB	Superconducting magnetic bearings
SMES	Superconducting magnetic energy storage
SOC	State of charge
SSC	Storage side converter
SVM	Space vector modulation
SVPWM	Space vector pulse width modulation
THD	Total harmonic distortion
ToU	Time of use
UPS	Uninterruptible power supply
VRM	Variable reluctance machine
VSI	Voltage source inverter

Nomenclature

A	Rotor surface area
a	Rotor inner radius
a_1	Bearing life adjustment factor for reliability
a_{skf}	Bearing life modification factor
b	Rotor outer radius
B	Friction of viscous
C	DC-link equivalent capacitance
C_D	Drag coefficient
C_s	Static load rating
D_p	Pitch circle diameter of the bearing
D_r	Rotor outer diameter
D_s	Shaft diameter
E	Stored kinetic energy
F_a	Bearing axial load
F_b	Load applied on the bearing
f_L	A factor dependent on bearing design and relative load
f_0	Bearing type and mode of lubrication factor
F_r	Bearing radial load
F_s	Static equivalent load
h	Rotor length
I	Moment of inertia
$I_{DC,G}$	DC current from the GSC
$I_{DC,S}$	DC current from the SSC
$I_{G,d}$	Direct axis component of the grid current
$I_{G,q}$	Quadrature axis component of the grid current
I_d	Direct axis stator current
I_q	Quadrature axis stator current
i_{abc}	Three phase stator currents
J	Flywheel rotor and MG combined moment of inertia
K	Rotor shape factor

κ	Ratio of specific heats
K_{n}	Knudsen number
k	Roughness coefficient
K_{ii}	Integral gain for current
K_{iv}	Integral gain for voltage
$K_{i\omega}$	Integral gain for speed
K_{pi}	Proportional gain for current
K_{pv}	Proportional gain for voltage
$K_{p\omega}$	Proportional gain for speed
m	Rotor mass
n	Number density
r	Rotor radius
R	Universal gas constant
T	Temperature
v	Rotor peripheral speed
x	Distance from the axis of rotation
λ	Mean free path of a molecule
μ	Viscosity
ρ	Air density
P	Equivalent dynamic load on bearing
V	Velocity
X	Bearing radial load factor
Y	Bearing axial load factor
d	Flywheel rotor to containment gap
n	Rotational speed
p	Exponent of the bearing life equation
ω	Angular speed
ω_e	Rotor electrical speed
ω_G	Grid frequency
$\omega_{\max}$	Maximum angular speed
$\omega_{\min}$	Minimum angular speed

y	Bearing load torque factor determined experimentally
z	Bearing load torque factor determined experimentally
ρ_m	Rotor mass density
σ_{max}	Maximum tensile strength
L_{10}	Bearing basic rating life in millions of revolutions
L_{10h}	Bearing basic rating life in operating hours
L_d	Direct axis inductance
L_f	Filter inductance
L_{nm}	SKF rating life for bearings in millions of revolutions
L_{nm}	Stator winding self and mutual inductance
L_{nmh}	SKF rating life for bearings in operating hours
L_q	Quadrature axis inductance
M_a	Mach number
P_u	Bearing fatigue load limit
P_w	Power loss
R_e	Reynolds number
R_{ed}	Couette Reynolds number
R_s	Stator winding resistance
T_B	Bearing torque
$TF_{OL,I}$	Open loop current transfer function
$TF_{OL,V}$	Open loop voltage transfer function
$TF_{OL,\omega}$	Open loop speed transfer function
T_L	Load torque
T_e	Electromagnetic torque
T_v	Speed dependent torque
$V_{DC,0}$	Initial DC bus voltage
V_{DC}	DC voltage of the inverter
$V_{G,d}$	Direct axis component of the grid voltage
$V_{G,q}$	Quadrature axis component of the grid voltage
V_a	VSI output voltage
V_{abc}	Three phase stator voltages

V_{tri}	Peak value of the triangular carrier
X_s	Static radial load factor
Y_s	Static axial load factor
v_0	Kinematic oil viscosity
λ_{abc}	Three phase stator winding flux
λ_m	Rotor field flux
τ_{xy}	Shear stress between two surfaces x and y
η	Efficiency
σ	Tangential momentum accommodation coefficient

Chapter 1 Introduction

1.1 Overview

World energy demand continues to increase, to meet the expanding needs of the households and industries, particularly with high growth rates such as Brazil, Russia, India and China (BRIC) and developing countries as indicated in *Figure 1.1*. This has led to increases in energy prices where traditional energy generation methods are less able to adapt, exacerbating the issues created by market deregulation, power quality problems, and pressures to limit carbon dioxide emissions [1, 2]. Traditional electricity systems are operating in one-way direction and with the radial configuration from the generation to the supply. In order for the demanded load and the generation supply to be balanced, the generating units must supply the demand at all timescales [3]. However, the demand varies seasonally, monthly or even daily, with the annual maximum demand lasting perhaps only for a few hours each year [1]. This requires the availability of large amounts of electrical energy that may be only needed for a short time each year; imposing increased cost and production of insufficient energy [3].

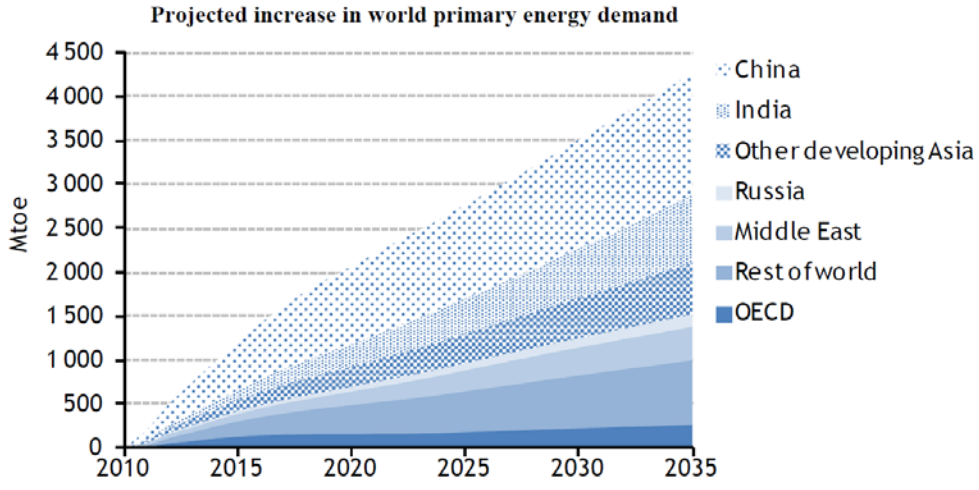

Figure 1.1. Projected increase in world energy demand *[4]*

Renewable energy sources (RES) and potential distributed generation (DG) were considered as supplements to traditional generation methods but are now being deployed as replacements [2]. They largely contribute to facilitating clean and

emission-free energy; increasing the energy supply whilst decreasing carbon footprints. According to the 2008 Climate Change Act and EU Renewable Energy Directive 2009, the EU is committed to reducing greenhouse gas (GHG) emissions to at least 80% of 1990 levels by 2050 [5, 6, 7, 8], requiring higher penetration of renewables and distributed generation. However, there are major challenges associated with the energy demand coming from the renewables, due to their intermittent nature across a range of timescales [9]. At a time when RES is supplying energy, there may be low demand, but when the energy is demanded, it may exceed RES energy production [2]. Also, there are monthly, seasonal, and annual fluctuations in RES supply, as their availability is always subject to weather conditions. On the other hand, the energy demand differs from time to time, which is unlikely to match the intermittences of RES, thus creating reliability problems [9, 10]. In addition, the traditional approach of controlling the energy generation and load demand during peak times by installing gas turbine generations will no longer be an ideal solution given their environmental impacts. As discussed in [10], gas-fired plants can provide reliable and flexible back up power due to their fast response to rapid changes in demand. However, gas turbine generators are sources of GHG emissions producing CO_2, which will lead to a wrong direction if 2050 renewable target is to be met [8]. Later in the thesis, it will be discussed how the demand side response can be used as a balancing mechanism to manage the unbalancing issue.

The solution to the problem of balancing can be met using energy storage systems (ESS). They are now a vital necessity to aggregate traditional generating plants to help meet an excessive demand and supplement the intermittent RES for their integration into the electrical network [11]. They are needed at different points within an electricity grid from generation to the customer level to balance electrical energy generation and demand. The process involves converting and storing electrical energy from an available source into another form of energy, which can be converted back into electrical energy when needed. The forms of energy storage conversion can be chemical, mechanical, thermal, or magnetic [1, 3]. ESS enable electricity to be produced

when it is needed and stored when the generation exceeds the demand. Storage is beneficial when there is low demand, low generation cost, or when the available energy sources are intermittent. At the same time, the stored energy can be consumed at times of high demand, high generation cost, or when no alternative generation is available [1, 2, 3].

Integration of ESS to the electrical grid enables transmission and distribution systems to operate at their rated capacity with increased efficiency and avoid the need for any further system investments. Transmission and distribution investment avoidance or deferral will be accomplished when ESS withstand the demand peaks that would otherwise lead to an overload of the existing system and the requirement for more feeders and other system upgrades [12].

At the distribution level, energy storage is typically needed to complement distributed generation providing back up for uninterruptible power supply (UPS) services. DG is mostly located at the customer level in order for the power to be generated at the point where it is being consumed. DGs are used to generate power at the scales demanded by the consumers, contrary to the conventional large-scale centralized power systems where power generating units are typically located far from the consumers and operated at their rated maximum demand. However, smaller capacity of generation (kW to a few MW) and higher possibility of line faults in DGs create load variations and voltage drops which further leads to stability problems at the distribution level. Integration of storage systems with DGs provides power flexibility and improves system stability. Penetration of DG will be more robust and further supported by advancements in energy storage technologies and availability of RES [11].

On the issue of instability, it is important to keep the frequency of the AC supply within around ±1% of mean otherwise the system collapses [13]. So far, the stability issue has been addressed with a combination of energy storage and demand-side management, where the former is mainly dominated by the use of large banks of Li-Ion batteries. The sub-second demand can be met by Li-Ion batteries with an

appropriate control electronics capable of providing duration of typically one to two hours allowing additional revenue streams such as arbitrage, load shifting and other grid ancillary services including long duration energy storage. Hence all attention has been drawn towards Li-Ion batteries and low storage, high power technologies such as supercapacitors and flywheels have been prevented to compete with them. The question might be whether other technologies can be considered to replace the deployment of large numbers of grid-scale Li-Ion batteries to meet the growing future storage needs? The answer to this question is not simple because there are other factors that will affect the future of storage with a lot of interdependencies [13].

The lack of recycling of Li-Ion batteries and their production relying on material from questionable sources is already a concern [14]. On the technical part, high penetration of renewables and distributed generation and potential deployment of electric vehicles in the near future will significantly affect the balance of the electrical grid. The balancing problem could be mitigated with the integration of a good fit storage system as well as delaying the charging periods of the electric vehicles to periods of low demand. However, this is limited by the nature and characteristics of the storage device where in the case of a Li-Ion battery with relatively the best cycle-life compared to other batteries, its lifetime will be compromised due to multiple charging or deep discharging as indicated in Figure *1.2* - developed based on a recent publication on projection of the future lifetime cost of electrical storage technologies from 2015 to 2050 [15].

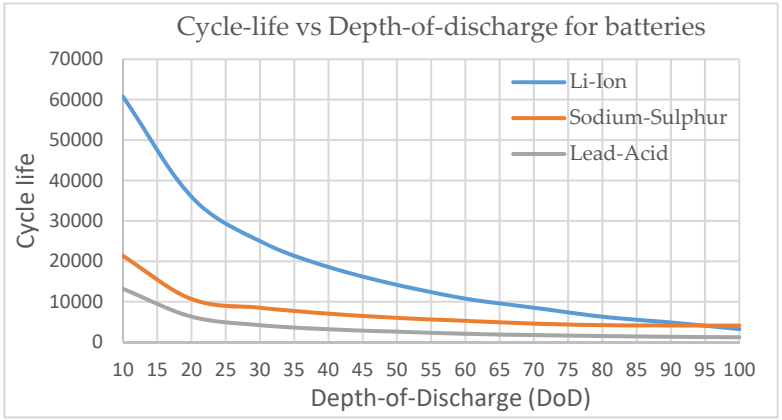

Figure 1.2. Li-Ion cycle life relative to depth-of-discharge *[15]*

Another technical innovation is demand-side response whereby demand can be controlled by delaying power draw for equipment which has a slow time constant. For example, heater-chiller units normally switching according to a thermostat could be delayed or started earlier. This is already being done and there may be other ways to time-shift the demand. Another technical effect is the expansion of interconnectors between regions or countries. Changes in energy storage needs and patterns are demanding energy storage technologies to respond accordingly. In the past, energy storage was mainly rated based on their energy capacity (in GWh) with one cycle per day. However, today the same systems are used up to 10 and 20 times a day, making the power capacity (in GW) rather important than the energy capacity [10]. Considering the future structure of the electrical grid and if market reform is done well, the best and most efficient technology will develop without the need for intervention and with the following major timescales:

- Fast response with high cycle storage
- Bulk storage with at least 8 hours rather than the 1-2 hours offered by Li-Ion
- More than a day to seasonal storage

It can be argued that the rationale for these timescales is the reformation of the market structure from one originally designed for a system of large centralised power stations and peaking plants to one fit for purpose for a system with high penetration of renewables, distributed generation and prosumers [13]. It is understood that no other technology but chemical storage can deliver energy from storage for more than a day, backed up by natural gas plants. For fast response and the 8 hours need, the Li-Ion batteries will be able to meet this criterion by lowering their C rating (ratio of kW/kWh) with the disadvantage of increasing the cost.

However, there is a desire to further reduce the energy storage costs by employing technologies with lower CO_2 emissions and lifetimes of over 20 years that are easily recyclable, unlike Li-Ion batteries. Flow batteries, compressed or liquid air, pumped hydro, gravity systems and engines operating based on renewable fuels can be better

candidates. Nevertheless, the sub-second response from the start-up cannot be met by any of the mentioned technologies which leaves a gap to be filled. If Li-Ion batteries are used to meet this gap, in addition to their main issue of suffering from limited cycle life, there would be an overlap of provision in duration as well. Therefore, the best choice is the lowest cost technology with low minutes of storage and the flywheel storage fits this perfectly.

A flywheel is a very simple storage device that stores energy in rotational momentum and can be operated as an electrical storage by integrating a direct drive MG. The electrical power in and out of the MG and power transfer to a load or the grid is controlled with a power electronics operated inverter in a similar way to a battery or any other non-synchronous device. In order to keep a reasonable size of the MG, the flywheel is operated between a maximum and a minimum speed (typically a third to a half its full speed) and is kept spinning by means of a small input power to make up for the system parasitic losses. The standby losses occurring due to aerodynamic drag or windage can be almost eliminated by use of a sealed casing which holds the required vacuum. The power level is controlled by the size of the MG and is independent of the rotor, providing the possibility of producing very high powers with a relatively small flywheel sufficient for a few 10's of seconds or minutes.

With advances in materials technology, bearings, and power electronics, the technology of flywheels for energy storage has significantly developed [16]. Flywheels with the main attributes of high energy efficiency, and high power and energy density, compete with other storage technologies in electrical energy storage applications, as well as in transportation, military services, and space satellites [17]. With storage capabilities of up to hundreds of MJ and power ranges from kW to GW, they perform a variety of important energy storage applications in a power system [18]. The most common applications of flywheels in electrical energy storage are for uninterruptible power supplies (UPS) and power quality improvement [19, 20]. The major contenders to flywheels for these applications are limited to electrochemical batteries and supercapacitors. However, the electrochemical battery is highly mismatched and

suffers from an insufficient cycle life, since the number of cycles per day is usually too high [21]. Particularly for power quality improvement, electrical disturbances are frequent but short, with the vast majority of them lasting for less than 5 seconds. Such disturbances can be effectively managed by flywheels and offer an improvement over batteries considering the instantaneous response time and longer life cycle of the former. Even with one cycle per day, an electrochemical battery would require approximately 3650 cycles to last for even 10 years which is unlikely under these circumstances. This can only be achieved if the depth of discharge is kept low and the battery is carefully managed, both electrically and thermally (see *Figure 1.2* of cycle life relative to DoD). It also requires specifying an energy storage capacity two to five times the required capacity, to reduce the depth of discharge, thus leading to a higher cost. Supercapacitors have been tested for these types of applications; however, with more or less the same capital cost as flywheels [3], their operational lifetime is relatively low (reaching up to 12 years) [2].

To make more use of an energy storage system and minimise its capacity in order to reduce the cost, it is more useful for it to be used many times a day, to allow for the time-shifting of demand and to feed into the grid at times of high demand. Interest in this new paradigm of how energy is used will be greatly enhanced once Time of Use (ToU) tariffs are in place in developed countries such as the UK. Whereas for developing countries with intermitted power grids or remote areas with no access to grid with the renewables and diesel generator being the only means of power supply, the need for fast response storage capable of withstanding multiple cycles a day becomes more important.

1.2 Objectives and research questions

This thesis describes the research on flywheel energy storage system (FESS) providing backup storage for ground power applications. The aim is to assess the application of flywheel systems integrated into an islanded solar PV system with a backup diesel generator providing reliable power for residential premises. The

flywheels are generally used for high power applications and the majority of manufacturers are providing short-term response flywheels with high power densities with durations of seconds to minutes of storage. Therefore, flywheels are not usually considered for ground power applications and chemical batteries (mostly Li-Ion type) are the commonly used type of storage for these applications. However, in some special circumstances, a hypothesis has been developed that a FESS may be better than chemical batteries. These circumstances are as follows:

- Islanded micro grids for domestic application as may be found in developing countries with weak or absent grids; here the power demand is highly intermittent and supplied inefficiently by diesel generators.
- Introducing solar PV as an additional power source as a low-cost means of reducing emissions is attractive but increases supply and demand imbalance, potentially generating a large number of cycles which would require the diesel generator to come on and off frequently.
- It is considered that if a chemical battery was used as an energy storage, it would degrade too quickly, hence the FESS with very high cycle life could be a more attractive and sustainable option overturning the default choice of ESS to be a chemical battery.

An additional motivation for the research is that in developing countries temperature control needed for batteries is difficult to achieve, supply of replacement batteries may be challenging and recycling of batteries is non-existent or worse, for instance is done in unsafe conditions by local people. Although it would be very useful to also prove what would be an additional hypothesis, it was beyond the scope of the research which focussed on the technical assessment in terms of savings of emissions. Specifically, this research focuses on the design and development of the modelling and simulation of the electrical characteristics of a FESS connected within a micro-grid islanded PV system with a backup diesel generator. The main aim of adding the FESS

is to reduce diesel fuel consumption and improve the reliability of the system to meet the power demand. In achieving this, the following research questions arise:

- Is there a good demand for a long-duration energy storage flywheel system in today's competitive energy storage market?
- Who are the competitors in the energy storage market and what are they offering? What are the technical benefits of this flywheel compared to other energy storage systems?
- How to design and integrate a flywheel storage system with a hybrid PV system and backup a diesel generator and what are the most suitable hybridisation strategies?
- How to implement an optimal charge-discharge strategy for the flywheel system to improve system efficiency and reliability?

1.3 Contributions of the research

In reference to the research questions, the main contributions of this research are summarised as follows:

- Assessment of a high inertia flywheel storage system with steel laminated rotor for longer duration storage and suitable for use at the residential level. The flywheel energy storage market is highly dominated by carbon composite based flywheels that are a good fit for fast response applications but not suitable for longer duration storage applications due to their lower energy density and higher discharge rate. The capital cost of composite flywheels is also a concern and what is proposed in this research is a flywheel system based on laminated steel rotor with the aim to overcome the higher cost of composite flywheels and safety issue of solid steel flywheels. This new type of flywheel system requires lower maintenance and is fully recyclable at the end of its prolific lifetime. Use of thinner steel laminates in the rotor improves the level of safety and the system will be suitable for longer duration storage

applications due to its higher inertia and higher energy density in comparison to carbon composite flywheels.

- Analysis of the flywheel loss model and determination of windage drag coefficients and bearing torque equations to govern the self-discharge rate and operational losses of the proposed flywheel system.
- Design and control of the flywheel storage system and associated MG and inverter system to determine optimal control strategies for charge-discharge and energy conversion of the system.
- Creating a model of a hybrid solar PV system and a backup diesel generator with an integrated high inertial flywheel storage for islanded residential applications. The main contribution to developing the hybrid model is the design and development of the energy storage part and the residential load model. The MATLAB/Simulink model of the flywheel system is developed based on the loss model for aerodynamic and bearing systems as well as the design of the entire control system. Except for the permanent magnet synchronous motor-generator, which is selected from MATLAB Simscape's built-in library, the entire model of the flywheel storage including design of the LC filter and SVPWM, the charge-discharge algorithm of the flywheel storage and its communication with the hybrid system are developed and designed from scratch.
- Assessment of the contribution of flywheel storage in reducing the diesel engine fuel consumption and improving the stability of the system in comparison to a system without an energy storage or the one with a chemical battery.

1.4 Methodology

This section describes the methodology applied in accomplishing the above mentioned research objectives and addressing the research questions. A generalised approach is to assess the level of contribution of a flywheel storage system in

combined operation with other energy sources in supplying power to residential premises in islanded conditions. This is achieved by evaluating a flywheel model based on different charging and discharging scenarios with the following steps in methodology:

a. A comprehensive literature review was conducted to address the emergence and history of flywheels and to understand their main characteristics and applications. This would provide a thorough analysis of the flywheel storage and identify other types of storage systems performing similar applications. Hence, a clear research direction would develop by identifying the research gaps in the literature.
b. The mathematics and modelling techniques of the FESS and its main components have been analysed resulting in the creation of an appropriate flywheel model serving the purpose of this study. This included analysis of the types of electric machines suitable for flywheel application and their controlling techniques, the types of bearings and their loss analysis, and the rotor and containment requirements. The developed model was used to perform simulations in real-life scenarios based on which the results will be analysed to evaluate the competency of the flywheel model for use in ground power applications.
c. The developed model of the flywheel was incorporated into an islanded micro-grid system model consisting of a solar PV system, diesel generator and FESS. The analysis, control, and development of the solar PV system and the diesel engine are discussed in detail. The solar PV data and parameters were selected based on the National Renewable Laboratory (NREL) System Advisor models that are available as open-source. The time of operation and energy production of the diesel generator was analysed from the simulation of the micro-grid model and its parameters were obtained from the technical datasheets published by the diesel engine manufacturers. Based on this, the produced energy and fuel consumption could be calculated easily. The demand and energy consumption data for residential premises is obtained from a high-resolution integrated electrical-thermal stochastic demand model developed by Loughborough University. This

data was used to develop different demand profiles at different times of the year to analyse the dynamic performance and energy production of the hybrid model.

The original aim was to use a load profile for a small village in a developing country with no access to electrical grid or with a weak intermittent grid. This would have made the analysis more realistic in terms of energy demand requirements for an islanded system. However, access to such data was not possible and as an alternative, the load demand profiles were generated using CREST Demand Model - a high-resolution energy demand model for building occupancies at the residential level developed by Loughborough University. The CREST model considers the natural behaviour of occupants in using appliances at home as determined based on UK time-use survey data. The data was used to create stochastic profiles of dwelling occupancy in order to consider different states such as the residents can be at home and active, at home and asleep, or away from home and active. The range of appliances used is also quite extensive taking into account all different types of consumers throughout the UK. The only difference between the load profiles generated by CREST model and that of a developing country (with a lot of sunny days) would be the inclusion of air-conditioning units during the summer. Despite this, the analysis could be repeated using the same methodology and principles with the only difference of added air-conditioning load and higher power rating of the system components to meet the higher demand.

d. An analysis of different charge-discharge strategies was conducted to determine the optimal operation of the flywheel storage in improving the efficiency and reliability of the hybrid model. Different 'what if' scenarios were evaluated and for each case, the contribution of the flywheel system as backup storage was analysed.
e. Finally, the simulation of the hybrid model was performed in MATLAB/SIMULINK environment and performance and energy production of

the solar PV system, the diesel generator, and the flywheel storage were analysed and compared.

1.5 Structure of the thesis

This thesis contains 7 chapters in addition to references and appendices. A brief description of the contents of the chapters are as follows:

Chapter 2 presents a brief background of the existence and emergence of flywheel storage systems from their early forms to the latest developments referred to as advanced flywheels. This is followed by a description of the structure and main components of the flywheel addressing the type and material of the rotor, the electric machines used in flywheels and a comparison of their technical parameters, the type and configuration of power electronics interface and bearing system as well as the containment requirements for safe operation of the flywheel system.

Chapter 3 provides a detailed description of the characteristics and applications of flywheel storage systems. The general attributes and drawbacks of flywheel storage compared to other storage systems providing similar applications are pointed out and some areas of advancements are discussed. A wide range of applications of flywheel systems in different sectors and a variety of scales is addressed in detail. An overview of some onsite installations and commercial projects for each application is provided and commercially available flywheel prototypes for stationary applications is addressed. An output from the research of Chapters 2 and 3 is available in open access as [22].

Chapter 4 describes different losses associated with flywheel storage and particularly focusing on aerodynamic and bearing friction losses. An assessment of the windage losses based on various flow regimes is presented and two different methods for calculation of aerodynamic losses in rarefied vacuum conditions are discussed and compared. Bearing sizing and selection as well as bearing life calculation for designing the bearing system are presented. Bearing loss calculations using the methods practiced by the bearing manufacturers are discussed in detail.

Finally, the system total losses and overall roundtrip efficiency considering the flywheel standby losses as well as the inverter and MG losses are calculated for different number of cycles per day.

Chapter 5 discusses the modelling and control of flywheel and its associated electrical machine and conversion system. Derivation of the mathematical model of the electrical MG is analysed and its controlling technique in performing energy conversion in the system is described. Control of the inverter and determination of the controller gains for charging and discharging states of the flywheel system are also discussed in detail.

Chapter 6 describes the operation and control of the flywheel storage system integrated into a micro-grid islanded solar photovoltaic (PV) system with a backup diesel generator. The MATLAB/Simulink developed models of the PV system, the diesel generator, and the flywheel system are presented and their combination forming a hybrid stand-alone system connected to a residential load through a common DC-link is analysed. The generation of the load profiles representing real-life energy consumption of residential dwellings is discussed in detail. Different energy supply strategies are developed and for each case, the results and analysis of the dynamic performance of the hybrid system supplying energy to different residential loads are presented. The generator fuel consumption and flywheel contribution as a storage system in reducing the CO_2 emissions are studied for different scenarios. Finally, this chapter concludes with an analysis of the possibility of a flywheel system as an alternative to chemical batteries providing back up storage for an autonomous solar PV system.

Chapter 7 presents the main findings of the research and conclusion of the work with a discussion on areas for further research.

Chapter 2 Description of Flywheel Energy Storage System

This chapter provides a description of flywheel energy storage systems (FESS) along with their structure and main components. The chapter is outlined as follows: Section 2.1 provides a brief background of flywheels, their history and principle of operation. This is followed by a description of a flywheel's general structure and main components including the rotor, electrical machine, power electronics, bearing system, and the casing incorporating vacuum system and rotor safety containment. Each component is described in detail and the main types and their significance are highlighted. The chapter is concluded with a summary in section 2.3.

2.1 Background

The flywheel has existed for thousands of years as one of the earliest mechanical energy storage systems. The first rotary tool known to humankind was the hand drill, which even did not need the flywheel to function properly [23]. The other rotary object to show a flywheel effect was spindle whorl. This rotary spindle was the first known object to maintain its rotations under its own inertia. Another ancient object performing the applications of flywheels was the potter's wheel that appeared about two millennia after the first spindle was known [23]. The existence of the potter wheel dates back to 3500 to 3000BC. This wheel was performing flywheel's functionality by maintaining its rotation as a result of an initial velocity to shape the pot. The energy stored by this wheel was suggested to be 500J (0.14Wh) at an estimated rotational speed of 100 rpm. Additionally, other forms of flywheels existed in Egypt in the 15th century BC for twisting strips of leather to make ropes for shipbuilding [23]. Flywheel applications were performed by similar rotary objects, such as the water wheel, lathe, hand mills, and other rotary objects operated by people and animals. These spinning wheels from the Middle Ages do not differ from those developed in the 19th or even 20th centuries. Since their early appearance, the spinning wheels have emerged in different forms and shapes but there were no substantial improvements until the two major developments in the 18th century when metal replaced wood in machine

constructions and flywheels established their usage in steam engines. Developments in cast iron and the production of iron resulted in the production of flywheels in one complete piece, with a greater moment of inertia for the same space. The use of cranks and flywheels, in the steam engines of Watt, Boulton, and Picard in the 1780s, have far improved the conversion of the reciprocating force into uniform rotary motion [24]. The word 'flywheel' appeared at the beginning of the industrial revolution (namely in 1784). At the time, flywheels were used on steam engine boats and trains and as energy accumulators in factories [25]. In the middle of the 19th century, as a result of further developments in cast iron and cast steel, very large flywheels with curved spokes were built. As an example, the first three-wheeled vehicle built by Benz in 1885 is shown in *Figure 2.1* [23]. In 1889, a fast engine of the time with higher inertia was supported by a disc type flywheel. Ten years later a similar flywheel was used in a 1.75 hp, 1500 rpm engine. Later in the 19th century, an alternative to flywheels was used as the prime mover, called the turbine. The emergence of turbines created some stress problems which forced the designers to develop and optimise the design. This stress distribution optimisation helped the design of the flywheels in an indirect way [22].

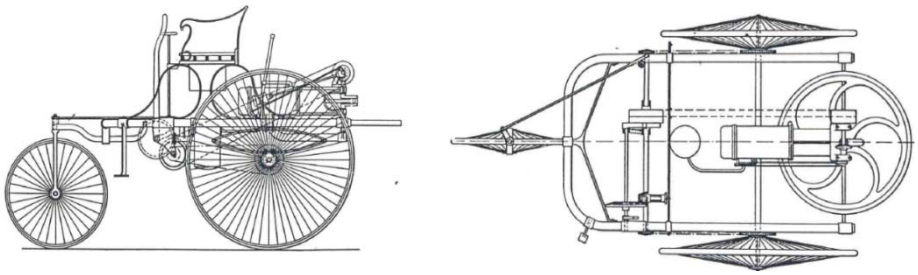

Figure 2.1. The first three-wheeled vehicle built by Benz in 1885 showing the large flywheel, placed with its axis in vertical position *[23]*

Furthermore, the design of steam turbines was an important step in the design and development of kinetic energy storage systems. The first turbo-generator operating at 18000 rpm was built in 1884 and a faster machine with 20000 rpm was established in 1897. Since the evolution of the steam turbines and turbo-generators, flywheels have been used in different applications throughout the history including

weapons, mine locomotives, inertial starter machines, electric railways, buses, and energy storage [23].

Over time, several shapes and designs have been implemented, but major developments came in the early 20th century when rotor shapes and rotational stresses were thoroughly analysed, and flywheels were considered as potential energy storage systems [26]. An early example of a flywheel system used in transport was the Gyrobus, powered by a 1500 kg flywheel, produced in Switzerland during the 1950s [27]. Advanced flywheels or new generation flywheels emerged after the two important developments in the 1960s. The first development was the advances in material with high strength from which flywheels with higher energy storage capacity were built. Secondly, awareness of ecological problems resulted in consideration of energy storage devices to contribute to the energy needs and reduce energy cost and pollution [23]. In the 1970s, energy costs increased which further increased the need and interest for energy storage. As a result, research and investments in the development of flywheel energy storage devices began, resulting in achievements such as helicopter hoist built by Lockheed, the R-32 subway car built by Garrett industries, and the city bus built by the Kursk Polytechnic Institute [23]. In all these application flywheels were made of steel discs which can be considered conventional compared to today's flywheel energy storage devices; especially in perspective of energy density which is improved significantly due to advancements in composite material. Fibre composite rotors were built later in the 1970s when flywheels were proposed for electric vehicles, stationary power back up, and space missions [18, 19]. In the 1980s, the production of flywheels was boosted by the emergence of relatively low-speed magnetic bearings [28].

Despite major developments during their early stages, the utilisation of flywheels has not been significant and has declined with the development of the electric grid. However, due to the recent improvements in materials, magnetic bearings, power electronics, and the introduction of high-speed electric machines, FESS has been established as a solid option for energy storage applications [17][29-31].

2.2 Structure and Components of FESS

A flywheel energy storage system (FESS) stores energy that is based on the rotating mass principle. It is a mechanical storage device which emulates the storage of electrical energy by converting it to mechanical energy. The energy in a flywheel is stored in the form of rotational kinetic energy. The main components in a FESS consist of a spinning rotor, motor-generator (MG), bearings, power electronics interface, and housing or containment for safeguarding the entire system. Schematic of a typical flywheel system suitable for ground-based power applications is shown in Figure 2.2.

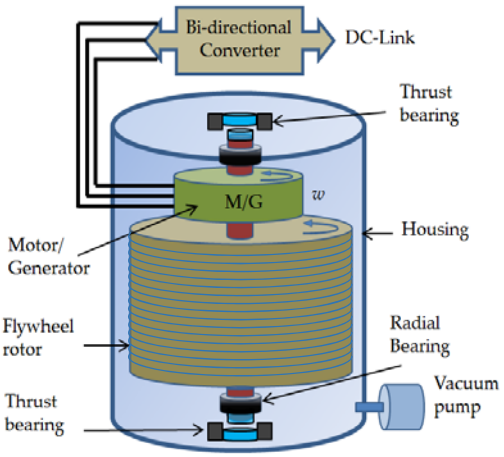

Figure 2.2. Structure and components of a flywheel

The input energy to the FESS is usually drawn from an electrical source coming from the grid or any other source of electrical energy. The flywheel accelerates as it stores energy and slows down when it is discharging to deliver the accumulated energy. The rotating flywheel is driven by an electrical MG performing the interchange of electrical energy to mechanical energy and vice versa [32]. It is charged when the MG operates as a motor by drawing power from the electrical source to accelerate the rotor up to a desired speed. The process is reversed to discharge the flywheel battery using the stored energy in the rotor to produce electrical power. In discharging mode, the rotor is decelerated and the MG is operated in generator mode. The flywheel and MG are coaxially connected so that controlling the MG enables control of the flywheel [33, 34].

2.2.1 Flywheel Rotor

The stored energy in a flywheel is determined by the rotor shape and material. It is linearly proportional to the moment of inertia and the square of angular velocity, as shown in Equation (2.1) [35]:

$$E = \frac{1}{2} I \, \omega^2 \tag{2.1}$$

where

E: stored kinetic energy (*Joules*)

I: moment of inertia ($kg.m^2$)

ω: angular speed (rad/s)

The useful energy of a flywheel within a speed range of minimum speed (ω_{min}) and maximum speed (ω_{max}) can be obtained by:

$$E = \frac{1}{2} I \, (\omega_{max}{}^2 - \omega_{min}{}^2) = \frac{1}{2} I \, \omega_{max}{}^2 \left(1 - \frac{\omega_{min}{}^2}{\omega_{max}{}^2}\right) \tag{2.2}$$

Typically, an electrically driven flywheel operates between (ω_{min}) and (ω_{max}) to avoid too great a voltage variation and to limit the maximum MG torque for a given power rating. The moment of inertia is a function of the mass and shape of the rotor. It is determined by the volume integral of rotor mass density (ρ_m) and square of the distance (x) from the differential mass element to the axis of rotation:

$$I = \int \rho_m \, x^2 \, dV \tag{2.3}$$

Flywheels are often built as solid or hollow cylinders, ranging from short and disc-type, to long drum-type [36]. For a solid cylinder flywheel, the moment of inertia is calculated using the geometry and mass of the rotor:

$$I = \frac{1}{2} m \, r^2 \tag{2.4}$$

Where m is representing the flywheel mass as

$$m = \pi \rho_m h r^2 \tag{2.5}$$

The moment of inertia can be represented as a function of the rotor dimension and density by substituting (2.5) into (2.4):

$$I = \frac{1}{2} \pi \rho_m h r^4 \tag{2.6}$$

where

r: rotor radius

m: rotor mass

h: rotor length

ρ_m: rotor mass density

For a hollow cylinder flywheel of outer radius *b* and inner radius *a*, as shown in Figure *2.3*, the moment of inertia is determined by:

$$I = \frac{1}{2} m \, (b^2 + a^2) \tag{2.7}$$

$$I = \tfrac{1}{2} \pi \rho_m h \, (b^4 - a^4) \tag{2.8}$$

Hence the energy stored in a hollow cylinder flywheel as a function of the rotor geometry, mass and speed can be calculated by

$$E = \tfrac{1}{4} \pi \rho_m h \, \omega^2 \, (b^4 - a^4) \tag{2.9}$$

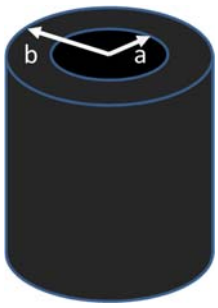

***Figure* 2.3.** Hollow cylinder flywheel

The maximum speed limit at which a flywheel may operate is determined by the strength of the rotor material, called tensile strength (σ) [37]. A suitable safety margin must be maintained, to keep the stress experienced by the rotor below the strength of the rotor material. The maximum stress of a thin rotating ring is given by:

$$\sigma_{max} = \rho_m \, v^2 = \rho_m \, r^2 \, \omega^2 \tag{2.10}$$

where

σ_{max}: maximum tensile strength

v: rotor peripheral speed

More complex equations are available for different rotor geometries; but for a given shape, the maximum stress is always proportional to (ρ_m), and the square of peripheral speed (v) equal to ($r\omega$). The effect of rotor geometries can be accommodated by introducing a shape factor *K*. The maximum specific energy and volume energy density are then given by:

$$\frac{E}{m} = K \frac{\sigma_{\max}}{\rho} \quad [\mathrm{J/kg}] \tag{2.11}$$

$$\frac{E}{V} = K\sigma_{\max} \quad [\mathrm{J/m^3}] \tag{2.12}$$

Equations (2.11) and (2.12) indicate that the specific energy (energy per mass unit) and energy density (energy per volume unit) of the flywheel are dependent on its shape, expressed as shape factor *K*. The shape of a flywheel is an important factor for determining the flywheel speed limit, and hence, the maximum energy that can be stored. The shape factor *K*, dependent on the flywheel geometry, is a measurement of flywheel material utilisation [37]. *Figure 2.4* indicates the values of *K* for the most common types of flywheel geometries.

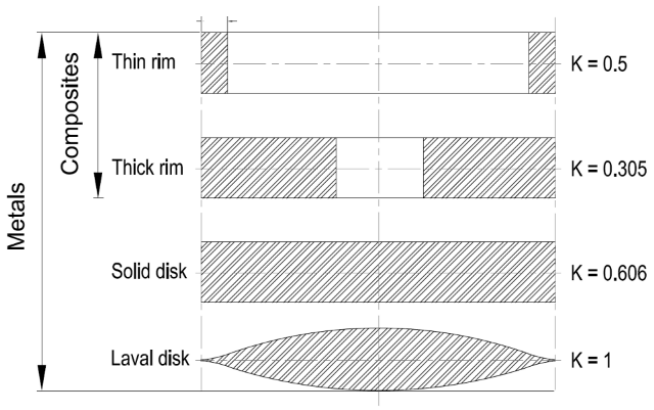

Figure 2.4. Different flywheel cross-sections *[37]*

According to Equation (2.1), the stored energy of a flywheel can be optimised by either increasing the spinning speed (ω) or increasing the moment of inertia (I). This allows two choices for flywheel design: low-speed FESS (typically up to 10,000 rpm) and high-speed FESS (up to 100,000 rpm) [26]. Low-speed flywheels are usually made of heavier metallic material and are supported by either mechanical or magnetic bearings or a combination of both. High-speed flywheels generally use lighter but strong composite materials and typically require magnetic bearings. The commonly used material for flywheel rotors is either metal or fibre composites. Metallic rotor choices can be either moderate-strength steel for low-cost options or maraging steel and titanium for higher specific energy requirements. Fibre composite material is made by embedding fibres in a matrix material such as epoxy. Typical fibres used are graphite, S-glass, E-glass, and Kevlar [38].

Table 2-1. Characteristics of material for use in flywheels *[18] [23]*

Material	**Density (ρ)**	**Tensile strength (σ)**	**Specific strength**	
Steel	***(kg/m³)***	***(MN/m²)***	***kJ/kg***	***Wh/kg***
AISI 4340 Steel	7830	1790	229	64
18 Ni-250 (Maraging)	8000	1860	233	65
HP 9-4-20	7830	1310-1480	167	46
HP 9-4-30	7830	1520-1660	194	54
Composites				
E-glass	2000	100	50	14
S2-glass	1920	1470	760	210
Carbon T1000	1520	1950	1280	350
Carbon AS4C	1510	1650	1100	300
Kevlar 49	1400	2700	1700	480
Graphite (Fibre)	1550-1600	2800	1400	390

Table 2-1 lists characteristics of more common material that can be used in flywheel rotors. Light alloys based on aluminium or magnesium are typically not used due to their more limited fatigue life compared to steels. Graphite, more commonly known as carbon fibre, is the strongest material with much higher specific strength than metals, but its main drawback is its high cost [39]. The price of high-speed flywheels can be up to five times higher than the cost of low-speed flywheels, according to [37]. The author notes that the cost of a flywheel system is governed by the design of the whole system, not the rotor, although this core element may dictate the design of the other elements in the system, hence the total cost.

A new class of intermediate speed flywheels, benefiting from the low cost of steel materials but a sufficiently high energy density, is also being developed, based on the use of laminated steel. This has the potential to offer low cost, but also compact, options [40]. Use of steel laminates can be advantageous in making a construction that eliminates the stress raising feature of a central hole and this increases the energy stored per unit mass by a factor of two for a given strength of material. This is apparent from Equation 2.11 and *Figure 2.4* with K being nearly double if the central hole is not present. The peripheral speed of this flywheel can be much higher that would be safe for a solid monolithic structure. The catastrophic fracture in the rotor by fatigue crack is restricted to a single laminate that will only release a small fraction of the energy contained.

Table 2-2. Comparison of rotor mass and volume ratio of steel and composite.

Attribute	**Carbon Fibre, V_{max} = 790 m/s a = 2/3 b[1]**	**Steel Laminate V_{max} = 427 m/s a = 0 (No hole)**
Mass	1	4.53
Volume	1	0.503

[1] a is the inner radius and b is the outer radius of a hollow flywheel

It is relatively simple to compare the intermediate speed flywheel rotor with a composite rotor for an assumed value of peripheral speed based on realistic maximum operating stresses in the two materials. The moment of inertia is a geometric value and the energy stored is then proportional to material density and square of speed

(Equation 2.9). This analysis is used to find the rotor mass and volume ratio of steel relative to composite as shown in *Table 2-2*. Interestingly the mass of the rotor is over 4 times higher but the volume is halved.

The peripheral speeds of composite rotors on commercially available flywheels are typically limited to less than 800 m/s, which is much lower than is achievable theoretically due to variation in material properties and diminishing returns when the weight and cost of containment outweigh the gains of operating at higher speeds. In many cases, rotor peripheral speeds are even less for these reasons. In a composite flywheel, the entire flywheel typically fails and even though the size of the fragments is small; all the energy is released at once. As an alternative to heavy containment, the flywheel can be buried but this adds cost in a different way.

2.2.2 Electric Machine

As discussed previously, the electrical machine or integrated MG is coupled to the flywheel, to enable the energy conversion and charging process of the flywheel. The machine, acting as a motor, charges the flywheel by accelerating it and drawing energy from an electrical energy source. The stored energy in the flywheel is extracted by the same machine, acting as a generator, and hence, the flywheel is slowed down during discharge. Common electrical machines used in FESS applications are the induction machine (IM), permanent magnet (PM) machine, and variable reluctance machine (VRM) [37].

An IM is used for high power applications due to its ruggedness, higher torque, and low cost. However, the main problems with IMs are their speed limitations, complex control, and higher maintenance requirements [41]. The squirrel cage type can be a less expensive option for slow response applications. Doubly fed induction machine (DFIM) recently used in FESS applications provides the advantage of lower power conversion rating in comparison to IM or PMSM. Due to its flexible control mechanism, it allows mitigated power electronics sizing [42]. An IM is widely used in

FESS-based wind turbine applications to enable the power smoothing of wind generation systems [42].

A VRM is very robust and has low idling losses and a wide speed range. It has a simpler control mechanism than IMs when it comes to high-speed operations. On the downside, it has a low power factor and low power density, as well as high torque ripples [41]. Both switched reluctance and synchronous reluctance types are applied in high-speed FESS applications [42].

A PM machine is a most commonly used machine for FESS because of its higher efficiency, high power density, and low rotor losses. It is widely used in high-speed applications due to the speed limitations of IMs, and the torque ripple, vibration, and noise of VRMs. The key problems with a PM machine are its idling losses due to stator eddy current losses, its high price, and its low tensile strength [37]. Brushless dc machine (BLDCM), permanent magnet synchronous machine (PMSM), and Halbach array machine (HAM) are the main types of PM machines used in FESS applications [42]. A detailed comparison between IMs, VRMs, and PMs addressing different aspects of these machines is presented in *Table 2-3*.

Table 2-3. Comparison of electrical machines suitable for use in FESS *[37] [43] [44]*

Machine	**Asynchronous**	**Variable Reluctance**	**Permanent Magnet Synchronous**
Power	High	Medium and low	Medium and low
Specific power	Medium (~0.7 kW/kg)	Medium (~0.7 kW/kg)	High (~1.2 kW/kg)
Rotor losses	Copper and iron	Iron due to slots	Very low
Spinning losses	Removable by annulling flux	Removable by annulling flux	Non-removable, static flux
Efficiency	High (93.4%)	High (93%)	Very high (95.5%)
Control	Vector control	Synchronous: Vector Control. Switched: DSP	Sinusoidal: Vector control. Trapezoidal: DSP
Size	1.8 L/kW	2.6 L/kW	2.3 L/kW
Tensile strength	Medium	Medium	Low
Torque ripple	Medium (7.3%)	High (24%)	Medium (10%)
Maximum/base speed	Medium (>3)	High (>4)	Low (<2)
Demagnetization	No	No	Yes
Cost	Low (22 €/kW)	Low (24 €/kW)	High (38 €/kW)
Advantages	Low cost	Low loss, high efficiency	Low loss, high efficiency
	Simple manufacture	Overcurrent capability	High power density
	Technology-matured	Excitation coil can repeat adjustment	High load density

	Adjustable power factor	Lower loss at starting torque	High torque density
	No demagnetization	Easy to dissipate heat	Small volume and simple structure
	High energy storage	Robustness of temperature overheat	low rotor resistance loss
	No running loss	High power density	No field winding loss
			Flexible shape and size
			Simple control mode
			High reliability
Disadvantages	High slip ratio of rotor	Complex structure	poor robustness of temperature
	Limited speed	Difficult to manufacture if switched reluctance type	Demagnetisation
	Larger volume	Low power factor	High cost
	Low power to quality ratio	Torque ripple, vibration and noise	Materials fragile
	High losses, low efficiency	Difficult to regulate the speed	Difficult air gap flux- field adjustment

To take advantage of both PMs and VRMs, hybrid PM reluctance machines have recently been developed. Some special types of machines designed for FESS applications are presented in [42] and the latest developments of MG for FESS are discussed in [43]. A special machine reported for flywheel applications is the bearingless homopolar ac machine with 3 sets of windings in its stator: dc field winding, three-phase torque producing winding and 2-phase 2-pole suspension winding [45]. The drawback of this machine is its unstable suspension problem that occurs at a certain level of field excitation at some speed levels. Another unconventional machine for use in FESS applications is a 12-phase output type. The output phases can be rectified by connecting to four three-phase rectifier bridges to supply a dc-link capacitor in parallel [46].

2.2.3 Power Electronics

The energy conversion in a FESS is accomplished by the operation of an integrated electrical machine and a bi-directional power converter. The power electronic converter topologies that can be used for FESS applications are DC-AC, AC-AC, and AC-DC-AC, or a combination of these. The switching devices of the power converters are selected based on their operational characteristics and application. These include bipolar junction transistor (BJT), metal oxide semiconductor field-effect transistor

(MOSFET), insulated gate bipolar transistor (IGBT), and thyristors (SCR, GTO, MCT) [47]. The commonly used switches are a silicon controlled rectifier (SCR), gate turn off thyristor (GTO), and IGBT. SCR and GTO have been traditionally used for variable frequency power converters. However, IGBTs have been more commonly adopted in recent years, due to its higher power capability and higher switching frequencies [18].

The widely used configuration of power converters in FESS is the back-to-back (BTB) or AC-DC-AC configuration that allows connection of the flywheel storage to an AC source (e.g. electrical grid) through a DC-link. The converters in the BTB topology are three-phase bridged semiconductor switches, often controlled by the pulse width modulation (PWM) technique [37]. The PWM uses rectangular pulses and modulates the width of these pulses to produce a variable waveform. The pulses are applied to the power electronics converter to produce a sinusoidal AC current from a DC input [48]. The grid side converter maintains the DC link voltage, where the machine side converter is used to control the operation of the MG and the flywheel.

A DC to AC converter, usually known as an inverter, produces an AC output of a desired magnitude and frequency from a fixed or variable DC input. Variable output waveforms are achieved by either varying the DC input or adjusting the gain of the inverter [49]. The widely used industrial applications of inverters for FESS are variable-speed ac motor drives, renewable energy, transportation, and uninterruptible power supplies (UPS) [50]. In wind power applications, an inverter is used to connect the FESS directly to the grid (*Figure 2.5*) or to the DC link of the wind generator (*Figure 2.6*) [51, 52].

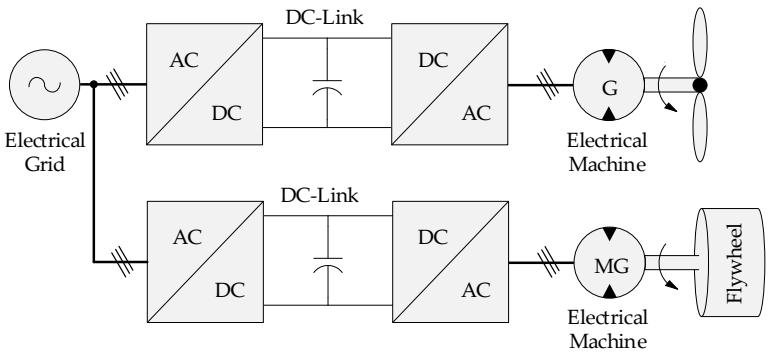

Figure 2.5. FESS with a BTB converter directly connected to the grid

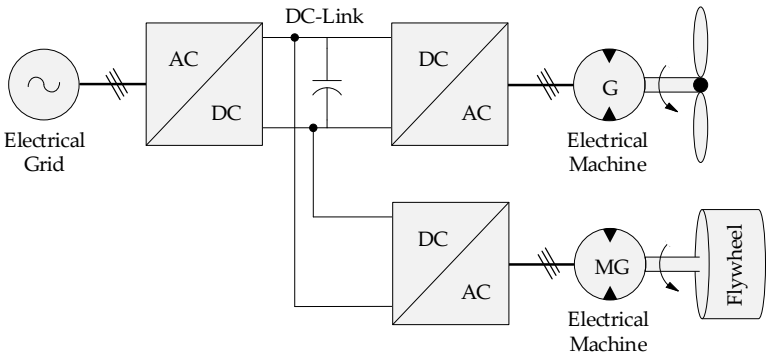

Figure 2.6. FESS with a DC-AC converter connected to the DC-link

In high power and high voltage applications, the two-level DC-AC inverters are limited to operating at a high frequency, due to switching losses and device rating constraints [53]. Multilevel inverters, with an additional DC link capacitor, can be used to generate higher voltages with a less transient dv/dt and reduced total harmonic distortion (THD) [54]. The common multilevel converter topologies in the industry are diode-clamped converters or neutral-point-clamped (NPC) converters, cascaded H-bridge (CHB) converters, and flying capacitor (FC) converters. A three-level twelve-pulse NPC converter topology for FESS is proposed in [55]. Two NPC converters are connected in BTB combination to connect the FESS to the point of common coupling (PCC) between the electrical grid and wind generation.

An AC to AC or matrix converter (MC) is an array of multiple bidirectional switches arranged in a way to allow the connection of any of the output phases of the converter to any of the input phases. MCs are used to modify the amplitude, frequency, and phases of the waveforms between the two asynchronous ac systems [53]. During its early stages, the AC-AC power converter was termed as a Forced Commutated Cycloconverter (FCC), as it mainly relied on forced commutated thyristors [54]. These converters became a viable alternative to BTB converters after the emergence of BJTs. A comparison of MCs and BTB converters is presented in [56]. MCs are compact in size and have a lower weight since there are no large capacitors or inductors required for energy storage. However, the lack of an energy-storing capacitor limits their maximum voltage transfer ratio to 86%. This limit can be exceeded, but with the cost of unwanted low-frequency components in the input and

output waveforms [54]. AC-AC converters can be used with FESS in dynamic voltage restorer applications to mitigate voltage sags [57]. The choice of the matrix converter improves the reliability of the system and increases the power density [58].

A cascaded DC-DC and DC-AC converter configuration can also be used for FESS applications connected to a DC microgrid. A three-phase full-bridge circuit in series with a bidirectional buck-boost converter is proposed in [59]. This combination has the potential to be used in a wider range of applications with the emergence of DC microgrid in the future.

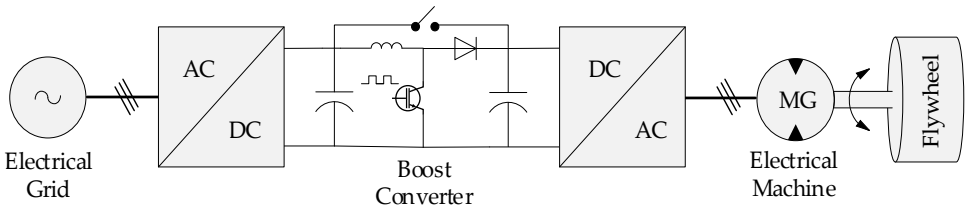

Figure 2.7. FESS connected to the grid via BTB configuration with a boost converter

In the cases where the discharging speed of the FESS is low, a DC-DC boost converter is connected at the DC link between the BTB converters to regulate the output voltage as shown in *Figure 2.7*. The boost converter can be bypassed by a switch during the charging intervals [60]. In [61], a Z-source inverter topology is used as an alternative to a boost converter. In this configuration, inverter output waveform distortion is reduced and the reliability of the system is greatly improved, because of the short circuit which can exist across any phase leg of the inverter.

A higher switching frequency for the inverter and rectifier reduces current ripples and increases control bandwidth, but switching losses will be increased. In addition, the fast switching of the power converter reduces higher-order harmonics to produce an improved sinewave. Harmonics can be further reduced by the introduction of AC filters on the AC side of the converter. Filters can reduce current ripples, winding deterioration, and hence, the losses [62, 63].

2.2.4 Bearings

Bearings are required to keep the rotor in place with very low friction, yet provide a support mechanism for the flywheel. The bearing system can be mechanical or

magnetic, depending on the weight, lifecycle requirements, and accepted level of losses [29]. Gas bearings cannot be used due to the vacuum within the enclosure. Traditionally mechanical ball bearings have been used, but these have higher friction compared to magnetic bearings and require higher maintenance because of lubricant deterioration [29]. These difficulties may be mitigated by using a hybrid system of magnetic and mechanical bearings. A magnetic bearing has no friction losses and does not require any lubrication but, if active, requires power to energize it. It stabilizes the flywheel by supporting its weight using permanent magnets [18]. Permanent (passive) magnetic bearings (PMB), active magnetic bearings (AMB), and superconducting magnetic bearings (SMB) are the main types of magnetic bearing systems [41]. A PMB has high stiffness, low cost, and low losses due to lack of current. However, it has limitations in providing stability and is usually considered as an auxiliary bearing system [37]. An AMB is operated by the magnetic field produced from current-carrying coils controlling the rotor position. It positions the rotor through a feedback system by applying variable forces which are determined based on the deviation of the rotor position due to external forces. An AMB has a high cost, a complicated control system, and consumes energy to operate, which indirectly adds to the system losses [41].

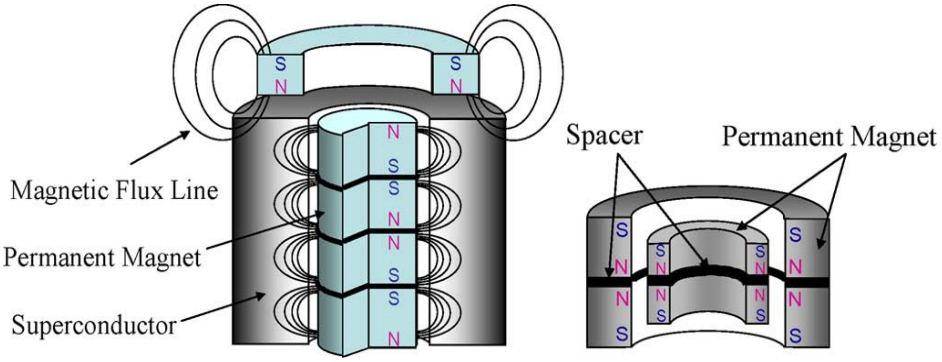

Figure 2.8. Structure of SMB (left) and PMB (right) *[64]*

FESS standby loss can be affected by the AMB mass. As a result, increasing the rotational speed and AMB mass add to the AMB iron and copper loss [36]. To ensure a good efficiency of the overall system, a compromise between speed and losses has to be made. An SMB provides a high speed, frictionless, long life, compact, and stable

operation. It is the best magnetic bearing for high-speed operation as it can stabilize the flywheel without electricity or a positioning system [18, 41]. An SMB requires a cryogenic cooling system as it operates at a very low temperature; but recently, it has been improved by using high-temperature superconductors (HTS). The main drawback of an SMB system is its very high cost [18, 29, 41]. The parasitic losses of mechanical bearings are about 5% of the total storage capacity per hour unless hybrid systems are used. This factor is about 1% for electromagnetic bearings [65] and can be further lowered to 0.1% by using HTS bearings [66]. The use of hybrid bearings will reduce the losses and complexity of the control system and also provide a stable and cost-effective solution [67]. A compact FESS assisted by hybrid mechanical-magnetic bearings is proposed in [68]. The magnetic levitation in the vertical orientation is maintained by the magnetic bearing, while the translational and rotational levitation is assisted by the mechanical bearing. In [64], a combination of SMB and PMB have been analysed to reduce the cost of the cooling system. The position of the flywheel rotor is controlled by the PMB and the SMB is mainly used to suppress the rotor vibrations. However, the capability of PMB in restraining the system during high speeds still remains in question.

2.2.5 Containment

The containment or housing has two purposes: to provide an environment for low gas drag and for the containment of the rotor in the event of a failure. The aerodynamic drag loss in a FESS increases with the cube of the rotational speed if the system is operated in atmospheric pressure [26]. These losses are reduced by mounting the flywheel in a vacuum enclosure to improve the system performance and safety. The housing or enclosure is the stationary part of the flywheel and is usually made of thick steel or other high strength material, such as composites. The container holds the rotor in a vacuum to control rotor aerodynamic drag losses by maintaining the low pressure inside the device, thus withstanding failures as a result of any possible rotor catastrophes [32]. Operating the system in such a low pressure requires a vacuum

pump and an efficient cooling system to handle the heat generated from MG and some other parts of FESS [26]. When the power into and out of the flywheel is via an electric machine, there are no rotary seals, so leakage can be very small. This means that the vacuum pump does not need to operate frequently, or can be eliminated with a sufficient sealing of the housing. The operation of the vacuum pump depends on the rotor type. Composite rotors have a very high tip speed requiring lower (harder) vacuum pressures and outgas, due to the nature of the polymer resin matrix materials in contrast to steel. An alternative approach is to use a gas mixture of helium and air, which reduces both the aerodynamic drag loss and the system cooling requirements [26].

In the event of rotor failure, composite rotors tend to break into numerous small fragments and its energy is dissipated by friction as the fragments rotate inside the casing. As this happens, the pressure is built up inside the casing and the endplates of the casing. If air enters during failure, then a much stronger dust type explosion must also be contained, leading to the need for stronger containment. Single piece steel rotors can burst into several fragments which will be difficult for the enclosure to withstand, so require very large containment systems. This issue can be mitigated by making the rotor from a stack of thinner discs, as explained in the section on rotors. This is because the catastrophic failure would release a fraction of the energy contained in the flywheel rotor. The enclosure design for high-speed FESS will contribute to half of the flywheel weight, whereas this factor would be two and half times larger for low speed FESS, according to [37]. However, this multiplier would be different from the perspective of most flywheel manufacturers who adopt a range of stances to justify safety including placing flywheels in bunkers for large composite rotors. Published literature on what is required to contain both composite and steel rotors is not readily available and, to the author's knowledge, no officially adopted standards currently exist. One recent publication has proposed a standard [69], which can be a useful step forward.

2.3 Chapter summary

This chapter provided a general background on the existence and emergence of flywheels since their early appearance thousands of years back. The second part of the chapter focused on the structure and components of FESS addressing their types and recent developments.

Early age flywheels were mostly made of wood until the industrial revolution that laid the foundation for the development of metallic flywheels. Recent improvements in material and advances in power electronics and electric machinery have promoted modern age flywheels which are mainly composite based benefitting from higher strength and lighter weight. However, steel rotor flywheels are also extensively in use due to their lower cost. On the recent developments, flywheel rotors made of laminated steel can be a potential alternative.

The common types of electric machines for flywheel applications are IMs, PM machines, and VRM. A detailed comparison of the machines was provided and PM was reported as the most widely used electric machine in FESS. This is due to its higher efficiency and power density, and lower rotor losses. The converter topologies that can be used in FESS are DC-AC, AC-AC, or a combination of both. The converters are often transistor operated and controlled by PWM technique. Despite developments of different multilevel converters (e.g. diode-clamped, NPC, CHB, FC), the back-to-back AC-DC-AC is still the widely used converter topology in FESS. The bearing system is required to keep the flywheel rotor in place and it can be mechanical, magnetic, or gas type bearings. The gas type bearing cannot be used in flywheels due to the vacuum requirement within the enclosure. Traditionally, mechanical ball bearings have been used in flywheels, but these require higher maintenance and have higher friction compared to magnetic bearings. The common types of magnetic bearings are PMB, AMB, and SMB. Each has its own operational requirements (e.g. energy, cooling, etc.) which adds to the cost. Sometimes as a trade-off between improved performance and the cost, a hybrid system of bearings is used. Combined mechanical and magnetic bearings is generally a preferred arrangement, however, a

combination of SMB and PMB is also explored as an option. Finally, the performance and safety of the flywheel system are improved by enclosing it in a solid containment. The enclosure is typically made of thick steel or a high strength material (i.e. composites) and must be equipped with a vacuum pump to maintain the pressure level inside the container. The thickness of the container and vacuum pumping requirement are related to the material and peripheral speed of the flywheel rotor. Composite rotors do not require as thick a containment as steel rotors, however, they must be frequently depressurised due to outgas generated from the polymer resin material.

Chapter 3 Flywheel Characteristics and Applications

This chapter is focused on flywheel energy storage systems characteristics and applications. Flywheels have experienced considerable improvement as a result of recent developments in construction material and bearings, power electronics and electric machines. They find applications in electrical energy storage as well as transportation, military services, and state-space satellites. The first part of this chapter describes the general attributes and drawbacks associated with flywheel storage systems. The second part is devoted to applications of flywheels as an energy storage system at different levels and scales where recent onsite industrial examples for each particular application is also provided. There is a scarcity of information available in the literature addressing recent onsite applications of flywheels. A number of reported examples for each application are collected from many sources and to the author's best of knowledge. The chapter is concluded with a brief summary and motivation for research direction.

3.1 FESS Characteristics

The main characteristics of flywheels are high cycle life (in the hundreds of thousands), long calendar life (more than 20 years), fast response, high round trip efficiency, high charge and discharge rates, high power and energy density [29], and low environmental impacts [1]. Another main attribute of the flywheel is that its state of charge can be easily measured from the rotational speed and is not affected by life or temperature [18]. On the downside, flywheel self-discharges at a much higher rate than other storage mediums and flywheels can be hazardous, if their rotors and containment systems are not designed safely.

Flywheels have a long lifetime and very low operational and maintenance requirements due to the fundamental nature of their storage method which does not require any physical or chemical change other than the state of stress. This leads to high cycle life, compared to many other energy storage systems, as long as stress levels are kept within fatigue life limits. Flywheels do not require long charge-discharge

cycles but can be charged and discharged rapidly, limited by the means of inputting or extracting power. They are not affected by the depth of discharge (DoD). The lifetime of commercially available flywheels is typically more than 20 years and a charge-discharge cycle life in excess of hundreds of thousands, with no deterioration in performance over the lifetime [2]. The technology is capable of transferring large amounts of power in seconds, with a high roundtrip energy efficiency in the range of 90%–95% for the best systems [3]. It can deliver its stored energy and recharge quickly, in a matter of seconds. It is an environmentally friendly technology and there are no emissions because of its operation, since the material used is not hazardous to the environment [32]. Particularly, steel rotor type flywheels are fully recyclable although recycling will not be needed for decades. The power and energy ratings of flywheels are independent and each can generally be separately optimised, based on the application of the energy storage. The power rating of a flywheel depends on the size of the MG and associated power electronics, where its energy rating is determined by the dimensions, geometric shape and speed of the rotor [2].

There are wide ranges of applications for flywheels in high power output short duration periods; however, given the available choices for rotor material, a longer storage period requires developing new rotor designs [17]. For example, increasing the rotor diameter will increase the inertia and extend the energy storage duration. Rotor lamination will also improve the energy storage capability of the flywheel since it allows higher rotor tip speeds for steel rotor. The size of FESS is an important characteristic which puts them in competition with other energy storage technologies. Flywheels can have power densities up to five to ten times that of batteries. Due to their relatively lower volume requirements and longer working life, they can replace batteries in certain applications, including in transportation and space vehicles [17].

3.2 Flywheel Energy Storage Applications

With the technical advances and improved composite manufacturing techniques, today's energy storage flywheels operate with storing capacity of up to hundreds of

Mega-Joules energy and Giga-Watts of power [18] which can be reached by arranging flywheels in banks, rather than using large machines [70]. Flywheel applications range from large scale at the electrical grid level, to small scale at the customer level [17, 18]. The best and most suitable applications of flywheels fall in the areas of high power for a short duration (e.g., 100 s of kW in 10 s of seconds) [71] , when frequent charge-discharge cycles are involved [17]. The most common applications are power quality such as frequency and voltage regulation [72], high power pulsed systems such as military vehicles [73], attitude control in spacecraft [27], UPS [50], load levelling [1], hybrid and electric vehicles and energy storage applications [74]. A description of some common applications associated with FESS including their onsite industrial installations is given in the following subsections.

3.2.1 Power Quality Enhancement

As part of the power quality requirements, the frequency and voltage of many electrical systems need to be maintained to an acceptable level and deviations should be avoided. For example, when the loads are added or taken out of a power grid, the system voltage and frequency will be reduced or increased since it is difficult for the supply side to compensate sufficiently quickly. Energy storage systems, especially those which are fast performing like flywheels, can quickly add or take power from the grid to keep the system voltage and frequency within a specified range [75]. Flywheels can easily arrange for ride-through applications for interruptions of up to 15 s long and provide a means of switching between power sources without any service interruptions [1]. Flywheels can operate for up to tens of minutes for reactive power support, spinning reserve, and voltage regulation, to supply reliable electric power and improve the power quality in applications such as communication facilities and computer server centres [1, 76]. As long as run-down losses are kept low, durations can be extended to several hours, without losing excessive amounts of energy.

On the application part, reported in 2001, Piller GmbH (Osterode, Germany) has installed flywheels in a facility which was powered by the utility grid and local generators [29]. The flywheel system was supplying a semiconductor fabrication facility in Dresden, Germany. The plant rating was 30 MW and the flywheel storage system could store 7kWh energy, which was good enough to allow switching between different energy sources within the power plant. Another flywheel system consisted of 17 flywheels to be combined with a total power rating of 4.75 MW, has been operated by Active Power (Austin, Texas). This flywheel system integrated with Caterpillar generators was supplying a plastic product manufacturer to provide power conditioning and protect it against power outages [17].

In North Western Australia, a flywheel system has been integrated into a town's power supply to support the increased power demand during the tourist season [77]. Coral Bay, a hybrid wind-diesel power station in Australia, consists of seven 320 kW low-load diesel generators with three 200 kW wind turbines. In 2007, the integration of a 500 kW flywheel virtual generator into the system allowed the wind turbines to provide up to 95% of Coral Bay's supply at peak times. The reported data shows that for nearly 900 h per year, 90% of the power station's total supply comes from wind generation. In addition, while maintaining the grid standards and improving the power quality, 80% of this total power is wind-generated for one-third of the year [77]. Another flywheel-based stabilisation system has been planned for the Marsabit wind farm, a remote community served by an isolated microgrid in northern Kenya. A 500 kW flywheel-based system will be integrated into the existing two 275 kW wind turbines and diesel generators. The PowerStore flywheel, designed and implemented by ABB, provides the means to stabilise the grid connection to maximise renewable energy penetration [78]. PowerStore is a flywheel-based stabilising generator which is mainly used for improving power quality. It enables the integration and control of renewable wind and solar energy in the electrical grid. Acting like a static synchronous compensator (STATCOM), it combines an 18 MWs (Megawatt-second) low-speed flywheel with solid state converters that absorb or inject full energy in 1

millisecond [79]. The range of models from 500 kW to 1.5 MW allows the configuration of either a grid support mode for MW scale grids or as a virtual generator for use in smaller isolated grids.

3.2.2 Frequency Regulation

Frequency fluctuations occur due to variations between the loads and supply, where one exceeds the other. When demand exceeds supply, the generating plants are slowed down by the extra load, thus decreasing the system frequency. On the other hand, the generators accelerate and the frequency increases whenever the generation exceeds the demanded loads [80]. The frequency fluctuates every second, as demand varies and generators turn on and off. To avoid this, frequency regulation is applied, which demands the generators to hold capacity in reserve, to maintain the stability of generation and consumption. This ramping up and down of the generators not only increases the fuel cost and emissions but also takes up to a minute or longer for some generating power plants to respond [81].

A frequency regulation service is a very cyclic application requiring thousands of charge-discharge cycles in a year. Any storage device in this application will be very rarely "resting", since it includes constant charging and discharging at variable rates, from very slow to rapid and deep cycling [82]. Today, grid operators look for 'fast-acting regulators' including flywheels and batteries to respond to the frequency regulation issue. Because of their fast response and frequent charge-discharge capabilities, flywheels are likely to dominate over batteries in this application. Similarly, the capability of flywheels to switch from full output to full absorption in seconds puts them on a par with the immediate energy produced by gas fired power plants. FESS can deliver twice as much frequency regulation for each megawatt of power that they produce while cutting carbon emissions in half [81]. The earliest, but the shortest lifespan of a flywheel system reported for frequency regulation using renewables, was installed in Shimane, Japan, in 2003. This 200 kW Urenco Power Technology Flywheel was installed by Fuji electric to reduce system fluctuations due to wind generation. The diesel generators supporting the 1.8 MW wind turbines were

operating at a higher efficiency since the excess demand and load fluctuations were managed by the integrated flywheel system. The system was decommissioned in 2004, as Urenco abandoned power quality operated flywheels and removed all previously installed units [77]. The largest power rated FESS for frequency regulation is the Joint European Torus (JET) Fusion Flywheel of the European Atomic Energy Community (EURATOM) located in Oxfordshire, UK [83]. JET uses the grid for powering electromagnets, and for generating fields to confine and ohmically heat hydrogen plasma. Experiments typically last 20 s and draw 1000 MW—a large fraction of the local Didcot Power Station's capacity [84]. There are two large flywheels capable of supplying up to 400 MW for 30 s and an additional 300 MW power is pulled from the grid to combine with the FESS, in order to satisfy the peak consumption of the JET pulse. The JET flywheels are charged up from the grid for several minutes, then quickly discharged into the required loads. Hence, distribution network congestion is avoided by reducing the demand on the grid during experiments [85]. On the latest industrial applications of flywheels reported for frequency regulation, a 20 MW flywheel-based facility provides frequency regulations services to New York Independent System Operator (NYISO) in Stephentown, New York [32]. The facility is built and operated by Beacon Power and comprises 200 flywheels, each with a power capacity of 100 kW. The tests during early trials showed that 1 MW of fast response flywheel storage could produce up to 30 MW of regulation service – two to three times better than an average Independent System Operator (ISO) generator. A second 20 MW frequency-regulation facility in the Hazle Township of Pennsylvania is commissioned by Spindle Grid Regulation, LLC. This zero emission facility is designed for 20 year-life and at least 100,000 full-depth discharge cycles. It is comprised of 200 Beacon Power 100 kW (25 kWh) flywheels connected in parallel, which can respond in less than 2 s [86]. One of the world's largest flywheel systems performing frequency regulation services in Japan is reported by [87]. The system capacity is 23 MW with an approximate cost of 4250 $/kW.

3.2.3 Voltage Sag Control

Voltage sag problems are created due to load unbalance or faults in the power grid, causing a decrease in voltage magnitude. Voltage sags due to unbalanced loads occur when large amounts of power for a short period of time is absorbed by the load, which will decrease the voltage and cause voltage drop problems [80].

Voltage sag has become one of the major power quality problems affecting sensitive loads such as modem industrial manufacturing like semiconductor production, food processing and paper making, sensitive microprocessors, and high frequency power electronic devices [88]. Further drawbacks of voltage sag in three-phase power networks are increased line losses, neutral conductor overloads, and extra rotating losses in drives [80]. About 92% of the power quality problems are as a result of voltage sag and 80% of these occasions last for only 20–50 ms [88].

Traditionally, voltage sag has been compensated for by generation reserves adding power to the system, when demanded. The recent approach is to engage energy storage systems in mitigating the voltage problems in power networks. The energy storage system is used to store the energy in times when excessive power is required, in order to keep the grid voltage fixed. This reduces the cost and eliminates the need for oversized generating units [80].

FESS, with their excellent characteristics, can be viable alternatives to other storage systems for this application. Particularly, fast response, high power density, and frequent charge-discharge cycle capability are the best attributes of flywheels for voltage compensation applications [80]. On the application part, a 10 MJ FESS for improving quality and reliability of power supply from the distribution network was tested in the year 2000. It was able to keep the voltage in the distribution network within 98%–102% and had the capability of supplying 10 kW of power for 15 min [18]. In 2005, a flywheel-based grid stabilising generator (PowerStore) commenced operation in Flores Island, Portugal. It has been used to perform a frequency and voltage ride through to safeguard conventional grids and allows the integration of

renewable generation from wind and solar sources. The PowerStore with a 500 kW rated power and 60 s duration capability is still operational [77].

3.2.4 UPS

A short term (seconds to minutes) energy storage device with control electronics is referred to as an uninterruptible power supply (UPS). It is one of the existing markets and the most successful application for high power flywheels to supply power for occasions which usually don't last longer than 15 s. More than 80% of the power outages last for less than a second [17] and 97% of them last for less than 3 s [19]; however, this causes voltage and frequency problems, as well as power interruptions. In these applications, the UPS, as backup storage, bridges the gap between the loss of the grid and the start of backup sources during an interruption.

The most developed and widely used storage medium in UPS applications is batteries. FESS can be used as a substitute or in combination with batteries in UPS systems [89]. In cases with only flywheels operating as backup storage, sufficient power is provided by the flywheel to run the system, until the power source is restored or a standby power source comes online. Depending on the level of power required, 10–15 s of back up support is enough to meet the demand loads, without transferring to the backup generator set [17, 19]. This is the case when power outages last less than 15 s. Meanwhile, in diesel-rotary UPS with diesel generators for long-term outages, the diesel engines commonly start and accept 100% load within 3–4 s and flywheels are best suited to bridge the power until the generators are fully operated and synchronized. As a result, either scenario can be accomplished with flywheels acting as energy storage systems for UPS applications. In addition, flywheels are used in combination with batteries in UPS systems requiring longer durations. A flywheel can deal with shorter interruptions, while batteries can be saved for longer outages. This will save the battery from frequent charge-discharge, which will further increase its lifetime [89]. Usually, flywheels and batteries are combined for applications requiring

a mix and match between energy density and cost, that otherwise cannot be achieved with a single operation of either of the storage systems [87].

Many manufacturers around the world have developed flywheel systems for UPS. To name a few, one of the earliest flywheels for on-site power applications was built in Munich, Germany, in 1973. It was rated for 155 MW power and 0.93 power factor, for a pulsed duration of 9.7 s. In the following years, this flywheel was complemented with two more flywheels to utilise a flywheel generator system for high energy fusion experiments. The system was fully commissioned in 1987 and the total rated power and pulsed duration capability of the system were increased to 387 MW and 12 s, respectively [77]. A hybrid microgrid supplying heat and electricity to an industrial airport facility on an island in Alaska was commissioned in 1999. Originally consisting of a 225 kW wind turbine, and two 150 kW diesel generators, the system was upgraded with a 160 kW FESS by Beacon technology in 2014. In addition to efficiency improvements, integration of the flywheel system has also provided fuel savings of up to 30% [77]. In 2001, a high power UPS system with 50 MW output and 650 MJ storage capacity was investigated. Its possible applications were large UPS systems, the energy supply of plasma experiments, and acceleration of heavy masses (aircraft catapult, pre-acceleration of spacecraft) [18]. In the same year, a medical centre in Dallas installed a flywheel/UPS/generator to deliver continuous power for a cardiac catheterization unit which was experiencing power disturbance problems due to power outages [89]. In 2002 a flywheel/UPS/generator was installed in Fort Monmouth to provide backup power and protect internet, intranet services and server backup equipment. This flywheel system replaced batteries because the battery system was aged and the cost of the new battery system was greater than the new flywheel system [89]. Piller GmbH has also installed a FESS in a combined heat and power station to supply a semiconductor facility in Dresden, Germany. The integrated 5 MW flywheel subsystem can supplement the 30 MW plant with 5 s storage [29]. A battery-free UPS system has been announced by VYCON to protect a light-out data centre located in Texas, US. The system will involve multiple 750 kVA double-conversion UPS

modules, paired with an 8 MW (300 kW power rating per unit) FESS. Deploying approximately 1MW of clean energy, a similar flywheel system has also been planned to protect EasyStreet Online Service's data centre in California, US [90]. Similarly, the control centre of Austin Energy is protected by a 4.8 MW flywheel UPS by VYCON. Austin Energy, one of the largest electric utilities in the US, supplies approximately 400,000 customers and a population of about one million. The attributes associated with a battery-free flywheel system are reduced downtime, no battery maintenance requirement, and savings on the cooling of the environment for batteries.

As part of the services at the grid level, both European and U.S. companies have developed flywheel systems that are functioning for different applications around the world [17, 29]. According to the U.S. Federal Energy Management Program (FEMP) [89], flywheels have been commercially available to supplement or replace batteries in UPS systems since 1998. However, in 2002, the technology was considered superior to lead-acid batteries and there were about 18 manufacturers of flywheels only for UPS systems in the U.S.A and Canada outlines a brief overview of a number of commercial flywheel manufacturers for stationary applications.

3.2.5 Transportation

In transportation, flywheels are used in hybrid and electric vehicles to store energy for use when harsh acceleration is required or to assist with uphill climbs. In hybrid vehicles, the constant power is provided by the internal combustion engines to keep the vehicle running at a constant optimum speed, reducing fuel consumption, air and noise pollution, and extending the engine life by reducing maintenance requirements [17, 29]. At the same time, energy from regenerative braking during vehicle slowdown is stored in the flywheel, which will be supplied back to provide a boost during acceleration or climbing hills [92]. The only competitors to flywheels in hybrid vehicle applications are chemical batteries and ultra-capacitors. However, ultra-capacitors suffer from a low energy density and higher cost. Flywheels rank better than batteries based on their longer life time, higher power density, higher

efficiency, and frequent charge-discharge capability [17]. Furthermore, flywheels are developed for rail applications, both for hybrid and electric systems. They also find a place in gas turbine trains for the same purpose. The desired speed and maximum weight of the train determine the power and energy requirements. It is estimated that 30% of the braking energy could be recovered by this system, due to receptivity issues [17]. In electrical vehicles with chemical batteries as their source of propulsion, flywheels are considered to cope well with a fluctuating power consumption. This will prolong the lifetime of the battery as its charge-discharge cycles become more regular [19]. In train energy recovery systems, flywheels are installed at stations or substations to recover energy through regenerative braking, and supply it back into the system for traction purposes. Flywheels are well suited for this application due to the high rate of charge-discharge cycles needed. In addition, it allows voltage sag control for transmission and distribution lines, without increasing the line capacity of the railway.

A number of flywheels for trackside energy recovery systems have been demonstrated by Urenco, VYCON Inc. and Calnetix [93]. Since the 1960s, Urenco Power Technologies (UPT) has been in operation and its manufactured flywheels are mostly made from carbon fibre composite. In transport applications, a number of trials of FESS installed on London Underground (LU) trains have been conducted in 2000-01. LU has tested a Urenco flywheel in the 500 to 600Hz range (up to 36000 rpm) on a 2.8 km track between South Ealing and Northfields. Three 100 kW flywheel energy storage units were tested on the Jubilee Line cars. The FESS was operated to receive regenerated energy from braking trains and provide energy for accelerating the trains [93].

In April 2014, VYCON Inc. installed a FESS for the Los Angeles Country Metropolitan Transportation Authority (LA Metro) Redline (MRL), to recover the braking energy from trains. MRL provides rail subway service connecting downtown to San Fernando Valley through six-car trains with AC or DC traction systems [94]. VYCON's flywheel, known as Metro's Wayside Energy Storage Substation (WESS), can recover 66% of the braking train energy [95]. The collected data, after six months

of operation, showed 20% energy savings (approximately 541 MWh), which is enough to power 100 average homes in California [94]. A total of 190 metro systems operating in 9477 stations and approximately 11,800 km of track has been reported globally [21]. The introduction of energy storage into rail transit for braking energy recovery can potentially reduce 10% of the electricity consumption while achieving cost savings of $90,000 per station [21]. Flywheels are also used in roller coaster launch systems to accumulate the energy during downhill movements and then rapidly accelerate the train to reach uphill positions, using electromagnetic, hydraulic, and friction wheel propulsion. The Incredible Hulk roller coaster at an adventure theme park in Orlando, Florida, uses several 4500 kg flywheels to propel the system. The flywheels charge continuously at about 200 kW and then discharge at 8 MW to launch the train [21].

Since the late 2000s, the use of flywheel hybrid storage systems in motorsports has seen major developments, beginning with Formula 1 and followed by the highest class of World Endurance Championship (WEC) [21]. Williams Hybrid Power (WHP), part of Williams Group of companies, pioneered the use of FESS in motorsport. WHP's electric flywheel was used in Porsche Motorsport on their 2010 911 GT3 R Hybrid endurance racing car. This car competed in several endurance races in 2010, including the 24 h Nürburgring race, where it led the race by two laps until 22nd h, before retiring due to an engine-related failure- an unrelated problem to the hybrid system. The following year, the GT3 R secured the first position in the VLN race at the Nordschleife [96]. Porsche hybrid's latest version, the 918 RSR hybrid concept sports car with electric flywheel energy storage, was announced at the 2010 Detroit Motorshow. In March 2012, WHP was announced as the hybrid energy storage supplier for Audi R18 e-Tron Quattro. WHP's entirely new design flywheel (150 kW power, 45,000 rpm speed) for Audi made history by becoming the first hybrid car to win Le Mans, the most demanding race in the world, in 2010, 2013, and 2014 competitions [97].

In public transport, city buses are an ideal application for electric flywheel hybridisation, due to their higher mass and frequent start-stop nature. The technology can save fuel and reduce greenhouse gas emissions by up to 30% [96]. The first

important application of flywheels in transport was gyro buses in Switzerland and Austria in 1950s. These buses were propelled by using the electricity from overhead lines and storing it in flywheels [87]. The recent applications include WHP's developed FESS for use in buses for the Go-Ahead Group on March 2012. It also developed a kinetic energy recovery system (KERS) for GKN Gyrodrive in April 2014. The GKN has recently demonstrated a design for use in city buses [98].

3.2.6 Spacecraft

Flywheels find applications in space vehicles where the primary source of energy is the sun, and the energy needs to be stored for the periods when the satellite is in darkness [29]. FES for the international space station (ISS) was discussed in 1961 and was first proposed in the 1970s [17]. In the mid- 1990s, due to improvements in high-strength composite fibres and magnetic bearings, interests were renewed in FESS for satellite applications. In 1994, The NASA Glen Research Centre with Space Vehicle Directorate of Air Force Research Laboratory initiated efforts to develop flywheels systems on satellites [29]. For the past decade, the NASA Glenn Research Centre (GRC) has been interested in developing flywheels for space vehicles. Initially, designs used battery storage, but now, FES is being considered to combine or replace batteries. The combined functionality of batteries and flywheels will improve efficiency, and reduce the spacecraft mass and cost [17]. The proposed flywheel system for NASA has a composite rotor and magnetic bearings, capable of storing an excess of 15 MJ and peak power of 4.1 kW, with a net efficiency of 93.7%. Based on the estimates by NASA, replacing space station batteries with flywheels will result in more than US$200 million savings [29]. It has been reported that a flywheel system would be significantly smaller and offer a better weight reduction than the use of NiH_2 battery devices for use on EOS-AMI-type spacecraft. It has been shown that the flywheel offers a 35% reduction in mass, 55% reduction in volume and a 6.7% area reduction for solar array [99]. FESS is the only storage system that can accomplish dual functions, by providing satellites with renewable energy storage in conjunction with

attitude control [27, 28]. Authors in [100] provide an algorithm for charge and discharge control of FESS in space applications. The permanent magnet operated flywheel system was tested for 60,000 rpm and is proposed as an alternative to batteries on spacecraft in the future.

3.2.7 Renewables

Flywheels can assist in the penetration of wind and solar energy in power systems by improving system stability. The fast response characteristics of flywheels make them suitable in applications involving renewable energy storage for grid frequency balancing. Power oscillations due to solar and wind sources are compensated for by storing the energy during sunny or windy periods and are supplied back when demanded [18, 19]. Flywheels can be used to rectify the wind oscillations and improve the system frequency; whereas, in solar systems, they can be integrated with batteries to improve the system output and elongate the battery's operational lifetime [18].

The authors in [37] indicate that the formation of a hybrid system by the addition of wind turbines and photovoltaic panels could not result in fuel savings, as expected. This is because synchronous diesel generators, even unloaded, will consume up to 40% fuel on full load. Diesel generators should only be started when demanded and shut down most of the time. Therefore, FESS can reduce frequent start/shut-down cycles of the diesel generators; thus reducing fuel consumption and bridging the power fluctuations [37]. There are great advantages of flywheels backing up solar photovoltaic (PV) system since they can cope with the high cycles due to the cloud passing, yet provide ride through, as long as standing losses are kept low. There has been a wide range of flywheel systems developed for the penetration of renewable energy systems. For example, ABB's PowerStore, Urenco Power, Beacon Power, and VYCON technology, have all provided flywheel-based systems for wind and solar applications. In 2005, a 350kW/5kWh flywheel system was installed in Flores Island, Portugal. Because of the improved network stability of the system at Flores, implementation of a similar system was encouraged in Graciosa Island in the

following years [92]. The purpose of these storage systems was to maximise the level of wind generation into the power systems of the mentioned islands [92]. On a larger scale, the world's first high penetration solar PV diesel power station was installed in 2010, supplying the towns of Nullagine and Marble Bar in Western Australia. A FESS is integrated as a UPS system, to allow maximum solar power injection during sunshine and ramp up diesel generators when the sun is obscured. This enables a saving of 405,000 litres of fuel and 1100 metric tons of greenhouse gas emissions each year. The incorporation of flywheels in the system has helped the PV system to supply 60% of the average daytime energy for both towns, generating 1 GWh of renewable energy per year [77]. In recent years, a 2-MW flywheel system is installed on Alaska's Kodiak Island to smooth out the varying power flows from wind turbines, replacing a 3-MW battery system which has been struggling with the frequent number of usages during a day [101]. Similarly, another project is designed to a smaller island in Alaska to run exclusively on wind power about 15% of the time. In this system, flywheels will provide all frequency and voltage support for the grid [101].

3.2.8 Military

In the military, a recent trend has been towards the inclusion of electricity in military applications, such as in ships and other ground vehicles, as well as for weapons, navigation, communications, and their associated intelligent systems. This use of electric energy at different rates and different power levels requires energy storage to respond rapidly and reliably to this variable nature of the energy demand [17]. Hybrid electric power is essential for future combat vehicles, based on their planned electrically powered applications. Flywheels appear as an appropriate energy storage technology for these applications. They can be combined with supercapacitors to provide power for high speed systems requiring power in less than 10 μs.

Flywheels are also likely to find applications in the launching of aircraft from carriers. Currently, these systems are driven by steam accumulators to store the energy; however, flywheels could replace these accumulators to reduce the size of the

power generating systems that would otherwise be sized for the peak power load [17]. A FESS is integrated into a microgrid serving the US Marine Corp in California, to provide energy storage applications throughout the entire distributed generation at the base [77]. The purpose of the project is to provide energy security to military facilities using renewable energy. It is a network of interconnected smaller microgrids that are nestled into a 1.1 MW bigger-scale microgrid, that includes solar PV systems, diesel generators, batteries, and 60 kW, 120 kWh FESS [102]. The flywheel storage is intended to decrease the dependency on diesel generators by about 40% and provide peak shaving applications by mainly supplying high power loads such as elevators. In addition to extending the lifespan of the batteries, the FESS was estimated to work for 50,000 cycles and have a lifespan of 25 years [102].

3.2.9 Global installed capacity of flywheel storage systems

According to California Energy Storage Alliance (CESA), the global installed capacity (MW) of ESS is approximately 2.7% of global installed electric capacity – where 98% of total storage capacity coming from pumped hydro and only 2% is shared between non-pumped hydro storage systems [77].

As reported in the database of China Energy Storage Alliance (CNESA) [103], there were 14 flywheel energy storage projects reported worldwide in 2015. Either in the planning, construction, or operation stage, the total estimated global installed capacity of FESS is approximately 1,027 MW. Although this figure was only 4.1% of the total market activity for energy storage over the period of 2013-2014, excluding pumped storage [77].

The major flywheel operator in the world is the USA region with five plants using flywheel energy storage. Beacon Power is a well-known flywheel storage provider with one of its onsite storage facilities located in Stephentown, New York, where 200 flywheels operate in parallel to provide 20 MW [104]. The flywheels are housed in 20 pods of 1 MW each and rated for 100 kW with a storage capacity of 25 kWh [105].

One of the recent projects reported by Off-Grid Energy Independence is Europe's largest and UK's first battery-flywheel system coordinated by Schwungrad Energie

Limited whose flywheel technology will be provided by Adaptive Balancing Power GmbH. The battery-flywheel system will connect to the Irish and UK grids to support energy demand. In the project's first stage, the flywheel system with 500 kW peak power rating and a storage of 10 kWh will be installed and tested in Ireland. Then it will be upgraded to 1 MW power with 20 kWh storage to be used as a hybrid system with the 2 MW battery facility at the University of Sheffield [106].

The global FESS market is projected to grow at a compound annual growth rate (CAGR) of 19.6% by 2020 [107], although this figure is anticipated to reach 8.93% by 2027 [108]. Based on the research findings and to the author's knowledge, there is limited information available in the literature addressing the global onsite installation of the flywheel projects. Despite their maturity level and global usage, flywheels are not yet an established technology and all the information and technical data are limited to the flywheel manufacturers' websites.

Description and examples of onsite industrial installations of the flywheel energy storage systems for different applications were addressed earlier in this chapter (sections *3.2.1-3.2.8*). *Table 3-1* outlines a brief overview of a number of commercial flywheel manufacturers for stationary applications.

Table 3-1. Comparison of the characteristic properties of different commercial flywheel systems, reproduced from *[91]* and manufacturers websites

	Piller Power Bridge	Active Power	Temporal Power	Beacon Power Gen 4	Rosseta T2	Vycon	Kinetic Traction Systems	Stornetic	PowerThru	Gyrotricity	Amber Kinetics
Origin	Germany	USA	Canada	USA	Germany	USA	USA	Germany	USA	UK	USA
Rated Power	1,600	250 kW	100-500 kW	100 kW	500 kW	500 kW	200 kW	22 kW	190 kW	25 kW	8 kW
Rated Energy Capacity	4 kWh	0.9 kWh	50 kWh	25 kWh	4 kWh	0.83 kWh	1.5 kWh	4 kWh	0.63 kWh	0.069 kWh	32 kWh
Application area	UPS	UPS	Voltage Stability/ Maintenance	Frequency Stability/ Maintenance	Recuperation	UPS, Recuperation	UPS, Power Quality, Micro-grid & Railway	Grid services, Railway	UPS	Frequency Stability, Railway	Micro-grid, Telecoms, Utilities
Maximum rpm	3,300	7,700	11,500	16,000	25,000	36,000	37,800	45,000	52,000	20,000	10,000
Bearing concept	Rolling bearings, relieved magnetically	Rolling bearings, relieved magnetically	Unclear	Rolling bearings, relieved magnetically	Rolling bearings	Active magnetic bearings	Magnetic & hydrodynamic bearings	Active magnetic bearings	Active magnetic bearings	Mechanical & magnetic bearings	Not stated
Flywheel material	Steel	Steel	Steel	Fibre composite	Fibre composite	Steel	Fibre composite	Fibre composite	Fibre composite	Laminated Steel	Steel
Topology[1]	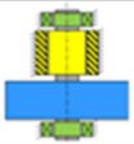	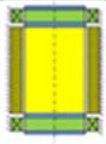	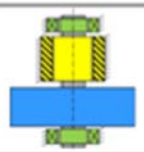	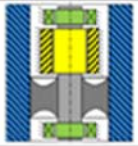	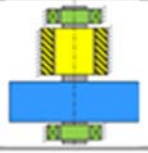		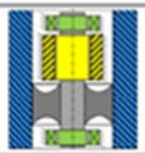	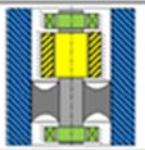		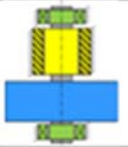	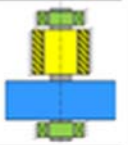
Configuration											

3.3 Chapter summary and research direction

Energy storage systems are key elements in improving efficiency by balancing electrical energy supply and demand. Today's energy paradigm requires an energy storage to be responsive with numerous cycles per day. This is due to the penetration of renewable energy sources and the emergence of smart meters into electrical networks which significantly affect the power quality and stability of the system. Flywheels with their associated attributes can provide energy storage services at the grid level as well as at the customer level. As was discussed earlier in the chapter, flywheel systems are generally used for high power applications providing power quality and ride through services. Majority of the manufacturers are providing a short-term response with the high power density and these are capable of responding within milliseconds and with durations of seconds to minutes. Rotors for these flywheels are either carbon composite or solid steel. In these applications, Li-Ion batteries are less suitable due to their ratio of power to the storage, the C rating, being closer to one and with high power applications demanding high numbers of cycles, life can be an issue. Therefore, flywheels are not commonly considered for ground power applications providing storage longer than 10's minutes. There has been a growing need for storing energy in residential premises that is attractive for providing arbitrage type storage for buildings with solar panels. Most of these are connected to a stable grid and the incentive for the consumer is to have storage behind the meter which reduces energy bills. Nevertheless, the need for the storage becomes more important in cases of intermittent grid or islanded solar PV systems in remote areas.

There is a need for research in this area as energy storage system of choice for residential PV systems is more typically an electrochemical battery, whereas flywheels have not been widely tested nor considered for this application. Of course the batteries are mass produced and are more cost effective compared to flywheels, but flywheels will still be a viable choice when it comes to numerous cycles per day. On the downside, batteries are temperature sensitive and take up more space than a flywheel for the same rated power to energy ratio. In addition, there is a growing

environmental concern when disposing of spent chemical batteries, particularly more difficult in less developed countries.

There are several advantages of FESS over chemical storage systems, but a flywheel is likely to incur a higher initial capital cost, although with high longevity, lifetime costs will be lower. As a means of reducing flywheel costs, what is being proposed here is FESS based on laminated steel with a view to overcoming the drawback of the aforementioned high initial costs of a high speed composite based system.

There are many publications addressing the mechanical aspects, such as the bearing systems and rotor dynamics of the flywheels. To name a few, rotor design and analysis of composite rotor FESS are discussed in [109]. Authors in [110] present modelling and simulation of the rotor of a composite flywheel at different speeds. Dynamic analysis and control of an active magnetic bearing FESS are studied in [111], and its vibration control for high speed applications is discussed in [112]. A model of a FESS with integrated bearing system is proposed in [67], a thorough analysis, design, and control of a novel flywheel assisted by hybrid mechanical–magnetic bearings is presented in [68], and a new concept of reducing overall cost by using combined superconducting and permanent magnet bearings in flywheel storage systems is discussed and analysed in [113].

A research area not widely explored is the modelling and simulation of the electrical characteristics of the systems of flywheels when used for ground power applications. Particularly, for small scale customer level where flywheels can support residential PV systems, limited research has been conducted and there are no commercially available flywheel storage systems for these applications. Filling this gap in the literature is necessary but remains a challenging task since the availability of practical data for FESS suitable for energy storage applications is very limited.

The operation of a flywheel system for ground power applications requires a large inertia system and, as a result, the speed acceleration will be lower. Control of the associated MG for such applications is different from that of a speed motor driving a

load such as a compressor where speed is requested and power is drawn to meet the load. It is vital to avoid speed fluctuations during zero speed start or at the time of transitioning the flywheel system between charging and discharging modes. Despite many publications in the area of controlling motors for flywheel applications, this issue is not widely discussed in the literature. Most are intended for high power short-term response applications focusing on high-speed low-inertia flywheel systems.

The application and control of a permanent magnet synchronous motor (PMSM) in FESS are addressed in a number of recent publications. The research on the performance of a high-speed PMSM operated FESS based on the torque and back-*emf* of the synchronous machine is presented in [114]. Authors in [115] analyse the rotor loss of a PMSM in a short-term high power FESS for UPS applications. References [50] and [88] discuss the modelling and control of PM synchronous machines in high power flywheel applications for use in UPS and voltage sag control, respectively. The control of PMSM drive applied to FESS is described in [116] and [117]; however, the latter is generally addressing the simulation aspect whereas the former is focused mostly on the space-vector modulation technique and current control of the machine. The design aspects of a high-speed PMSM for flywheel applications is discussed in [118] with more emphasis on the rotor and stator design part including the material selection, armature reaction and demagnetisation, influence of magnet configuration, etc. To the authors best of knowledge, there are very few publications addressing the operation of electrical machines for flywheel storage systems providing energy storage services at the small scale residential level.

This study therefore presents a simulation and analysis of a permanent magnet synchronous motor (PMSM) operated flywheel system using MATLAB/Simulink. A detailed model of a higher inertia FESS suitable for ground power applications at the residential level is discussed and its dynamic performance under different charge-discharge scenarios is analysed. The model is combined with a hybrid solar PV and backup diesel generator system for improving fuel consumption and reducing the frequent start/shut-down cycles of the diesel engine as well as the carbon emissions.

Chapter 4 Flywheel Loss Calculations

The main sources of loss in a flywheel part of the flywheel energy storage system are aerodynamic and bearing friction losses. There are other significant losses in the motor-generator and power conversion electronics but these are dealt with in Chapter 5. Although the aerodynamic and bearing friction losses are typically small in a well-designed flywheel, the energy losses can become significant since the flywheel normally operates continuously when integrated over time. It is the purpose of this chapter to assess the losses using the latest available information and allow a loss model to be developed for the simulation for a given set of design choices. Determination of drag coefficients based on various flow regimes using two different calculation methods is discussed in section 4.1. Detailed bearing loss calculations using the methods practiced by the bearing manufacturers are provided in section 4.2. The overall efficiency and system standby losses due to bearing and drag losses are then calculated in section 4.3 and the chapter is concluded in section 4.4.

4.1 Aerodynamic or windage drag loss

The aerodynamic loss, normally called the windage loss, is due to the friction drag between the rotating flywheel rotor and surrounding air, whereas the bearing loss is generally dependent on the rotor weight and type of lubrication used. The windage loss at atmospheric pressure conditions will usually be unacceptably high in terms of waste of energy as is demonstrated later in a calculation. High windage losses may also result in overheating of the flywheel rotor and must be controlled by enclosing the flywheel in a containment to create a vacuum environment. The losses reduce with a higher vacuum (i.e. lower absolute pressure), but not proportionally. It is possible to eliminate them entirely if the vacuum is very high but this is often not practical for reasons explained. The higher the level of vacuum, the harder it is to maintain due to leaks and outgassing from internal materials. There will always be some level of leakage and the higher the vacuum, the more gas will pass through the leak due to the increased pressure ratio. Also, once the leakage gas passes into the casing, the same mass of gas will increase the vacuum pressure more in the case of a high vacuum than

a lower vacuum. Most solid materials and liquids such as lubricating oil will liberate gas when subject to vacuum and this is called outgassing. The higher the vacuum, the greater the gas released by this mechanism. Lubricating oil that might be needed for the bearing system could even boil if the vacuum is too high. A final issue with the level of vacuum, very much related to leaks and outgassing, is the maintenance of the vacuum using a pump. If the vacuum level is not too high and given the electrical connection allows the casing to be hermetically sealed, a low cost solution will be to pump the casing down intermittently. This eliminates the power loss of running a vacuum pump continuously and the wear on the pump. If sealing is very effective, it might be that the pump can be taken away and vacuuming down done as a maintenance item carried out every few years. Again, the lower the level of vacuum needed, the more likely this cost reducing strategy could be adopted.

The windage loss in a flywheel occurs due to friction between the rotor and surrounding gas or air, depending on the type of enclosure. It is proportional to the cube of speed and would become intolerable in terms of waste energy and overheating if the level of pressure is not controlled [119]. A casing is hence necessary to provide low pressure vacuum environment and reduce windage losses. However, as the pressure is reduced far below atmospheric pressure to what is called the rarefied condition, the flow regime changes and calculation of windage drag losses must be done in another way. The fluid behaviour must be analysed by kinetic theory as it cannot be predicted by physics of continuum fluid mechanics given the gas particles are too far apart from each other.

4.1.1 Flow types based on pressure

The flow types in terms of the degree of rarefaction can be generally classified as continuum flow, slip flow, transition flow, Couette flow and free molecular flow. The transition between each state can be determined based on dimensionless Knudsen (K_n) number. Couette flow occurs for the special case when the gap between the casing and flywheel rotor becomes small and friction loss increases greatly due to boundary layer effects. The transition between continuum and molecular flow is determined by

Knudsen number which is defined as the ratio between the mean free path of a molecule (λ) and the dimension of the object under consideration (d), the latter being the gap between the rotor and the casing [120]. The Knudsen number can also be defined in relation to dimensionless parameters Mach number (M_a) and Reynolds number (R_e) by

$$K_n = \frac{\lambda}{d} = \left(\frac{\pi\kappa}{2}\right)^{\frac{1}{2}} \frac{M_a}{R_e} \tag{4.1}$$

In Equation 4.1, the Mach number and Reynolds number can be defined by the relations:

$$M_a = \frac{V}{(\kappa RT)^{\frac{1}{2}}} \tag{4.2}$$

$$R_e = \frac{\rho d V}{\mu} \tag{4.3}$$

where

ρ: air density

κ: ratio of specific heats

R: universal gas constant

T: temperature

V: velocity

d: flywheel rotor to containment gap

μ: viscosity

As the pressure inside the flywheel containment is reduced, the molecules are sufficiently spaced apart and the flow regime turns into rarefied free molecular flow. The mean free path of molecules become much larger than the length of the flow and the motion of the molecules can be regarded as a Maxwellian distribution since the molecular collisions between the surfaces are completely neglected [120]. In free molecular flow, the continuum approximations using fluid mechanics are invalid as the viscosity varies based on pressure and temperature; hence, the fluid behaviour

needs to be determined by kinetic theory [121]. Solutions for such operational regimes are determined based upon statistical methods or analytical solutions.

The theoretical analysis of the flow of gases is generally characterised by the Boltzmann equation where solutions to the limiting cases of continuum flow ($K_n = 0$) and free molecular flow ($K_n \to \infty$) can be derived. However, for more practical cases and better analysis of the flow of gases, the transition between these two cases will be of great importance and requires an approximate solution for a range of Knudsen numbers. Since the early work of Millikan [122], several authors have developed approximate solutions of Boltzmann equation valid for an entire range of K_n including strong rarefaction case ($K_n \to \infty$) [123, 124]. In this research, the work of Beck [123] and Alofs and Springer [125] are analysed and the results are compared at a different speed and pressure levels.

4.1.2 Determination of the drag coefficient

Beck derived an equation for shear stress between two infinitely extended plates x and y under rarefied condition separated by a distance d and moving with constant relative velocity V:

$$\tau_{xy} = \frac{1}{2}\zeta\left[\mathrm{mn}V\left(\frac{RT}{2\pi}\right)^{\frac{1}{2}}\right] \tag{4.4}$$

The value of ζ in Equation (4.4) is dependent on the Knudsen number and is valid for the case where the temperature difference between two plates is quite negligible ($\frac{T_x}{T_y} = 1$).

$$\zeta = \frac{4K_n}{1 + 2K_n} \tag{4.5}$$

where

τ_{xy}: shear stress between two surfaces x and y

m: molecular mass

n: number density

The force exerted on an object moving through a fluid with relatively large velocities is given by:

$$F_D = \frac{1}{2}\mathrm{m}\, C_D V^2 \tag{4.6}$$

Where the drag coefficient C_D is a dimensionless quantity that is a function of speed, roughness and geometry of the object. Using Equation (4.6), the drag coefficient as a function of shear stress for cylindrical surfaces can be represented by:

$$C_D = \frac{2\tau_{xy}}{\rho V^2} \tag{4.7}$$

Substituting Equations (4.4) and (4.5) in Equation (4.7) and simplifying gives:

$$C_D = \frac{4K_n}{1+2K_n}\left(\frac{1}{M_a(2\pi\kappa)^{\frac{1}{2}}}\right) \tag{4.8}$$

Using the derived expression (4.8) for C_D and substituting Equation (4.1) in Equation (4.7), the shear stress as a function of Mach number and Reynolds number is given by:

$$\tau_{xy} = \rho V^2\left(\frac{1}{M_a(2\pi\kappa)^{\frac{1}{2}} + R_e}\right) \tag{4.9}$$

Finally, using Beck's equation for shear stress, the power loss due to windage of a rotating cylindrical flywheel of radius (r) and length (h) can be calculated by:

$$P_w = \tau_{xy} A r \omega \tag{4.10}$$

$$P_w = \left(\frac{2\pi\rho h r^4}{M_a(2\pi\kappa)^{\frac{1}{2}} + R_e}\right)\omega^3 \tag{4.11}$$

Equation (4.11) is valid for the entire range of Knudsen numbers and hence can be used to calculate the drag loss of vacuum operated flywheel under rarefied gas

environment. It gives reasonable agreement with results obtained by Lees and Liu [126]. If the temperature difference between the flywheel and the casing is neglected, it gives good agreement to experimental results of Kuhlthau [127].

Alofs and Springer [125] have also derived an expression for shear stress to determine drag in cylindrical coquette flow of rarefied gases. They combined equations developed by Kennard [128] and Bower and Talbot [129] for free molecular plane coquette flows in order to include the tangential momentum accommodation coefficient in calculating the shear stress. The expression developed by Alofs [125] is given by:

$$\tau_{xy} = \frac{1}{2}\,\rho V \left(\frac{2RT}{\pi}\right)^{\frac{1}{2}} \left(\frac{a}{b}\right)^{2} \left[\frac{\sigma}{2-\sigma}\right] \tag{4.12}$$

where

a: inner radius of cylinder

b: outer radius of cylinder

σ: tangential momentum accommodation coefficient

The expression for power loss due to windage can be derived by substituting Equation (4.2) and Alofs' shear stress expression (4.12) in Equation (4.10):

$$P_w = \left(\frac{2\pi\rho h a^6}{M_a (2\pi\kappa b^4)^{\frac{1}{2}}}\right)\left[\frac{\sigma}{2-\sigma}\right]\omega^3 \tag{4.13}$$

The experimental findings of Alofs show that Equation (4.13) is valid for a wide range of Knudsen numbers. However, for the case of low gas densities in free molecular flow where $K_n > 7$, an average value of $\sigma = 0.972$ is proved to be valid.

4.1.3 Aerodynamic drag loss calculations at atmospheric pressure

The windage losses are due to the friction between the rotating flywheel rotor and surrounding gas or air, depending on the type of enclosure. These losses are proportional to the cube of speed and can become significant at atmospheric pressure

levels, which will be unacceptable in terms of waste of energy. Calculation of the windage loss at atmospheric pressures is presented here for an indication of the scale how these losses are increasing with speed. The power loss equation for resisting drag torque of a rotating cylinder is given by [119]:

$$P_{W1} = \frac{1}{32} k h C_D \pi \rho \omega^3 {D_r}^4 \tag{4.14}$$

The torque coefficient C_D is typically determined by measurement and depends on the Couette Reynolds number:

$$R_{ed} = \frac{\rho D_r d \omega}{2\mu} \tag{4.15}$$

$$C_D = \begin{cases} 10 \dfrac{\left(2d/D_r\right)^{0.3}}{{R_{ed}}^1} & R_{ed} < 64 \quad (4.16) \\ 2 \dfrac{\left(2d/D_r\right)^{0.3}}{{R_{ed}}^{0.6}} & 64 < R_{ed} < 5 \times 10^2 \quad (4.17) \\ 1.03 \dfrac{\left(2d/D_r\right)^{0.3}}{{R_{ed}}^{0.5}} & 5 \times 10^2 < R_{ed} < 10^4 \quad (4.18) \\ 0.065 \dfrac{\left(2d/D_r\right)^{0.3}}{{R_{ed}}^{0.2}} & 10^4 < R_{ed} \quad (4.19) \end{cases}$$

where

k: roughness coefficient (k=1 for smooth surfaces, typically k=1-1.4)

D_r: rotor outer diameter

d: air gap between the rotor and container

R_{ed}: Couette Reynolds number

ρ: air density

μ: viscosity

Similarly, the power loss due to the windage friction losses at the rotor end surfaces can be calculated using [130]:

$$P_{W2} = \frac{1}{64} C_D \rho \omega^3 \left({D_r}^5 - {D_s}^5\right) \tag{4.20}$$

where D_s is the shaft diameter and C_D is now a function of the tip Reynolds number given by

$$R_{er} = \frac{\rho \omega {D_r}^2}{4\mu} \tag{4.21}$$

$$C_D = \begin{cases} \dfrac{3.87}{{R_{er}}^{\frac{1}{2}}} & R_{er} < 3 \times 10^5 \quad (4.22) \\ \dfrac{0.146}{{R_{er}}^{\frac{1}{5}}} & R_{er} > 3 \times 10^5 \quad (4.23) \end{cases}$$

The windage losses due to the rotating parts of the flywheel considering the atmospheric pressures is calculated by adding the power loss Equations (4.14) and (4.20). The specification of the flywheel system and air density values at 20°C and atmospheric pressure conditions are given in *Table 4-1*.

***Table 4-1**. Flywheel specifications and air properties*

Property	Unit	Value
Mass (m)	kg	524
Rotor outer diameter (a)	mm	410
Rotor axial length (h)	mm	500
Rotor air gap (d)	mm	1-5
Rotor shaft diameter (D_s)	mm	25
Max peripheral velocity (v)	m/s	430
Gas constant for air (R)	J K^{-1}/kg	287
Viscosity coefficient (μ)	kg m^{-1}/s	1. 8 × 10^{-5}
Specific heat ratio (κ)	-	1.4
Couette Reynolds number (R_{ed})[1]	-	26900
Tip Reynolds number (R_{er}) [1]	-	5514451

[1] Rotor air gap = 1 mm, Temperature = 40°C

Determining the Reynolds number for each case identifies Equation (4.19) for calculation of P_{W1} and Equation (4.23) for calculation of P_{W2}, respectively. Therefore, the total power loss at different rotor air gaps and atmospheric pressure are calculated and presented in *Table 4-2*.

Since the windage losses at atmospheric pressure increase with the cube of speed, it can be seen that the power loss level can be extremely high even at medium speeds (15-20 krpm). Increasing the radial gap between the flywheel rotor and containment can also increase the losses. For example, if the speed is kept constant at

20,000 rpm and the air-gap is changed from 1mm to 5mm, the increase in the windage losses will be approximately 560 W. For higher speeds, even a small radial gap of 1mm will incur significant windage losses.

***Table 4-2**. Windage losses (W) at varying radial gaps and atmospheric pressure conditions*

Speed (rpm)	Rotor air-gap				
	1 mm	2 mm	3 mm	4 mm	5 mm
1,000	4.68×10^{-1}	4.97×10^{-1}	5.14×10^{-1}	5.24×10^{-1}	5.38×10^{-1}
5,000	$5.85\times10^{+1}$	$6.21\times10^{+1}$	$6.43\times10^{+1}$	$6.59\times10^{+1}$	$6.72\times10^{+1}$
10,000	$4.68\times10^{+2}$	$4.97\times10^{+2}$	$5.14\times10^{+2}$	$5.28\times10^{+2}$	$5.38\times10^{+2}$
15,000	$1.58\times10^{+3}$	$1.68\times10^{+3}$	$1.74\times10^{+3}$	$1.78\times10^{+3}$	$1.82\times10^{+3}$
20,000	$3.74\times10^{+3}$	$3.97\times10^{+3}$	$4.12\times10^{+3}$	$4.22\times10^{+3}$	$4.30\times10^{+3}$
25,000	$7.31\times10^{+3}$	$7.76\times10^{+3}$	$8.04\times10^{+3}$	$8.24\times10^{+3}$	$8.41\times10^{+3}$
30,000	$1.26\times10^{+4}$	$1.34\times10^{+4}$	$1.39\times10^{+4}$	$1.42\times10^{+4}$	$1.45\times10^{+4}$

Considering the significant level of windage losses in atmospheric pressure conditions, the operation of the flywheel in vacuum conditions becomes vital and, as a result, the calculation methods used for atmospheric conditions are not valid for rarefied vacuum conditions. Therefore, the standby windage loss of the system at different speeds and pressure levels is estimated with the help of Equations 4.1- 4.3 and expressions derived by Beck (4.11) and Alofs (4.13).

***Table 4-3**. Windage losses (W) - Alofs' method*

Speed (rpm)	Pressure (Pa)					
	0.001	0.01	0.1	1	10	100
1,000	3.82×10^{-4}	3.82×10^{-3}	3.82×10^{-3}	3.82×10^{-1}	3.82	$3.82\times10^{+1}$
5,000	9.55×10^{-3}	9.55×10^{-2}	9.55×10^{-1}	9.55	$9.55\times10^{+1}$	$9.55\times10^{+2}$
10,000	3.82×10^{-2}	3.82×10^{-1}	3.82	$3.82\times10^{+1}$	$3.82\times10^{+2}$	$3.82\times10^{+3}$
15,000	8.60×10^{-2}	8.60×10^{-1}	8.60	$8.60\times10^{+1}$	$8.60\times10^{+2}$	$8.60\times10^{+3}$
20,000	1.53×10^{-1}	1.53	$1.53\times10^{+1}$	$1.53\times10^{+2}$	$1.53\times10^{+3}$	$1.53\times10^{+4}$
25,000	2.39×10^{-1}	2.39	$2.39\times10^{+1}$	$2.39\times10^{+2}$	$2.39\times10^{+3}$	$2.39\times10^{+4}$
30,000	3.44×10^{-1}	3.44	$3.44\times10^{+1}$	$3.44\times10^{+2}$	$3.44\times10^{+3}$	$3.44\times10^{+4}$

***Table 4-4**. Windage losses (W) - Beck's method*

Speed (rpm)	Pressure (Pa)					
	0.001	0.01	0.1	1	10	100
1,000	4.08×10^{-4}	4.08×10^{-3}	4.05×10^{-2}	3.79×10^{-1}	2.31	4.72
5,000	1.02×10^{-2}	1.02×10^{-1}	1.01	9.48	$5.78\times10^{+1}$	$1.18\times10^{+2}$
10,000	4.08×10^{-2}	4.08×10^{-1}	4.05	$3.79\times10^{+1}$	$2.31\times10^{+2}$	$4.72\times10^{+2}$
15,000	9.18×10^{-2}	9.18×10^{-1}	9.11	$8.53\times10^{+1}$	$5.21\times10^{+2}$	$1.06\times10^{+3}$
20,000	1.63×10^{-1}	1.63	$1.62\times10^{+1}$	$1.52\times10^{+2}$	$9.25\times10^{+2}$	$1.89\times10^{+3}$
25,000	2.55×10^{-1}	2.55	$2.53\times10^{+1}$	$2.37\times10^{+2}$	$1.45\times10^{+3}$	$2.95\times10^{+3}$
30,000	3.67×10^{-1}	3.67	$3.65\times10^{+1}$	$3.41\times10^{+2}$	$2.08\times10^{+3}$	$4.25\times10^{+3}$

Results of windage loss calculations for a constant air gap of 1 mm and pressure levels of 0.001 Pa, 0.01 Pa, 0.1 Pa, 1 Pa, 10 Pa and 100 Pa, are presented in *Table 4-3* for Alof's method and *Table 4-4* for Beck's method. Each pressure level is tested for different speeds ranging between 1,000–30, 0000 rpm. Although the considered flywheel system has an operating speed range of 10,000–20, 0000 rpm and pressures of 10 Pa and 100 Pa will not be reached due to vacuum operation, calculations beyond these limits are performed for a better comparison of the methods derived by Beck and Alofs. The agreement of the two methods at a different speed and pressure levels is also tested and compared.

Comparing the two methods for pressure levels below 1 Pa ($0.001 < Pa < 1$), loss values slightly deviate but are still valid with small percentage error that can be neglected. Both methods give quite a close correlation at 1 Pa. However, for pressures greater than 1 Pa ($1 < Pa < 100$), windage losses of the two methods do not match and deviate quite far away as the pressure level increases. *Table 4-3* shows that Alofs expression is valid for an entire range of Knudsen numbers and its validity is not affected by the changes in pressure level. On the other hand, Beck's drag loss equation is valid for strong rarefied conditions and large Knudsen numbers. As the pressure increases, the Knudsen number is reduced and Beck's expression gives an error for pressures above 1 Pa.

The correspondence of Beck's and Alofs' calculation methods is also examined by calculating windage losses at different air gaps ranging between 1–5 mm as shown in *Figure 4.1* . The speed range is further extended to 40,000 rpm since the air gap effect on windage loss is more evident at larger speeds.

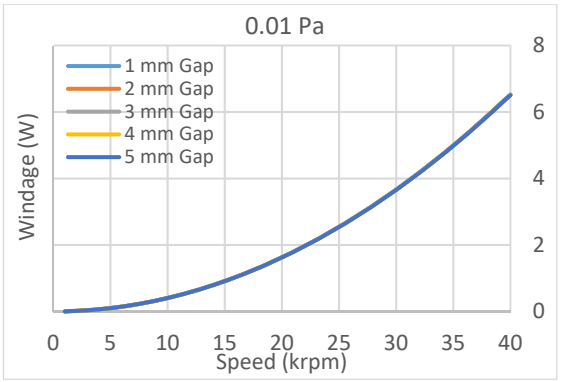

(a) Beck

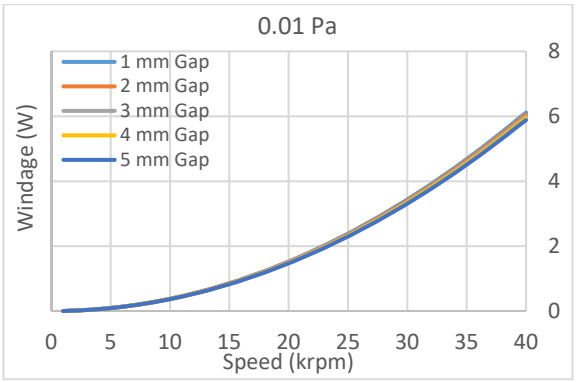

(b) Alofs

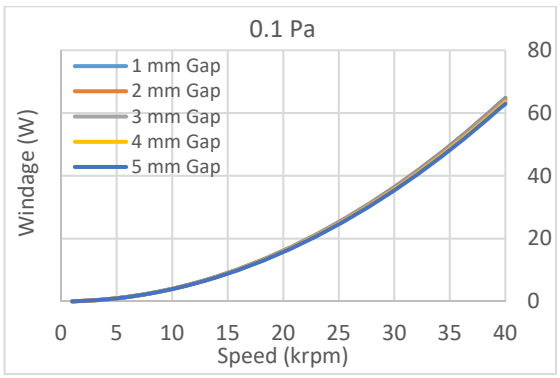

(c) Beck

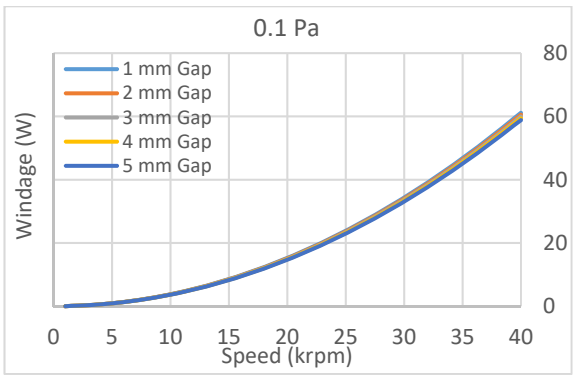

(d) Alofs

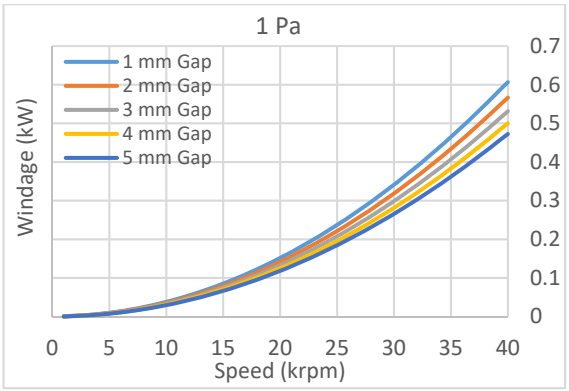

(e) Beck

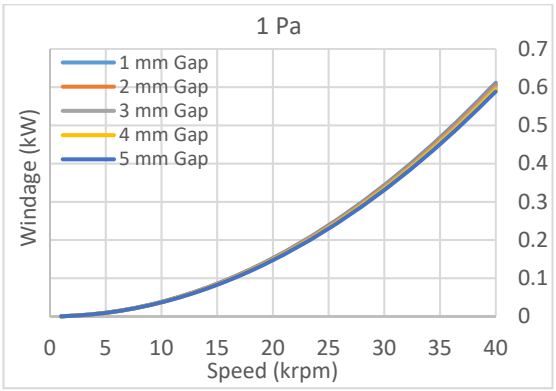

(f) Alofs

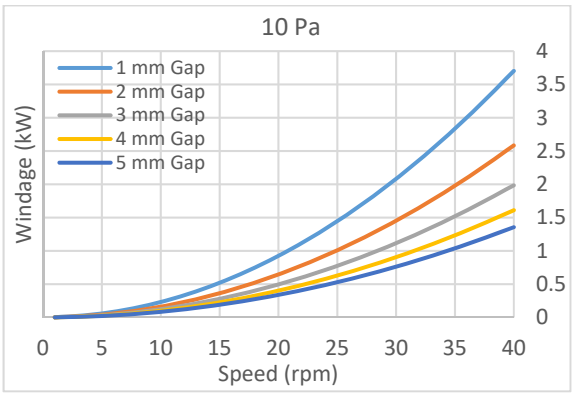

(g) Beck

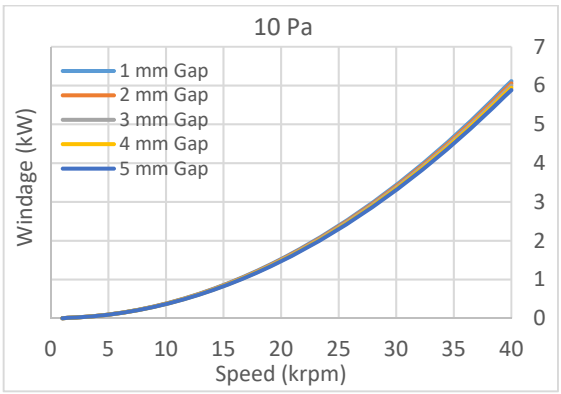

(h) Alofs

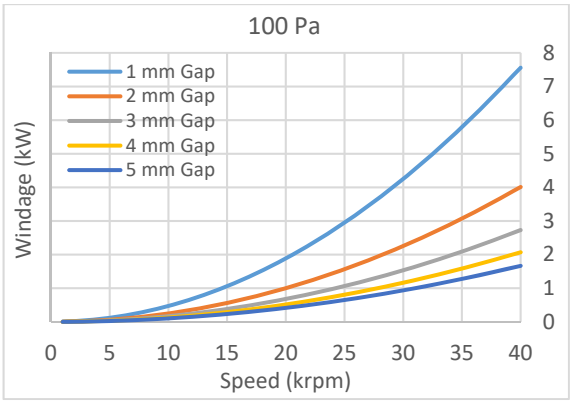

(i) Beck

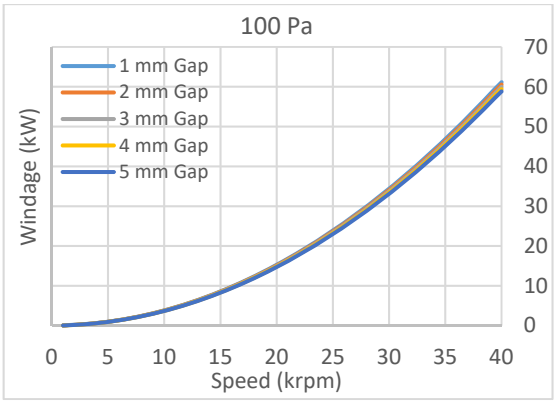

(j) Alofs

***Figure* 4.1.** *Aerodynamic drag loss at different air gaps and pressures using Beck's and Alofs method*

The estimation of losses at lower pressures show that air gap variations do not affect the windage loss and both methods give satisfactory results matching each other (*Figure 4.1a-d*). Beck's windage losses at 0.01 Pa are the same for all air gap values where Alofs' results slightly decrease as the air gap increases. Both methods correspond to each other and are quite close when the pressure is increased to 0.1 Pa. Similarly, when the pressure reaches 1 Pa, Alofs' method is not affected by air gap variations whereas Beck's windage losses decrease as the air gap increases. The discrepancy between the two methods is propagated when the pressure level is further increased to 10 Pa and 100 Pa as shown in (Figure *4.1g-j*). Therefore, both calculation methods give accurate results at lower pressures and are not affected by the air gap differences. As the pressure increases beyond 1 Pa, Beck's windage losses change significantly since it is dependent on the air gap.

The results obtained confirm that Beck's method is valid for rarefied gas conditions with low-pressure level and will introduce errors as the pressure increases. In addition, at large pressures, any small increase in the air gap will contribute to rarefication of the medium and hence the windage loss will be reduced. This condition can be seen that a change of air gap from 1 mm to 5 mm at 100 Pa and 20,000 rpm will reduce the windage loss to approximately 1.5 kW (*Figure 4.1i*). Furthermore, the loss reduction is significantly changed to 6 kW when the speed is increased to 40,000 rpm.

In contrast, Alofs' windage losses stay quite consistent for all pressure levels and are not affected by the air gap alterations.

Finally, the windage loss for continuum and molecular flow regimes as a function of the flywheel pressure level is shown in Figure *4.2*. The losses in the molecular region are calculated based on rarefied gas conditions using the approximation methods developed by Beck and Alofs, whereas for the case of continuum regimes, the calculation methods for atmospheric conditions are used. For each flow regime, it is shown that the level of losses for the two conditions of 1mm and 5 mm radial gap is quite close and not significantly affected by changing the pressure level. Although the flywheel system will be operating in molecular regime due to vacuum conditions and well below the 10 Pa pressure level, to the author's best knowledge, there is no theory or test available to show the windage losses in the transition region between continuum and molecular flow regimes.

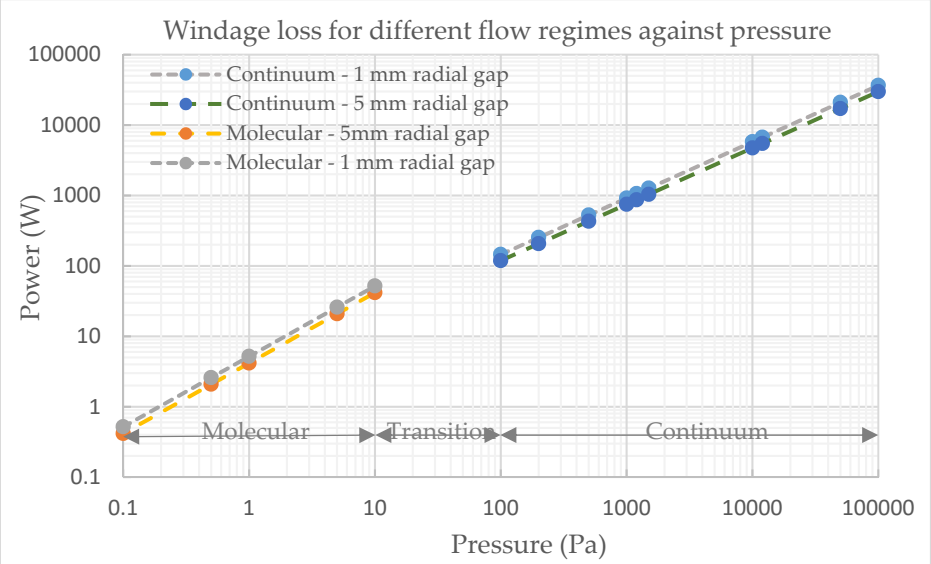

***Figure 4.2**. Windage loss against pressure for continuum and molecular flow regimes*

4.2 Bearing loss calculations

The overall losses in ball bearings can be estimated by considering the slip and shear stress at interacting surfaces within the bearing. However, predicting the torque and power loss of bearing through analytical models is complex and still limited in accuracy in some applications. This is due to the level of difficulty associated with

satisfactorily quantifying the relationship between the state of lubricant within the bearing cavity and the applied lubricant conditions. Practical experience shows that increase in the amount of lubricant will generally increase the bearing friction, and hence, the torque. Although some percentage of it can be accounted for by some of the lubricant filling the bearing cavity, control of the amount of lubricant in the cavity to the amount of lubricant supply still is complex and needs to be determined empirically [131]. Therefore, an empirical approach developed by Palmgren [132] favoured in industry and by bearing manufacturers, such as SKF and NSK, is usually considered for estimating bearing torque and power loss. He determined the empirical factors for all types of rolling bearings and developed equations for the frictional torque.

According to Palmgren, the torque of a rolling bearing (T_B) consists of two components: one speed dependent (T_v) and the other load dependent (T_L) [131, 132].

$$T_B = T_L + T_v \tag{4.24}$$

The load term T_L is determined by bearing type and load:

$$T_L = f_L F_b D_p \tag{4.25}$$

where

F_b: load applied on the bearing (N)

D_p: pitch circle diameter of the rolling element (inches)

f_L : a factor dependent on bearing design and relative load that can be obtained by

$$f_L = z({}^{F_s}/_{C_s})^y \tag{4.26}$$

where

F_s: static equivalent load (N)

C_s: static load rating (N) (*Table 4-5*)

y, z: load torque factors determined experimentally (*Table 4-6*)

The static equivalent load is a theoretical load that is assumed to produce a contact stress equivalent to the maximum stress when the bearing is operating under actual practical conditions. It is calculated using Equation (4.27) and the greater of the two values should be accounted for the static equivalent load on radial bearings.

$$F_s = max((X_s F_r + Y_s F_a)\ ,\ \ F_r\ ) \tag{4.27}$$

where

F_r: radial load (N)

F_a: axial load (N)

X_s: static radial load factor (*Table 4-6*)

Y_s: static axial load factor (*Table 4-6*)

***Table 4-5**. Values of permissible static load factor fs [131]*

Operating Conditions	Lower Limit of $f_s = C_s/F_s$	
	Ball Bearings	Roller Bearings
Low-noise applications	2.0	3.0
Bearings subjected to vibration and shock loads	1.5	2.0
Standard operating conditions	1.0	1.5

***Table 4-6**. Values of load factor, torque factor and lubrication factor [131] [133]*

	Equivalent Load Factors		Load Torque Factors		Lubrication Factor, f_0		
Bearing type	*Xs*	*Ys*	*z*	y	Oil mist/injection	Oil bath /grease	Oil bath/jet
Single row radial	0.6	0.5	0.0007	0.55	0.7 - 1.0	1.5 – 2.0	3.0 – 4.0
Angular contact, (α = 15°)	0.5	0.47	0.001	0.33	1.0	3.0	6.0
α = 20°	0.5	0.42	0.001	0.33	1.0	3.0	6.0
α = 25°	0.5	0.38	0.001	0.33	1.0	3.0	6.0
α = 30°	0.5	0.33	0.001	0.33	1.0	3.0	6.0
α = 35°	0.5	0.29	0.001	0.33	1.0	3.0	6.0
α = 40°	0.5	0.26	0.001	0.33	1.0	3.0	6.0
Angular contact double row	-	-	-	-	2.0	6.0	9.0

The load factor in Equation (4.25) is calculated based on the magnitude and direction of the applied load given by:

$$F_b = max((0.9\ F_a\ ctn\ (a) - 0.1\ F_r)\ ,\ \ F_r\ ) \tag{4.28}$$

Finally, the speed-dependent component of the bearing torque is the combined effect of the speed and viscous shearing of the type of lubricant used for the bearing:

$$T_v = \begin{cases} 1.42 \times 10^{-5}\, f_0\, (v_0 n)^{\frac{2}{3}}\, {D_p}^3, & v_0 n > 2000 \\ 2.30 \times 10^{-3}\, f_0\, {D_p}^3 \quad , & v_0 n \leq 2000 \end{cases} \tag{4.29}$$

where

n: bearing speed (rpm)

v_0: kinematic oil viscosity (centistokes)

f_0: factor dependent on bearing type and mode of lubrication (*Table 4-6*)

4.2.1 Bearing sizing and selection

Selection of bearing for use in flywheel applications is dependent on a combination of parameters including bearing static and dynamic load, operational speed and an acceptable level of maintenance. In addition to supporting the flywheel weight and dynamic forces during the operating range of 10-20 krpm, the selected bearing is required to have a satisfactory life with low maintenance and an acceptable level of losses. Suitable bearing types for high-speed applications are hydrodynamic bearings, air foil bearings, different types of magnetic bearings and rolling element bearings [134]. Hydrodynamic bearings are suitable for high-speed applications under vibrating conditions and air foil bearings can operate at high speed under high temperature levels as they do not require lubrication and the bearing surfaces are kept apart by pressurised air. However, the former needs special treatment of oil lubrication system and the latter requires pressurised air which makes them unsuitable for flywheels due to their requirements and a higher level of costs. Since the flywheel is operating in vacuum and leakage and friction loss due to shaft seals need to be avoided, magnetic bearing and rolling element types are the only choices available. However, magnetic bearings and particularly active magnetic type are expensive and complex and cannot withstand larger acceleration and gyroscopic forces. They also need rolling bearings as back up in case of power failure. With these

considerations and based on manufacturers recommendations, the flywheel rotor is balanced by a combination of passive magnetic bearing and radial ball bearings. The majority of the weight is vertically levitated by the passive magnetic bearing which theoretically has no losses and two relatively small diameter ball bearings are used to radially stabilise the spinning rotor. In order to keep the spinning rotor around its axis, soft springs can be mounted on ball bearings to accommodate for any small out of balance. Angular contact ball bearings are generally a good choice and give excellent life if the bearing is maintained well and the temperature is not allowed to exceed the limits of the lubricant. Calculation of the bearing life and lubrication selection are discussed in upcoming subsections.

4.2.2 Bearing lubrication selection

The type of lubrication in rolling elements determine the operating temperature as well as the speed limit and bearing losses. Oil lubrication allows the highest speed operation due to having lower friction and better cooling characteristics. The downside is that it may require more frequent maintenance and additional equipment for oil pumping. In the case of oil lubrication, the power loss generally increases with the rate of supply of lubricant to the bearing. The running temperature initially increases to a maximum and then decreases due to the cooling effect of the oil lubricant [131]. As an alternative, high pressure oil feed systems provide good temperature control but their oil supply system is sophisticated and requires a high pressure pump equipped with filter and oil cooler adding to the overall cost of the system. Grease is another option and serves best in terms of maintenance requirements and life expectancy. However, it doesn't have the same cooling effect as oil lubrication method and the speed limit will be lower compared to oil lubrication. Fortunately, the speed of the steel rotor is not particularly high so bearings can operate using grease lubrication without difficulty. In terms of loss estimate, however, in addition to lubricant viscosity, the quantity and mode of supply also affect the temperature range and power loss in bearings. Finally, the pressure level for vacuum

operation is also important and care must be taken that the vapour pressure level of the selected lubricant meets the condition for high or medium vacuum levels. Hence a nominal lubrication method preferred in the majority of the bearing systems is either oil mist or grease lubrication method [131].

The type of lubricant for the two radial bearings supporting the flywheel is selected by considering the above requirements. The lower bearing will have the highest load and act as a register bearing by taking the net axial load. Therefore, it is oil-lubricated by creating an oil mist so its temperature is kept at the lowest. On the other hand, the top ball bearing will be grease lubricated because getting an oil mist to this bearing is difficult and will possibly develop an oil mist around the rotor which will contribute to windage losses. The selection of grease lubricant can be justified since this bearing is lightly preloaded by the attached springs and will not experience significant load variations. Hence heat generation and temperature control will not be an issue.

4.2.3 Bearing life

Bearing life as defined by the bearing manufacturers is the duration that it can safely endure load under rotating conditions. The rolling surfaces experience a high number of cyclic stresses that can lead to cracks under or at the surface. Surface cracks will cause material breaks on the surface of the rolling elements and would leave a pit. Signs of fatigue pit are usually in the form of noise or vibration and this indication is considered to be the end of bearing life. However, this failure mode is still safe and the bearing can operate for sufficient time before remedial action is taken [131]. For flywheel applications where maintenance requirements are favoured to be at a minimum and bearing breakdown could lead to a catastrophic failure, fatigue life calculation becomes an important step in bearing selection and design process.

4.2.3.1 Basic rating life

There are many factors that can affect the operational life of bearing systems. These include errors in bearing design and selection, improper mounting and

inadequate maintenance. Aside from these factors, a simple calculation of the bearing fatigue life can be estimated based on basic rating life. It is defined as the total number of operating hours completed by a number of selected bearings (operating individually and under the same conditions) when 10% of them fail to function due to flaking [133]. The following relation calculates basic rating life for ball bearings as a function of bearing load:

$$L_{10} = (C/P)^p \tag{4.30}$$

$$L_{10h} = \frac{10^6}{60n} L_{10} \tag{4.31}$$

where

L_{10}: basic rating life (at 90% reliability), millions of revolutions

L_{10h}: basic rating life (at 90% reliability), operating hours

C: basic dynamic load rating (N) is the constant load on the bearing that it can withstand for a rating life of one million revolutions

P: equivalent dynamic load (N)

n: rotational speed (min^{-1})

p: exponent of the life equation (3 for ball bearing, 10/3 for roller bearing)

4.2.3.2 Dynamic equivalent load

The load applied on the bearing, in rare cases, will be purely axial or radial and generally, it will be a combination of both. The resultant load on the bearing will swerve in magnitude and direction that makes it quite difficult to calculate the equivalent load. The dynamic equivalent load is a hypothetical load that is assumed to act at the centre of the bearing and give the same effect as the bearing was experiencing a radial or an axial load only. In the case of radial bearings, this theoretical load is considered as pure radial load and is expressed as a dynamic equivalent radial load. It can be approximated by:

$$P = XF_r + YF_a \tag{4.32}$$

where

P: equivalent radial load (N)

F_r: radial load (N)

F_a: axial load (N)

X: radial load factor (*Table 4-7*)

Y: axial load factor (*Table 4-7*)

***Table 4-7**. Values of load factors X and Y for angular contact bearings [133]*

Nominal Contact Angle	$\frac{F_a}{C_s}$	e	$\frac{F_a}{F_r} \leq e$		$\frac{F_a}{F_r} > e$	
			X	Y	X	Y
15	0.178	0.38	1	0	0.44	1.47
	0.357	0.40				1.40
	0.714	0.43				1.30
	1.070	0.46				1.23
	1.430	0.47				1.19
	2.140	0.50				1.12
	3.570	0.55				1.02
	5.350	0.56				1.00
18	-	0.57	1	0	0.43	1.00
25	-	0.68	1	0	0.41	0.87
30	-	0.80	1	0	0.39	0.76
40	-	1.14	1	0	0.35	0.57
50	-	1.49	-	-	0.73	1
55	-	1.79	-	-	0.81	1
60	-	2.17	-	-	0.92	1

The value of axial load factor (Y) is dependent on the contact angle. As the contact angle of angular contact ball bearings increases with the increase of axial load, this variation is adjusted by the ratio of basic static load rating (C_s) and axial load (F_a). The values of X and Y are determined based on the ratios ($\frac{F_a}{C_s}$) and ($\frac{F_a}{F_r}$) as given in *Table* 4-7.

4.2.3.3 Modified rating life

In Equations 4.30 and 4.31, factors such as lubrication, errors in bearing design and selection, improper mounting, inadequate maintenance and environmental conditions are not considered in calculating the bearing life. Therefore, basic rating

life for modern high quality bearings will be considerably different and it will deviate from the actual service life in a given application. Bearing life calculations considering the above mentioned factors are quite computational and require test data. A simplified approach practiced by many bearing manufacturers is the inclusion of modification and adjustment factors to supplement the basic rating life equations and give an estimation of the fatigue life rating close to practicality. The modified life equations based on the adjustment factors proposed by SKF take the form [135]:

$$L_{nm} = a_1 a_{skf} (C/P)^p \tag{4.33}$$

$$L_{nmh} = \frac{10^6}{60n} L_{nm} \tag{4.34}$$

where

L_{nm}: SKF rating life (at 100 – n% reliability), millions of revolutions

L_{nmh}: SKF rating life (at 100 – n% reliability), operating hours

a_1: life adjustment factor for reliability (*Table 4-8*)

a_{skf}: life modification factor (Fatigue load limit, lubrication and operating conditions)

***Table 4-8**. Values of the life adjustment factor a_1 [135]*

Reliability	**Failure probability**	**SKF rating life**	**Factor**
	n	L_{nm}	a_1
%	%	*Millions revolution*	-
90	10	L_{10m}	1
95	5	L_{5m}	0.64
96	4	L_{4m}	0.55
97	3	L_{3m}	0.47
98	2	L_{2m}	0.37
99	1	L_{1m}	0.25

The factor a_1 is an adjustment factor when calculating the modified life of the bearing. It shows the percentage of the failure when the bearing completes millions of revolutions. The value of a_{skf} is a function of viscosity ratio (κ) for lubrication condition, the level of contamination in the bearing (η_c) and the ratio of the fatigue

load limit to the acting bearing equivalent load ($\frac{P_u}{P}$). These values are obtained from the tables and diagrams by the manufacturers provided in Appendix A.

4.2.4 Bearing friction losses

The load and specifications for the bearings are summarised in *Table 4-9*. The lower bearing will have the highest load by taking the net axial load of approximately 5% of the rotor weight. The top bearing will be supported by the attached springs and a light preload based on bearing manufacturers will be considered for this bearing.

***Table 4-9**. Bearing loads and specifications*

Property (Unit)	**Lower bearing**	**Top bearing**
Axial load F_a (N)[1]	260	80
Radial load F_r (N)	100	160
Load ratio $(F_a/F_r) > e \; or < e$ (Table 4-7)	2.60	0.53
Radial load factor X (contact angle = 25)	0.41	1.0
Radial load factor Y (contact angle = 25)	0.87	0
Equivalent load P (N)	267	160

[1] Flywheel rotor: mass (kg) = 524, outer diameter (mm) = 410, height (mm) = 500

The radial load on the bearings is not fixed and is estimated using ISO 1940/1 for a balance quality grade of G0.4 [136]. This gives an unbalanced force of approximately 260 N although this will not be achieved since it will be significantly reduced due to the presence of the soft mounting springs. Opposite to the case of axial loads, most of the radial load will act on the top bearing since the length of the MG moves the lower bearing further away from the flywheel rotor. Hence, 160 N is assumed for the top bearing and 100 N for the lower bearing. The type and specification of the bearings and factors and parameter for bearing life calculations are presented in *Table 4-8* to *Table 4-11*.

***Table 4-10**. Angular contact super precision ball bearing specifications [135]*

Bearing SKF 7005 CD/P4A	**Principle dimensions**			**Basic load ratings**		**Fatigue load limit**	**Max speed**
	Bore diameter	Outside diameter	Width	Dynamic	Static		
	d	**D**	**B**	**C**	**Cs**	**P_u**	
	mm	mm	mm	kN	kN	kN	krpm
Top bearing (Grease lubricate)	25	47	12	9.56	5.2	0.22	36
Lower bearing (Oil lubricate)	25	47	12	9.56	5.2	0.22	56

***Table 4-11**. Values of life modification factor [135]*

	Actual operating viscosity				Rated viscosity	κ	η_c	a_{skf}[1]
	Oil-mist (mm^2/s)		Grease (mm^2/s)		nd_m			
	40°C	100°C	40°C	100°C	mm^2/s			
Top bearing	-	-	26	4.5	7	0.64	0.4	2.5
Lower bearing	16	4	-	-	7	0.57	0.5	4

[1] See Appendix A for specifications and diagrams

Bearing friction loss is calculated by selecting the bearing type and the lubrication method described above. The load dependent torque and speed dependent torque on the bearings are calculated by substituting the relevant parameters into Equations (4.25) and (4.29). The results of calculated bearing losses at different speeds for both bearings supporting the flywheel rotor are presented in *Table 4-12*.

***Table 4-12**. Results of bearing standby loss calculations*

Speed (rpm)	Bearing friction losses (W)				
	Lower bearing loss		Top bearing loss		Total loss
	P_L	P_v	P_L	P_v	P
1,000	0.4	0.08	0.13	0.38	1
5,000	2	1.2	0.7	5.6	10
10,000	4	3.7	1.3	17.6	27
15,000	6	7.3	2	34.5	50
20,000	8	11.7	2.7	55.8	78
25,000	10	17	3.3	81	111
30,000	12	23	4	109.5	149

Most of the estimated losses occur on the top bearing and the majority comes from the speed dependent loss component. This is partially due to larger radial load assumed for this bearing but it is mainly related to the type and mode of lubrication. As the speed increases, the speed related losses for the top bearing increase much greater compared to its load related losses. This is not the case for the lower bearing since it is oil lubricated and the viscosity and mode of lubrication contributions are small. Hence, the type of lubrication determines the implication of load related and speed related losses.

***Table 4-13**. Results of bearing life calculations*

Bearing type	Description	Speed (1000 rpm)						
		1	5	10	15	20	25	30
Top	Basic rating life (1000h)	3555	711	356	237	178	142	119
	Modified rating life at 95% reliability (1000h)	5688	1138	569	379	284	228	190
Lower	Basic rating life (1000h)	765	153	77	51	38	31	26
	Modified rating life at 95% reliability (1000h)	1959	392	196	131	98	78	65

Bearing life calculations for both bearings operating at different speeds are shown in *Table 4-13*. Opposite to strong dependency of the bearing losses on lubrication type, the applied load mainly challenges the bearing life and the type of lubrication has less of an effect. It is dependent on the equivalent load and the type of bearing. Since the same type of bearing has been selected for both the top and lower bearings, the larger equivalent load on the lower bearing greatly reduces its estimated lifetime. The equivalent load on the lower bearing is 40% higher than the top bearing. If we compare both bearings at 20,000 rpm, the estimated basic life of the top bearing is 178,000 h while that of the lower bearing is 38,000 h. The modified rating life of the top and lower bearings are 284,000 h and 98,000 h, respectively. Therefore, despite the lower bearing having a relatively less viscous lubricant compared to the grease-lubricated top bearing, a 40% increase in its equivalent load will reduce its basic lifetime by 78% and modified rating life by 65%. In addition, factors such as dynamic load rating (C) and fatigue load limit (P_u) will also affect the bearing life rating. Selecting a different type of bearing with lower C value will have a shorter bearing life rating.

4.3 System total losses and efficiency

In order to determine the overall efficiency of the system, total standby losses including windage and bearing friction losses must be taken into account. The flywheel self-discharge rate increases nonlinearly as the speed and pressure increase. The windage losses vary with pressure and speed although bearing losses are only speed dependent. Hence the combined run down losses will be a combination of different powers of speed due to multiple power loss expressions (P_L, P_v *and* P_w) included in the calculations. Air gap variations will also have a significant effect at

higher pressures, but a gap of 1 mm is considered as a worst-case. The standby self-discharge rate at different pressures of 0.01 Pa, 0.1 Pa and 1 Pa is shown in *Figure 4.3*. The flywheel is considered to be initially fully charged and running at 20,000 rpm, and then left on standby mode for 24 hours without any further recharging.

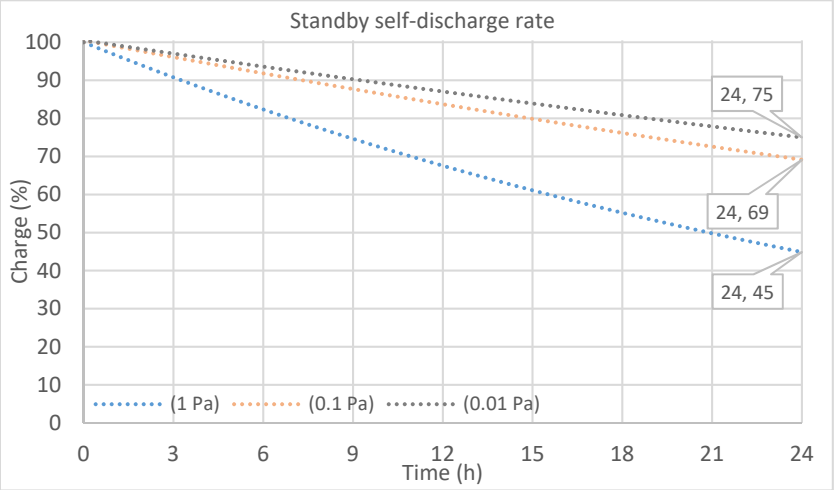

***Figure 4.3**. Flywheel standby discharge rate during 24 hours*

The 24-hours run down losses at lower pressures are smaller and giving 25% and approximately 30% discharge at pressures of 0.01 Pa and 0.1 Pa, respectively. However, when the pressure is increased to 1 Pa, the discharge rate is almost doubled to 55% and approximately 2740 Wh energy is lost in 24 hours. This is because of the exponential increase of the windage losses with respect to pressure rise. At lower pressures, the windage losses are insignificant and bearing friction losses dominate the standby losses. At 1 Pa and at higher speeds, the windage losses increase substantially while the rate of change of bearing losses will be relatively the same. Since the flywheel will be operating in a vacuum and a pressure of 0.01 Pa could be easily maintained, 1 Pa pressure will not be reached and can be considered as the maximum operating pressure limit. In addition, this analysis is performed based on the assumption that the flywheel performs only one charge-discharge cycle per day and then left on standby for the course of 24 hours. However, if the number of cycles per day increases, the energy loss during standby periods will become smaller as shown in *Table 4-14*.

***Table 4-14**. Flywheel standby discharge rate relative to number of cycles*

No. of cycles	Standby self-discharge rate (%)		
(Per day)	(0.01 Pa)	(0.1 Pa)	(1 Pa)
1 (0.5 h)	24	30	54
5 (2.5 h)	23	29	53
10 (5 h)	20	25	47
20 (10 h)	15	19	37
30 (15 h)	10	12	25
40 (20 h)	4	5	12
45 (22.5 h)	2	3	7

The flywheel is a C2 rating (5 kWh, 10kW) taking 30 min charge-discharge time between 50% charge to fully charged and back to 50% state of charge. For 10 cycles per day, the flywheel will be idling for 19 hours and this gives 47% discharge rate if the pressure reaches the maximum of 1 Pa. The self-discharge rate is reduced to quite an acceptable level of 25% for 30 cycles and this is further improved to 12% and 10% if the pressure is reduced to 0.1 Pa and 0.01 Pa, respectively. The standby losses will be far reduced for 40 and 45 cycles but this will not be realistic since the maximum possible number of cycles per day is 48 and the flywheel would hardly rest. A compromise must be made between the number of cycles and standby losses based on the level of pressure in the vacuum. For instance, the self-discharge rate of 25% can be reached for 10 cycles at 0.1 Pa or 30 cycles at 1 Pa. Therefore, 10 cycles per day is considered as an acceptable compromise for calculating the run down losses and system efficiency. This will give a self-discharge rate of 4.7% per cycle in the extreme conditions of a 1 mm air gap and a pressure level of 1 Pa. The self-discharge rate in terms of initial stored energy E_0 and available energy $E_{(t)}$ after a time period can be determined by Equation 4.35.

$$\eta_{self-discharge} = \frac{E_{(t)}}{E_0} \tag{4.35}$$

The efficiency of the system can be calculated considering the system conversion efficiency while charging (η_{charge}) and discharging ($\eta_{discharge}$) which are dependent on the energy losses in the electrical machine and related power electronics. The overall efficiency per cycle of the flywheel system (η_{sys}) including the run down losses

can be calculated by assuming an efficiency of 98% for power electronics and 95% for the MG (electrical machine) giving an overall round trip efficiency of approximately 83%. Accordingly, the maximum standby losses of 230 W can be confirmed by combining the windage losses (*Table 4-3* & *Table 4-4*) with the bearing friction losses (*Table 4-12*) for an operating speed of 20,000 rpm. The remaining operational losses are approximately 310 Wh per cycle.

The following assumptions are made for calculation of the aerodynamic drag and bearing friction losses in PMSM-Flywheel unit:

- The flywheel rotor is considered as a drum type steel laminated solid cylinder. There are no internal losses within the rotor itself.
- The clearances between stationary and rotating components are small, such that the boundary layers on stationary and rotating surfaces merge.
- The windage losses are calculated under maximum operating conditions of 1 Pa pressure at 40 °C and a maximum speed of 20,000 rpm. Although the flywheel system will be maintained well below the aforementioned pressure and temperature ratings due to vacuum conditions.
- Density values are calculated from temperature and pressure using ideal gas law.
- Windage on the motor-generator is neglected, since its rotor diameter is much smaller than that of the flywheel rotor, and it will be quite insignificant since the power law on diameter for windage is 4 (Equations 4.11 and 4.13).
- It is assumed that the combined axial load on the bearing system is 10% of the total flywheel rotor weight with the rest taken by the passive magnetic bearing.
- Analysis of external forces on the bearings is neglected as the flywheel is operating in stationary ground condition and the movement effects such as those for vehicles uses are not present.
- The bearing losses are calculated assuming the radial out of balance forces are much higher than would be present since the bearings are soft mounted. However,

it may be that a balance grade of 0.4 is not achievable or the effect of soft mounting on reducing radial losses is less than expected.

4.4 Chapter summary

This chapter provided the calculation method and analysis of bearing friction and aerodynamic losses of a steel rotor flywheel operating within a speed range of 10-20 krpm under vacuum conditions. Bearing and windage loss equations using two different methods, derived by Beck and Alofs, are analysed and the results are compared. Analysis of the windage losses was performed at different pressure levels (0.001-100 Pa) and the results of both methods indicated good correlation at lower pressures. It was shown that Alofs drag coefficient was valid for all range of Knudsen numbers as it is not affected by the air gap. However, Beck's windage losses increased as the air gap decreased and, therefore, this method is only valid for rarefied gas conditions with low-pressure level and will introduce errors as the pressure increases beyond 1 Pa. The estimated losses of the bearing system at higher speeds showed that the speed-dependent loss component was dominant in relative to load dependent component if grease lubrication was used. This was partially related to the radial load on the bearing but was mainly affected by the type and mode of lubrication. On the other hand, it was not the case for oil-lubricated bearings since the viscosity and mode of lubrication contributions at higher speeds were smaller compared to the load effects on the bearing.

The standby losses were calculated for a different number of cycles per day and it was shown that the run down losses of the flywheel system are 25% in 24 hours at 10 cycles per day. The round trip efficiency of the system is calculated to be 83% giving approximately 230 W for standby losses and leaving about 310 Wh per cycle for other losses while the flywheel is operational. The loss analysis is performed for the worst-case scenario under extreme conditions of 1 mm air gap and pressure level of 1 Pa, although this will not be reached since the flywheel is operating in vacuum conditions.

Chapter 5 Modelling and Control of Flywheel Energy Storage System

The power conversion system involving different forms of energy storage systems can be presented as shown in *Figure 5.1*. It shows the connection of the flywheel storage to an electrical grid through a DC-link, however, the same configuration can be used when connecting other storage systems (batteries, supercapacitors, or SMES) to the grid. All storage types link to the same DC bus and they are connected to the grid at the point of common coupling (PCC). The components that the storage systems commonly share are the switchgear, transformer, AC filter and the grid side converter (GSC) which communicates with storage side converter (SSC) to maintain the voltage at the DC link [137].

What generally differentiates between the operation of a flywheel storage system and other storage systems is the topology of the SSC. It functions as a bidirectional AC-DC inverter or rectifier to control the supply of power in and out of the flywheel, whereas, in the case of other storage systems such as batteries, supercapacitors and SMES, it performs as a bidirectional DC-DC converter to communicate between the DC-link and the storage device. For flywheels, the converters are arranged in a cascaded bidirectional back to back AC-DC-AC configuration to perform power flow in both directions with the help of the associated control system.

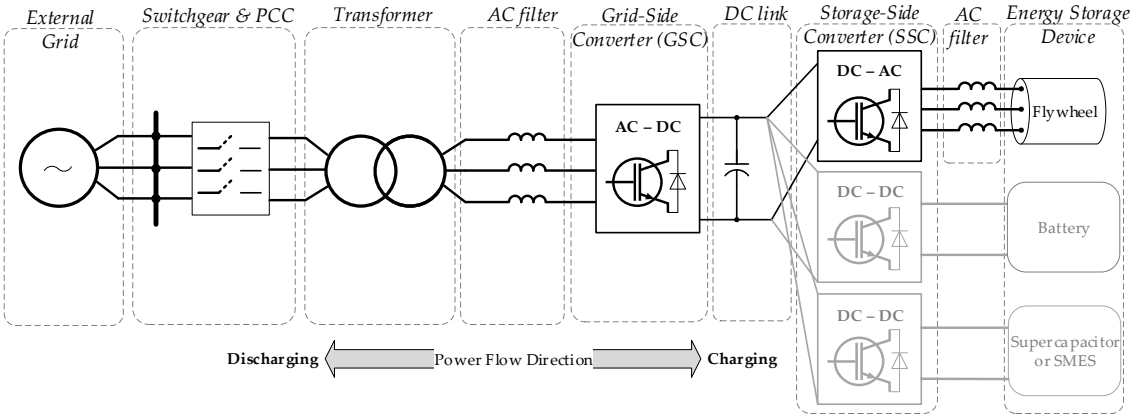

***Figure 5.1**. General configuration of power conversion system involving different energy storage systems adapted from [137]*

A generalised topology of the FESS connected to an electrical supply with bi-directional power flow is shown in Figure 5.2. The FESS and the grid are connected

through the DC-link and back-to-back converters. The function of the GSC is to control the power flow from/to the grid while the SSC controls the operation and flow of power in and out of the MG connected to the flywheel rotor. The working principle of the FESS can be discussed in three modes of operation: charging mode, discharging mode, and standby mode. During charging, SSC draws power from the DC-link to run the MG and accelerate the flywheel. MG is operating as a motor, SSC as an inverter, and GSC as a rectifier to maintain the DC-link voltage. While in discharging, the operation of both converters is reversed and the flywheel is decelerated to deliver the stored energy and maintain the DC-link voltage. The standby mode is when the flywheel spins at a constant fixed speed and no energy conversion occurs except for a small power fed into the flywheel to maintain speed. The fixed speed for standby is typically chosen to be the speed at which the flywheel is at 50% SOC to allow an equal amount of energy to be stored or released in the case that it is not clear which will be required. In a more sophisticated control system where the state of other power generating elements is known, the standby speed can be changed and will depend on the state of these other elements.

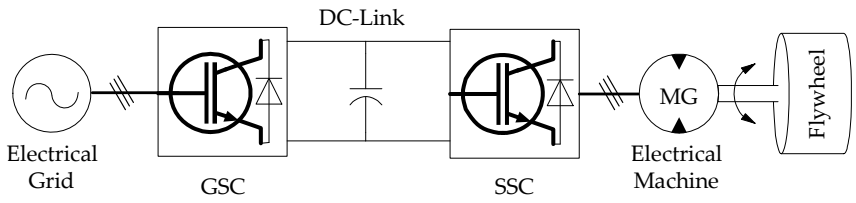

***Figure 5.2**. FESS with back-to-back bidirectional power converters*

In this chapter mathematical modelling and control of FESS including GSC, the DC-link, SSC and the electrical machine are presented. The mathematical model of the selected MG is presented in section 5.1. The controlling structure and operation of the FESS during different charge-discharge states are described in section 5.2. This also includes control of the DC-link, the SSC and the GSC. The chapter is concluded in section 5.3 where the design of torque, speed and voltage PI controllers are discussed and calculation methods of their respective gain parameters are presented.

5.1 Description and mathematical model of Permanent magnet synchronous machine

The electrical machine is the vital component of the FESS considering the fact that the flywheel rotor is just a high inertia rotating mass coupled to the shaft of the electrical machine. The energy conversion is supported by controlling the operation of electrical MG. In this research, a permanent magnet synchronous motor (PMSM) is considered to perform both motoring and generating tasks by operating as an integrated electrical machine. It is widely used in motion control applications due to its compact structure, low inertia, high specific power, high steady-state torque density and higher efficiency [138]. Based on its attributes and owing to its fast dynamic response, PMSM is usually considered for high-speed flywheel applications compared to induction machine (IM) and variable reluctant machine (VRM). Due to its simple method of control, lower mass and low losses, it has been broadly used in numerous variable speed applications in recent years [139-142]. Contrary to the other motors, a PMSM has no windings on the rotor and it operates based on the magnetic field produced by its own permanent magnets. It can be simply analysed with the help of voltage equations for the stator windings given by [47]:

$$\boldsymbol{V}_{abc} = R_s \boldsymbol{i}_{abc} + \frac{d\boldsymbol{\lambda}_{abc}}{dt} \tag{5.1}$$

where:

$$\boldsymbol{V}_{abc} = \begin{bmatrix} V_a \\ V_b \\ V_c \end{bmatrix},\ \boldsymbol{i}_{abc} = \begin{bmatrix} i_a \\ i_b \\ i_c \end{bmatrix},$$

$$\boldsymbol{\lambda}_{abc} = \begin{bmatrix} \lambda_a \\ \lambda_b \\ \lambda_c \end{bmatrix} = \begin{bmatrix} L_{aa} & L_{ab} & L_{ac} \\ L_{ab} & L_{bb} & L_{bc} \\ L_{ac} & L_{bc} & L_{cc} \end{bmatrix} \begin{bmatrix} i_a \\ i_b \\ i_c \end{bmatrix} + \lambda_m \begin{bmatrix} Cos(\omega_e t) \\ Cos(\omega_e t - \frac{2\pi}{3}) \\ Cos(\omega_e t + \frac{2\pi}{3}) \end{bmatrix}$$

The electromagnetic torque (T_e) expression can be represented by:

$$T_e = \lambda [i_a \quad i_b \quad i_c] \frac{d}{d\theta} \begin{bmatrix} \lambda_m Cos(\omega_e t) \\ \lambda_m Cos(\omega_e t - \frac{2\pi}{3}) \\ \lambda_m Cos(\omega_e t + \frac{2\pi}{3}) \end{bmatrix} \tag{5.2}$$

where;

$\boldsymbol{V}_{ab}$: Three-phase stator voltages (V)

$\boldsymbol{i}_{abc}$: Three-phase stator currents (A)

$\boldsymbol{\lambda}_{abc}$: Three-phase stator winding flux (V/rad/s)

R_s : Stator winding resistance (Ω)

L_{nm} : Stator winding self and mutual inductance (H)

λ_m : Rotor field flux (V/rad/s)

T_e : Electromagnetic torque (N.m)

ω_e : Rotor's electrical speed (rad/s)

In order to develop a mathematical model of PMSM and facilitate the analysis, the following assumptions are considered:

- The induced electromagnetic force (EMF) is sinusoidal
- The air gap between the rotor and stator is uniform
- Magnetic saturation and iron losses are neglected
- Eddy current and hysteresis losses are negligible

The above-mentioned losses are neglected since their effect is small in comparison to other losses in the system. However, while considering the flywheel in standby mode and calculating the overall efficiency of the system, these losses are approximated and included in modelling energy flows discussed in the next chapter.

Equations (5.1) and (5.2) of the PMSM indicate a nonlinear time-varying and multi-variable coupled system. The coefficients of the differential equation are time-varying and the induced voltages, currents, and flux linkages change continuously while the electric circuit is in relative motion. This makes the modelling of the PMSM complex and mathematical transformations are required to decouple the variables and refer the time-varying quantities to a common reference frame. This helps to control the machine and, therefore, the three-phase system is transformed into an equivalent two-dimensional system called direct and quadrature (*d-q*) axes frame or *rotating*

reference frame as shown in *Figure 5.3* [143]. The transformation of three-phase *a-b-c* voltage equations to their respective *d-q* equations is presented in appendix B.

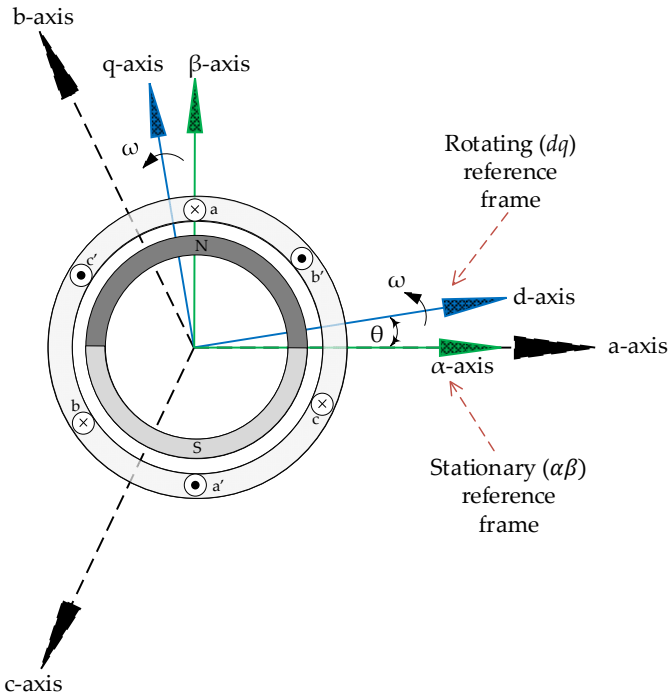

***Figure 5.3**. Transformation of a-b-c to rotating reference frame and stationary reference frame adapted from [143]*

As illustrated in Figure *5.3*, the *rotating reference frame* makes an angle θ with the fixed stator phase A (a-axis) and q-axis is orthogonal to d-axis. Since the stator magnetomotive force (mmf) rotates at the speed of rotation of the rotor, this transformation allows separation of flux producing and torque producing components of the AC motor along d-axis and q-axis, respectively [47]. Transformation of Equation (5.1) gives simplified voltage balance equations of the PMSM in d-q rotating reference frame as follows:

$$V_q = R_s I_q + \omega_e \lambda_d + \frac{d\lambda_q}{dt} \tag{5.3}$$

$$V_d = R_s I_d - \omega_e \lambda_q + \frac{d\lambda_d}{dt} \tag{5.4}$$

Where

$$\lambda_d = L_d I_d + \lambda_m \tag{5.5}$$

$$\lambda_q = L_q I_q \tag{5.6}$$

Substituting above in Equations (5.3) and (5.4) and simplifying and rearranging gives:

$$V_q = R_s I_q + L_q \frac{dI_q}{dt} + \omega_e L_d I_d + \omega_e \lambda_m \tag{5.7}$$

$$V_d = R_s I_d + L_d \frac{dI_d}{dt} - \omega_e L_q I_q \tag{5.8}$$

Similarly, the electromagnetic torque developed by the motor in terms of *d-q* components can be obtained as:

$$T_e = \frac{3}{2}\frac{P}{2}(\lambda_m I_q + (L_d - L_q) I_d I_q) \tag{5.9}$$

Considering a non-salient cylindrical rotor PMSM, the magnetic resistance is the same in all directions and equal inductances ($L_d = L_q$) can be assumed. The electromagnetic torque in Equation (5.9) can be simplified and will depend only on the rotor flux (λ_m) and stator current (I_q):

$$T_e = \frac{3}{2}\frac{P}{2}\lambda_m I_q \tag{5.10}$$

Finally, the relation between the mechanical and electromagnetic torque is presented by:

$$T_e = J\frac{d\omega_m}{dt} + B\omega_m + T_L \tag{5.11}$$

where;

I_d : Direct axis stator current (A)

I_q : Quadrature axis stator current (A)

L_d : Direct axis inductance (H)

L_q : Quadrature axis inductance (H)

J: Combined moment of inertia of the PMSM and flywheel (kg·m²)

B : Friction of viscous (N·m/rad/s)

P : Number of poles

T_L : Load torque (N·m)

T_e : Electromagnetic torque (N·m)

ω_m : Rotor's mechanical speed (rad/s)

5.2 Control of the Permanent Magnet Synchronous Machine

The operation of AC motor drive systems is primarily controlled by varying the torque of the machine to control the position and speed of the load as desired. Depending on the application, average torque control and instantaneous torque control are the main controlling methods of AC motors [144]. Average torque control (also called scalar control) is used in applications where the motor operates at an average speed under steady-state conditions. Constant V/f control (voltage magnitude and frequency control) is a type of average torque control that works based on control of the average current of the motor. The major limitation of scalar control is that it cannot control the dynamic behaviour of the AC motor and, therefore, instantaneous torque control is needed to achieve high-performance operation. The torque of AC motors is instantaneously controlled using Vector Control technique where both the magnitude and direction of the motor currents are controlled. Field-oriented control (FOC) and direct torque control (DTC) are the main controlling techniques for instantaneous torque operations where the former is more popular and widely used despite its higher level of complexity [144]. The operation of FESS requires variable speed control and instantaneous torque changes are required for high performance and smooth operation for the entire speed range. In this study, the Field-oriented Vector Control method has been used to control the operation and dynamic performance of the PMSM operated flywheel during the acceleration and deceleration modes.

5.2.1 Permanent Magnet Synchronous Machine Vector Control

The vector control of PMSM helps the control of the stator three-phase currents since there are no currents from the rotor. The direction of the current flow is controlled by the SSC (inverter) using the switching control. The switching of the PMSM inverter is controlled with pulse width modulation (PWM) technique using space vectors. The vector control technique that is also referred as field-oriented control, is based on the measurement of motor three-phase currents and their transformation into a system of coordinates rotating with the rotor of the machine

[145]. It decomposes the stator currents into decoupled magnetic-generating component and torque-generating component that allows separate closed-loop control of flux and torque of the machine, respectively. Using FOC, control of PMSM can be simplified and implemented similar to control structure of a separately excited DC machine.

The position of the rotor can be determined using sensorless control or an absolute position sensor (e.g. resolver or encoder). Then the rotor is aligned with phase A knowing that the direct (flux-generating) axis is also in line with phase A. Hence the relative position of the rotor with respect to d-axis is set to zero and the flux-generating component of the stator current (I_d) becomes orthogonal with that of torque-generating component (I_q). The current vector makes a 90-degree angle with the rotor axis and, as a result, ($I_d = 0$) is assumed for maximum electromagnetic torque generation and simpler control structure [146]. For further clarification of the FOC technique, the process can be generally summarised as follows:

Three-phase stator currents of the motor are converted to two-dimensional rotating d-q frames using Clark-Park transformation. The magnetic flux-generating part is represented by (d) component and the torque-generating part is represented by (q) component of the rotating frame. The decoupled d-q components are passed through independent PI controllers to be controlled separately. Then, the transformation from d-q rotating frames to three-phase sinusoidal currents is performed with Inverse Clark-Park transformation and space vector pulse width modulation (SVPWM) as shown in *Figure 5.4*.

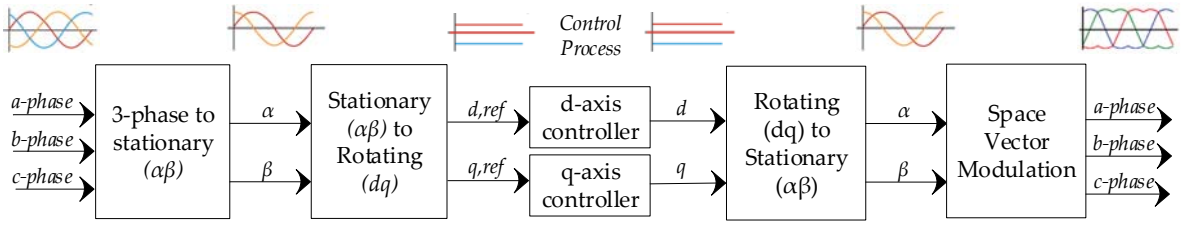

***Figure 5.4**. Vector control transformation adapted from [146]*

The controlling principle of PMSM can be described with the following general steps [146]:

- Measure the motor quantities (stator three-phase currents and the rotor position)
- The three-phase stator currents *a-b-c* are converted to two-axis reference frame α-β using Clark Transformation.
- The α-β currents are then converted to rotor *d-q* reference frame using Park Transformation.
- The stator current components (I_d) and (I_q) are separately controlled. The d-axis current (I_d) is used to control the flux and the q-axis current (I_q) is to control the torque production. The measured *d-q* currents are compared with reference *d-q* currents and the error is regulated and controlled with PI controllers.
- A speed regulator is used to compare the measured speed with the reference speed whose output is provided as the input to the q-axis controller to produce the torque.
- The outputs of the current PI controllers (controlling the error of *d-q* currents) are transformed back to the two-phase α-β system to generate the input space vectors to the inverter
- The inverter switches are turned on and off to control the current flowing to the motor. This switching operation and control of the inverter are employed using space vector pulse width modulation (SVPWM) technique.
- The PMSM is then controlled with the output three-phase voltages generated by the inverter

A detailed description of Clark and Park transformations is provided in Appendix B and SVPWM technique is presented in Appendix C.

5.2.2 Space Vector Pulse Width Modulation Controlled Inverter

In variable speed applications where a change of speed is required at every instant, the electrical machine is supplied from a separately controlled power source that can produce variable supply voltages according to the requirements of the motor operation. These power sources are three-phase inverters consisting of transistor switches that can be operated and controlled to generate voltage pulses with variable

width to control the speed of the motor. The width and generation of pulses can be controlled using pulse width modulation (PWM) technique. As a result, the amplitude and frequency of the stator voltages of the PMSM can be controlled and hence the machine will operate at the desirable speeds.

Space vector pulse width modulation is an advanced and computational modulation technique which is possibly the best method for controlling variable AC drives. This technique is used to generate the inverter gating signals by sampling a reference signal regularly [48]. Space vector modulation (SVM) transforms the voltage vectors into pulse width modulation (PWM) signals through which the switching of the inverter is controlled. SVPWM enables inverter IGBT switches to turn ON and OFF in a particular pattern to produce the required voltage across the stator windings of an AC drive. *Figure 5.5* shows a voltage source inverter (VSI) with IGBT transistor and anti-parallel diode switches connected to a PMSM through an LC filter.

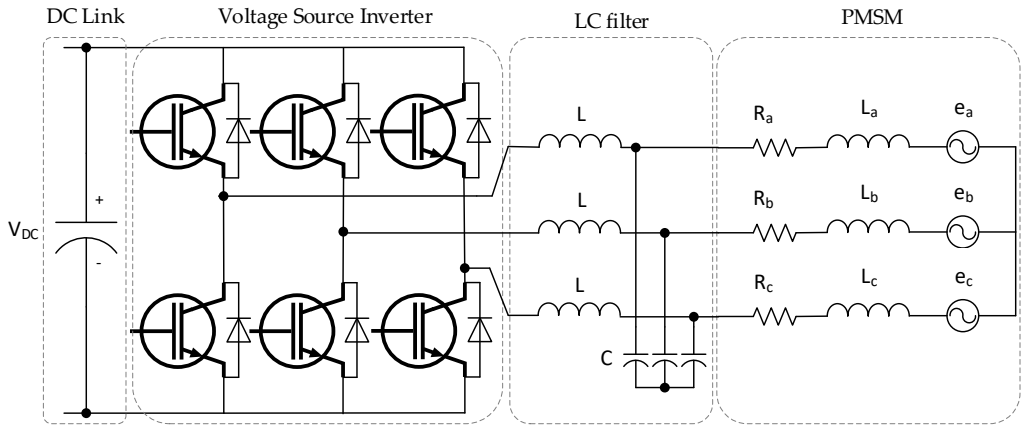

***Figure 5.5**. Circuit diagram of VSI and PMSM [142]*

In comparison to sinusoidal pulse width modulation, SVPWM provides a better DC voltage utilization with decreased total harmonic distortion (THD). Therefore, the speed and torque fluctuations are reduced and overall performance of the motor drive is improved [147]. The principle of operation and detailed description of the SVPWM technique is discussed in Appendix C.

5.2.3 Operation and control of the PMSM and converters

The control block diagram of the PMSM-Flywheel in both charging (motoring) and discharging (generating) states is presented in *Figure 5.6*. The operation of the SSC is controlled by cascaded control loops with an inner current loop and an outer speed loop to regulate the speed of the PMSM. The controlling operation of the cascaded loops is performed using PI controllers. In the inner control loop, the three-phase stator currents are measured and transformed to two-axis *d-q* currents using Clark-Park transformation. The decoupled *d-q* currents are controlled separately with PI current controllers to control the flux and torque of the MG. The *d*-component of the current is the flux producing component and *q*-component is the torque producing component [148]. Similarly, in the outer loop, the PMSM speed is measured and regulated by comparing it with the reference speed. The output of the speed PI regulator is applied as the reference *q*-current component for the current PI regulator to control the torque accordingly.

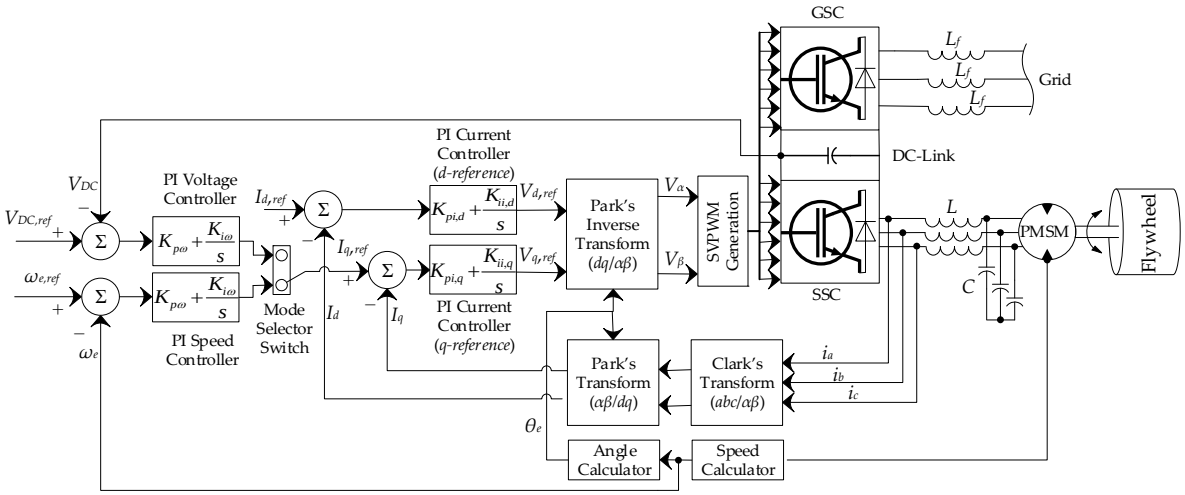

***Figure 5.6**. Block diagram of FESS controlling scheme*

On the other hand, during the discharge mode when the DC-bus voltage drops below a threshold value, a voltage controller is required to adjust and control the system current to regulate the DC-link voltage. This action is controlled by the GSC which functions to maintain a constant DC voltage and regulate the reactive power exchange with the grid [137]. A simplified equivalent circuit of the GSC connected to the

external grid through an inductive filter is shown in *Figure 5.7*. For ease of analysis, the grid and the GSC are considered as ideal AC voltage sources.

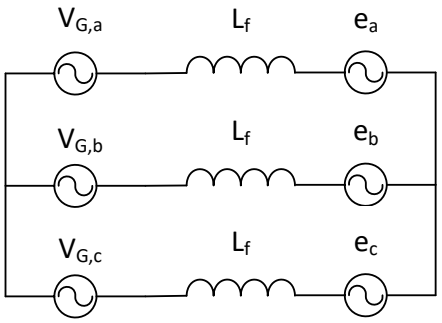

***Figure 5.7**. Equivalent circuit diagram of GSC and the grid*

The mathematical equations of the voltages and currents based on the provided equivalent circuit of the GSC, simplified in rotating *d-q* reference frame, can be expressed as follows:

$$V_{G,q} - e_q = L_f \frac{dI_{G,q}}{dt} + \omega_G L_f I_{G,d} \tag{5.12}$$

$$V_{G,d} - e_d = L_f \frac{dI_{G,d}}{dt} - \omega_G L_f I_{G,q} \tag{5.13}$$

where,

$V_{G,q}$: Quadrature axis component of the grid voltage (V)

$V_{G,d}$: Direct axis component of the grid voltage (V)

$I_{G,q}$: Quadrature axis component of the grid current (A)

$I_{G,d}$: Direct axis component of the grid current (A)

ω_G : Grid frequency (rad/s)

L_f : Filter inductance (H)

The model and control of the GSC converter can be implemented based on the set of equations presented in (5.12) and (5.13). As shown in *Figure 5.6*, the input measurements are the DC-link voltage (V_{DC}) and three phase sinusoidal currents flowing from the grid. Hence the outer speed loop in charging mode is replaced with the outer voltage loop in discharging mode. Similar to the motoring mode where the speed is regulated by the extracting energy from the source, the generating mode

allows the DC-link voltage to be measured and regulated by comparing it with the reference voltage ($V_{DC,ref}$). The alternating currents are transformed to rotating d-q reference frame currents (I_d) and (I_q). The direct current component (I_d) of the converter is compared with rethe ference current ($I_{d,ref}$) flowing from the converter and the error is regulated using a PI controller. In the same way, the output of the voltage PI controller is regulated as an input for the current PI controller. Then the outputs of the PI controllers are transformed to sinusoidal voltages in stationary reference frames α-β which will produce inputs signals of the SVPWM to control the switching of the IGBT transistors of the GSC.

In the same way, the model and control of the DC-link are implemented by neglecting the internal power losses in power conductors. The DC-link acts as a bridge between the GSC and SSC and its power loss (P_{DC}) is the difference between the power from the GSC (P_G) and the power from the SSC (P_S) given by:

$$P_{DC} = P_G - P_S \tag{5.14}$$

Similarly, the power consumed by the DC-link capacitor is given by:

$$P_{DC} = \frac{1}{2} C \frac{d}{dt} {V_{DC}}^2(t) \tag{5.15}$$

The time dependent DC-link voltage $V_{DC}(t)$ is calculated with the following integral:

$$V_{DC}(t) = V_{DC,0} + \frac{1}{\mathrm{C}} \int_0^t (I_{DC,G} - I_{DC,S}) dt \tag{5.16}$$

where,

$V_{DC,0}$: Initial DC bus voltage (V)

$I_{DC,G}$: DC current from the GSC (A)

$I_{DC,S}$: DC current from the SSC (A)

C : Equivalent capacitance of the DC-link (Farads)

Considering the charging mode when power flows from the GSC to the SSC, the power from the GSC expressed in d-q rotating reference frame can be represented by [137]:

$$P_G = \frac{3}{2}(V_{G,d}I_{G,d} + V_{G,q}I_{G,q}) \tag{5.17}$$

As the FESS operates between a minimum and maximum speed range for better utilisation of its useful energy, the speed loop is required to determine and monitor the flywheel's state of charge. In order to operate within the specified speed range, the status of the rotor speed and position in any state of operation is essential for controlling flywheel's torque and flux. In addition, the DC-link voltage can be maintained through the voltage feedback loop in either states of charging or discharging. This allows control of the power from the PMSM and hence its torque, provided that the motor speed is known.

5.3 PI Controller Design

The operation of the PMSM-Flywheel is controlled using a proportional-integral (PI) cascaded control structure. The controller is designed to follow the changes in position, speed and torque of the machine to a set of reference values. Due to its flexibility, it is widely used in industry to control the position and velocity of AC motor drives. It consists of segregated control loops with the outermost position loop followed by the inner speed loop and the innermost current (torque) loop as shown in *Figure 5.8*. This technique requires the response time of the current loop to be the fastest compared to the speed and position loops [149, 150].

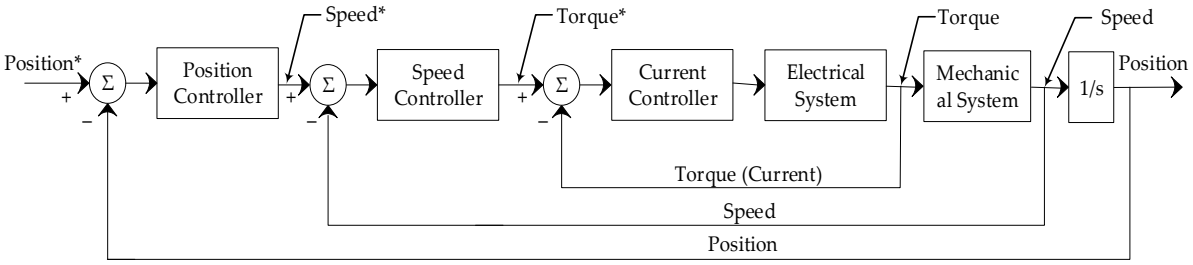

***Figure 5.8**. General cascaded control structure [149]*

The parameters of the PI controllers are determined based on the mathematical equations of PMSM derived in the rotor *d-q* reference frame. Equations (5.7-5.9) indicate that *d-q* axis stator currents are not decoupled and the cross-coupling terms such as $\omega_e L_q I_q$, $\omega_e L_d I_d$ and $\omega_e \lambda_m$ make the model nonlinear [151]. The torque

magnitude is related to both *d-q-axis* currents which may possibly contribute a negative torque [152]. Equations (5.7) and (5.8) can be decoupled using the input-and-output linearisation and feedforward manipulation technique [153]. Another method to decouple and linearise the system equations is the assumption of applying $I_d = 0$. This maximises the torque/current ratio and allows decoupling of torque and flux of PMSM to be analysed similar to a PMDC machine. Therefore, Equations (5.7) and (5.8) can be simplified as follows:

$$V_q = R_s I_q + L_q \frac{dI_q}{dt} + \omega_e \lambda_m \tag{5.18}$$

$$V_d = -\omega_e L_q I_q \tag{5.19}$$

$$\frac{P}{2}(T_e - T_L) = J\frac{d\omega_e}{dt} + B\omega_e \tag{5.20}$$

where

$$T_e = \frac{3}{2}\frac{P}{2}\lambda_m I_q \tag{5.21}$$

and

$$\omega_e = \frac{P}{2}\omega_m \tag{5.22}$$

5.3.1 Current (Torque) controller

The torque of PMSM is controlled to overpower the inertia and motion resistance of the machine and set the speed as close as possible to the reference value ($\omega_{e,ref}$). The difference in speed can be calculated by comparing the controlled speed ω_e to the reference speed ($\omega_{e,ref}$) which allows determination of the required torque to overcome the speed error ($\Delta\omega = \omega_{e,ref} - \omega_e$) and track the reference speed. This torque will set the reference value for electromagnetic torque ($T_{e,ref}$). The required acceleration of the motor can be calculated using Equation (5.20) such that the motor must generate torque (T_e) to accelerate and overcome the load torque (T_L) in order to track the reference speed.

Since the electromagnetic torque of a cylindrical rotor PMSM is a function of the rotor flux and stator current (Equation 5.21), it is always better to produce the torque by keeping the stator current at the smallest possible value. The ratio between

the electromagnetic torque and stator current is given by ($T_e/sqrt({I_d}^2 + {I_q}^2)$) [154]. This ratio will be minimum for $I_d = 0$, and it aligns the stator current vector with *q-axis*. Since the rotor flux is collinear with *d-axis*, the stator current and rotor flux vectors will become perpendicular to each other. As a result, the reference torque ($T_{e,ref}$) can be determined using Equation 5.21 and by establishing $I_d = 0$. This allows regulation of the I_q component of the stator current which is provided as an input for the reference torque ($T_{e,ref}$) according to:

$$I_q = \frac{4}{3P\lambda_m} T_e = C * T_e \tag{5.23}$$

Assuming $T_L = 0$ and substituting (5.21) in (5.20) gives:

$$J\frac{d\omega_e}{dt} + B\omega_e = \frac{3}{2}(\frac{P}{2})^2 \lambda_m I_q = K_T I_q \tag{5.24}$$

Ignoring friction of viscosity (B) and combining Equations (5.18) and (5.24) into a cascaded control structure gives the following block diagram:

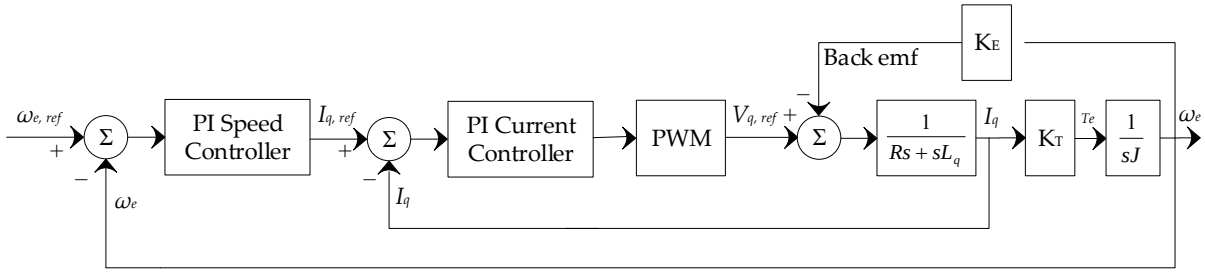

***Figure 5.9**. Cascaded current and speed control loop of PMSM – Motoring mode*

Since the flux of a PMDC machine is constant and the induced back-*emf* is directly related to current ($e_a = \frac{K_T K_E}{sJ} I_q$), the block diagram can be further simplified as shown in *Figure 5.10*.

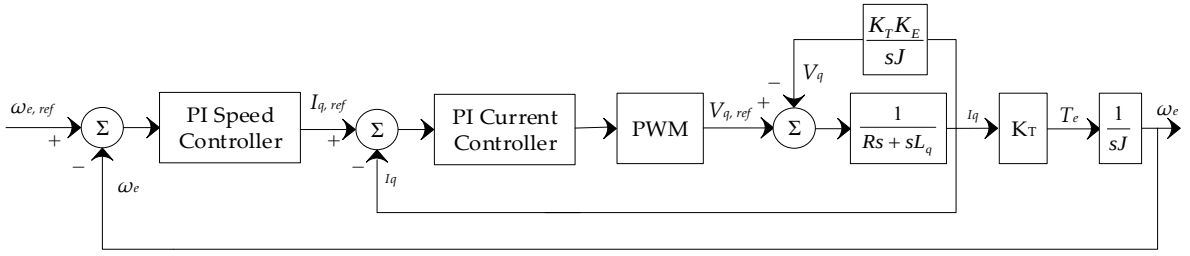

***Figure 5.10**. The simplified current control loop of PMSM – Motoring mode*

Since the PMSM-Flywheel system is a high inertia system and the back-*emf* is inversely proportional to inertia (J), the feedback loop can be neglected and the current controller loop is further reduced as in *Figure 5.11*.

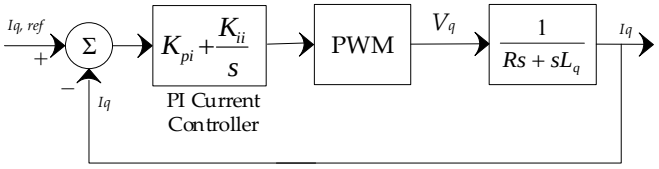

***Figure 5.11**. The reduced current control loop of PMSM – Motoring mode*

Considering that the PWM pulses are provided by a full-bridge inverter whose switching frequency (in kHz) is higher than the fundamental frequency (in Hz), it can be modelled as a voltage source inverter (VSI) by ignoring the dynamics of the PWM switches [155].

$$V_a = K_{PWM} V_R \tag{5.25}$$

And

$$K_{PWM} = \frac{V_{DC}}{V_{tri}} \tag{5.26}$$

where,

V_a = VSI output voltage

V_R = Control signal from the regulator

V_{DC} = DC voltage of the inverter

V_{tri} = Peak value of the triangular carrier

Therefore, the open-loop transfer function of the inner current loop can be written as:

$$TF_{OL,I} = \left(\frac{K_{pi}s+K_{ii}}{s}\right)\left(\frac{V_{DC}}{V_{tri}}\right)\left(\frac{1}{R_s+sL_q}\right) \tag{5.27}$$

The proportional gain K_{pi} and integral gain K_{ii} of the PI current controller can be determined by substituting the PMSM and inverter parameters in (5.27). Detailed calculation method for derivation of K_{pi} and K_{ii} is provided in Appendix D.

Considering the above where the dynamics of the inverter switches are ignored and the system dynamic is mainly dependent on the LC filter, the equivalent circuit of the inverter system in *Figure 5.5* can be presented as follows:

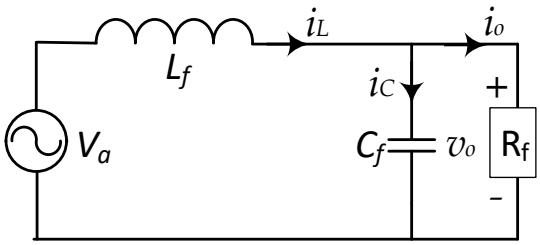

***Figure 5.12**. Inverter and LC filter equivalent circuit*

The state-space representation of the system in *Figure 5.12* can be obtained by selecting the inductor current i_L and output voltage v_o as the state variables [155]:

$$\begin{bmatrix} \dot{i_L} \\ \dot{V_o} \end{bmatrix} = \begin{bmatrix} 0 & -1/L_f \\ 1/C_f & 0 \end{bmatrix} \begin{bmatrix} i_L \\ V_o \end{bmatrix} + \begin{bmatrix} 1/L \\ 0 \end{bmatrix} V_a + \begin{bmatrix} 0 \\ -1/C_f \end{bmatrix} i_o \tag{5.28}$$

The dynamic model of the inverter based on Equation 5.28 can be represented in block diagram form as shown in *Figure 5.13*.

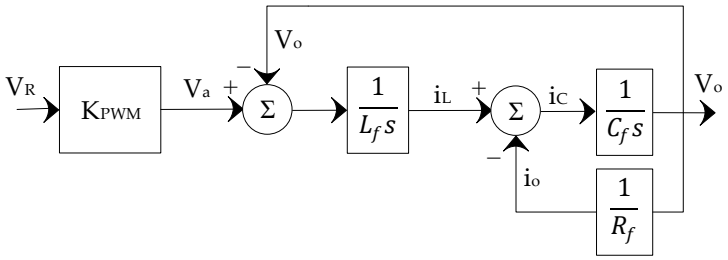

***Figure 5.13**. Dynamic linear model of the inverter system*

This model has been used in designing the voltage PI controller in an upcoming section.

5.3.2 Speed controller

The PI gains of the speed controller can be calculated when the response time of the speed loop is selected to be slower than that of the current loop. If the difference in response time is assumed to be one order of magnitude, the current loop can be represented by an ideal unity gain as in *Figure 5.14*.

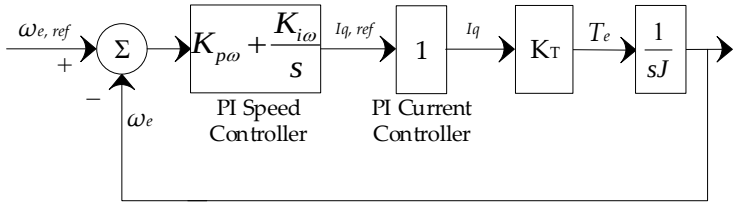

***Figure 5.14**. Simplified speed control loop of PMSM – Motoring mode*

The open-loop transfer function of the speed loop in *Figure 5.14* can be presented as follows:

$$TF_{OL,\omega} = \left(\frac{K_{p\omega}s+K_{i\omega}}{s}\right)(1)\left(\frac{K_T}{sJ}\right) \tag{5.29}$$

Substituting the values of the torque constant (K_T) and inertia (J), the proportional gain $K_{p\omega}$ and integral gain $K_{i\omega}$ of the PI speed controller can be calculated. Detailed calculation method for derivation of $K_{p\omega}$ and $K_{i\omega}$ is provided in Appendix D.

5.3.3 Voltage controller

A similar approach can be applied to calculate the PI controller gains of the voltage regulator during the discharging phase of the PMSM-Flywheel. The voltage controller is used to maintain the DC-link voltage stable and as close as possible to the reference voltage ($V_{DC,ref}$). It consists of two cascaded loops such that the outer control loop provides reference quadrature current ($I_{q,ref}$) for the inner current control loop. Considering a full-bridge voltage source inverter with the filter inductance L_f, capacitance C_f and resistance R_f, the structure of the current and voltage loops can be represented as shown in the following block diagram (*Figure 5.15*).

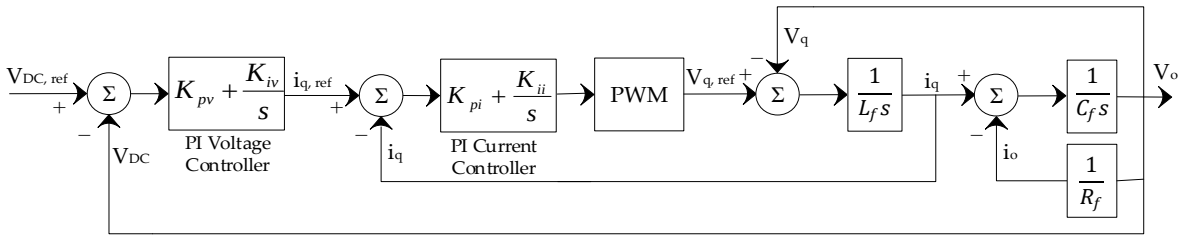

***Figure 5.15**. Cascaded voltage and current loop of PMSM – Generating mode*

Simplifying the current loop in the above block diagram gives:

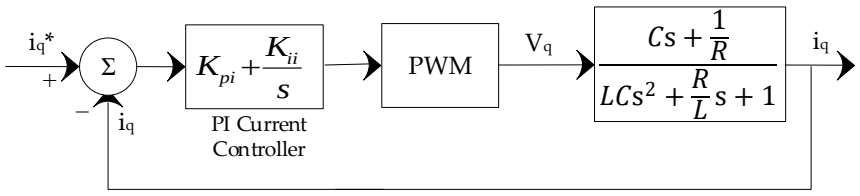

***Figure 5.16**. Reduced current control loop of PMSM – Generating mode*

The open-loop transfer function of the inner current loop in *Figure 5.15* can be determined as:

$$TF_{OL,I} = \left(\frac{K_{pi}s+K_{ii}}{s}\right)(K_{PWM})\left(\frac{Cs+\frac{1}{R}}{LCs^2+\frac{L}{R}s+1}\right) \tag{5.30}$$

Similar to the speed loop controller design, the PI gain parameters of the voltage loop are calculated by replacing the current closed-loop with a unity gain. Considering $V_{G,d} = 0$ strategy and neglecting the losses in power converter where the dynamics of the PWM switching can be ignored, the input current into the DC-link from the GSC can be obtained using Equation (5.17).

$$I_{DC,G} = \frac{3}{2}\left(\frac{V_{G,q}I_{G,q}}{V_{DC}}\right) \tag{5.31}$$

Equation 5.31 provides a linear relationship between $I_{DC,G}$ and $I_{G,q}$ which can be used to build the transfer function for the DC-link and design the gains of the voltage PI controller. The block diagram of the DC-link controller is presented as follows:

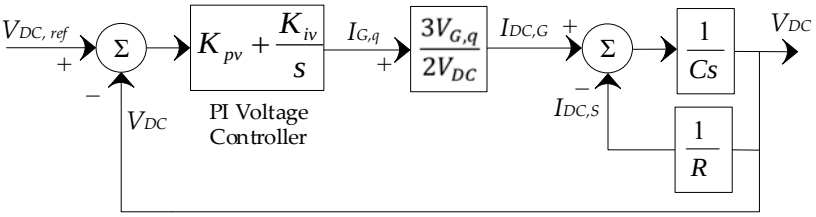

***Figure 5.17**. Reduced voltage control loop of PMSM – Generating mode*

Selecting the bandwidth of the voltage loop one order of magnitude smaller than the current loop simplifies open-loop voltage transfer function as follows:

$$TF_{OL,V} = \left(\frac{K_{pv}s+K_{iv}}{s}\right)\left(\frac{3}{2}\frac{V_{G,q}I_{G,q}}{V_{DC}}\right)\left(\frac{1}{Cs+\frac{1}{R}}\right) \tag{5.32}$$

The proportional and integral gains of the PI voltage controller can be determined by substituting the values of parameters C and R in Equation (5.32). Detailed calculation method for derivation of K_{pv} and K_{iv} is provided in Appendix D.

The gain parameters of the PI controllers in both charging and discharging states of the FESS can be determined based on the derived mathematical relations presented above. The designed parameters set the gains of the PI controllers in terms of electrical parameters of the electrical machine, power converters, DC-link and LC filter. However, for higher accuracy and better real-time performance of the system, the PI controllers are further tuned using MATLAB to compensate for any possible errors and the assumptions made in the design process.

Chapter 6 Modelling, analysis and results

This chapter describes the modelling and analysis of an islanded solar photovoltaic (PV) system with a backup diesel generator (DGen) providing power to a residential load. Typically, an electrical storage system would be integrated with a solar PV system in order to improve system efficiency and reliability. The most established choice of energy storage for such applications is electrochemical battery storage and particularly, the Lithium-ion type. It can provide services ranging from millisecond response for demand management to durations of hours required for backup storage and grid ancillary services. This has limited the high power, low storage technologies such as flywheels and supercapacitors competing with Li-Ion batteries. However, given the demand in residential premises and intermittent nature of the power produced from the PV system, the need arises for a fast response and high cycle storage also providing bulk services throughout the day. In addition, there is a desire to employ technologies that have lifetimes of over 20 years with low CO_2 in manufacture which is easily recyclable, unlike Li-Ion. It is proposed that flywheels with their attributes such as long calendar life, fast response time, high charge-discharge rates, and with low environmental impacts can be real contenders to Li-Ions in this application. It is here that the testing of this hypothesis is reported in terms of developing a control strategy, quantifying energy savings and assessing how the flywheel will perform as compared with a battery.

In this study, the choice of a flywheel storage system as an alternative to battery storage in an autonomous hybrid solar PV and diesel generator systems is analysed. The model of a combined islanded PV system, FESS and diesel generator supplying a dynamic variable load has been implemented in MATLAB/Simulink and the results are presented and analysed in detail. All system components including the PV system, diesel generator, FESS and the residential load are connected to a common DC bus for better utilisation of the energy and ease of control (*Figure 6.1*).

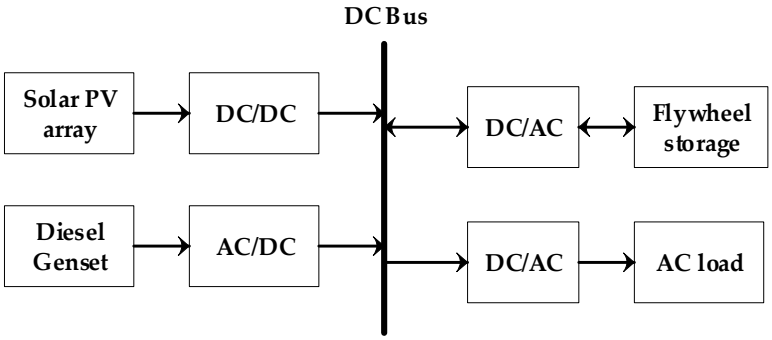

Figure 6.1. General configuration of a PV, DGen and FESS connected to a load via the DC bus

The connected AC load has been chosen to be a typical residential load with variable demand throughout the day so that the operation and communication between the available sources of energy (PV, DGen and FESS) are tested for close to real-life conditions. The load demand profiles were generated using CREST Demand Model, which is a high-resolution energy demand model for building occupancies at the residential level [156]. The load demand model is explained in greater detail in Section 6.5.

This chapter is divided into seven sections. The model of FESS implemented in MATLAB/Simulink is presented in section 6.1. The models of the diesel generator and solar PV system are discussed in sections 6.2 and 6.3, respectively. Section 6.4 describes the formation of the hybrid model. The residential load and creation of the demand profiles are described in section 6.5. Simulated results of the hybrid PV–DGen–FESS model are presented with the analysis in section 6.6 and the chapter is concluded with a discussion in section 6.7.

6.1 Flywheel energy storage model

The detailed analysis of the aerodynamic and bearing mechanical losses associated with the operation of the flywheel system in vacuum conditions were presented in Chapter 4. The mathematical model, analysis and control of the PMSM–Flywheel was discussed in Chapter 5. Now, the model of the designed flywheel system developed in MATLAB/Simulink software tool is presented in this chapter.

Figure 6.2 shows a simplified model of the flywheel storage system consisting of a permanent magnet synchronous MG connected to an electrical grid via a DC link.

The torque command governs the motoring or generating states of the MG based on which the charging and discharging states of the flywheel is determined. The output generated signals indicate the electromagnetic torque and 3-phase stator currents of the MG as well as the state of charge (SOC) and stored energy of the flywheel storage system.

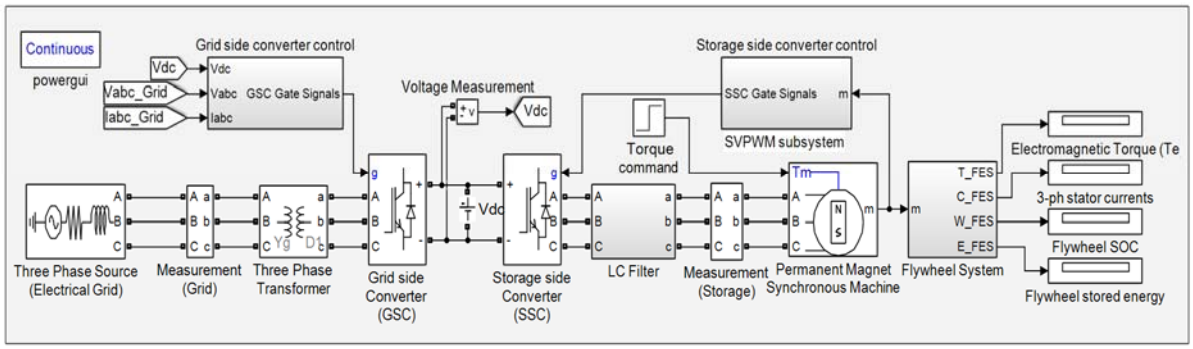

Figure 6.2. *Simplified model of a PMSM operated flywheel connected to an electrical grid*

There are two feedback controlling schemes in place to provide the means of communication between the flywheel and the grid and maintain the voltage level at the DC-link. The power flow from the grid side is controlled by switching the gates of the IGBT/Diode operated converter. The DC-link voltage and three-phase voltages and currents from the power grid are measured and regulated by comparing with respective reference values to generate the gating signals for the grid side converter (GSC). Similarly, the gating signals of the storage side converter (SSC) are generated through a feedback loop from the terminals of the PMSM. However, the controlling scheme of the SSC is more complicated because it has to maintain the DC-link voltage and control the speed of the flywheel during its charge, discharge and standby modes. This is implemented using SVPWM as shown in Figure 6.3.

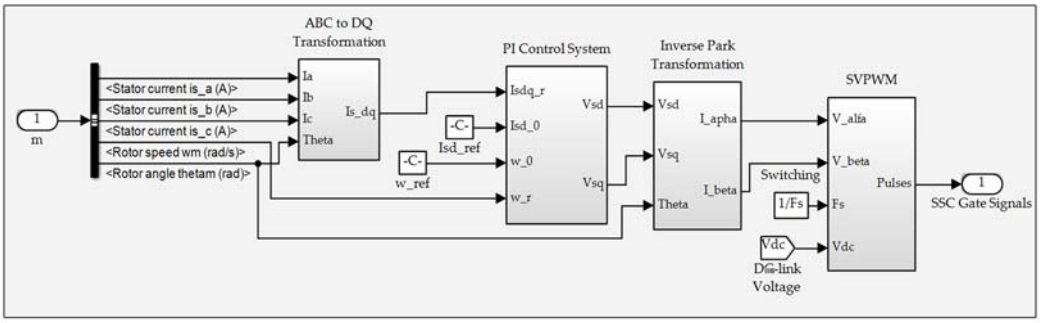

Figure 6.3. *Space vector pulse width modulation (SVPWM) subsystem*

Three-phase stator currents (*abc*) of the electrical machine are measured and converted to *direct-quadrature* (*dq*) axis currents. Then a PI controller is used to regulate the (*dq*) currents and rotor speed (ω_m) by comparing each with their respective reference values. This provides the reference voltage signals for the SVPWM technique, which also requires a switching frequency input and measured DC-link voltage to produce SSC gating signals. As a result, the voltage at the DC bus can be maintained by regulating the speed of the flywheel through the signals from the stator currents of the connected MG.

There are different topologies of connecting a FESS to a load or another source of energy. This simplified model is used as a generalised configuration for better exploration of the energy transfer from/to the flywheel using associated control schemes. Later in section 6.4, it is shown how the electrical grid is replaced with a combined solar PV and DGen system to represent an autonomous system.

6.2 Diesel generator model

The model of the diesel generator implemented in MATLAB/Simulink is shown in Figure *6.4*. This model is developed using the built-in Simulink blocks available in MathWorks computing environment [157]. The synchronous diesel engine is connected to an IGBT/Diode operated AC-DC converter to be controlled to maintain the voltage level at the DC bus when the engine is generating power. A synchronous diesel engine was chosen rather than a variable speed generator since it is most likely that this type of lower-cost device would be already available and the solar PV and FESS would be added to an existing system to reduce cost and avoid replacement of the entire system. The switching operation of the converter on the generator side is controlled based on the status of the voltage at the DC bus (V_{DC}) and the output voltages (V_{abc_Gen}) and currents (I_{abc_Gen}) of the diesel engine. Each parameter is measured and compared with its respective reference value to compensate for the errors using a PI controller. A similar control scheme was applied for controlling the switching mechanism of the GSC when connected to the FESS.

The MATLAB built-in synchronous machine block requires two inputs and produces multiple output signals that can be retrieved from BusSelector signal connected to the output of the machine. The set of inputs are the field voltage and either a reference input mechanical power (P_m) or rotor speed reference (ω_m). *Figure 6.5* shows the list of output signals generated at the terminals of the machine on the left and the selected output signals for display on the right.

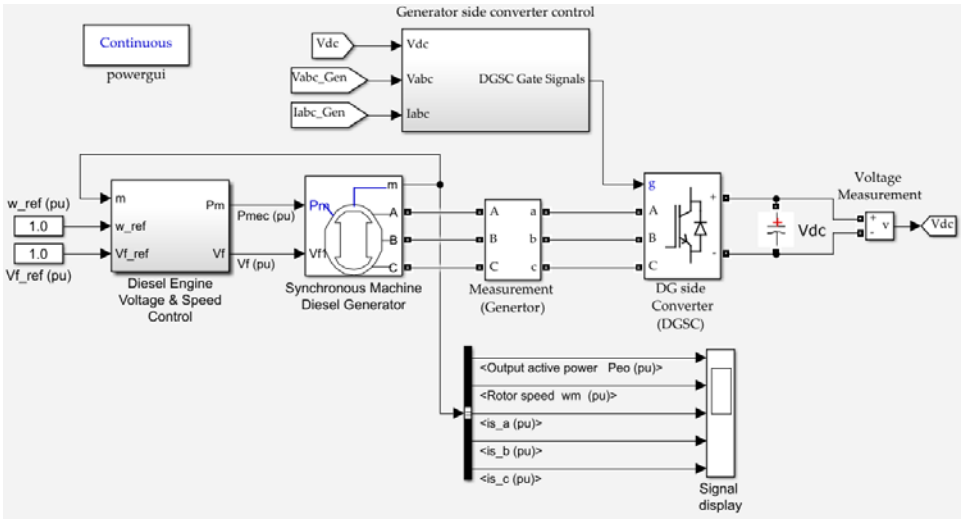

Figure 6.4. *Diesel generator model with AC-DC converter*

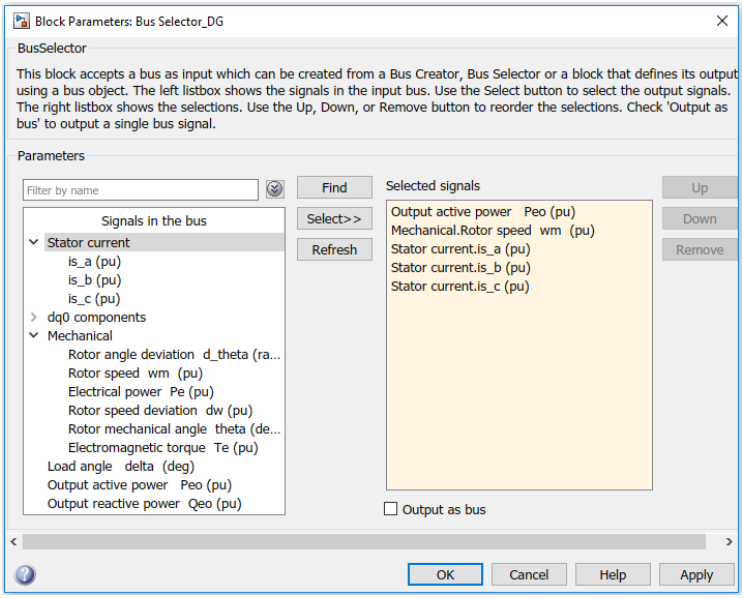

Figure 6.5. *Output signals generated by the synchronous diesel engine*

The operation of the machine is controlled by governing the speed and voltage of the machine through a feedback loop from its output terminal. The rated values of the speed and voltage are set as reference and compared with their respective measured

values retrieved from the feedback loop. The error in each case is regulated to produce the machine inputs (*Figure 6.6*).

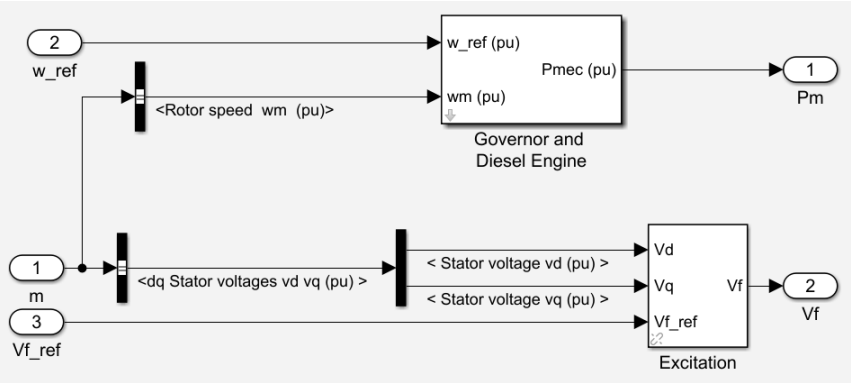

Figure 6.6. *Diesel engine speed and voltage control subsystem*

The excitation field voltage (V_f) of the machine is generated by comparing the *measured* (*dq*) voltages of the stator with the *reference* field voltage (V_{f_ref}) and regulating the *error* using a PI controller. Similarly, the *measured* rotor speed is compared with the *reference* rotor speed and *error* is regulated using a PI controller as shown in *Figure 6.7*. Then the regulated output of the speed PI controller is used to calculate the machine torque and hence the input mechanical power (P_m).

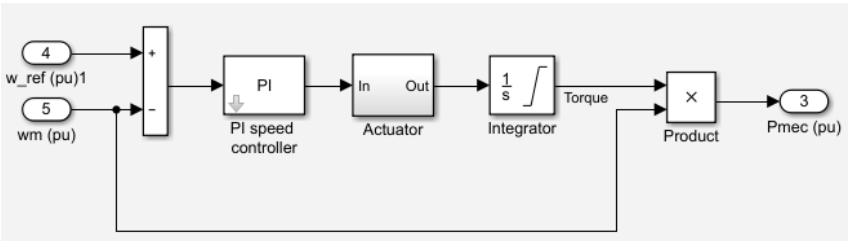

Figure 6.7. *Diesel engine governor subsystem*

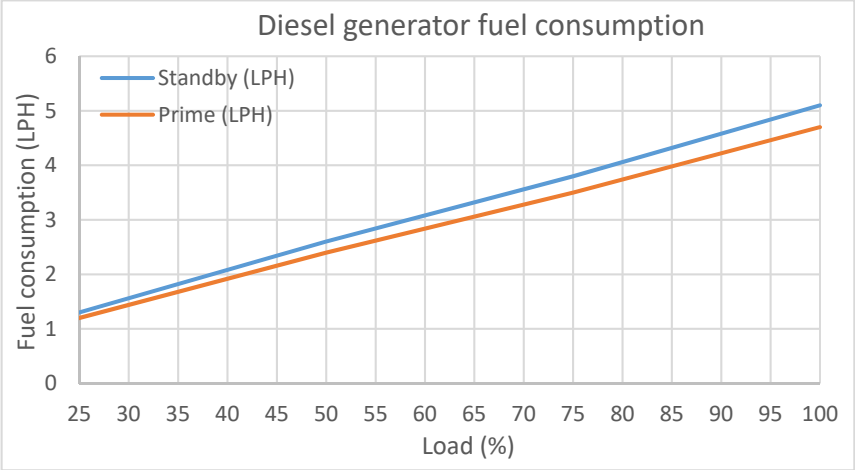

Figure 6.8. *Diesel engine fuel consumption relative to the load*

The diesel engine model can be connected to an AC or a DC load, however, it is integrated to the PV system and flywheel at the DC-link which serves as the point of common coupling between the energy sources and the load. The fuel consumption of the diesel engine relative to load for standby and prime conditions is shown in *Figure 6.8*. Full specification sheets of the diesel generators are provided in Appendix E.

6.3 Solar PV system model

The model of a solar PV array system connected to the DC-bus through a boost DC-DC converter is shown in Figure 6.9. The MATLAB/Simulink built-in PV array block requires the sun irradiance (W/m^2) and cell temperature ($deg.C.$) as inputs and produces PV voltage ($V_{\_PV}$) and PV current ($I_{\_PV}$) as outputs. The parameters of the PV module can be user defined or selected from a wide range of pre-set modules from National Renewable Laboratory (NREL) System Advisor Model. Further details on the mathematical model and the internal circuit of the PV module is available on the MathWorks website [158].

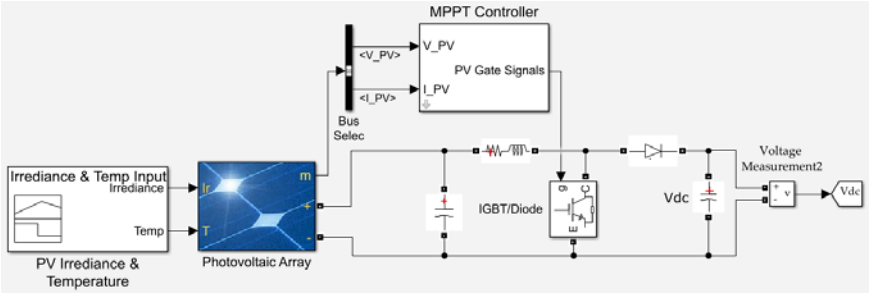

Figure 6.9. *Model of solar PV array system with a boost DC-DC converter*

An important feature of MATLAB's PV array system is that it generates current-voltage (I-V) and power-voltage (P-V) characteristics plots based on a specified irradiance and temperature level. This can be generated for one cell or for the entire array of cells connected in parallel. *Figure 6.10* shows I-V and P-V characteristics of one module for different irradiances of 100, 500 and 1000 (W/m^2) at a constant 25°C. The parameters of the selected PV module are presented in *Table 6-1*. It can be seen that the current rating of the module stays constant until the maximum voltage of 39.8 V is reached. Then the current drops for higher voltages beyond 39.8 V indicating that the maximum power is produced at this particular voltage level. This shows the

importance of maximum power point tracking (MPPT) and how the P-V characteristic graph allows determination of the corresponding current and voltage magnitudes at the maximum power production level.

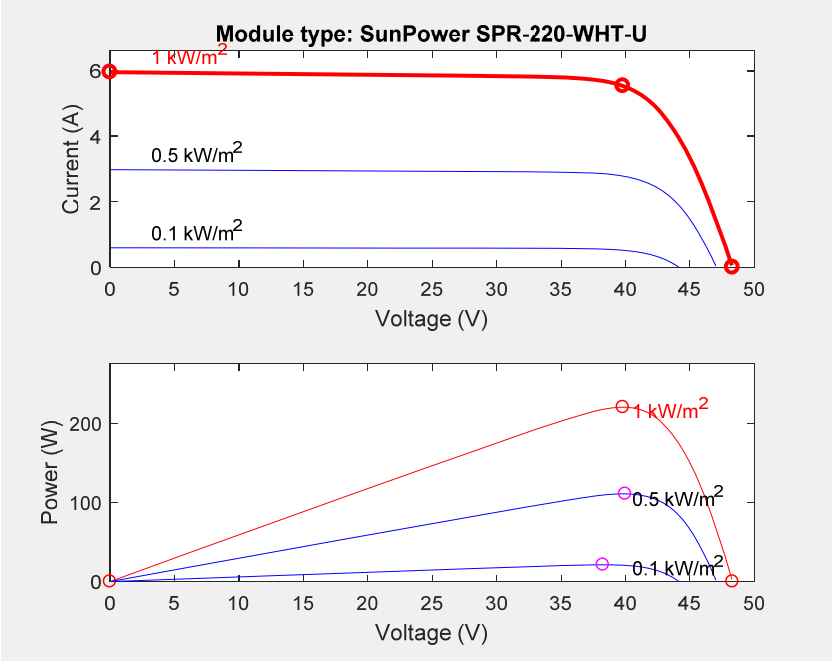

Figure 6.10. *I-V and P-V characteristics of one module at 25°C and specified irradiances*

Table 6-1. *SunPower SPR-220-WHT-U PV module parameters*

Parameter (unit)	Value
Maximum power (W)	220.094
Open circuit voltage (V)	48.3
Voltage and maximum power point (MPPT) V_{mp} (V)	39.8
Current at maximum power point (MPPT) I_{mp} (A)	5.95
Short-circuit current Isc (A)	5.95

The characteristic plots of I-V and P-V generated for 12 parallel strings each with 7 series modules are shown in *Figure 6.11*. The waveforms are equivalent to the one module plots but the voltage and current ratings are for the combined 72 modules (7 series x 12 parallel). Each module produces 220 W producing a total power of nearly 15.8 kW for 72 modules as can be seen in the lower graph (*Figure 6.11*).

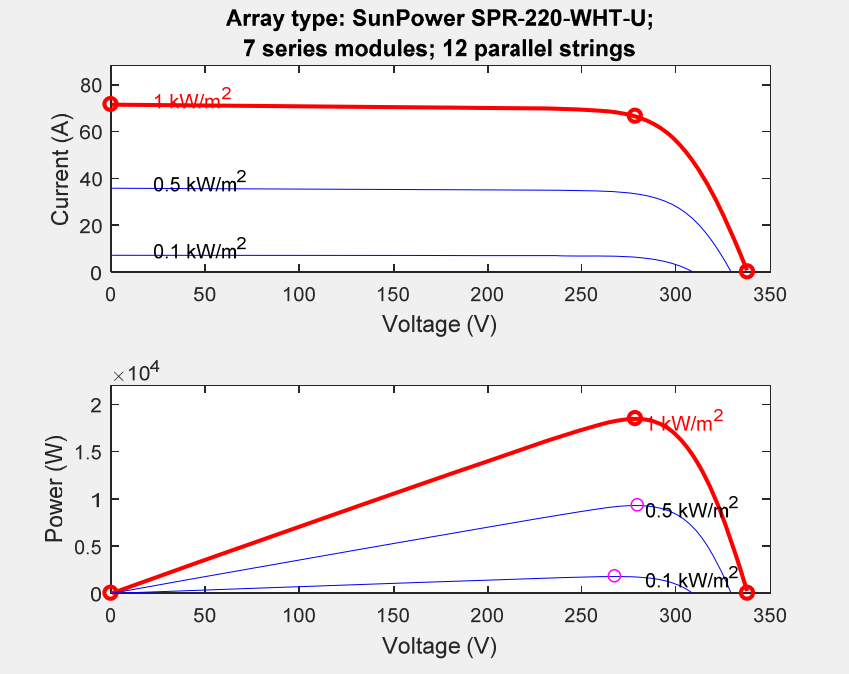

Figure 6.11. *I-V and P-V characteristics of 12x7 PV arrays at 25°C and specified irradiances*

The characteristic plots for constant irradiance of 1000 (W/m^2) and variable temperatures of 25, 45 and 60°C are presented in *Figure 6.12*. It is interesting to see that the power generation below a certain voltage level (i.e. 200V) is the same for all temperature levels; however, the modules with lower temperature level have a higher level of MPPT and vice versa.

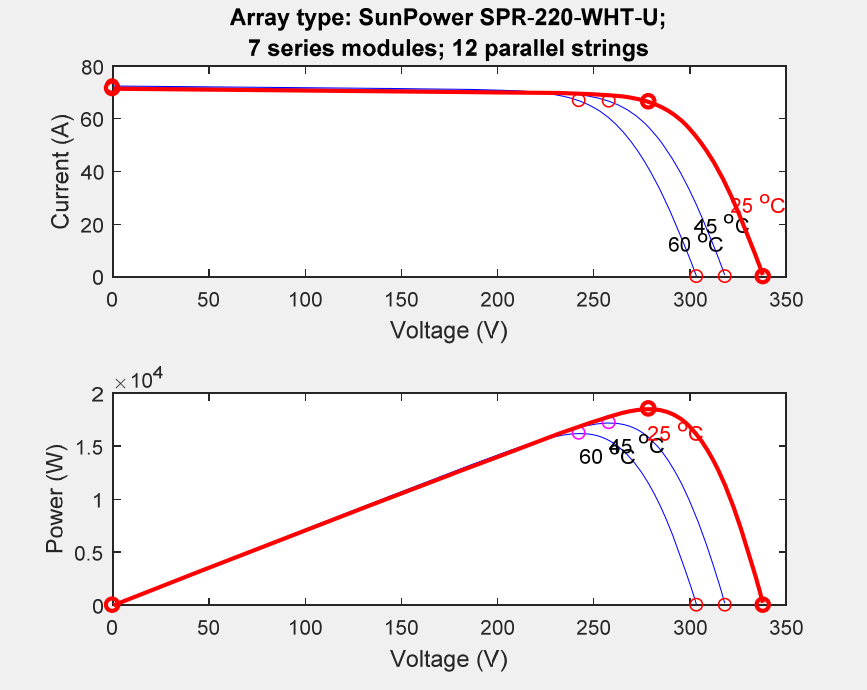

Figure 6.12. *I-V and P-V characteristics of 12x7 PV arrays at 1000 (W/m^2) & specified temperatures*

Considering the P-V characteristics of the PV module and significance of the MPPT in maintaining the voltage at the DC-bus, an MPPT controller is essential to provide the gate signals for the IGBT/Diode switch of the boost converter (*Figure 6.9*). The MPPT controller measures the voltage and current of the PV module and uses an integral regulator to minimise the error. The regulator output produces a duty cycle correction which is compared with an initial reference duty cycle as shown in *Figure 6.13*. Finally, the calculated duty cycle is provided as an input to a PWM generator to provide switching pulses for the boost converter (*Figure 6.14*).

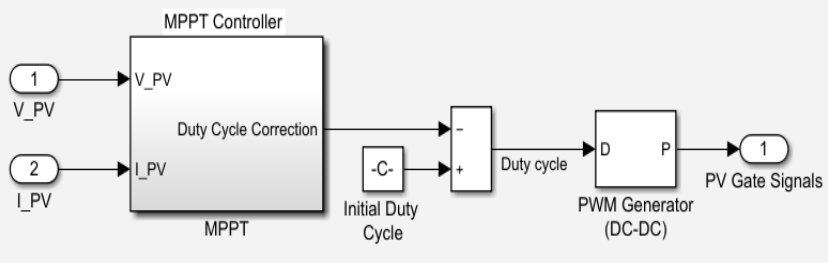

Figure 6.13. *PV module MPPT controller subsystem*

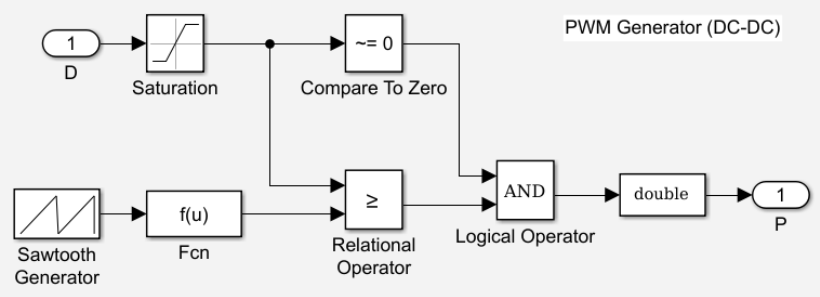

Figure 6.14. *PWM generator subsystem*

The PV module in this section is adapted from the existing PV array examples available in MathWorks [158]. The MPPT controller presented here is developed using "Incremental Conductance" technique [159]. The mathematical relationships in developing the PV model and associated MPPT control is not the scope of this thesis and is not described here. Details of the PV model and a variety of MPPT controlling techniques are addressed in references [160, 161].

6.4 Solar PV – DGen – FESS hybrid model

The simplified model of the standalone hybrid solar PV array with backup diesel generator connected to a FESS is shown in Figure 6.15. The model is implemented in

MATLAB/Simulink showing the interconnection of the hybrid system to a DC-link serving as the point of common coupling between the load and the hybrid system. The hybrid model is developed based on the controlling schemes and standalone models of the flywheel, PV system and diesel generator discussed in previous sections. The main difference here is that the model of the flywheel system previously connected to an electrical grid (see Figure 6.2) is now connected to the solar PV system serving as the main source of energy supply. The set of parameters for each subsystem is provided in *Table 6-2*. The parameters of the PV system are selected from the NREL system advisor models available in MATLAB. The diesel generator parameters are based on the manufacturer's data sheets provided in Appendix E and the PMSM parameters are provided by the manufacturer but cannot be referenced for reasons of confidentiality.

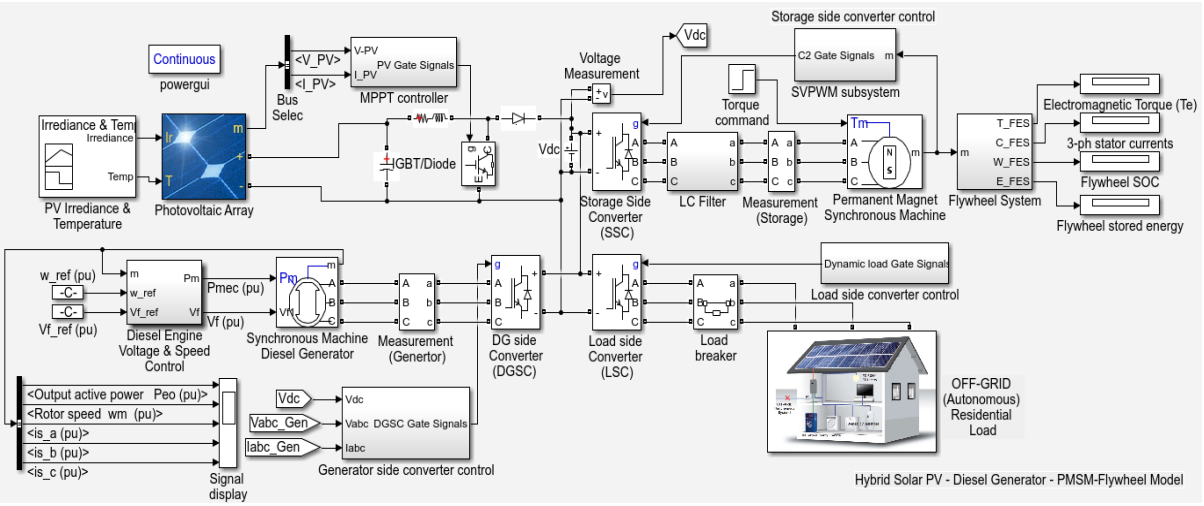

Figure 6.15. *An autonomous PV-DGEN-FESS hybrid model connected to a residential load*

The connected dynamic three-phase load is updated on a timely basis from a lookup table that stores the energy consumption data of residential households. Full details of the load with an in-depth description of the development of the load model is discussed in the next section.

Table 6-2. *Parameters of the hybrid FESS-PV-DGen model*

Energy source	Parameter	Value (Unit)
PMSM-FESS	Stator resistance	0.20 (Ω)
	Armature inductance ($L_d = L_q$)	0.0438 (H)
	Inertia	11 ($kg.m^2$)
	Number of poles	2 (poles)
	Power rating	10 (kW)
	Energy storage rating	5 (kWh)
	Input voltage	380 (V)
	Rated frequency	417 (Hz)
	Inverter switching frequency	10 (kHz)
	Filter damping resistance	0.75 (Ω)
	Filter capacitance	40 (μF)
	Filter inductance	0.64 (mH)
Diesel Generator (Synchronous Machine)	Nominal power	15 (kW)
	Line-to-line voltage	380 (V)
	Rated frequency	50 (Hz)
	Number of poles	4 (poles)
Solar PV array (2 parallel strings x 10 series-connected modules per string)	Sun Power SPR-315E-WHT-D NREL System Advisor Model	
	Maximum power	315 (W)
	Open circuit voltage	65 (V)
	Voltage at maximum power point	54.7 (V)
	Current at maximum power point	5.76 (A)
	Sun irradiance	500 (W/m^2)
	Cell temperature	40 (deg. C)
	DC-link voltage	600 (V)

The main contribution in developing the hybrid model in *Figure 6.15* is the design and development of the energy storage part and the residential load model – both discussed in detail in sections 6.1 and 6.5, respectively. The model of the flywheel system is developed based on the mathematical relations derived for dynamics of the system in Chapter 2 and the aerodynamic and bearing system losses calculated in Chapter 4. The mathematical modelling and control of the FESS during charge-discharge conditions and the development of the SVPWM model is also another important contribution of this thesis. Except for the permanent magnet synchronous MG which is selected from MATLAB Simscape's built-in library, the entire model of the flywheel storage including the LC filter is designed from scratch. The model of the residential dynamic load and control of the load side converter have also been designed and implemented in this work. In addition, control of the PV system's DC-DC boost converter using MPPT as well as control of the diesel generator side

converter have also been modified and integrated to the FESS through a DC-link, which allows reliable operation of a hybrid PV-DGen-Flywheel system. The Simulink blocks for synchronous machine diesel generator, photovoltaic array, DG side converter and load side converter have all been selected from Simscape library.

6.5 The residential load model

The Centre for Renewable Energy Systems Technology (CREST) at Loughborough University has developed a high-resolution stochastic model of integrated electrical-thermal demand at the domestic level. The freely downloadable model calculates electrical demand based on appliances, lighting demand, and active resident occupancy [156]. To account for load variations and random load spikes, the model uses a bottom-up approach to create "spikiness" from simulation of switching the appliances *on* and *off*. Similarly, the natural behaviour of occupants in using the appliances at home is determined based on UK time-use survey data [162]. The data is used to create stochastic profiles of dwelling occupancy in order to consider different states such as the residents can be at home and active, at home and asleep, or away from home and active. An 'active profile' represents the likelihood of occupants undertaking variable activities throughout the day, which is naturally related to the use of appliances and hence the electrical demand [163]. The key parameters required for generating the load profiles are day of the month, month of the year, type of the day (weekday or weekend), number of dwellings and the total number of residents in a single dwelling unit. Figure 6.16 and Figure 6.17 show typical load profiles in February generated for ten dwellings each with five residents. Typically there are two peak times during the course of 24 hours where the time of the peak is generally dependent on the type of the day - whether a weekend or a weekday. The first peak time on a weekday starts early morning where the occupants wake up early and are mostly active until they leave the house. The second peak time occurs when the occupants return home and are quite active for the next three or four hours (Figure 6.16). However, the peak times on a weekend are pretty much shifted and the

occupants typically wake up late and sleep late. Also, the load distribution is quite irregular throughout the day and the occupants are active but perform different tasks at different times (Figure 6.17). The energy consumption on a weekend is also higher in comparison to a weekday given the occupants are mainly at home.

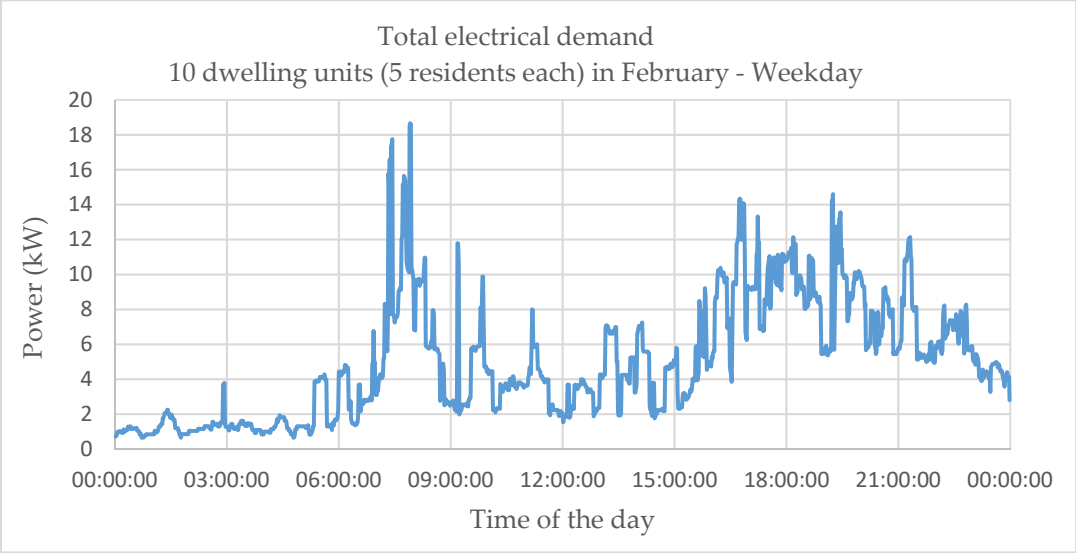

***Figure 6.16**. Total electricity demand for 2 dwelling units on a weekday in February*

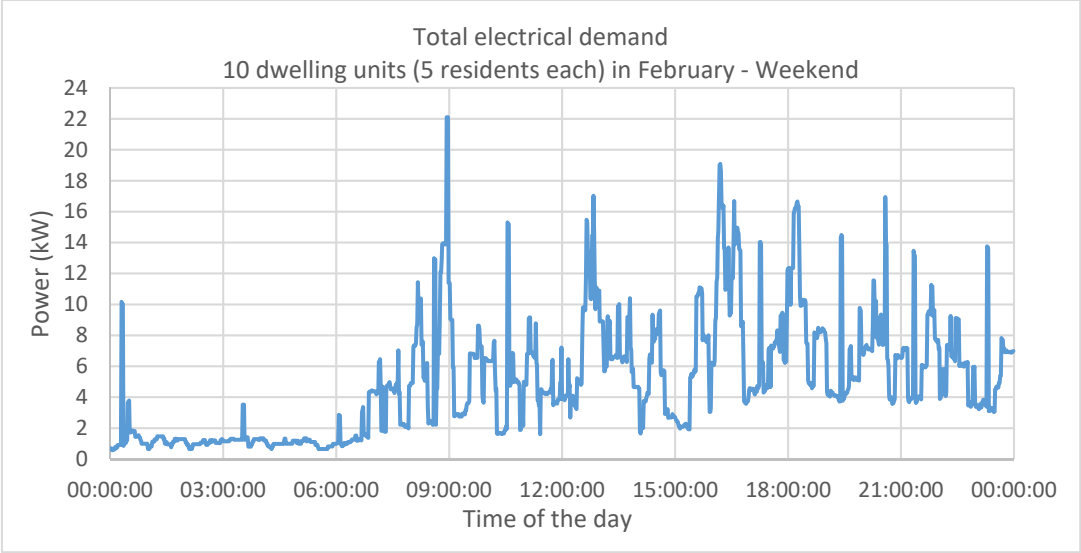

***Figure 6.17.** Total electricity demand for 2 dwelling units on a weekend in February*

Considering the load pattern described earlier, three different load demand profiles were created using CREST demand model to study and analyse the dynamic performance of the hybrid FESS, PV and DGen system while providing power to each of the load demands. The load profiles - generated for the weekends and at different

times of the year - demonstrate total electrical demand for ten dwellings each with five residents. The weekend is selected since the total demand for a weekend is usually higher compared to a weekday and also the load peaks and load spikes are inconsistent and unpredictable as they occur at different times of the day and do not follow any specific pattern. Hence the designed system will be tested under extreme conditions and for worst-case scenarios. For ease of analysis and a better comparison of the results, a duration of 3 three hours is considered for each case. From each load profile, the peak times with the highest load demand and more frequent load variations are selected for analysis.

a) Load profile 1

Profile 1 represents total electrical demand for 10 dwellings on a January weekend (Figure 6.18). The morning peak demand starts to increase after 8 am and will diminish at 1 pm. The afternoon peak demand starts at 3 pm and lasts until 8:30 pm including a random spike at around 7 pm. The load demand for a duration of 3-hours between 17:30 – 20:30 is selected for analysis (Figure 6.19). This includes 15 kW peak demand during which the performance of the hybrid system will be of quite an importance.

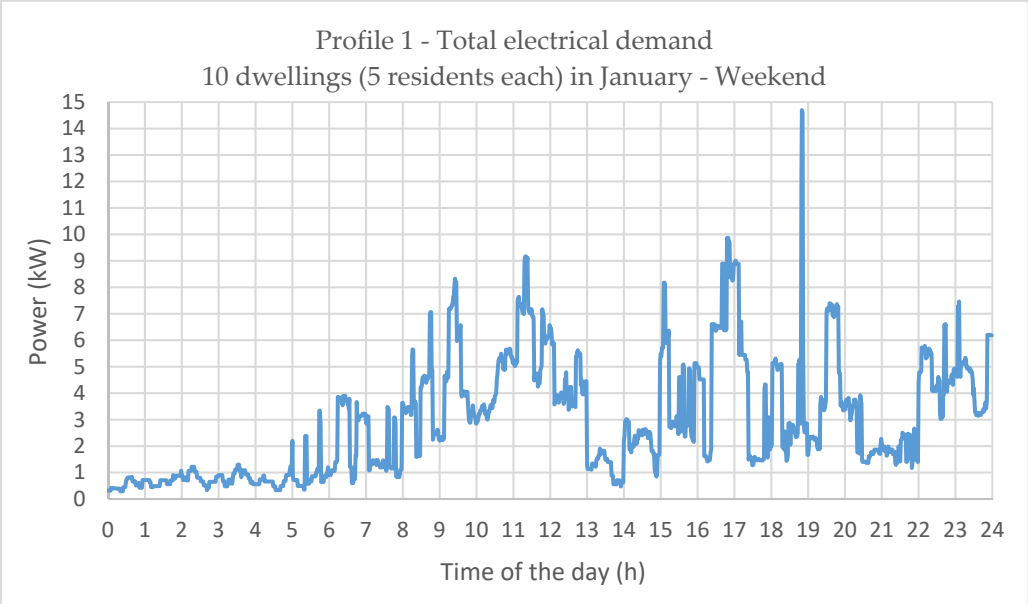

Figure 6.18. *24 hour total electrical demand – Profile 1*

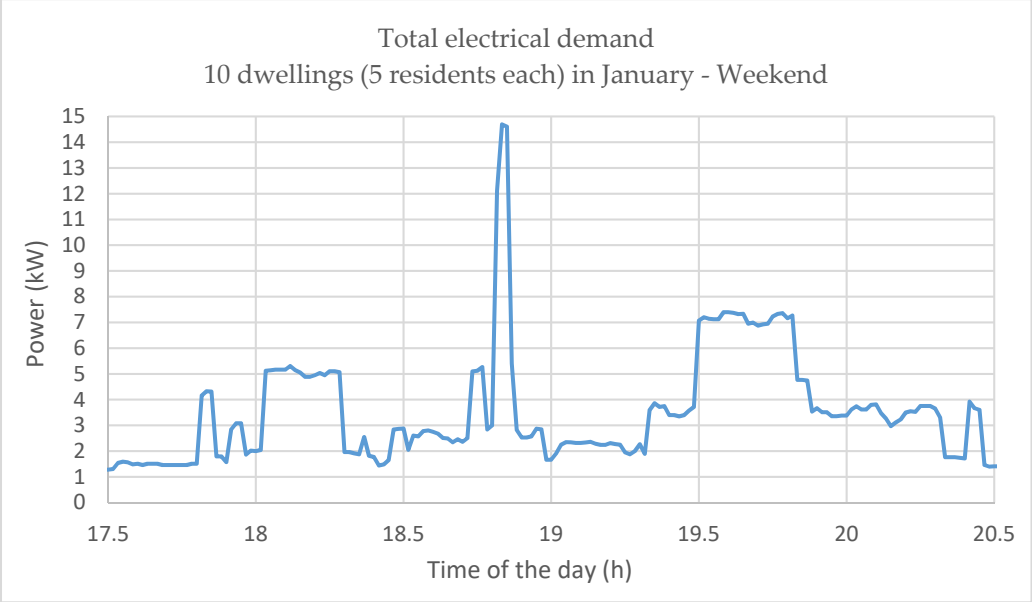

Figure 6.19. *3-hour (17:30 – 20:30) total electrical demand – Profile 1*

From the perspective of the solar PV system or diesel generator, it will be a challenge to provide energy for this type of load (especially during the afternoon peak). The average demand for this load profile is about 5 – 6 kW but the PV system and the diesel engine must be designed for the maximum load of 15 kW even though it lasts for a short period of only 5 minutes. This is when integration of a storage system becomes important and FESS suits best for such conditions providing bulk power in a short duration.

b) Load profile 2

Profile 2 represents total electrical demand for 10 dwellings on an April weekend (*Figure 6.20*). This profile is relatively different to profile 1 because the peak times last longer and are relatively scattered throughout the day. The morning peak lasts between 9 am and 3 pm while the afternoon peak starts at around 3 pm and lasts until 10 pm. The average load demand is also higher in the afternoon peak and therefore, the 3-hour peak time between 3:30 pm and 6:30 pm is selected for analysis (*Figure 6.21*). During this time, the load profile experiences the most fluctuations and the highest peak demand also falls within this period. Hence the energy source, whether it is going to be a PV system, a DGen, a FESS, or a combination of these, will be hardly resting.

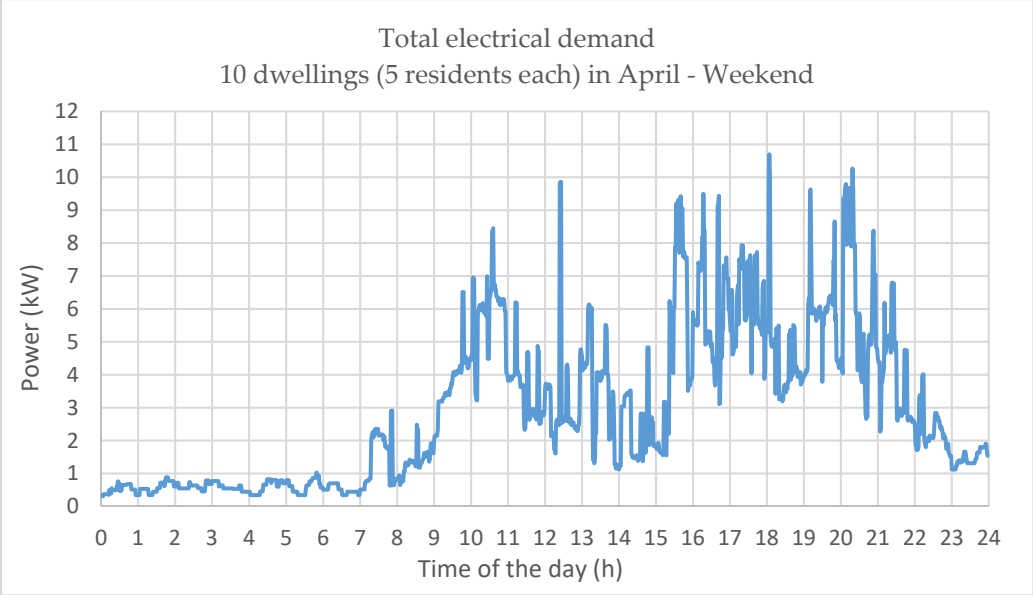

Figure 6.20. *24 hour total electrical demand – Profile 2*

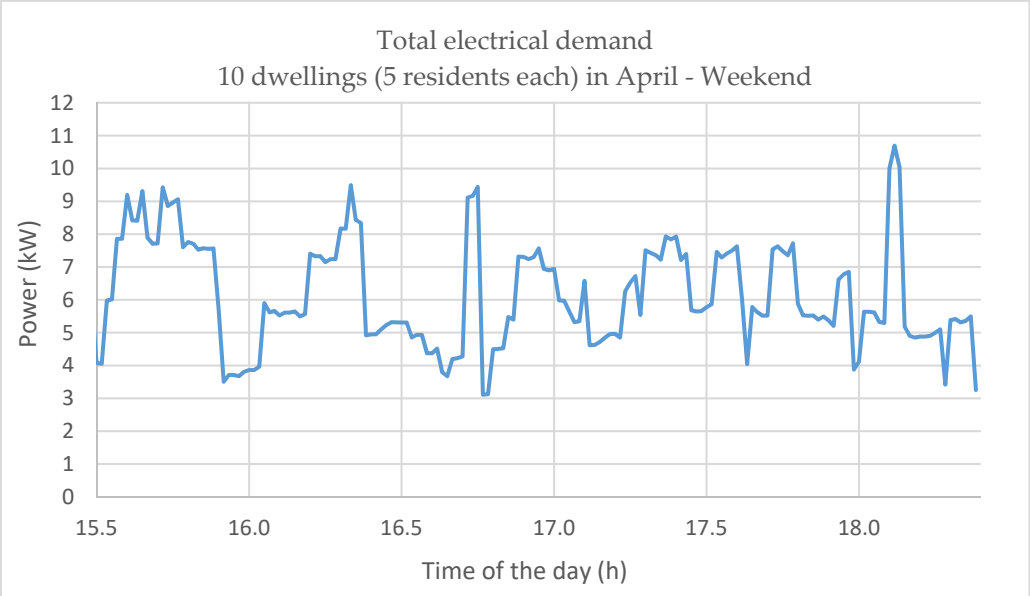

Figure 6.21. *3-hour (15:30 – 18:30 pm) total electrical demand – Profile 2*

c) Load profile 3

Figure 6.22 shows load profile 3 representing the total electrical demand for 10 dwellings on a weekend in August. Opposite to load profiles 1 and 2, the load demand is distributed in three peaks each with a different pattern and time distribution. The morning peak starts early and lasts approximately 2 hours with two sharp spikes reaching a maximum of up to 15 kW. The demand starts to increase again after 10:30 am and descends back at 12 pm. The afternoon peak demand lasts longer (4 pm – 12 am) with numerous load fluctuations, which is quite similar to the afternoon peak

demand for load profile 2. Hence, the designed system will be tested for a similar situation under load profile 2, but with higher peak demands with longer durations. Therefore, the morning peak demand between 6:00 – 9:00 am is considered for analysis (*Figure 6.23*).

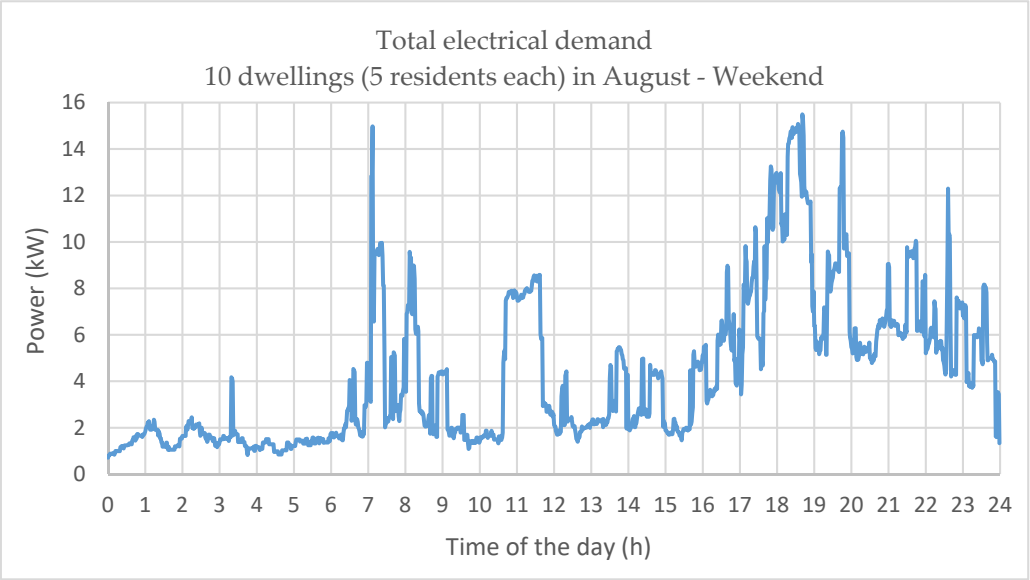

Figure 6.22. *24 hour total electrical demand – Profile 3*

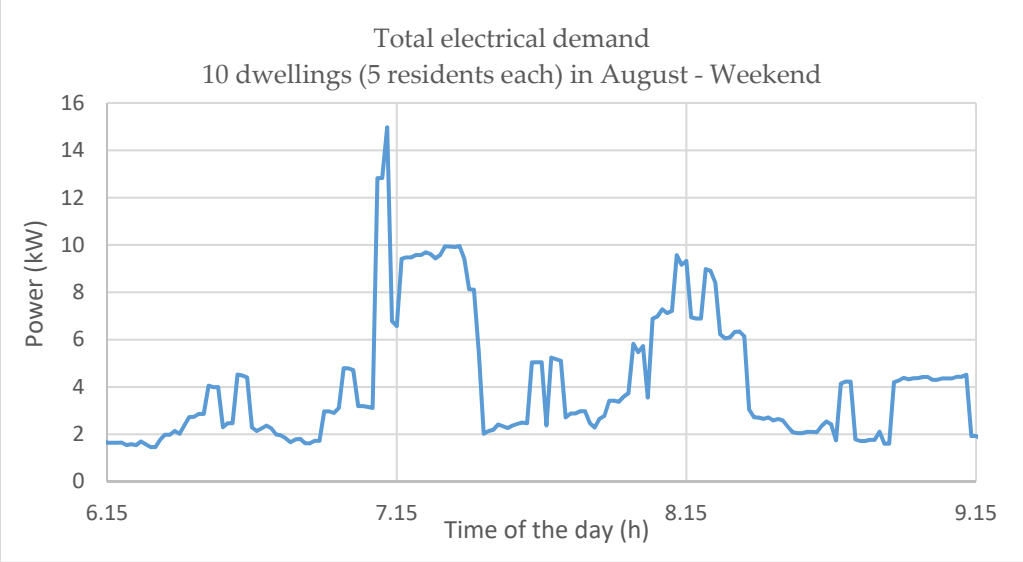

Figure 6.23. *3-hour (06:15 – 09:15 am) total electrical demand – Profile 3*

Considering the generated load profiles and referring to *Figure 6.1* where the load is connected to a common DC bus between the DGen, PV system, and FESS, it will be interesting to test the operation and dynamic performance of the system in supplying

energy to these load demands. This is implemented under three different energy supply strategies discussed as follows:

6.5.1 Strategy 1

In this strategy the PV system and the DGen are considered to share the load demand with no storage in place. It is assumed that the days are sunny and the PV source can continuously produce power where any outside disturbances such as a change in irradiance due to a cloud pass, temperatures changes, system failure, etc. are ignored. The PV panels will generate a constant power to supply an average load demand and any sharp peaks including load variations above the specified average rating will be covered by the backup diesel generator. The benefit is that the PV system will be reasonably sized to supply a constant load rather than a large and expensive system with multiple solar panels to match the maximum load demand. Similarly, the DGen will operate as a backup with the aim to help reduce fuel consumptions. For a fair comparison between load profiles 1, 2 and 3, the power ratings of the PV and the diesel engine will be considered the same in all cases. The power rating of the PV system is designed for 6 kW to supply the average load and the diesel generator is designed to produce 15 kW to account for the maximum load demand for all load profiles.

There are many disadvantages of a standalone PV- DGen system that can be improved with the introduction of an energy storage system. The diesel generator will not run efficiently as it has to be designed for the maximum demand load and must catch up with the load variations going up and down. When turned off, it does not come on instantly meaning that there is a possibility for load curtailment since solar PV system cannot be entirely relied upon due to partial or fully cloudy days. Therefore, the customers will most likely experience power outages - at least during the transfer of power from PV to DGen and vice versa. In addition to the technical issues, the operation of diesel engines has environmental and economic impacts due to CO_2 emissions and cost of fuel consumption, respectively. Introduction of a storage system will not only help with the technical issue but also reduce the negative impacts to a certain level.

6.5.2 Strategy 2

In this strategy the impact of the integration of FESS - as a storage system - into the combined diesel generator and solar PV system is investigated. It is believed that the introduction of the flywheel will improve overall system reliability by taking the load off the generator as well as filling the gaps between the supply and demand due to any system instabilities.

Similar to strategy 1, the PV system is sized to supply the average load and charge the storage device when there is excess energy available. The load above the average rating is initially covered by FESS and the diesel generator will be turned off for fuel savings. It will come on only when the power source from either of the PV system or FESS is not available. For example, the flywheel is already discharged and the PV system cannot provide power due to a cloud pass or when the load demand is above its maximum rating. Considering this, the storage device will come on and off multiple times during the day which will suit flywheel applications.

As for strategy 1, both PV and DGen will have the same maximum power ratings of 6 kW and 15 kW, respectively. If the load is greater than 6 kW, the FESS will take over from PV and start discharging to supply the demand. In occasions where the load is less than 6 kW and the flywheel is fully charged, the flywheel will switch to standby mode. If both PV and FESS fail to supply the load, the generator will come on. It will turn off as soon as the power is available from either of the PV or FESS sources. The flywheel is a C2 rating type with 10 kW PMSM integrated MG capable of storing 5 kWh when operating between 10,000 – 20,000 rpm. Therefore, it can provide power to the load when it is between 6 kW – 15 kW. The power transfer flow chart of the hybrid FESS, PV and DGen system for strategy 2 is shown in *Figure 6.24*. Typically, the flywheel is operated between a minimum and maximum speed (i.e. a third to a half its full speed) for better utilisation of its useful energy and to keep a reasonable size of the MG. This allows the system spinning by means of a small input power to make up for the system parasitic losses. Therefore, the fixed speed for standby mode is chosen

to be the speed at which the flywheel is at 50% SOC to allow an equal amount of energy to be stored or released in the case that it is not clear which will be required.

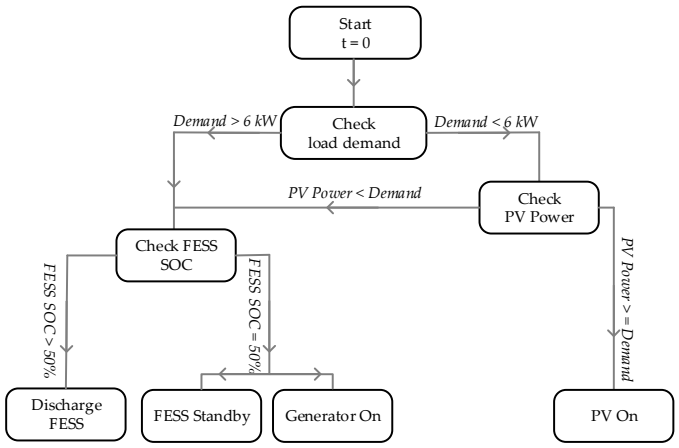

Figure 6.24. *Flow chart of FESS, PV and DGen power transfer - strategy 2*

In a more sophisticated control system where the state of other power generating elements is known, the standby speed can be changed and will depend on the state of other elements. The control algorithm of the hybrid model can be improved by using some optimisation techniques such as bi-level optimisation. For the ideal operation of the hybrid system incorporating flywheel energy storage, selection of the charge-discharge states of the flywheel system needs to be optimised based on non-linear power flow constraints. The optimal selection of the energy sources (solar PV, DGen, or FESS) in supplying the load is the main objective, however, reducing the cost and carbon emissions of the system while satisfying the load demand and avoiding any violations of the power flow constraints adds complexity to the system and cannot be addressed using the simplistic approach applied here. It requires a detailed analysis using an optimisation technique which is left for future work.

6.5.3 Strategy 3

In the previous two strategies for energy transfer, the solar PV system was considered to be operating under ideal conditions with no major interruptions during the day. However, this is not always the case in real-life situations as there will be occasions where the PV cannot produce power due to low irradiance. In strategy 3, the worst-case scenario is considered and it is assumed that the PV system is not available and

the load demand must be shared between the backup diesel generator and flywheel storage system. To help reduce the load on the generator and improve its efficiency, there are a number of possibilities to implement a charge-discharge strategy for the flywheel as described below:

6.5.3.1 Scenario 1

Initially the flywheel is fully charged and the generator is turned off. First, supply the load by discharging the flywheel until it reaches 50% SOC. Then turn on the generator to supply the load and recharge the flywheel. Once the flywheel charge reaches a certain level, it can switch to standby mode or discharge again to turn the generator off for fuel saving. This charge-discharge process can be continued until an alternative source of energy is available. The advantage is that the generator can operate at constant power and will be turned off when the flywheel is providing power. However, the downside is that the generator must be able to supply the load and charge the flywheel simultaneously- implying that it must be able to generate at least 25 kW (15 kW maximum demand plus 10 kW for charging the FESS)- which is not going to be an ideal solution especially during high demand periods.

6.5.3.2 Scenario 2

Operate the diesel generator within a maximum and minimum load range where the flywheel will be used to meet the demand outside this range. The flywheel will come on when the load is below the minimum or above the maximum operating range of the generator. This will improve the efficiency of the generator as it is not following the load variations up and down, but the fuel consumption will be higher due to its continuous operation.

In this scenario the maximum operating range for the generator can be set to 5 kW since its maximum rating is 15 kW and 10 kW must be allowed for charging the flywheel. During the flywheel charging period, the total load on the generator will be 15 kW and this leads to generator operating at its maximum generating capacity – leading to lower efficiency and higher fuel consumption. The situation could be further complicated when the demand is above the rating of the generator but the

flywheel charge is at a minimum. It will lead to either a load interruption or the generator must operate beyond its specified rating to cover the demand. Also, there are times that the generator will be operating at its maximum but the demand is low and the flywheel is already fully charged. In this case, despite running efficiently at a lower rate, the generator will be producing excessive energy.

6.5.3.3 Scenario 3

In this scenario, as a combination of the previous two scenarios, the diesel generator will supply the average load and the flywheel will cover the peak demand – similar to strategy 1 when the baseload was supplied by the solar PV system. The generator will not produce excessive energy but will follow the load before the demand is above the average and the flywheel takes over. When the flywheel is on, the generator is turned off until the flywheel charge reaches 50% SOC or the demand is lower than the specified average. The main challenge here is when to charge the flywheel so the charging period does not fall at the same time with the maximum demand or peak interval. Therefore, an ideal charging period will be during low demand intervals when the load is less than 5 kW since the generator is rated for 15 kW and the flywheel power rating is 10 kW. The advantage of this scenario over scenarios 1 and 2 is that the diesel engine will operate well below its maximum generating capacity including the flywheel charging periods. Further, the generator will be turned off on some occasions for fuel saving. The downside is that the generator will not be able to provide power instantly when it is turned back on. Typically it will approximately take 15 seconds for a diesel generator to turn on and provide full power. This can be well managed by delaying the transfer of power supply from the flywheel to the generator. For these reasons, scenario 3 was used for the simulation and analysis of the energy transfer between the diesel generator and flywheel in the absence of the PV system.

6.6 Results and analysis

In this section the simulated results of the hybrid PV-DGen-FESS model connected to a residential load are presented and analysed. The dynamics and energy transfer of the system is studied under three different strategies where each strategy is considered for three load profiles. Therefore, the system performance is tested and analysed for nine scenarios indicating the power outputs of the flywheel, solar PV, and the diesel generator in supplying power to the load. Some other important parameters such electromagnetic torque and state of charge of the flywheel, three-phase voltages and currents of the diesel generator, the voltage output of the PV array, and voltage at the DC bus, are also presented to show the conformity of the model. However, the results are somewhat limited in terms of solar irradiance and simulation period during which the system performance is analysed. The analysis is performed under constant irradiance conditions by assuming that the PV system is not affected by irradiance intermittency such as a cloud pass and it can provide an average power during the sunny periods. Since the residential load is dynamically variable and the demand fluctuations are unpredicted, this assumption was made for ease of comparison between the dynamic performance of the PV system, the diesel generator and the flywheel storage in supplying power to the load. Otherwise, the analysis of the hybrid system will be quite complex to account for load fluctuations and irradiance intermittency at the same time. Another limitation was the simulation period, which was restricted to 3-hours in order to avoid MATLAB/Simulink run time error. Due to the complexity of the hybrid model involving a variety of MATLAB blocks as well as different converters with their corresponding power electronics switching, a compromise between simulation speed and accuracy had to be made. Since the system is studied during the peak load times, 3-hour simulation will be good enough to analyse the energy flow and performance of the hybrid model and compare the results.

6.6.1 *Strategy 1 – Diesel generator and PV system only*

Strategy 1 is applied when the total electrical demand is shared between the PV system and the diesel engine in the absence of an energy storage system. It is assumed the days are sunny and the PV array can produce power constantly to supply an average demand load of 6 kW. The load variations above 6 kW are covered by the backup diesel generator which is sized for the maximum demand load of 15 kW. The simulated results for each load profile are presented in the upcoming subsections.

6.6.1.1 Strategy 1 – Profile 1

Figure *6.25* shows the power outputs of the PV system and the diesel generator in supplying the load profile 1. This is a simple scenario since there are only two occasions that the demand is higher than 6 kW and the diesel engine is needed to turn on. The solar PV is catching up with the load until about t = 80 mins when the diesel generator comes on. The generator is on for less than 5 minutes and will switch off as soon as the load is below 6 kW. Next time the generator is called just after t = 120 mins to cover the supply shortage of approximately 2 kW (*Figure 6.25c*).

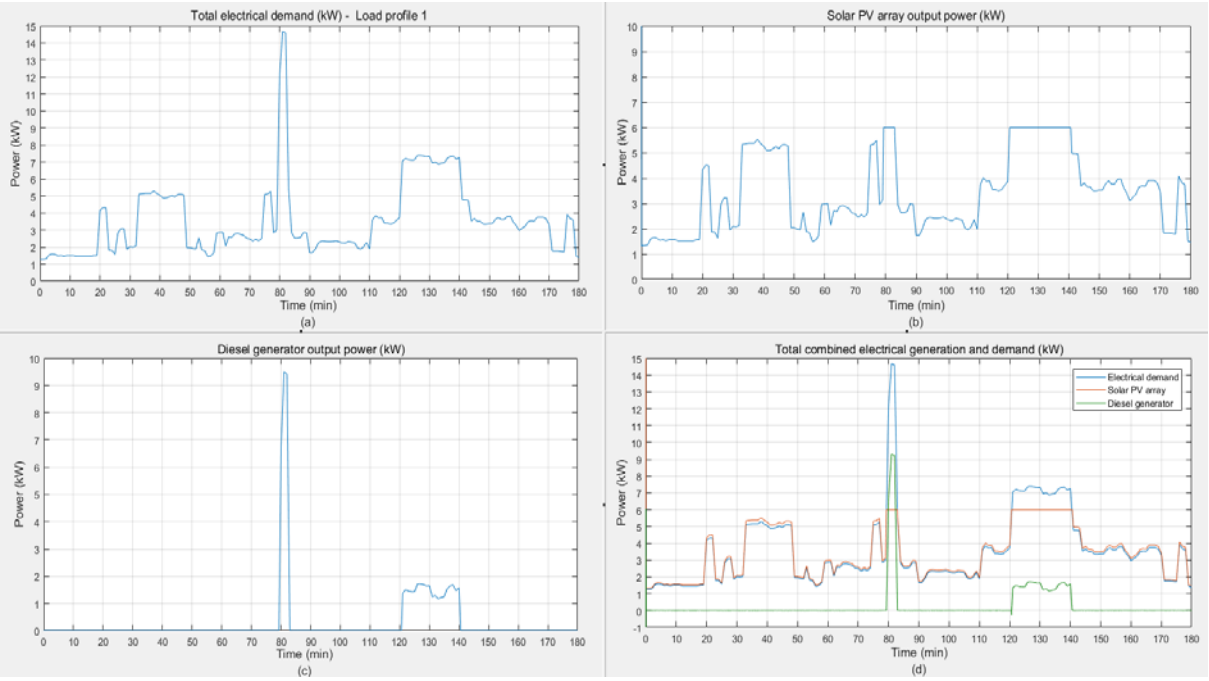

Figure 6.25. *Total electrical power (a) Load profile 1; (b) PV array; (c) Diesel generator; (d) Combined generation and demand*

The power curves in *Figure 6.25d* show how the PV system and the diesel generator share the load between them. The small discrepancy between the power

output of the PV and the load demand is because of the energy conversion losses of the system converters.

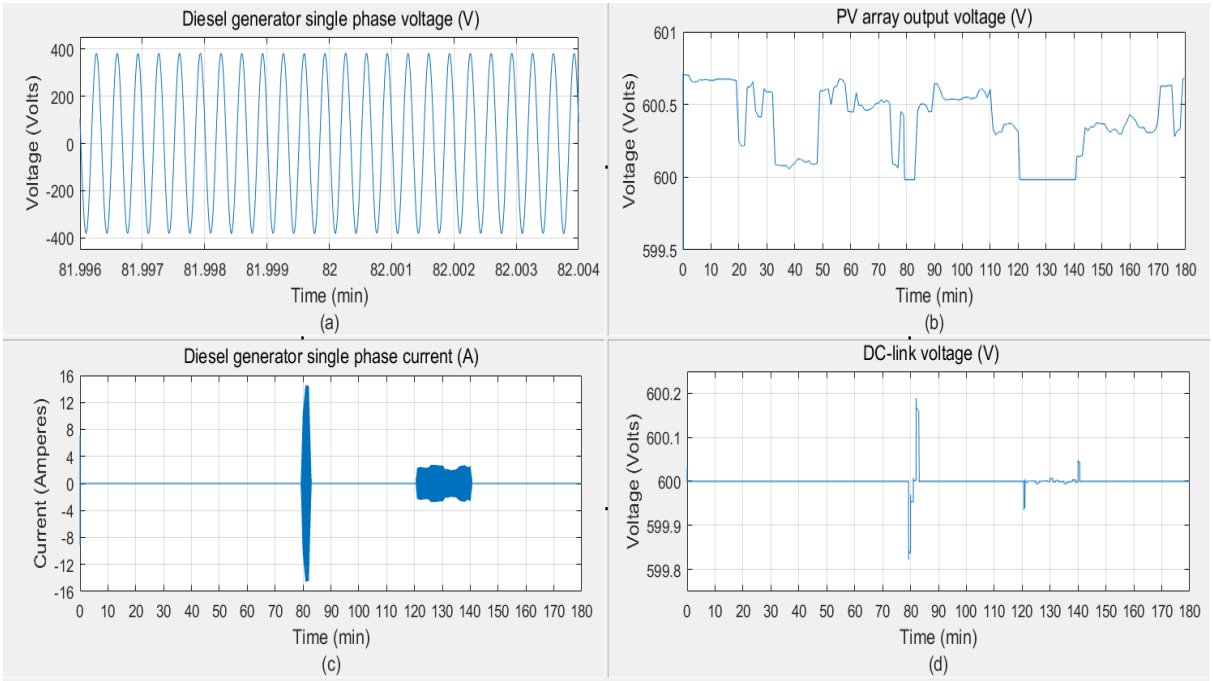

Figure 6.26. *System parameters (a) Diesel generator single-phase voltage; (b) PV array output voltage; (c) Diesel generator single-phase current; (d) DC-link voltage*

The system parameters showing the compliance of the currents and voltages of the generator and the PV system to their respective power output curves are shown in *Figure 6.26*. The generator output voltage stays constant at the instant the load is at maximum, whereas, the current waveform varies with respect to the power curve in *Figure 6.25*c (t = 80 mins). The PV array output voltage varies in accordance to load variations and is at minimum when the PV system is supplying a maximum of 6 kW. Some voltage spikes are generated during the times of transfer of power supply between the PV and the generator (*Figure 6.26d*), but these voltage variations are quite small and within ±0.2 V which is not a major concern. The DC-link voltage is mostly maintained at 600 V with a negligible percentage error.

6.6.1.2 Strategy 1 – Profile 2

The situation discussed for profile 1 is not usually present in real-life scenarios and, therefore, profile 2 is selected to analyse the system performance under an exacerbated and unfavourable demand condition with many peaks and spikes. The power outputs of the PV and diesel generator supplying power to load profile 2 is

shown in *Figure 6.27*. It can be seen that the generator is hardly rested and it turns on and off almost ten times in 3-hours. The PV system follows the load demand up to 6 kW where any supply shortage beyond the limit of the PV system is covered by the diesel engine (*Figure 6.27d*).

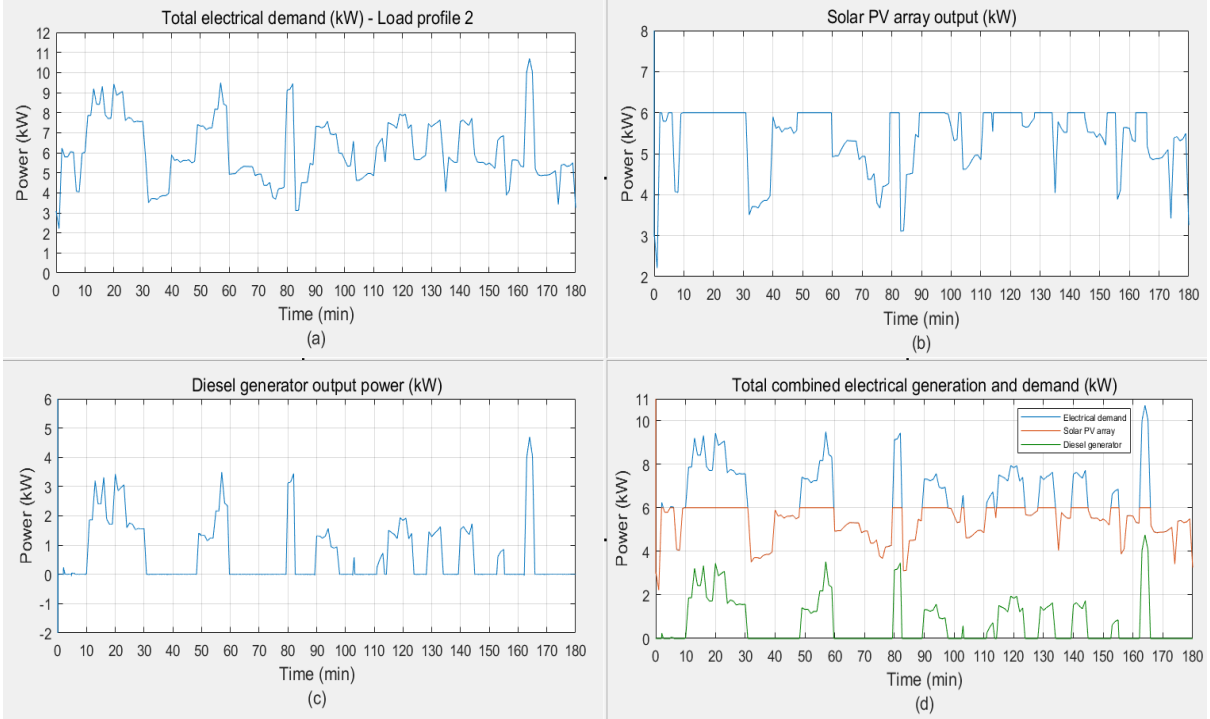

Figure 6.27. *Total electrical power (a) Load profile 2; (b) PV array; (c) Diesel generator; (d) Combined generation and demand*

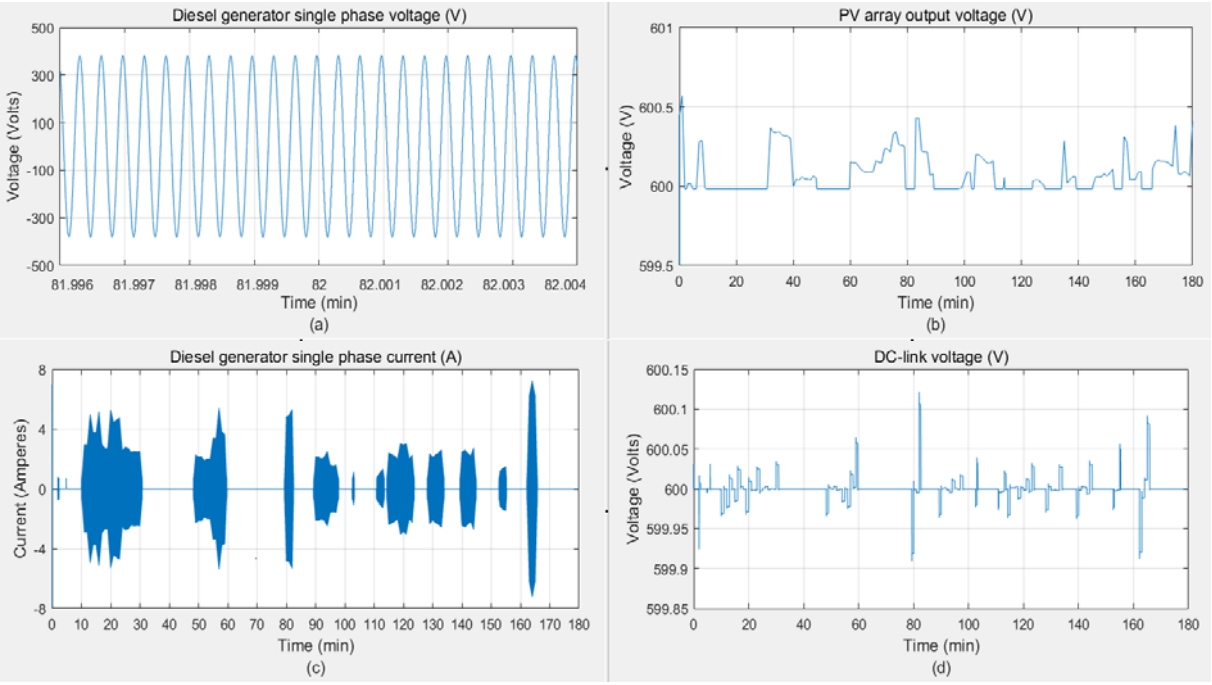

Figure 6.28. *System parameters (a) Diesel generator single-phase voltage; (b) PV array output voltage; (c) Diesel generator single-phase current; (d) DC-link voltage*

The system parameters including voltages and currents of the diesel generator and the PV system as well as the DC bus voltage are shown in *Figure 6.28*. The generator voltage stays constant while the single-phase current waveform of the generator and output voltage of the PV system follow their corresponding power output curves. The DC bus experiences many fluctuations due to the instant power transfer from the PV to the generator and vice versa. However, these variations can be negligible since they are very small and do not last long, which shows the compliance of the system controllers in maintaining a stable system.

6.6.1.3 Strategy 1 – Profile 3

Profile 3 shows a load demand with a large spike and two main peaks each lasting approximately more than 20 mins – a situation between load profiles 1 and 2 (Figure *6.29*). Similar to before, the PV system follows the load until it reaches 6 kW and the backup diesel generator is turned on to cover for the supply shortage. The generator is turned on at about t = 55 mins and will stay on for about 20 minutes covering for the large load spike and peak load period. During this period, the PV system is providing 6 kW and the difference between the load demand and PV generation is supplied by the generator. Same is applied when the generator is turned on again for the next peaking time, but it will be lightly loaded since the supply shortage is small (*Figure 6.29d*). The plots for the single-phase current of the generator and the DC bus voltage reflects the introduction of the generator into the system at the time of power transfer between the PV and DGen (*Figure 6.30*).

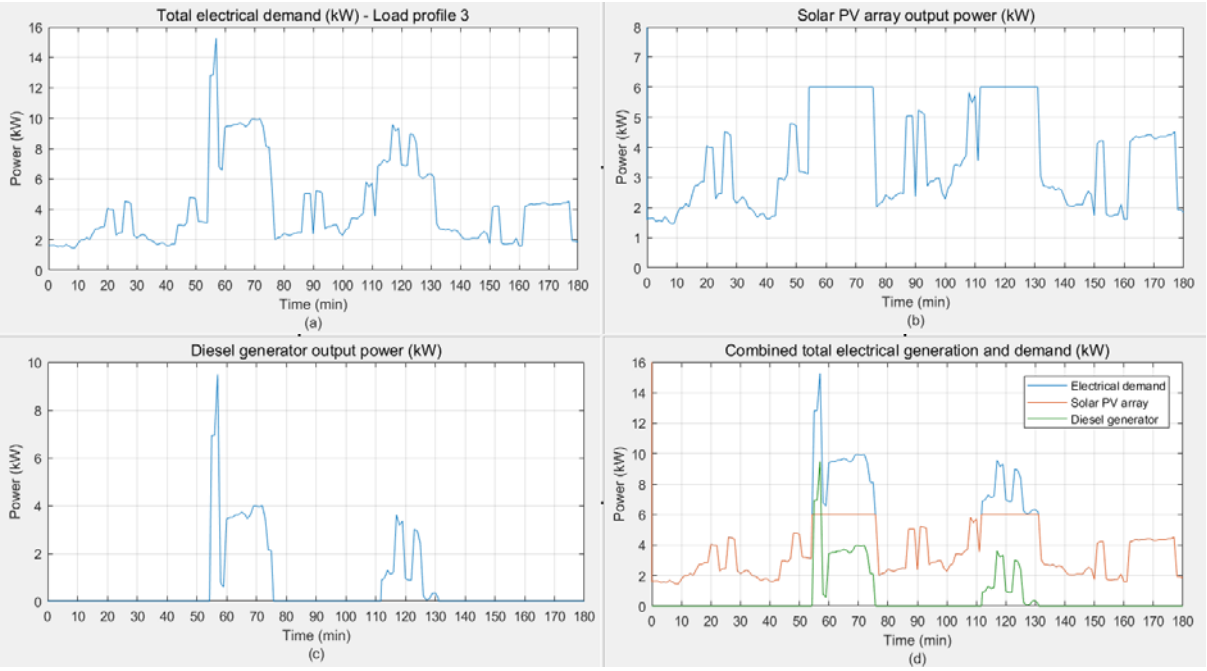

Figure 6.29. *Total electrical power (a) Load profile 3; (b) PV array; (c) Diesel generator; (d) Combined generation and demand*

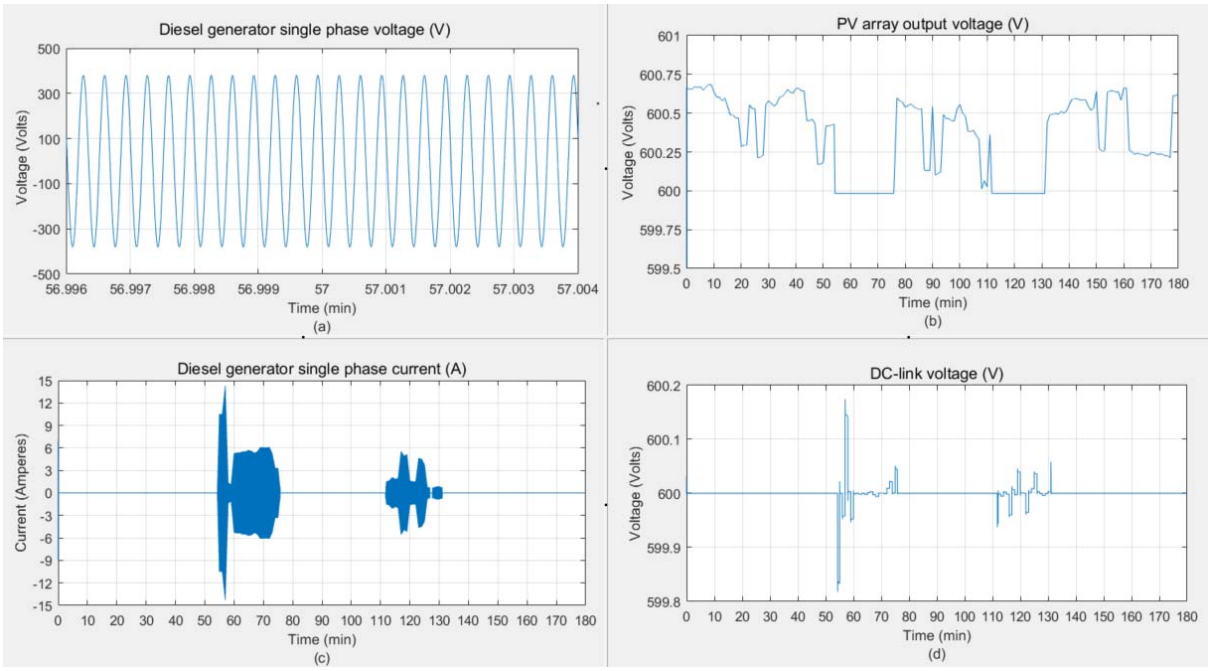

Figure 6.30. *System parameters (a) Diesel generator single-phase voltage; (b) PV array output voltage; (c) Diesel generator single-phase current; (d) DC-link voltage*

6.6.2 Strategy 2 – Combined flywheel, diesel generator and PV system

Strategy 2 investigates the option of adding a storage system to the stand-alone PV and diesel generator system. The purpose is to off-load the diesel generator as much as possible to improve system efficiency and reduce fuel consumption and CO_2 emissions. The PV system has been sized for 6 kW maximum and this is kept the same

for all scenarios for a fair comparison. The diesel generator is sized for the maximum load demand to account for the cases when neither of the PV or FESS is available. Lastly, the flywheel system is designed to provide a constant power of 10 kW with an energy rating of 5 kWh.

The charge-discharge of the flywheel in strategy 2 is controlled based on the communication of the PV system with the load. It is discharged when the demand is above 6 kW rating of the PV system. It supplies power to the load until it reaches its minimum state of charge at 50%. If the flywheel is discharged to its minimum and the demand is still higher than 6 kW, the backup diesel generator will turn on to supply the load. At the times of excess PV supply due to lower demand, the surplus available power is utilised to charge the flywheel. The FESS acts as an intermediate energy source owing to its fast response characteristic. The simulated results of the hybrid systems dynamic performance during the energy transfer for each load profile is discussed in the following subsections.

6.6.2.1 Strategy 2 – Profile 1

The load profile 1 and power output of the solar PV system along with the state of charge of the flywheel system is shown in *Figure 6.31*. Throughout the course of 3-hours for profile 1, the demand is mostly lower than the maximum rating of the PV system except for the two peaks arising at t = 80 mins and t = 120mins, respectively. With the flywheel initially at its minimum 50% charge, there is surplus energy available to charge it up to more than 95% before it discharges at t = 80 mins to cover the peak demand (Figure *6.31c*). After brushing the short load spike, it starts to charge again unit it reaches 100% SOC and switches to standby mode for approximately 18 minutes (t = 102 - 120 mins).

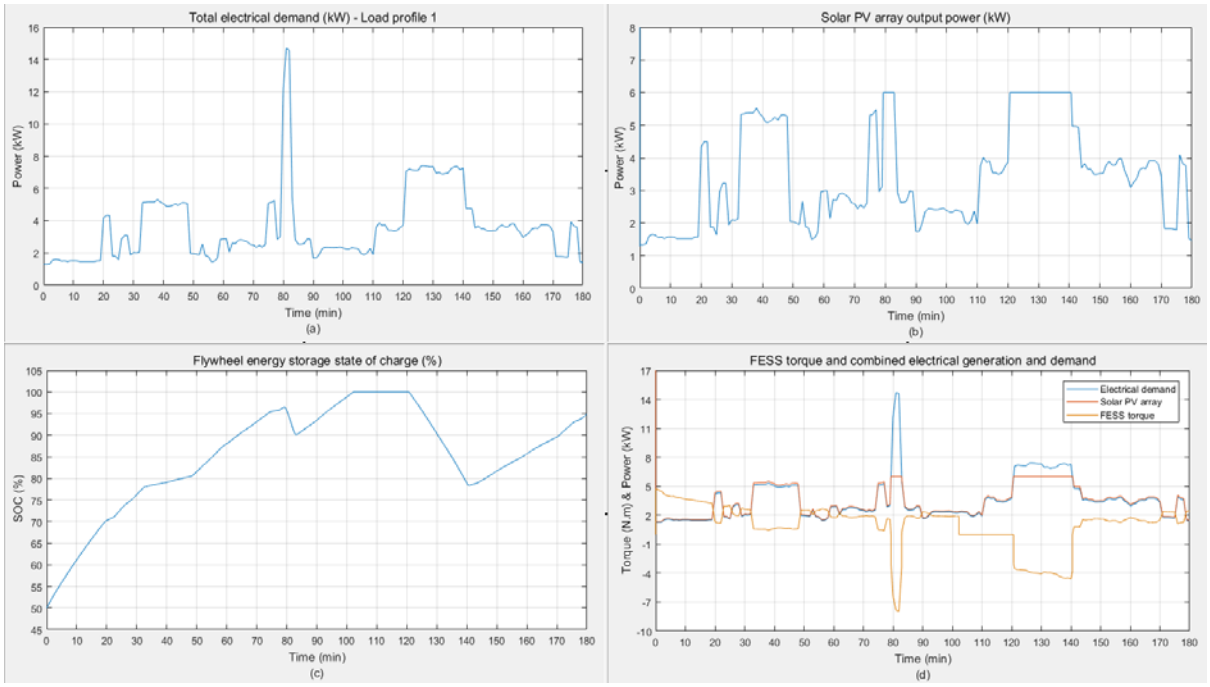

Figure 6.31. *(a) Load profile 1; (b) PV array output power; (c) Flywheel state of charge; (d) Flywheel torque and combined generation and demand*

The combined plots in Figure *6.31*d indicate how the FESS utilises the available excess energy of the PV system during charging. When the demand is low, more power is available and, therefore, the positive (charging) torque is higher. The same can be concluded about the negative (discharging) torque which occurs during the peak demand times where the flywheel discharges to supply the surplus in demand (t = 120 - 140 mins). The zero torque condition shows the flywheel standby status (t = 102 - 120 mins).

Comparing the scenarios for the cases of with and without the storage, it can be seen that the integration of the flywheel fully rested the diesel generator and it was not called at all even during the times of peak demand.

6.6.2.2 Strategy 2 - Profile 2

Compared to load profile 1, the conditions for load profile 2 is quite challenging since the demand is varying for the whole 3-hour period with many lengthy peaks. This implies that the backup energy sources (i.e flywheel or diesel generator) will be in service continuously (Figure *6.32*). The first peak demand appears at t = 10 mins when the load is above 6 kW and the flywheel is needed to cover the surplus in

demand. However, since the flywheel is at its minimum charge level (50% SOC), it switches to standby mode and the generator is called to supply the load (*Figure 6.32c, d*). Shortly after, at about t = 30 mins, when the load demand decreases, the flywheel starts to charge with the surplus power available from the PV system. This charging and discharging process of the flywheel continues until the end but the charge state is not improved due to the nature of demand. It partially helps the diesel generator with the peak demands, but despite this, the generator is still active and running frequently- catching up with the supply shortage from the PV system (*Figure 6.32d*). It can be seen that the generator is turned on when the FESS is in standby mode. Otherwise, the flywheel will be either charging or discharging.

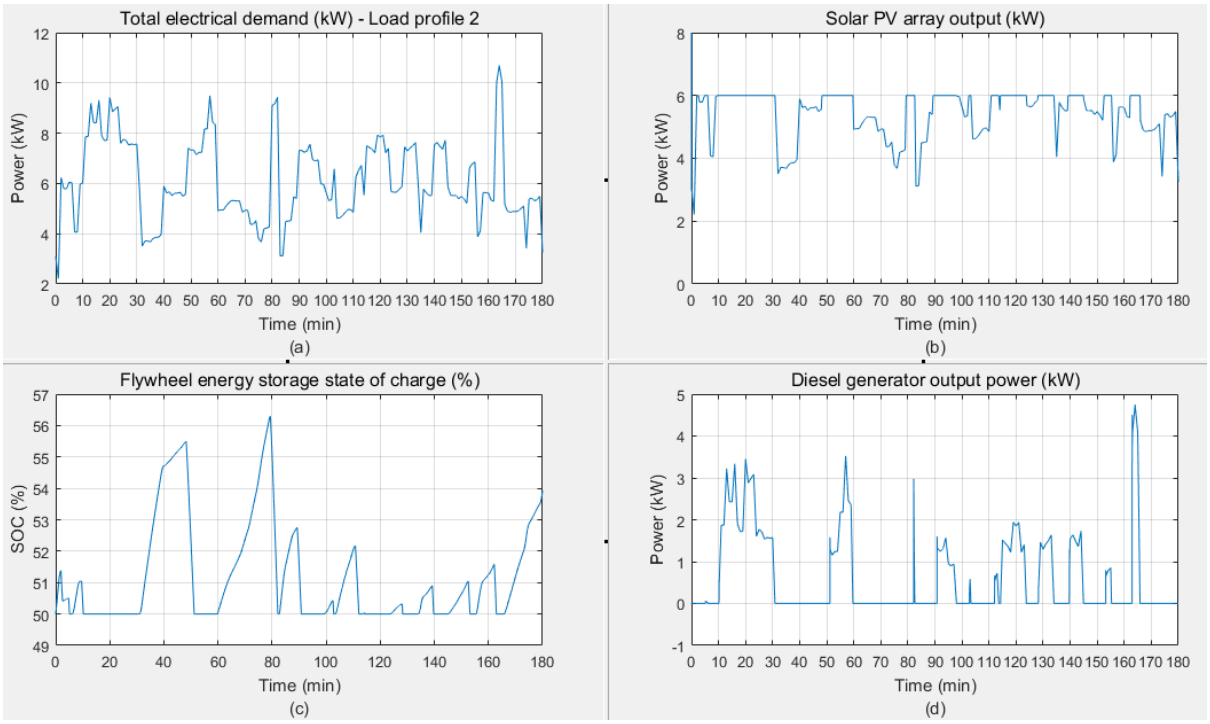

Figure 6.32. *(a) Load profile 2; (b) PV array output power; (c) Flywheel initially at 50% state of charge; (d) Diesel generator output power*

The above situation can be improved if the flywheel is initially 100% charged and can deliver energy immediately when demanded. Since the major peak demands appear at the beginning of load profile 2, a fully charged flywheel can keep the generator *off* for a longer period as shown in *Figure 6.33*. The flywheel discharges at t = 10 mins and covers the excess demand for about 85 minutes before it reaches 50% state of charge

and switches to standby. The power output plot of the diesel generator shows how the flywheel has reduced the operation time of the generator (*Figure 6.33d*).

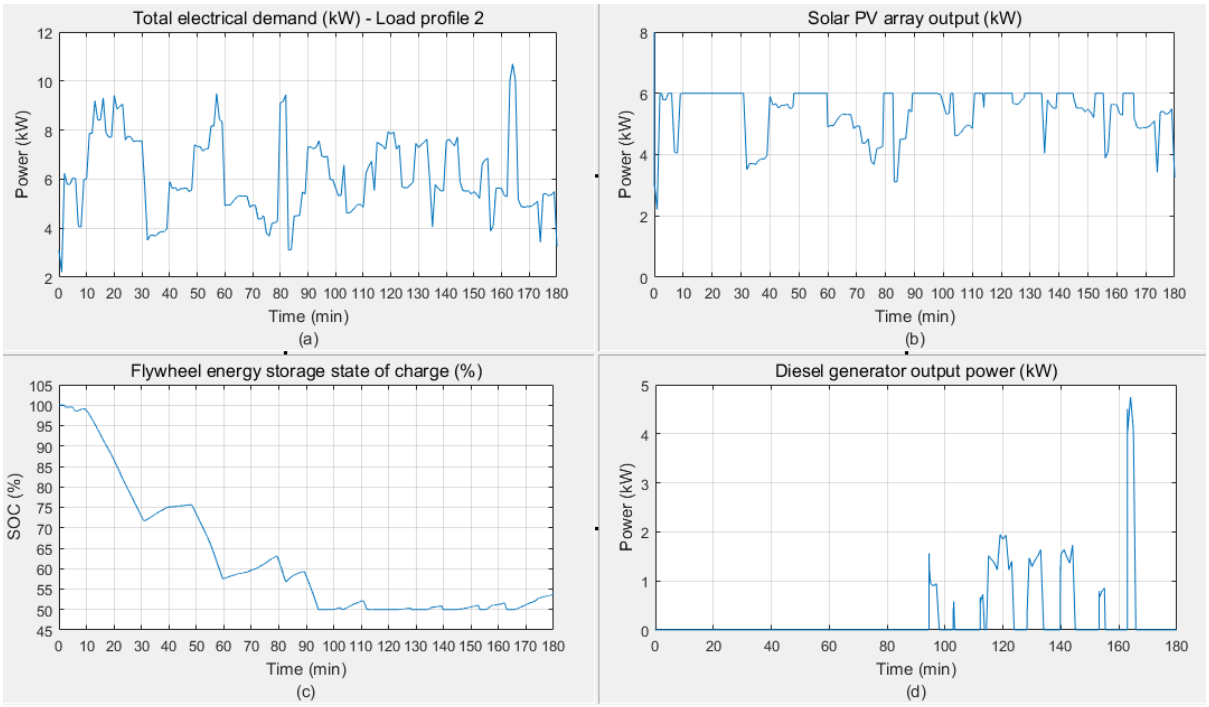

Figure 6.33. *(a) Load profile 2; (b) PV array output power; (c) Flywheel initially at 100% state of charge; (d) Diesel generator output power*

The results of the analysis show that the initial charging condition of the flywheel is vital in reducing the load on the generator. Therefore, the system is examined for 50, 75, and 100% state of charge scenarios and the results are presented in *Figure 6.34* and *Figure 6.35*. The voltage and current of the diesel generator and PV system for the case of 100% charged flywheel is shown in *Figure 6.36*, showing the compliance of the model at the time of power transfer from one energy source to another. There is a large current spike at t= 164 mins due to a sudden increase in the load and commanding an instant engagement of the diesel generator. The DC-link voltage drop is also slightly more than 5V at this instant, although it lasts for a very short period and is not too greatly deviated from the acceptable ±5 percent voltage drop level.

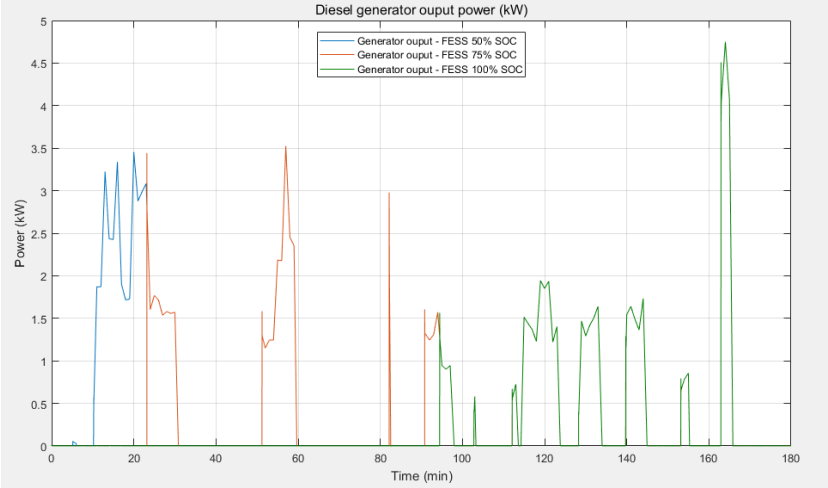

Figure 6.34. *Generator output power based on the initial state of charge of the flywheel system*

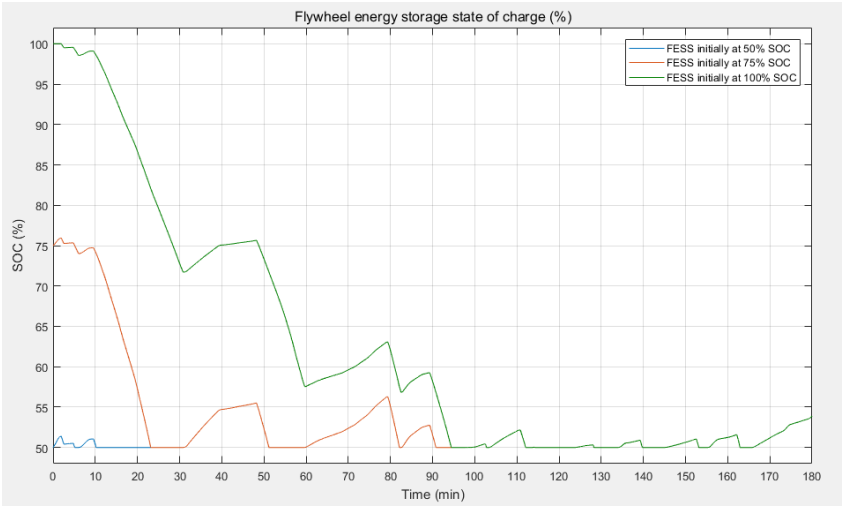

Figure 6.35. *Flywheel charge-discharge plots at different states of charge*

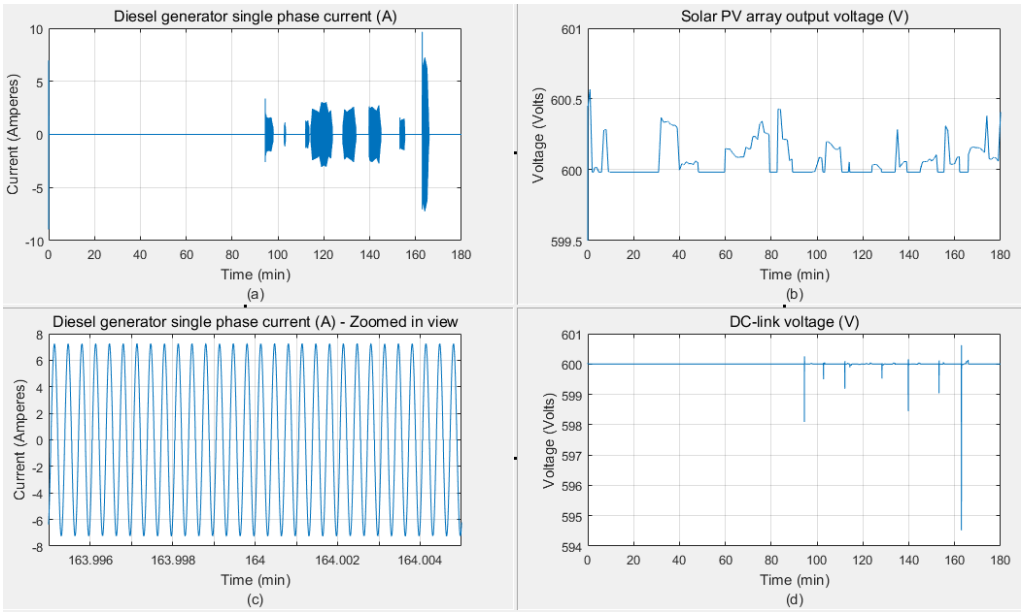

Figure 6.36. *System parameters (a) Diesel generator single-phase current; (b) PV array output voltage; (c) Diesel generator single-phase current- zoomed-in view; (d) DC-link voltage*

6.6.2.3 Strategy 2 – Profile 3

The operation of the hybrid system in supplying power to load profile 3 is shown in *Figure 6.37*. There are two main peak demands that would require power contribution from the FESS in addition to the PV system. However, the main difference to the previous scenarios is that the higher demand appears later and the surplus power from the PV system allows the flywheel to charge before it is called for action at about t = 55 mins. Due to the higher peak demand, the flywheel discharges faster and reaches its minimum charge level before switching to standby (*Figure 6.37c*). Hence, although lasting for a short period, there are only two occasions that the flywheel runs out of power and the generator is turned on to take the surplus demand (*Figure 6.37d*).

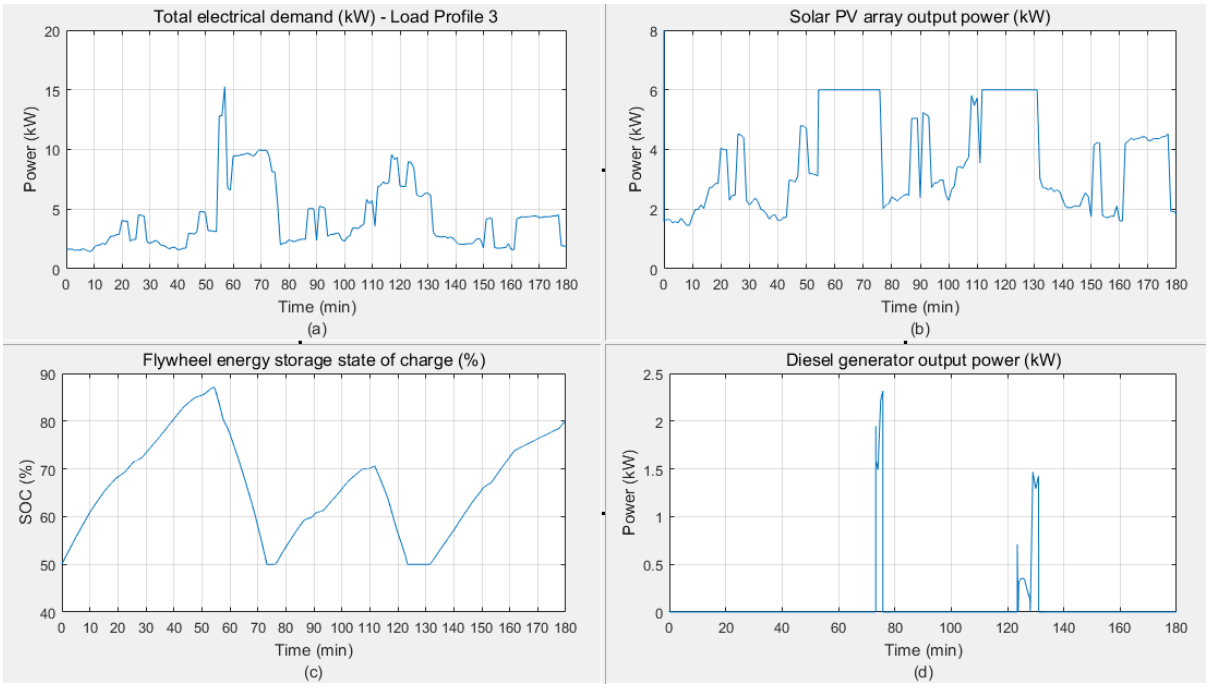

Figure 6.37. *(a) Load profile 3; (b) PV array output power; (c) Flywheel initially at 50% state of charge; (d) Diesel generator output power*

The system performance and communication between the PV system, the flywheel and the backup generator are shown in *Figure 6.38a*. Notice how the flywheel utilises the surplus energy from the PV system to charge. The generator currents comply with the generator power output plots. The DC bus voltage is maintained

constant for the whole duration by the PV and FESS except when the diesel generator comes on and introduces small voltage fluctuations (*Figure 6.38d*).

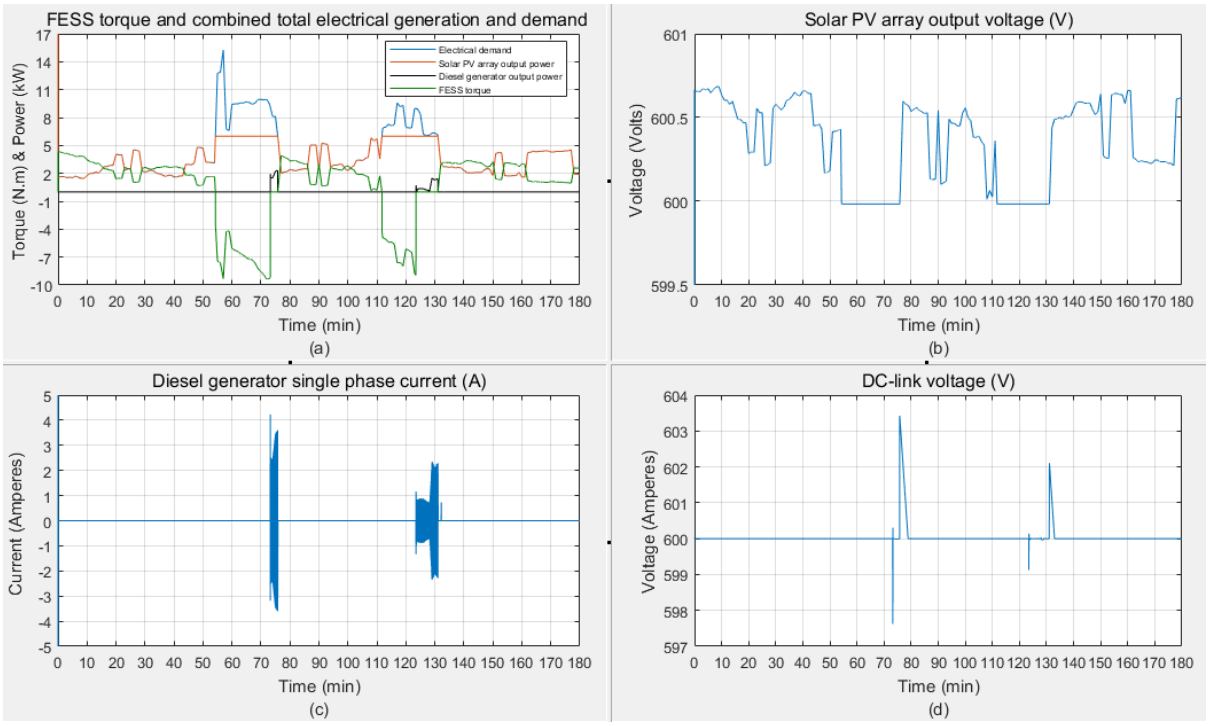

Figure 6.38. *(a) Combined operation of the FESS, DGen and PV system; (b) PV array output power; (c) Diesel generator current; (d) DC-link voltage*

In the above scenario, if the flywheel was initially at 75% state of charge, the generator would not be needed at all and the peak demands can be fully covered by the FESS. This is because the flywheel is reaching 100% charge before the first peak demand appears and it will have enough energy stored to brush up the peak loads.

6.6.3 Strategy 3 – Diesel generator and flywheel only

Strategy 3 considers the scenarios when the PV system is not available and the load demand is shared between the flywheel and the diesel generator. The main challenge is the charge and discharge time of the flywheel that should not happen at the time with the peak demand. Otherwise, the diesel generator must be sized for full load plus the power rating of the flywheel. The diesel generator will be supplying the baseload and the flywheel will perform peak shaving. It will be charged during the times of low demand when there is surplus power available from the diesel generator. There are times that the available surplus power exceeds 10 kW and can be fully utilised to charge the flywheel. However, a power rating of 5 kW is allocated for

charging of the flywheel in order for the generator to run efficiently and operate lower than its full load rating. On the other hand, while the flywheel is discharging, the generator will be turned off for fuel-saving and the flywheel will be set to discharge at its full 10 kW rating to supply the demand load. The flywheel is considered at 100% initial state of charge for all scenarios.

6.6.3.1 Strategy 3 – Profile 1

Similar to the previous scenarios in strategies 1 and 2, the load profile 1 is a simple case with two main peaks and one sharp peak. The FESS is initially at standby with 100% state of charge before it starts to discharge shortly after t = 30 mins as shown in Figure *6.39*. During this time, the demand is below 10 kW power rating of the flywheel and the diesel generator is turned off. As soon as the flywheel covers the peak demand, it switches to standby mode and the generator comes on. The sharp peak at about t = 80 mins is also covered by the flywheel and then right after, it is charged by the generator since the load demand is low between t = 85 - 110 mins. The generator power output increases while the flywheel is charging (*Figure 6.39b*). Similarly, the flywheel starts to discharge again to cover the second peak demand starting at t = 120 mins. Finally, the flywheel is switched to standby mode and the generator is turned on to supply the load.

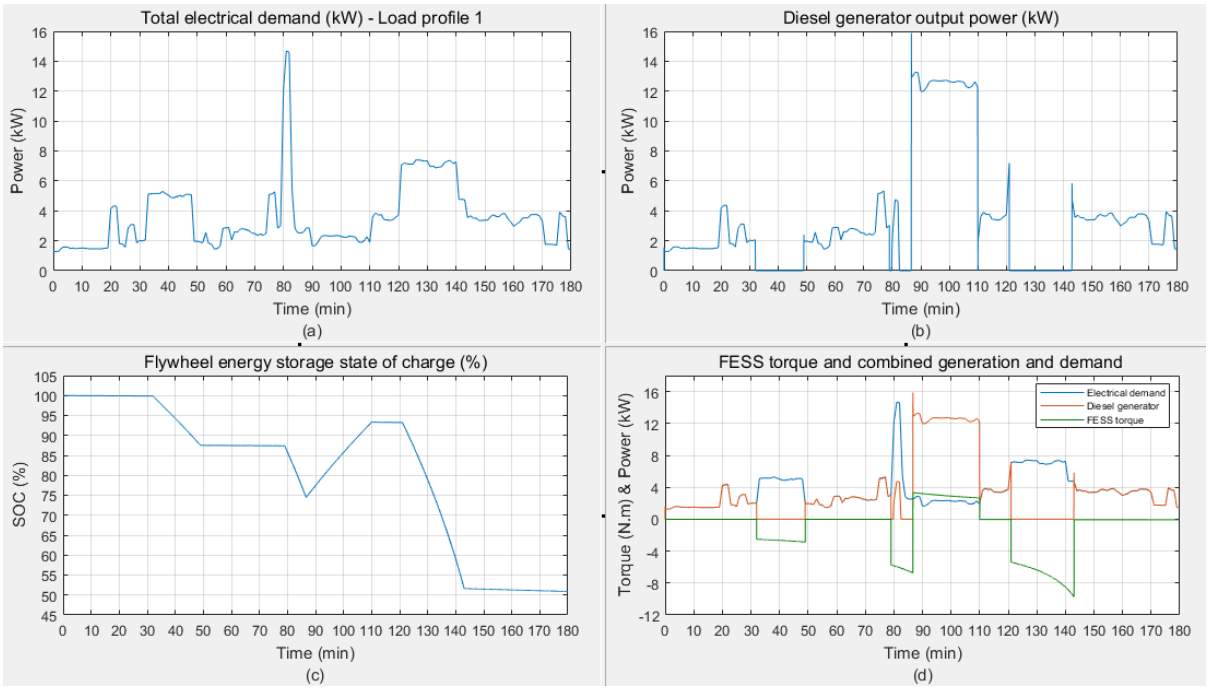

Figure 6.39. *(a) Load profile 1; (b) Diesel generator output power; (c) Flywheel state of charge; (d) Combined operation of the flywheel and diesel generator*

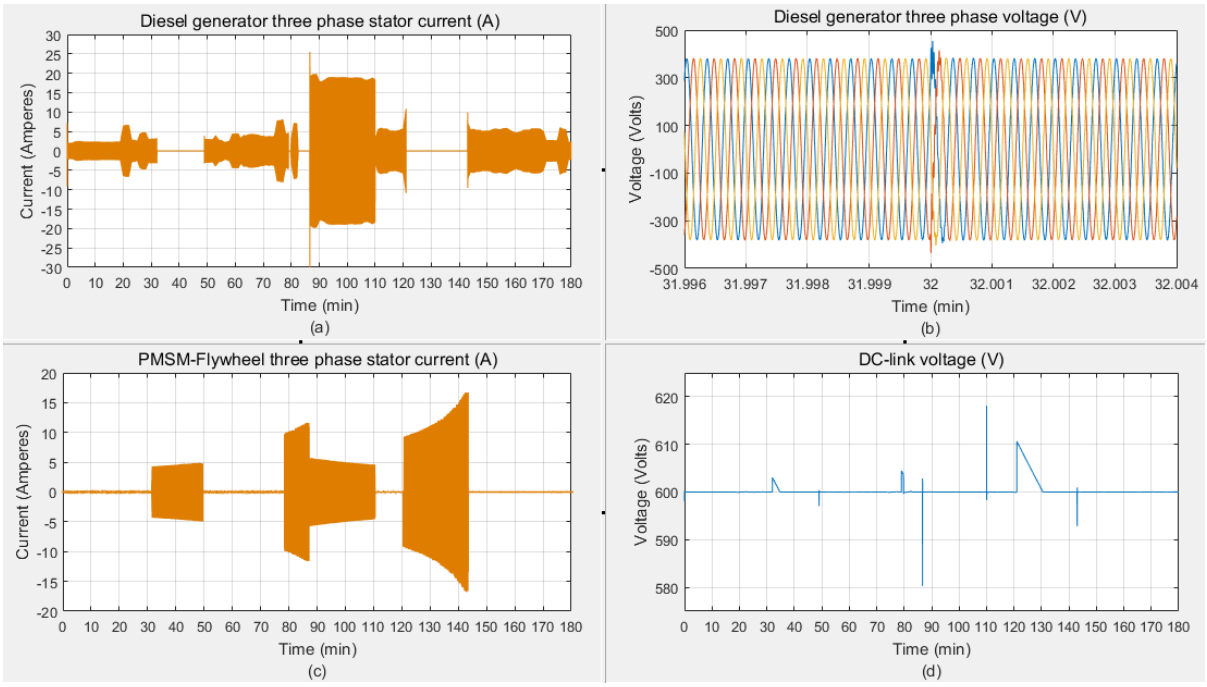

Figure 6.40. *(a) Diesel generator three-phase current; (b) Diesel generator three-phase voltage; (c) Flywheel three-phase stator currents; (d) DC-link voltage*

The accuracy and compliance of the model can be analysed from the current and torque waveforms of the flywheel as well as the voltage waveforms of the diesel generator and the DC bus. The charge-discharge torque of the flywheel with respect to the load demand and available surplus power from the generator is shown in Figure *6.39d*. The three-phase currents of the MG of the flywheel corresponding to its charge-

discharge torque is shown in *Figure 6.40c*. All waveforms show good correspondence between the flywheel, the generator, and the DC bus.

6.6.3.2 Strategy 3 – Profile 2

The load profile 2 is supplied by the combined operation of the diesel generator and FESS similar to profile 1. Since the load demand is quite fluctuating and has many peaks, the flywheel will not be as efficient as it was with profile 1. As shown in Figure *6.41*, the flywheel supplies power during the first two peaks and then switches to standby mode to save energy for the sharp load peak that starts slightly before t = 160 mins. Despite the flywheel covering for the two major peak demands, the diesel generator is on and off most of the time (*Figure 6.41b*).

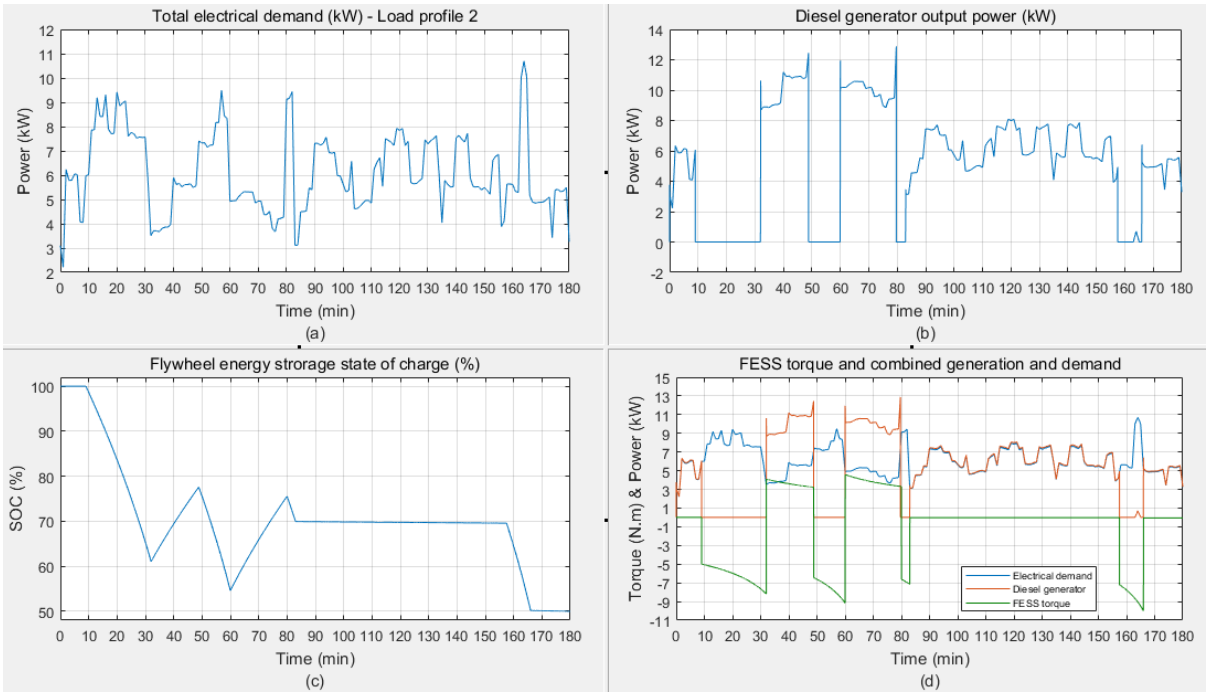

Figure 6.41. *(a) Load profile 2; (b) Diesel generator output power; (c) Flywheel state of charge; (d) Combined operation of the flywheel and diesel generator*

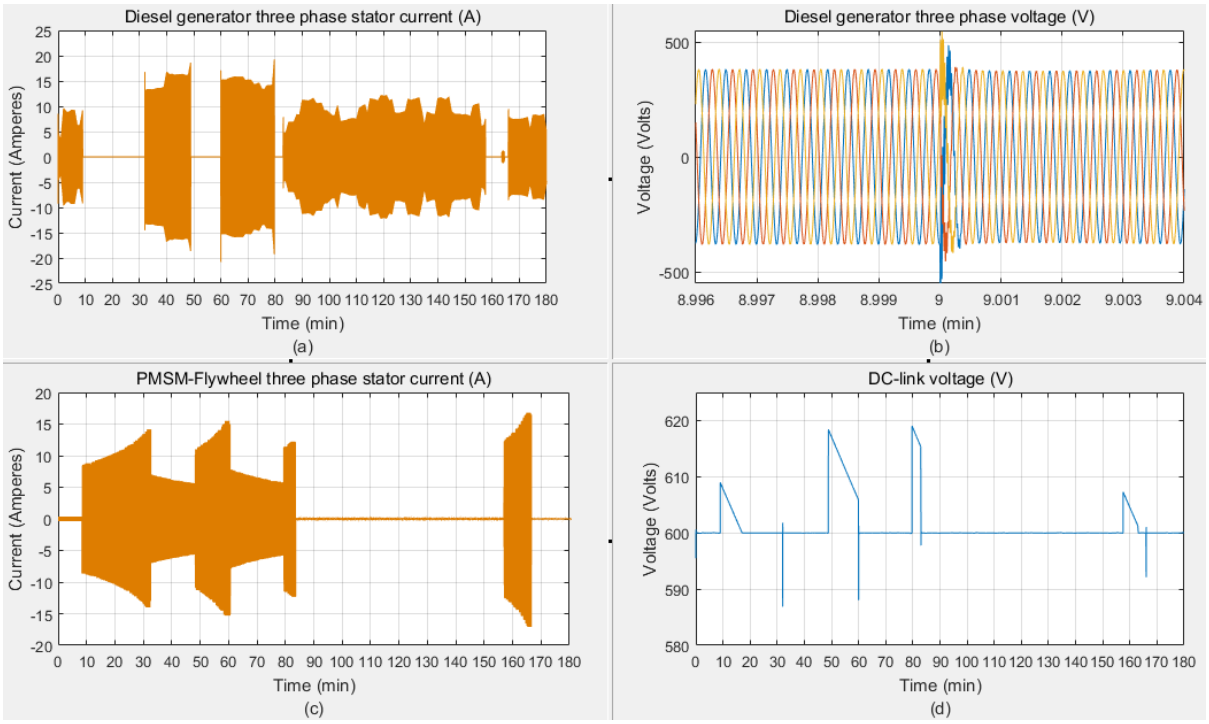

Figure 6.42. *(a) Diesel generator three-phase current; (b) Diesel generator three-phase voltage; (c) Flywheel three-phase stator currents; (d) DC-link voltage*

The current and torque waveforms of the flywheel and the voltage waveforms of the diesel generator have good correspondence and show the accuracy of the model. The DC bus fluctuations are higher compared to the previous cases and this is due to the demanding nature of the load that keeps the generator close to its maximum limits and hence affecting the DC-link voltage.

6.6.3.3 Strategy 3 – Profile 3

The load demand in profile 3 can be managed better by the stand-alone operation of the flywheel and diesel generator. The flywheel supplies both peak demands and the generator is not operated during these periods (Figure *6.43*). This keeps the generator output power below 6 kW except for the charging periods of the FESS, which is still within 8 kW. If the flywheel was not contributing, the generator would be running and following the load for the full period of 3-hours with no idling time. The combined operation of the flywheel and diesel generator can be analysed in *Figure 6.43d*. The corresponding three-phase currents and voltages along with the DC bus voltage are shown in *Figure 6.44*. Notice the DC-link voltage spikes that are quite

smaller compared to the previous case for profile 2. This is due to the lower demand that allows the diesel generator to operate well below its maximum limit.

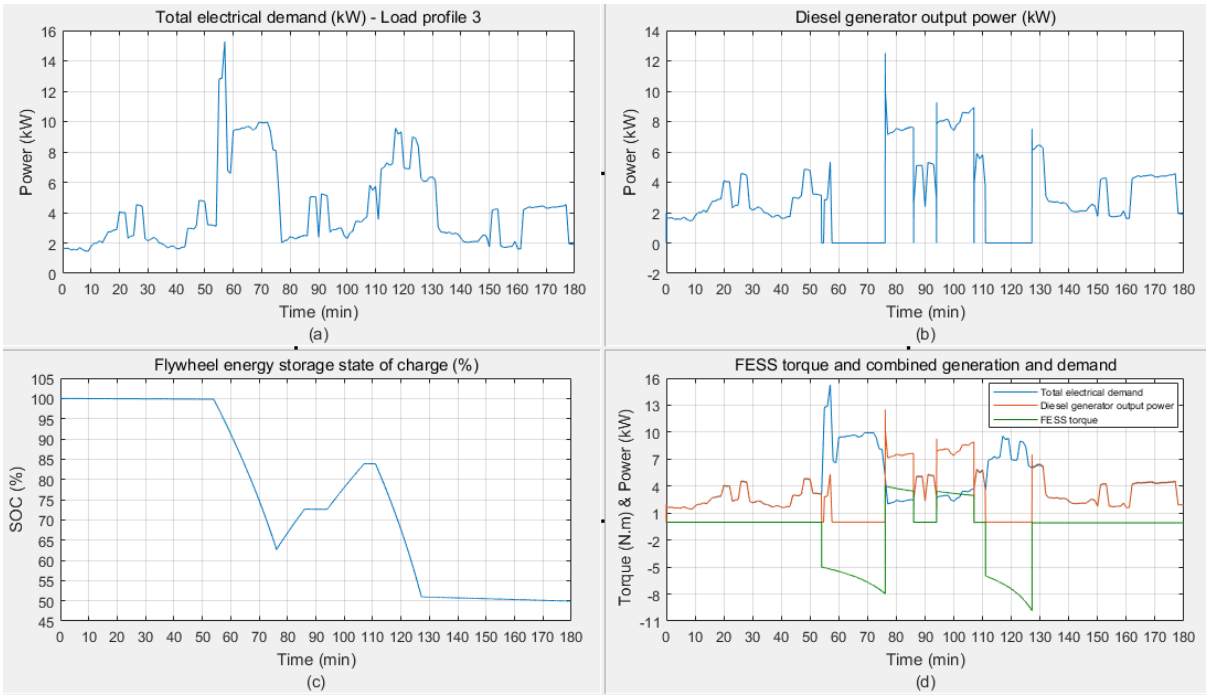

Figure 6.43. *(a) Load profile 3; (b) Diesel generator output power; (c) Flywheel state of charge; (d) Combined operation of the flywheel and diesel generator*

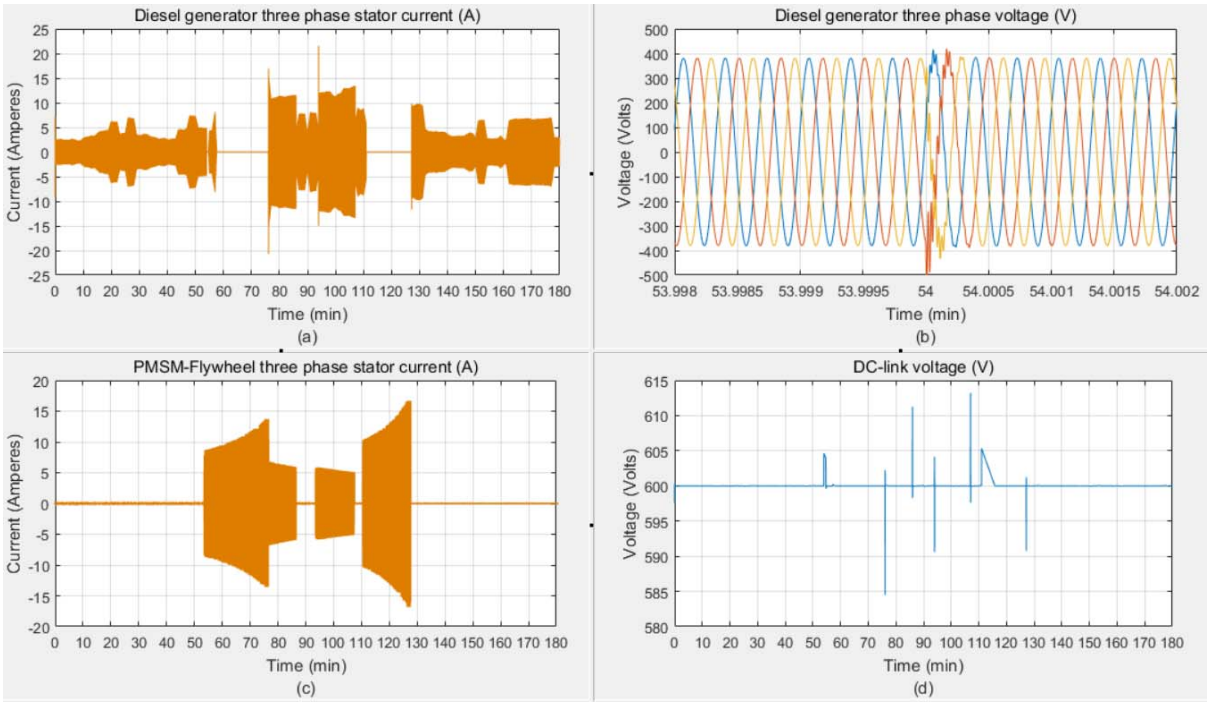

Figure 6.44. *(a) Diesel generator three-phase current; (b) Diesel generator three-phase voltage; (c) Flywheel three-phase stator currents; (d) DC-link voltage*

6.6.4 *Analysis of flywheel storage impact on generator fuel consumption*

The operation of the diesel generator in each of the above scenarios has been dependent on the level of contribution of the flywheel storage system. There have been instances that the demand has been fully supplied by the combined operation of the PV system and flywheel while the generator was completely turned off for the whole period. On the other hand, the higher demand on some occasions (i.e. profile 2) mostly required full engagement of the flywheel storage as well as the backup diesel engine. An analysis of the flywheel system contribution in reducing generator fuel consumption is discussed in this section. Generator fuel consumption and fuel cost savings for all different load profiles were calculated including the cases when the generator is in partial or full operation. The diesel generator models are selected from the two different manufacturers where the full specification sheet for each model is provided in Appendix E. The simulated results tabulated in *Table 6-3, 6-4 and 6-5* show the generator's produced energy (kWh) along with the fuel consumption (litres) and maximum fuel cost savings (£) for all different load profiles.

Table 6-3. *Diesel generator fuel consumption - Strategy 1*

	Generator model	The ratio of consumption at % load		Energy generated in 3-hours	Fuel consumed		Max Fuel cost in 3-hours[1]
		(*l*/*kWh*)		(*kWh*)	(*l*)		(£)
		75%	100%		75%	100%	
Strategy 1	PERKINS[2]	0.23	0.31	1.253	0.29	0.39	0.51
Profile 1	GREAVES[3]	0.25	0.33	1.253	0.31	0.41	0.54
Strategy 1	PERKINS[2]	0.23	0.31	2.156	0.50	0.67	0.87
Profile 2	GREAVES[3]	0.25	0.33	2.156	0.54	0.71	0.93
Strategy 1	PERKINS[2]	0.23	0.31	1.914	0.44	0.60	0.77
Profile 3	GREAVES[3]	0.25	0.33	1.914	0.48	0.63	0.82

[1]Cost of fuel = 1.3 (£/*l*) [2]PERKINS Generator C22 D5 [3]GREAVES POWER Generator G20-II

Table 6-4. *Diesel generator fuel consumption - Strategy 2*

	Generator model	The Ratio of consumption at % load		Energy generated in 3-hours	Fuel consumed		Max Fuel cost in 3-hours[1]
		(*l*/*kWh*)		(*kWh*)	(*l*)		(£)
		75%	100%		75%	100%	
Strategy 2	PERKINS[2]	0.23	0.31	0	0	0	0
Profile 1	GREAVES[3]	0.25	0.33	0	0	0	0
Strategy 2							
Profile 2	PERKINS[2]	0.23	0.31	1.962	0.45	0.61	0.80
(FESS 50% SOC)	GREAVES[3]	0.25	0.33	1.962	0.5	0.65	0.84
Strategy 2							
Profile 2	PERKINS[2]	0.23	0.31	1.567	0.36	0.49	0.63
(FESS 75% SOC)	GREAVES[3]	0.25	0.33	1.567	0.4	0.52	0.67
Strategy 2							
Profile 2	PERKINS[2]	0.23	0.31	1.144	0.26	0.36	0.46
(FESS 100% SOC)	GREAVES[3]	0.25	0.33	1.144	0.3	0.38	0.5
Strategy 2							
Profile 3	PERKINS[2]	0.23	0.31	0.7124	0.16	0.22	0.29
(FESS 50% SOC)	GREAVES[3]	0.25	0.33	0.7124	0.2	0.24	0.31

[1]Cost of fuel = 1.3 (£/*l*) [2]PERKINS Generator C22 D5 [3]GREAVES POWER Generator G20-II

Table 6-5. *Diesel generator fuel consumption - Strategy 3*

	Generator model	The ratio of consumption at % load		Energy generated in 3-hours	Fuel consumed		Max Fuel cost in 3-hours[1]
		(*l*/*kWh*)		(*kWh*)	(*l*)		(£)
		75%	100%		75%	100%	
Strategy 3	PERKINS[2]	0.23	0.31	8.05	1.85	2.496	3.24
Profile 1	GREAVES[3]	0.25	0.33	8.05	2	2.657	3.45
Strategy 3	PERKINS[2]	0.23	0.31	12.2	2.81	3.78	4.92
Profile 2	GREAVES[3]	0.25	0.33	12.2	3.05	4.026	5.23
Strategy 3	PERKINS[2]	0.23	0.31	7.515	1.73	2.33	3.03
Profile 3	GREAVES[3]	0.25	0.33	7.515	1.88	2.48	3.22

[1]Cost of fuel = 1.3 (£/*l*) [2]PERKINS Generator C22 D5 [3]GREAVES POWER Generator G20-II

Table 6-6. *Diesel generator fuel consumption – Standalone and without FESS*

	Generator model	The ratio of consumption at % load		Energy generated in 3-hours	Fuel consumed		Max Fuel cost in 3-hours[1]
		(*l*/*kWh*)		(*kWh*)	(*l*)		(£)
		75%	100%		75%	100%	
Strategy 3	PERKINS[2]	0.23	0.31	8.651	1.990	2.682	3.49
Profile 1	GREAVES[3]	0.25	0.33	8.651	2.163	2.855	3.71
Strategy 3	PERKINS[2]	0.23	0.31	14.35	3.3	4.45	5.78
Profile 2	GREAVES[3]	0.25	0.33	14.35	3.59	4.74	6.16
Strategy 3	PERKINS[2]	0.23	0.31	10.14	2.33	3.14	4.10
Profile 3	GREAVES[3]	0.25	0.33	10.14	2.54	3.35	4.35

[1]Cost of fuel = 1.3 (£/*l*) [2]PERKINS Generator C22 D5 [3]GREAVES POWER Generator G20-II

The results of the analysis show that the flywheel had no impact in strategy 1 because the standalone PV system and the diesel generator provided energy to the load and the system was analysed for the case where no storage is available. In strategy 2, a combination of all three sources was considered and flywheel's involvement and contribution in reducing diesel consumption were dependent on its initial state of charge for load profile 2, was maximum for load profile 1 and substantial for load profile 3. However, in strategy 3, the PV system was not available and only the diesel generator and flywheel storage were providing power to the load. The flywheel system's impact in this scenario has been important as can be seen by comparing *Table 6-5* and *Table 6-6*.

Table 6-7. *FESS impact on reducing generator fuel consumption and fuel cost*

FESS contribution		**Strategy 2**					**Strategy 3**		
		P1	*P2*			*P3*	*P1*	*P2*	*P3*
Flywheel initial state of charge (%)		50	50	75	100	50	100	100	100
DGen output (kWh)	*Without Flywheel*	1.067	2.3	2.3	2.3	1.95	8.65	14.35	10.14
	With Flywheel	0	1.96	1.57	1.14	0.71	8.05	12.2	7.51
DGen energy reduction (%)		100	15	32	50	64	7	15	26
DGen fuel cost saving in 3-hours (£)		0.46	0.15	0.31	0.5	0.53	0.26	0.92	1.13
DGen fuel cost saving per day (£)		3.68	1.2	2.48	4	4.24	2.08	7.36	9.04
DGen fuel cost saving per year (£)		1350	440	905	1460	1550	760	2690	3300

A summary of diesel generator consumption and fuel savings in relation to FESS's impact is shown in *Table 6-7*. Interestingly, in some occasions in strategy 2 where all PV, DGen and FESS were operating as a hybrid system, the flywheel storage could reduce the generator energy production by up to 100%. For the case of load profile 2 where both flywheel and diesel generator were quite busy due to the nature of the demand, the FESS can contribute up to 50% of the DGen load to bring down the fuel consumption and contribute in approximately £1,500 savings per year. In the worst case when the flywheel was initially 50% charged with no available energy to supply the load, still it has contributed in reducing the operation of the diesel engine by 15% with nearly £450 savings per year. In contrast, in strategy 3, the flywheel impact in terms of percentage reduction in diesel generator supply has not been significant; however, the fuel cost savings are quite vital. The yearly savings due to the reduction

in fuel consumption have been almost £2700 and £3300 for load profiles 2 and 3, respectively.

The results of the analysis show that the flywheel system was operating with at least two cycles during the course of 3-hours. Depending on the type of the load and initial state-of-charge of the flywheel, in some cases, the number of cycles was increased to three or four. Assuming the same charge-discharge ratio for a full day would give 10 cycles per day, 3650 cycles per year and 73,000 cycles over 20 years lifetime of the flywheel system. In order for a storage device to perform such number of cycles, it will come on and off multiple times during the day which will suit flywheel applications. It shows that despite the higher initial capital cost of the flywheel system, its lifetime cost will be lower due to its higher longevity.

Introduction of a FESS as a backup storage system not only provides fuel reductions and fuel savings but also increase diesel generators efficiency and lifetime. It adds stability to the system that would, otherwise, cannot be achieved with a standalone PV system backed up by the diesel generator. In addition, from the environmental perspective, reducing the service of the diesel generator will reduce greenhouse gases due to CO_2 emissions.

6.6.5 Analysis of levelised cost of storage (LCOS) for flywheels

There are several advantages of FESS over other storage systems, however, selection of the storage of choice is application dependent and it is quite challenging to determine the most cost effective and realistic option given the diversity of different storage technologies in terms of their performance characteristics and cost. An appropriate and widely practiced tool for a cost comparison of storage technologies is the levelised cost of storage (LCOS) which is used to quantify the cost per unit of discharged energy for a particular storage system and application. Performing LCOS analysis for flywheel systems requires updated technology parameters (cost and performance data) which is quite sparsely available in the literature. Especially for the case of laminated steel rotor flywheels where the focus of the industry is merely

towards carbon composite rotors and availability of technical data is solely limited to composite flywheels. In order to compare LCOS for flywheels with other storage technologies performing similar applications, results of a comprehensive methodology for projecting the future levelised cost of electricity storage technologies are presented here. Authors of [15] have performed an analysis for the determination of LCOS for 9 technologies in 12 power system applications from 2015 to 2050. Results can be generated via the interactive online version of the model that is made available to test and analyse the storage technologies based on their application requirements, cost and performance data verified by industry experts. Monte-Carlo simulation is used to account for any uncertainty and variation in the technical data.

The storage technologies that are characterised by fast response time and are suitable for small scale storage applications are flywheels, Li-ion batteries and supercapacitors. The common applications between these technologies that are included in the analysis are primary response, secondary response, black start and power quality. The results of the projected LCOS for each application is presented and compared for all three storage technologies. Figures 1-5 show the mean and range of LCOS for flywheels, Lithium-ion batteries and supercapacitors.

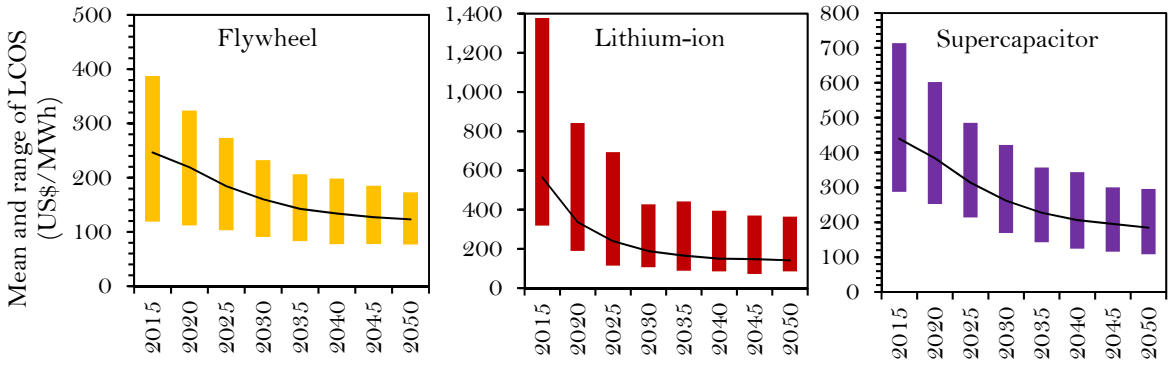

Figure 6.45. *LCOS projections for primary response reproduced from [15] (Left) Flywheel; (Middle) Lithium-ion (Right) Supercapacitor*

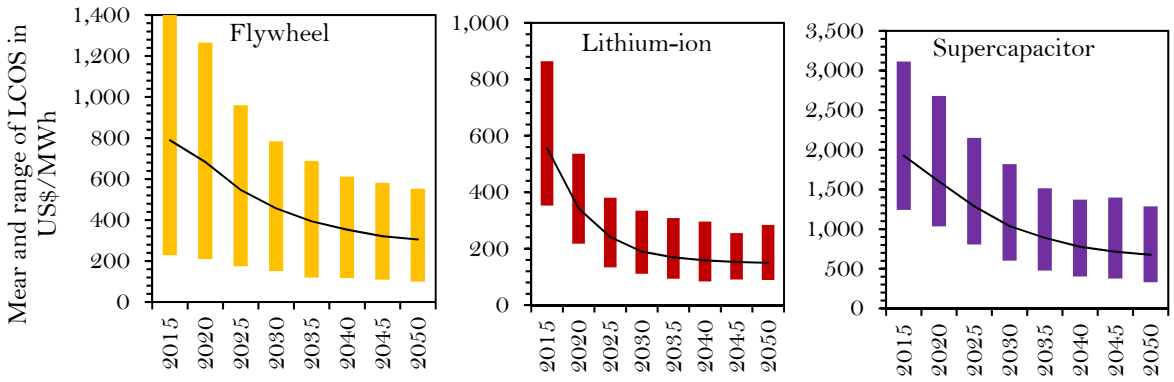

Figure 6.46. *LCOS projections for secondary response reproduced from [15] (Left) Flywheel; (Middle) Lithium-ion (Right) Supercapacitor*

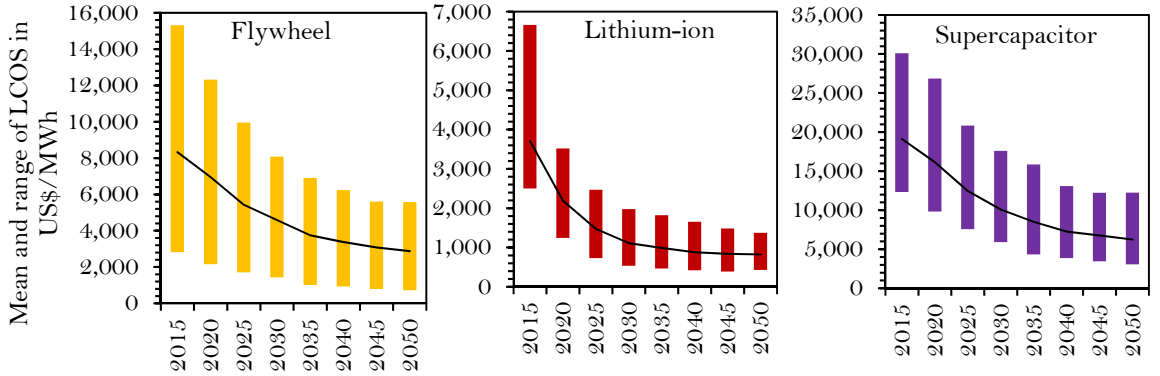

Figure 6.47. *LCOS projections for power quality reproduced from [15] (Left) Flywheel; (Middle) Lithium-ion (Right) Supercapacitor*

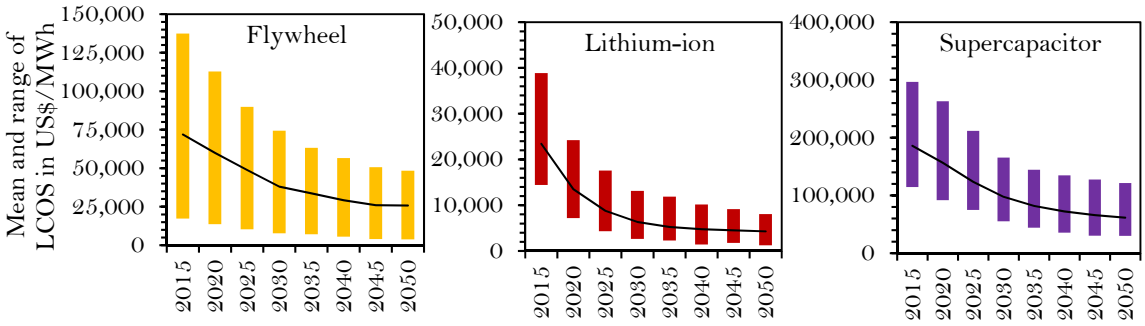

Figure 6.48. *LCOS projections for black start reproduced from [15] (Left) Flywheel; (Middle) Lithium-ion (Right) Supercapacitor*

The results of the analysis show that flywheels exhibit the lowest LCOS for primary response application in 2015 (270 US$/MWh) compared to Li-ion batteries (365 US$/MWh) and supercapacitors (384 US$/MWh). The projected LCOS in 2050 also shows that flywheels (96 US$/MWh) will still be more cost-effective than both Li-

ion (141 US$/MWh) and supercapacitors (185 US$/MWh). On the other hand, Li-ion will be the cost-effective technology with lower LCOS for secondary response between 2015 to 2050. Flywheels will still remain to be much economical compared to supercapacitors but they will always be more expensive in comparison to Li-ion batteries by approximately 200 US$/MWh. By 2050, flywheel storage systems exhibit a significant reduction in LCOS for power quality and black start applications although Li-ion batteries are predicted to be the most cost-effective option for these applications. In comparison to flywheels, they will be ten times and five times cheaper in the black start and power quality applications, respectively.

The primary response is dominated by flywheels and their only contender will be Li-ion batteries. It is the opposite in other applications especially for black start and power quality where Li-ion batteries are predicted to dominate all storage technologies by 2030 [15]. Yet flywheel storage appears to be the second-best technology and it can contest the dominance of Li-ion batteries for these applications if the capital cost is reduced. Because the LCOS analysis is performed based on the cost and performance data for composite flywheels, the range of LCOS values for flywheels is larger in comparison to batteries and supercapacitors. This is due to the variations and uncertainties in available technical data for flywheels which still remains a challenge and many assumptions have to be made until flywheels are mass-produced and emerge as an established technology like batteries. Since the data for steel flywheels are sparsely available and LCOS analysis cannot be performed by neglecting or estimating the cost and performance parameters, it can be argued that if steel laminated rotor data was considered instead, flywheels would exhibit much lower LCOS for the above-mentioned applications. Use of steel laminates in the rotor of flywheel not just reduces the capital cost but also improves some important parameters such as self-discharge rate, discharge duration and calendar life. Steel rotors will have higher inertia and hence the self-discharge rate will be lower and discharge duration will be higher. Sustainability and fully recyclability of steel as well

as its low maintenance requirement will allow a longer operational life for steel rotor flywheels.

6.7 Chapter summary and conclusion

This chapter explained the model of an autonomous hybrid solar PV system with a backup diesel generator and a flywheel storage system all connected to a common DC bus supplying power to a residential load. The model of the load was developed from CREST demand model which is a high resolution (minute-by-minute) energy demand model for building occupancies at the residential level. Different load profiles were generated and the hybrid model was analysed under three strategies namely, strategy 1 for the case of combined PV and diesel generator system without the presence of flywheel storage, strategy 2 for all three sources combined together to form a hybrid system, and strategy 3 to account for the scenario where the PV system is not available and the demand load is shared between the flywheel and the diesel engine. The individual models of the PV system, the diesel generator, the residential load and FESS implement in MATLAB/Simulink environment was briefly discussed and their combination as a hybrid system was presented. For the residential load, the original aim was to use the load profile for a small village in a developing country with no access to electrical grid or with a weak intermittent grid. This would have made the analysis more realistic in terms of energy demand requirements for an islanded system in a developing country where the current designed hybrid model will be directly applicable. However, access to such data was not possible and as an alternative, the load demand profiles were generated using CREST Demand Model. This residential demand model considers the natural behaviour of occupants in using appliances at home and it was used to create stochastic profiles of dwelling occupancies in order to consider different states such as the residents can be at home and active, at home and asleep, or away from home and active. The range of appliances used is also quite extensive taking into account all different types of consumers throughout the UK. The only difference between the load profiles

generated by CREST model and that of a developing country (with a lot of sunny days) would be the inclusion of air-conditioning units during the summer. Despite this, the analysis could be repeated using the same methodology and principles with the only difference of added air-conditioning load and higher power rating of the system to meet higher demand.

The results of the analysis showed the dynamic performance and communication between the system components when supplying power to the load. The compliance and conformity of the model were verified with the system output plots including the voltage, current, and power outputs of the PV system and the diesel generator, the charging toque, state of charge, and three-phase stator currents of the PMSM-Flywheel, and the DC-link voltage during transient and steady-state conditions. The performance and operation of the hybrid system have been generally dependent on the nature of the demand load and the level of contribution from the backup flywheel storage system. There have been instances that the PV system and the FESS have fully supplied the load allowing the diesel engine to be turned off for the whole period. On the contrary, the higher demand in some instances (i.e load profile 2) has fully engaged both the FESS and the diesel engine although the impact of the flywheel has been insignificant. Despite this, in the worst case, the flywheel storage has decreased the load on the generator by nearly 15% providing an annual fuel savings of worth £450 per annum. Whereas in some other cases, the flywheel's contribution to reducing the generator operation has been 32% and 50% when its initial charge state was 75% and 100%, respectively. The flywheel's initial state of charge at the beginning of the simulation has been important in determining its level of contribution as backup storage. For the case of load profile 2 with higher demand at the beginning, the flywheel's impact was more evident at 75% and 100% SOC but had no major effect at 50% SOC. However, in the cases of load profiles 1 and 3 with lower initial demand, there has been excess energy available to charge the flywheel and, as a result, the energy from the storage was not immediately needed. Therefore, the flywheel's initial charge state has been irrelevant and was initially set at 50% SOC. Considering the

three case studies based on which the analysis was performed, the maximum savings due to the reduction of the generator fuel consumption has been £760 per annum for load profile 1, £2700 per annum for profile 2, and £3300 per annum for the case of load profile 3.

Integration of the FESS as a backup storage system not only provides fuel reductions and fuel savings but also increases the diesel engine's efficiency and lifetime. It adds stability to the system and helps reduce greenhouse gases reduction due to CO_2 emissions. The authors in [37] indicate that the formation of a hybrid system by the addition of wind turbines and photovoltaic panels could not result in fuel savings, as expected. This is because the diesel generators, even unloaded, will consume up to 40% of fuel at full load. Diesel engines should only be started when demanded and shut down most of the time. Therefore, flywheel storage systems can reduce frequent start/shut-down cycles of the diesel generators; thus reducing fuel consumption and bridging the power fluctuations [37]. There are great advantages of flywheels backing up solar PV systems since they can cope with the high cycles due to the cloud passing, yet provide ride through, as long as standing losses are kept low. There has been a wide range of flywheel systems developed for the penetration of renewable energy systems. For example, ABB's PowerStore, Urenco Power, Beacon Power, and VYCON technology, have all provided flywheel-based systems for wind and solar applications [77].

The energy storage system of choice for residential PV systems is more typically an electrochemical battery, whereas flywheels have not been widely tested nor considered for this application. The batteries are mass-produced and are believed to be more cost-effective compared to flywheels, but flywheels could still be a viable choice when it comes to numerous cycles per day. On the downside, batteries are temperature sensitive and take up more space than a flywheel for the same rated power to energy ratio. In addition, there is a growing environmental concern when disposing of spent chemical batteries, particularly more difficult in less developed countries. There are several advantages of FESS over chemical storage systems, but a

flywheel is likely to incur a higher initial capital cost, although with high longevity, lifetime costs will be lower. As a means of reducing the capital costs, what is being proposed here is a FESS based on laminated steel with a view to overcoming the drawback of the aforementioned high initial costs of a high-speed composite based flywheel system. On the number of cycles, the results of the analysis show that the flywheel system was operating with at least two cycles during the course of 3-hours. In some instances, the number of cycles was increased to three or four depending on the type of load and initial state-of-charge of the flywheel. If the same ratio were assumed for a full day, then the number of charge-discharge cycles for the flywheel system would reach at least 10 cycles per day, 3650 per year and 73,000 over 20 years. Considering this, the storage device will come on and off multiple times during the day which will suit flywheel applications.

For the flywheel system to perform 73,000 cycles in 20 years, the level of maintenance will be fairly low and is only limited to maintenance of the bearing system and the vacuum pump. Assuming that the speed and vacuum level is maintained well, the chances of failure of the steel laminated rotor or any catastrophe will be quite low for such number of cycles and there will be no replacement cost for any major components of the system. For example, Beacon POWER which is in commercial operation as a leading carbon composite flywheel manufacturer for at least 10 years, has more than 400 flywheels in commercial operation with each flywheel capable of performing more than 175,000 full depth of discharge cycles over its lifetime. Beacon flywheels have accumulated more than 7 million hours with no major safety issues or events recorded [70]. For a steel laminated rotor operating at rated speed and full depth of discharge cycles with the bearing assembly discussed in Chapter 4, the bearing life time calculations (*Table 4-13*) show a basic maintenance requirement of every 4 years which could be only a normal inspection or lubrication maintenance. However, the modified rating life calculations indicate a maintenance requirement of every 11 years which occurs only once over the entire lifetime of the flywheel system. Nevertheless, the level of maintenance in a flywheel system is far

more sophisticated than what is anticipated here and is highly dependent on the number of cycles, rated speed, depth of discharge rate, the vacuum level in the vessel, etc. Typically a flywheel system is equipped with sensors and controls to alert the operator if any maintenance is required and automatically shuts down the system in case of emergencies.

In contrast, if a chemical battery (i.e. Li-Ion type) was used to arrange for backup storage services under such circumstances, it will be experiencing multiple charge-discharge cycles per day with some cycles not even fully completed. This will reduce the life cycle of the battery and will degrade its performance, hence justifying the choice of using flywheel storage as an alternative to batteries for such applications. Based on life estimates from [15], for a Li-Ion battery to perform 73,000 cycles, the cells would need to be replaced more than 5 times over the 20 years based on a C1, 10kWh battery operating with a 50% depth of discharge. For the same number of cycles and depth of discharge rating, a Sodium-Sulphur battery would need to be replaced 12 times and a Lead-Acid type would be replaced 28 times in 20 years. Similarly, the replacement of the Li-Ion battery cells will be 12 times if the battery operates with an 80% depth of discharge (*Figure 1.2*). This assumes the battery was kept within an ideal temperature range and with a good battery management system.

The projected lifetime cost estimations in 2015 to 2050 for flywheels and Li-ion batteries show that flywheels will have lower levelised cost of storage (LCOS) in primary response but will remain the second-best technology in secondary response, black start and power quality applications. It has been argued that the estimated LCOS will be much lower for steel rotor flywheels given the cheaper cost, recyclability and low maintenance requirements associated with the use of laminated steel in the rotor of the flywheel systems. Therefore, considering the calculated annual savings and the impact of the flywheel in providing backup storage and off-loading the diesel engine in autonomous PV systems, the payback time can be far quicker than anticipated with the bonus of introducing a green technology with at least 20 years of active operation.

It is worth mentioning that the analysis in this chapter has been performed for worst-case scenarios such as considering the weekends with worst periods of demand with higher peaks and spikes rather than a normal weekday with predictable load demand. Despite this, the flywheel's impact in improving the efficiency and reliability of the system has been vital and the annual fuel saving has been quite significant. However, a normal charge-discharge condition without severe loading conditions would allow the flywheel to hold charge for longer periods despite taking part in peak load shaving which usually lasts for shorter periods.

Lastly, the presented research work described the assessment of small-scale energy storage flywheel systems for use in residential premises with highly intermittent or non-existent grid infrastructure which is more applicable in developing countries. Based on the results of the analysis and considering the fuel cost savings associated with use of flywheels as a backup storage, the question is whether energy consumers in developing countries will be willing to invest in this new technology given the cheaper cost of diesel and abundant use of diesel generators as a default alternative choice of energy production? The answer to this question is not simple and requires a rigorous analysis from a technical and economical perspective. It depends on the size of the load and the average length of time the load is supplied by the flywheel storage. The consistency of electrical grid and availability of the renewable energy sources will also have a great impact in selecting between the flywheel storage and the diesel engine; nevertheless, at least for the near future until an established choice of storage emerges, neither of the two could be completely overruled and keeping both options as a supplement to each other might be an ideal solution.

At a glance, ignoring the environmental issue of diesel engines, it can be argued that flywheels are best for high wattage loads with shorter run times, while diesel generators would be ideal for longer and consistent run times. However, this would be a very generalised and incomplete conclusion and a thorough economic analysis is needed to develop a business model for flywheels. For example, flywheels need to be

deployed in islanded states or through microgrids to improve resilience. Sharing the benefits of flywheel deployment in these projects compared to a carbonised diesel engine option will have a positive impact on the incentive of the energy consumers. In addition, poor quality of diesel and major health threats associated with it will drive the decision to use flywheels as a clean source of energy from the environmental and human health perspective compared to cost.

Chapter 7 Conclusions

This research presented a review of the flywheel energy storage system with reference to its main components and applications. The structure and components of the flywheel were introduced and the main types of rotors, electric machines, power electronics, and bearing systems for FESS were described in detail. The main applications of flywheels in power quality improvement, uninterruptible power supply, transportation, renewable energy systems, and energy storage were explained, and some commercially available flywheel storage prototypes, along with their operation for each application, were also discussed. Flywheels with the unique characteristics of very high cycle and calendar life are the best technology for applications demanding these requirements. High power capability, instant response, and ease of recycling are additional key advantages. Given that the demand for energy storage is expanding substantially, and that FESS has these unique attributes, the future for flywheels remains very bright, even in a time when the cost of Li-ion and batteries with other chemistries continues to reduce.

The presented research work described the assessment of small-scale energy storage flywheel systems for use in residential premises with highly intermittent or non-existent grid infrastructure. This was addressed by modelling and analysis of a flywheel system integrated into an autonomous solar PV system with a backup diesel generator supplying residential loads based on a number of different energy transfer strategies. Flywheel storage was utilising to reduce generator fuel consumption and improve the reliability of the system in comparison to a system without storage. Had chemical battery storage been used it would suffer from too much degradation given a large number of discharge cycles needed, so it is believed flywheels offer a good alternative to batteries for this application.

7.1 Thesis summary and main findings of the research

The demand for energy is increasing due to population growth rates and increased electricity demand by the households and industries particularly in

developing countries as average income increases. Environmental concerns, demand variations and slow responsiveness of the traditional power systems require integration of renewable energy sources and distributed generation to be integrated into electrical networks. However, the issue is exacerbated due to the intermittent nature of the energy coming from renewables. This further requires aggregation of energy storage systems as a vital component in electrical systems to balance the demand and generation and also improve the reliability and stability of the system. Therefore, different scale energy storage systems with their unique characteristics have been used to complement today's electrical networks. At the distribution level and particularly in residential premises where longer duration storage is needed, the energy storage services are generally limited to chemical batteries meeting sub-seconds to hourly demands or even daily demands. This trend has limited the advancement of high power technologies such as flywheel and supercapacitors for these applications. For the case of flywheels and whether they can be used as an alternative to chemical batteries in residential applications, a summary of the major findings of this research is presented as follows:

Chapter 1 provided an overview of the need for energy storage systems in today's modernised electrical networks by addressing their associated benefits such as balance of supply and demand, transmission and distribution investment avoidance or deferrals, power quality and stability improvement, and complementing the integration of renewables and distributed generation at the distribution level. In addition, the role and characteristics of energy storage systems in the future structure of the electrical grid was discussed and a comparison of the attributes and drawbacks of both Li-Ion batteries and flywheel storage for such circumstances were analysed.

Chapter 2 provided a detailed description of flywheel energy storage systems. After presenting a brief background on the emergence and development of different forms of flywheel systems throughout history, their structure and components were described. The type and material of the flywheel rotor, power electronics and conversion system, types of bearings and containment have been discussed in detail.

It was concluded that the early age flywheel rotors were mostly made of wood and then progressed to metals. With the emergence of strong fibre materials in the 1970s, there was renewed interest in flywheels with lighter rotors. Currently there are commercial designs based on steel or composite, whereas recent developments in material and advancements in electric machinery and their associated power electronics have mostly promoted composite based flywheels mainly considered by the majority of FESS manufacturers. However, the lower cost of steel rotor flywheels has also kept them in extensive use. To reduce the safety issue of steel rotors and benefit from their cheaper cost, as a compromise between steel and carbon composite, this research proposes a flywheel storage system based on steel laminated rotor providing longer duration storage.

The common types of electric machines for flywheel applications are induction machines, permanent magnet machines, and variable reluctance machines. A detailed comparison of the machines was provided and it was concluded that permanent magnet type is the most widely used electric machine in FESS applications. The converter topologies that can be used in flywheels are application dependent and are typically DC-AC, AC-AC, or a combination of both.

The bearing system is required to keep the flywheel rotor in place and it can be mechanical, magnetic, or gas type bearings. The gas type bearing cannot be used in flywheels due to the vacuum requirement within the enclosure. Traditionally, mechanical ball bearings have been used in flywheels, but the common types of magnetic bearings recently used are PMB, AMB, and SMB. Sometimes as a trade-off between improved performance and cost, a hybrid system of bearings is used. Combined mechanical and magnetic bearings is generally a preferred arrangement, however, a combination of SMB and PMB is also explored as an option. Finally, the performance and safety of the flywheel system are improved by enclosing it in a solid containment. The enclosure is typically made of thick steel or a high strength material (i.e. composites) and must be equipped with a vacuum pump to maintain the pressure level inside the container. The thickness of the container and vacuum pumping

requirement are related to the material and peripheral speed of the flywheel rotor. Composite rotors do not require as thick a containment as solid steel rotors; however, the use of steel laminated rotors allows the containment to be much thinner compared to what is required for a solid steel rotor and is also thinner than composites.

The characteristics and applications of flywheels are presented in Chapter 3. The main attributes of FESS are their high cycle life and long calendar life in excess of 20 years with a high charge and discharge rate, fast response, and high round trip efficiency. They are an environmentally friendly technology and the steel rotor types, in particular, can be fully recycled. The main drawbacks of flywheels are their higher self-discharge rate and safety issues associated with rotor failure if the containment is not sufficient.

A survey of the literature showed that the most suitable applications of flywheels fall in the areas where high power for short duration is required suggesting power quality and UPS applications as the best fit applications. Some other applications such as high power pulsed systems for combat vehicles, attitude control in space satellites, hybrid and electric vehicles, and energy storage services are also performed by flywheel systems.

Chapter 3 also discussed the recent onsite industrial installations and examples of FESS for each particular application. A number of reported examples for each application was collected from many sources although there is a scarcity of information available in the literature addressing the industrial instalments of flywheels. Finally, a comparison of the characteristics and properties (i.e. C-rating, rotor topology and material, application area, and configuration) of some common flywheel manufacturers around the world for use in stationary applications was also presented.

Chapter 3 concludes with a description of the research direction developed based on the findings in the literature which shaped the remaining chapters of the thesis. Considering that the rotor is the key technology in any flywheel system, its design has been generally limited by the two options of solid metallic steel or carbon fibre

composites. For the case of solid steel rotors, flywheels must be either operated at low enough speeds to avoid any rotor bursts or a thick containment must be provided to allow for higher speeds, often an underground bunker. The composite material is superior to steel in terms of specific strength (around 10 times better than steel) and leads to rotor weight around 3-4 times less than solid steel. However, it was shown that for the same storage, the overall volume of the composite rotor is almost twice that of steel. In addition, the failure of composite rotor flywheels in an explosive mode shows that both steel and composite rotors require a very thick containment, adding to the overall cost of the flywheel system. Therefore, the use of steel laminates for the rotor was considered to overcome the safety and cost issues and also provide longer duration storage - something that is not generally practiced by the majority of the flywheel manufacturers. In contrast to solid steel rotors, use of steel laminated rotors requires a thinner containment because at the time of failure only a small part of the rotor is released and can be easily contained. Considering this and full recyclability of steel allows such flywheels to be used in buildings without extra safety requirements or the need to be buried under the ground. Hence, an emerged research area not widely addressed in the literature was the assessment of flywheels providing back up storage for small scale residential customers. Particularly for the cases of the intermittent electrical grid or standalone systems supplied by renewables sources, the use of flywheel storage has been quite limited. In achieving this objective, the modelling and simulation of a large inertia flywheel system with its associated electrical machine and conversion system was considered to be addressed in detail. The developed model was aimed to be integrated into a hybrid system of solar PV and diesel generator to assess the contribution of the flywheel system in improving the generator fuel consumption and overall reliability of the system.

Chapter 4 described the loss analysis of the considered flywheel system with more focus on the methods for calculation of aerodynamic and bearing friction losses. Different aerodynamic flow regimes based on different pressure levels were discussed and determination of the drag coefficient for the case of a flywheel system operated in

rarefied vacuum conditions was analysed. For a better approximation of the losses, two different windage calculation methods as developed by Beck and Alofs were analysed and compared. It was shown that both methods give consistent results below 1 Pa pressure level. As the pressure was increased beyond 1 Pa, Beck's method of windage losses introduced errors due to its dependence on the air gap between the boundary layers. However, Alofs' method was shown to be valid for the entire range of Knudsen numbers - staying quite consistent for all pressure levels and not affected by the air gap alterations. In addition to rarefied vacuum conditions, the windage losses were also calculated for high-pressure continuum flow regimes to give an indication of the scale how these losses increase with speed if the flywheel was operating under atmospheric pressures.

Bearing sizing and selection was discussed in detail and analysis of bearing friction losses based on empirical approaches favoured in the industry by bearing manufacturers such as SKF and NSK was also provided. The flywheel rotor is stabilised by a combination of radial ball bearing and passive magnetic bearing as a balance between friction and maintenance requirements of the ball bearing and complexity of the magnetic bearing that cannot withstand larger acceleration and gyroscopic forces. The majority of the rotor weight is vertically levitated by the passive magnetic bearing which technically has no losses if the field is uniform. For the two ball bearings used to accommodate for rotor out of balance, it was shown that the combined losses for both the top and lower bearings were approximately 80 Watts for 20,000 rpm and 110 W for 25,000 rpm. For a given speed of 20,000 rpm, the bearing basic life calculations were approximated as 178,000 hours and 38,000 hours for the top and lower bearings, respectively. However, for the same speed rating, the modified rating life for 95% reliability as proposed by bearing manufacturers was 284,000 hours for the top bearing and 98,000 hours for the lower bearing.

Chapter 4 was concluded with an approximation of system total losses and efficiency. The standby self-discharge rate of the flywheel system over the course of 24 hours was determined to be 75%, 70%, and 45% for the pressure levels of 0.01 Pa,

0.1 Pa, and 1 Pa, respectively. Also, the maximum standby losses due to windage and bearing friction losses for an operating speed of 20,000 rpm was approximately 230 W.

The modelling and control of a flywheel storage system were presented in Chapter 5. The general configurations of storage systems in a generalised power conversion system was discussed and the converter topologies for each storage system was described. The converter in a FESS function as a bidirectional AC-DC inverter to control the supply of power in and out of the flywheel, whereas in the case of other storage systems such as batteries, supercapacitors and SMES, it performs as a bidirectional DC-DC converter to communicate between the DC-link and the storage device. For flywheels, the converter system was shown to be arranged in a cascaded bidirectional back to back AC-DC-AC configuration to perform power flow in both directions with the help of an associated control system. The controlling of the converters at the storage side and at the grid side was analysed with the help of mathematical equations and circuit diagrams. A detailed mathematical model of the permanent magnet synchronous machine used as a MG unit in the flywheel system was also discussed and its controlling technique for the charging and discharging modes of the FESS was analysed. The final section of Chapter 5 described the design of the controllers for the operation of the flywheel system and its MG and converters. The speed, torque and voltage controllers including determination of their associated gain parameters were analysed in detail.

Chapter 6 presented the model, analysis, and results of the flywheel system integrated into an autonomous solar PV system for residential applications. The residential model and generation of different load profiles for a specified number of houses were described in detail. The developed model of a hybrid solar PV system, a backup diesel generator (DGen), and flywheel storage connected to a residential load were presented. The operation of the hybrid system was analysed based on a number of strategies to account for close to real-life situations such as PV-DGen system without storage, DGen-FESS without solar PV, and a combined PV-DGen-FESS. For each case, the communication and responsiveness of the model in terms of supplying

the total electrical demand and the outputs of the PV system and the diesel generator as well as the flywheel storage was analysed and the results were given. The analytical results for the electrical characteristics of the system such as currents and voltages of the generator and flywheel system, output voltage of the PV system and the DC-link voltage were also presented.

Chapter 6 also discussed the analysis of generator fuel consumption based on the above-mentioned scenarios. It was shown that the availability of the flywheel storage had a great impact on the fuel consumption of the diesel engine. The findings of this research showed that in some conditions, the flywheel contribution had led to about 60% reduction in operation time of the diesel generator. The impact of the FESS was dependent on its initial state of charge as well as the complexity of the demand. The calculated minimum annual fuel cost savings imposed by the flywheel system for the cases of DGen-FESS and combined PV-DGen-FESS was about £760 per year and £450 per year, respectively. On the other hand, in scenarios where the stored energy of the flywheel was fully utilised to supply the demand and the diesel engine was quite rarely engaged, a maximum annual fuel cost saving of £3,300 per year was achieved.

A comparison of projected lifetime cost estimations in 2015 to 2050 for flywheels and Li-ion batteries showed that flywheels will have lower levelised cost of storage (LCOS) in primary response but will remain the second-best technology in secondary response, black start and power quality applications. It was also discussed that the estimated LCOS will be much lower for steel rotor flywheels given the cheaper cost, recyclability and low maintenance requirements associated with the use of laminated steel in the rotor of the flywheel systems. Finally, it was concluded that the use of a flywheel storage system was not only limited to generator fuel reductions and fuel savings but could also increase the diesel engine's efficiency and lifetime. It adds stability to the system that would, otherwise, cannot be achieved with a standalone PV system backed up by the diesel generator. In addition, from the environmental perspective, reducing the service of the diesel generator will reduce greenhouse gases due to CO_2 emissions.

7.2 Recommendations for future research

This research provided an assessment of flywheel storage for use in residential applications where the customers have no access to an electrical grid and solar PV systems are used as the main source of energy supply. Chemical batteries have been the most common and well-established choice of storage for such applications. The higher capital cost and the safety issue of flywheels have been a major obstacle to their emergence for residential energy storage applications. Although the flywheel is one of the earliest forms of energy storage, compact, reliable, low maintenance flywheels have only become available relatively recently. The numbers produced have been small, and the use of more exotic materials and their processing, such as carbon fibre composites, have kept the cost at about five times higher than steel flywheels. New innovative designs based on steel could overcome the safety concern for highly stressed rotors, which can now operate at much higher tip speeds than was considered safe for monolithic steel rotors [164]. The use of steel laminates in the rotor of the flywheel can reduce both cost and safety issues since it allows provision of a thinner rotor containment with a smaller volume. Steel has the benefit that the material and processing routes are well established and understood to the supply base which is already there, for low-cost manufacturing at the all critical batch scales of 10s to 1000s. Steel is easily recyclable in comparison to batteries, although recycling will not need to be done for decades given an effective infinite calendar life and cycle life of many 10s of thousands.

In contrast, leaving technical issues aside, batteries can have significant environmental and social impacts. Based on a very recent publication on study of energy storage and environmental challenges of batteries [14], the negative environmental impact of batteries can be in the form of toxic fumes, GHG emissions, and hazardous waste that will be generated during manufacturing, recycling or disposal, transportation, collection, usage and storage. Due to high energy consumption during their manufacturing, environmental containments produced by the batteries is significant compared to processes of other energy storage systems. The

collection, disposal and recycling of batteries is a costly process requiring adequate facilities which will be difficult to implement and remains as a major challenge for less developed countries. Li-Ion batteries that are known to have the least level of toxic substances compared to other types of batteries, can generate between 120 and 200 kg $CO_{2\text{-eq}}$/kWh during the recycling process [165], although the recycling and collection rate of used Li-Ion is very low and limited to only 3% at present [166, 167].

Considering the attributes and drawbacks of both chemical batteries and flywheel storage systems, there are many technical and non-technical aspects of both technologies that can be compared and analysed. This research addressed the use of flywheel technology for standalone residential applications. An analysis of the flywheel storage combined with a solar PV system and a diesel engine was presented. The impact and contribution of the flywheel in improving system stability and generator fuel consumption were analysed. A research area recommended for future work is the individual assessment of flywheel and battery storage for a standalone solar PV system. Use of batteries for such applications has been widely analysed in the literature, however, like-for-like comparison of both storage technologies for the same application will be an area of interest. Considering a solar PV system with a backup diesel generator and a storage type of flywheel or battery storage, an analysis of the life cycle impact of each storage system will be of great importance.

The advantages of using steel laminates instead of solid steel or carbon composites in flywheel rotors have been discussed in detail. In case of a failure, the use of steel laminates in the flywheel rotor allows only a small fraction of the rotor energy to be released and this doesn't happen instantly or will not explode as in the case of a carbon composite rotor. The rotor containment can be thinner and as a result, the cost will be reduced and the safety will be significantly improved. However, the manufacture of the rotor from laminations of steel requires accuracy and is quite challenging in comparison to the construction of a solid steel rotor. The level of complications in the design and manufacturing process is further increased if different flywheel rotor shapes such as Laval disks with curves are produced. This would require more

detailed assessment and although this innovation is currently limited to cylindrical rotors with thin circular sheets of steel laminates, experimental testing for a number of commonly used flywheel rotor shapes will be a subject of interest for future research.

The solar irradiance of the PV system is another important parameter that will affect the level of contribution of the storage system. In the present work, a randomly generated set of data was used where the periods of low irradiance were ignored assuming a minimum level of sunshine is always present and the PV system can always generate a minimum power except for the times of a cloud pass or at night. The performance of the solar PV system based on real-life irradiance data for a village or small town in a remote area of a country will test the storage technologies to their limits (i.e. deep discharge, multiple cycles per day, instant response, etc.) which can be studied as a subject of further research.

Analysis of the flywheel storage in current work was performed at the times of peak demand and mostly for the cases with many load fluctuations. This was assessed for the two cases of combined PV-DGen-FESS and DGen-FESS without the presence of a solar PV system. For the latter case where the demand is shared between the diesel engine and the flywheel, the storage system would be challenged for a large number of cycles and depth of discharge and this will not be a suitable fit for the battery if it was used instead of the flywheel. However, if the same system was tested for the non-peak demand conditions and with reasonable load fluctuations, the battery storage might be a better fit in comparison to flywheel storage. Therefore, an assessment of a combined operation of flywheel and battery for improving the efficiency of a solar PV system while reducing environmental impact and cost is recommended for future researchers.

The design and analysis of the current work were performed in MATLAB/Simulink where the dynamics of the system at different stages of charging, discharging, and standby states have been analysed and compared. MATLAB/Simulink provides the flexibility in designing the controller algorithm and

allowing recalibration of the system at the times of higher energy demand, solar irradiance fluctuations and switching between different charge-discharge states. Alternatively, the model of the hybrid PV-DGen-FESS could also be implemented using HOMER Pro software to evaluate the system from a techno-economic point of view. HOMER Pro has many advantages that would be quite essential and of great importance when designing small scale micro-grid networks. The software uses non-differential optimisation which is much simpler and faster compared to MATLAB/Simulink. The computational time is significantly reduced and thousands of simulations can be performed in a few seconds. Another important feature of HOMER is its embedded sets of rules for controlling the generator and storage system with respect to the availability of renewable energy source. It can be managed using the Cycle Charging Dispatch Strategy or Load Following Dispatch Strategy depending on the sensitivity of the primary load, the engagement of the storage bank and the level of cost savings [168]. However, on the other hand, HOMER Pro has some limitations and does not include an algorithm for AC optimal power flow which will lead to not capturing frequency and voltage variations and hence, system transients cannot be analysed. Also, it is highly simplistic optimisation algorithm limits the capability of the software to investigate complex systems and perform stability analysis [169]. Therefore, for future research, it will be interesting to develop the model of the hybrid system and compare its dynamic performance using both software packages.

References

[1] H. Chen, T. N. Cong, W. Yang, C. Tan, Y. Li and Y. Ding, "Progress in electrical energy storage system: A critical review," *Progress in Natural Sciences: ScienceDirect,* vol. 19, pp. 291-312, 2009.

[2] I. Hadjipaschalis, A. Poullikkas and V. Efthimiou, "Overview of current and future energy storage technologies for electric power applications," *ScienceDirect: Renewable and Sustainable Energy Reviews,* vol. 13, pp. 1513-1522, 2009.

[3] P. Medina, A. W. Bizuayehu, J. Catalao, E. Rodrigues and J. Contreas, "Electrical Energy Storage Systems: Technologies' State-of-the-Art, Techno-Economic Benefits and Applications Analysis," in *2014 47th IEEE Hawaii International Conference on System Science*, 2014.

[4] Organisation for Economic Co-operation and Development (OECD), "Energy: OECD Green Growth Studies," 2011. [Online]. Available: www.oecd.org/publishing. [Accessed 01 02 2018].

[5] F. C. F. Tim , "Energy Storage: The Missing Link in the UK's Energy Commitments," Institution of Mechanical Engineers, London, UK, April 2014.

[6] "UK Renewable Energy Roadmap Update," Department of Energy and Climate Change, London, UK, November 2013.

[7] P. Taylor, R. Bolton, D. Stone, X.-P. Zhang, C. Matin and P. Upham, "Pathways for Energy Storage in the UK," The Centre for Low Carbon Futures 2050, UK, 27 March 2012.

[8] G. Strbac, M. Aunedi, D. Pudjianto, P. Djapic, F. Teng, A. Sturt, D. Jackravut, R. Sansom, V. Yufit and N. Brandon, "Strategic Assessment of the Role and Value of Energy Storage Systems in the UK Low Carbon Energy Future," Energy Future Labs, Imperial College London, London, UK, June 2012.

[9] P. C. Del Granado, S. W. Wallace and Z. Pang, "The Value of Electricity Storage in Domestic Homes: A Smart Grid Perspective," *Energy Systems,* vol. 5, pp. 211-232, 2014.

[10] DG ENER Working Paper, "The Future Role and Challenges of Energy Storage," European Commission, Directorate-General for Energy.

[11] Q. Fu, A. Hamidi, A. Nasiri, V. Bhavaraju, S. Krstic and P. Theisen, "The Role of Energy Storage in a Microgrid Concept-Examining the Opportunities and Promise of Microgrids," IEEE Electrification Magazine, February 2014.

[12] B. D. Manz, R. Piwko and N. Miller, "Look Before You Leap: The Role of Energy Storage in the Grid," *IEEE Power and Energy Magazine,* vol. 10, no. 04, pp. 75-84, August 2012.

[13] K. R. Pullen, "The Role of Flywheel Energy Storage in Decarbonised Electrical Power Systems," Energy Learning: United Nations UNEP-European Energy Centre EEC, [Online]. Available: https://energy-learning.com/index.php/opinion/78-what-s-new/162-flywheel-energy-storage. [Accessed 09 November 2018].

[14] A. R. Dehghani-Saniji, E. Tharumalingam, E. Dusseault and R. Fraser, “Study of Energy Storage Systems and Environmental Challenges of Batteries,” *ELSEVIER: Renewable and Sustainable Energy Reviews ,* vol. 104, pp. 192-208, 2019.

[15] O. Schmidt, S. Melchior, A. Hawkes and L. Staffell, “Projecting the Future Levelized Cost of Electricity Storage Technologies,” *Joule,* vol. 3, pp. 81-100, January 2019.

[16] P. W. Parfomak, “Energy Storage for Power Grids and Electric Transportation: A Technology Assessment,” Congressional Research Service-CRS Report for Congress, March 2012.

[17] R. Hebner and A. Walls, “Flywheel Batteries Come Around Again: Kinetic energy storage will propel applications ranging from railroad trains to space stations,” *IEEE Spectrum,* vol. 39, pp. 46-51, 2002.

[18] B. Bolund, H. Bernhoff and M. Leijon, “Flywheel energy and power storage systems,” *Renewable and Sustainable Energy Reviews,* vol. 11, p. 235–258, 2007.

[19] R. Sebastian and R. Pena Alzola, “Flywheel energy storage systems: Review and simulation for an isolated wind power system,” *Renewable and Sustainable Energy Reviews,* vol. 16, pp. 6803-6813, 2012.

[20] A. Emadi, A. Nasiri and S. B. Bekiarov, “Uninterruptible Power Supplies and Active Filters,” in *Power Electronics and Applications Series*, Washington DC, USA, CRC Press, 2005, pp. 19-24.

[21] D. Bender, “FLYWHEELS,” Sandia National Laboratories, Albuquerque, New Mexico and Livermore, California, May 2015.

[22] M. E. Amiryar and K. R. Pullen, “A review of Flywheel Energy Storage System Technologies and Their Applications,” *Applied Sciences, MDPI,* vol. 7, no. 3, pp. 286-307, 2017.

[23] G. Genta, Kinetic Energy Storage: Theory and Practice of Advanced Flywheel Systems, London, UK, 1985.

[24] H. W. Dickinson, “A Short History of the Steam Engines,” *Cambridge University Press, Cambridge, United Kingdom,* pp. 79-82, 2011.

[25] R. S. Shelke and D. G. Dighole, “A Review paper on Dual Mass Flywheel system,” *International Journal of Science, Engineering and Technology Research (IJSETR),* vol. 5, no. 1, pp. 326-331, 2016.

[26] R. Östergard, “Flywheel Energy Storage—A Conceptual Study,” *Master's Thesis*, Uppsala, Sweden, Uppsala Universitet, 2011.

[27] V. Babuska, S. M. Beatty, B. J. deBlonk and J. L. Fausz, “A Review of Technology Developments in Flywheel Attitude Control and Energy Transmission Systems,” in *2004 IEEE Aerospace Conference Proceedings*, Big Sky, MT, USA, 6-13 March 2004.

[28] J. G. Bitterly, “Flywheel technology past, present, and 21st-century projections,” *In IEEE Aerospace and Electronic Systems Magazine vol. 13, no. 8*, Honolulu, HI, USA, 1998.

[29] H. Liu and J. Jiang, “Flywheel energy storage—An upswing technology,” *Energy and Buildings in ScienceDirect,* vol. 39, pp. 599-604, 2007.

[30] R. Pena-Alzola, D. Campos-Gaona and M. Ordonez, “Control of Flywheel Energy Storage Systems as Virtual Synchronous Machines for Microgrid,” in *In Proceedings of the 2015 IEEE 16th Workshop on Control Modelling for Power Electronics (COMPEL)*, Vancouver, BC, Canada, 2015.

[31] J. G. De Oliveira, *Power Control Systems in a Flywheel based All-Electric Driveline,* Uppsala, Sweden: Uppsala, Universitet, 2011.

[32] A. A. Akhil, G. Huff, A. B. Currier, B. C. Kaun, D. M. Rastler, S. B. Chen, A. L. Cotter, D. T. Bradshaw and W. D. Gauntlett, “SANDIA REPORT: DOE/EPRI 2013 Electricity Storage Handbook in Collaboration with NRECA,” Sandia National Laboratories, TN, U.S.A, 2013.

[33] Z. Guo, X. Mu, Z. Bai and B. Cao, “Research on the Control of Flywheel Battery,” *Journal of Applied Sciences,* vol. 7, no. 12, pp. 3312-3316, 2007.

[34] X. Zhang and J. Yang, “An improved discharge control strategy with load current and rotor speed compensation for high-speed flywheel energy storage system,” in *In Proceedings of the 17th International Conference on Electrical Machines and Systems (ICEMS)*, Hangzhou, China, October 2014.

[35] S. Samineni, B. K. Johnson, H. L. Hess and J. D. Law, “Modeling and Analysis of a Flywheel Energy Storage System with a Power Converter Interface,” in *International Conference on Power Systems Transients-IPST 2003 in New Orleans*, New Orleans, USA, 2003.

[36] L. Bakay, M. Dubois, P. Viarouge and J. Ruel, “Mass-losses relationship in an optimized 8-pole radial AMB for Long Term Flywheel Energy Storage,” in *Proceedings of the IEEE AFRICON 2009*, Nairobi, Kenya, 2009.

[37] R. Sebastian, J. Quesada, A. Colmenar and Pena-Alzola, “Review of flywheel based energy storage systems,” in *Proceedings of the 2011 International Conference on power engineering, energy and electrical drives*, Malaga, Spain.

[38] J. Firebaugh, *Design Options for a Flywheel Energy Storage System, Master's thesis, Department of mechanical engineering, University of Washington,* 2007.

[39] K. M. Farhani, *Modeling and Analysis of a Flywheel Energy Storage System for Voltage Regulation,* Toronto, Ontario, Canada: Master's thesis. Ryerson University, 2010.

[40] “Dynamic Boosting Systems (DBS),” Laminated Steel Energy Storage Flywheel Technology, [Online]. Available: http://www.dynamicboost.com/flywheel-technology-energy-storage. [Accessed 18 September 2018].

[41] M. I. Daoud, A. S. Abdel-Khalik, A. Massoud, S. Ahmed and N. H. Abbasy, “On The Development of Flywheel Storage Systems for Power Systems Applications: A Survey,” *In Proceedings of the 20th International Conference on Electrical Machines (ICEM)*, Marseille, France, 2012.

[42] M. A. Awadallah and B. Venkatesh, “Energy storage in flywheels: an overview,” *Canadian Journal or Electrical and Computer Engineering,* vol. 38, no. 2, pp. 183-193, 2015.

[43] Y. Yali, W. Yuanxi and S. Feng, “the Latest Development of the Motor/Generator for the Flywheel Energy Storage System,” in *2011 International Conference on Mechatronic Science, Electric Engineering and Computer,* Jilin, China, August 2011.

[44] L. Chang, “Comparison of AC drives for electric vehicles - A report on experts' opinion survey,” in *IEEE Aerospace Systems Magazine*, Fredericton, NB, Canada, August 1994.

[45] E. Severson, R. Nilssen, T. Undeland and N. Mohan, “Suspension Force Model for Bearingless AC Homopolar Machines Designed for Flywheel Energy Storage,” in *7th IEEE GCC Conference and Exhibition (GCC)*, Doha, Qatar, 17-20 November 2013.

[46] W. Keyin, L. Dezhi, M. Jin, O. Yangbin, Z. Xiaofei and C. Junquan, “Design and Simulation of a 12-Phase Flywheel Energy Storage Generator System with Linearly Dynamic Load,” *IEEE Transactions on Applied Superconductivity,* vol. 20, no. 03, pp. 1050 - 1054, June 2010.

[47] E. L. Carrillo Arroyo, “Modelling and Simulation of Permanent Magnet Synchronous Motor Drive System,” University of Puerto Rico, San Juan, Puerto Rico, 2006.

[48] K. Mounika and B. K. Babu, “Sinusoidal and Space Vector Pulse Width Modulation for Inverter,” *International Journal of Engineering Trends and Technology (IJETT),* vol. 4, no. 4, pp. 1012-1017, April 2013.

[49] M. H. Rashid, N. Kumar and A. Kulkarni, Power Electronics: Devices, Circuits, and Applications, 4th Edition ed., Essex, UK: Pearson, Essex, UK, 2014.

[50] L. Zhou and Z. Ping Qi, “Modeling and Control of a Flywheel Energy Storage System for Uninterruptible Power Supply,” in *In Proceedings of the 2009 International Conference on Sustainable Power Generation and Supply*, Nanjing, China, April 2009.

[51] M. Khaterchi, j. Belhadj and M. Elleuch, “Participation of Direct Drive Wind Turbine to the Grid Ancillary Services using a Flywheel Energy Storage System,” in *201O 7th International Multi-Conference on Systems, Signals and Devices*, Amman, Jordan, June 2010.

[52] N. S. Gayathri and N. Senroy, “Wind turbine with flywheel for improved power smoothening and LVRT,” in *In Proceedings of the IEEE Power and Energy Society General Meeting*, Vancouver, BC, Canada, July 2013.

[53] M. Rashid, Power Electronics Handbook, 3rd Edition ed., London, UK: Butterworth Heinemann, 2011.

[54] B. M. Wilamoswski and J. D. Irwin, The industrial Electronics Handbook: Power Electronics and Motor Drives, 2nd Edition ed., New York, NY, USA: CRC Press, Taylor and Francis Group, 2011.

[55] G. O. Suvire and M. G. Molina, “Improving the Integration of Wind Power Generation Into AC Microgrids Using Flywheel Energy Storage,” *IEEE Transactions on Smart Grid,* vol. 3, no. 4, pp. 1945-1954, December 2012.

[56] T. Friedli, J. W. Kolar, J. Rodriguez and P. W. Wheeler, “Comparative Evaluation of Three-Phase AC–AC Matrix Converter and Voltage DC-Link Back-to-Back Converter Systems,” *IEEE transactions on industrial electronics,* vol. 59, no. 12, pp. 4487-4510, December 2012.

[57] P. Gamboa, S. Ferreira Pinto, J. Fernando Silva and E. Margato, “A Flywheel Energy Storage System with Matrix Converter Controlled Permanent Magnet Synchronous Motor,” in *Proceedings of the 2008 International Conference on Electrical Machines*, Vilamoura, Algarve, Portugal, September 2008.

[58] B. Wang and G. Venkataramanan, “Dynamic Voltage Restorer Utilizing a Matrix Converter and Flywheel Energy Storage,” *IEEE Transactions On Industry Applications,* vol. 45, no. 1, pp. 222-231, January/February 2009.

[59] X. Chang, Y. Li, W. Zhang, N. Wang and W. Xue, “Active Disturbance Rejection Control for a Flywheel Energy Storage System,” *IEEE Transactions On Industrial Electronics,* vol. 62, no. 2, pp. 991-1001, February 2015.

[60] A. Elserougi, A. M. Massoud and S. Ahmed, “Flywheel Energy Storage System based on boost DC-AC converter,” in *In Proceedings of IET Conference on Renewable Power Generation (RPG 2011)*, September 2011.

[61] Z. Jibin, L. Kai, Z. Mei and H. JianHui, “Simulation of Flywheel Energy Storage System (FESS) Using Z-Source Inverter,” in *In Proceedings of the 2010 International Conference on Electric Machines and Systems*, Incheon, Korea, October 2010.

[62] H. Kim and S.-K. Sul, “A Novel Filter Design for Output LC Filters of PWM Inverters,” *Journal of Power Electronics,* vol. 11, no. 1, pp. 74-81, January 2011.

[63] W. Santiago, “Inverter Output Filter Effect on PWM Motor Drives of a Flywheel Energy Storage System,” National Aeronautics and Space Administration, Glenn Research Center, 2004.

[64] M. Subkhan and M. Komori, “New Concept for Flywheel Energy Storage System Using SMB and PMB,” *IEEE Transactions On Applied Superconductivity,* vol. 21, no. 3, pp. 1485-1488, June 2011.

[65] S. Sabihuddin, A. E. Kiprakis and M. Mueller, “A Numerical and Graphical Review of Energy Storage Technologies,” *Energies,* vol. 8, no. 1, pp. 172-216, March 2015.

[66] M. Strasik, P. E. Johnson, A. C. Day, J. Mittleider, M. D. Higgins, J. Edwards, J. R. Schinler, K. E. McCrary, C. R. McIver, D. Carlson, J. F. Gonder and J. R. Hull, “Design, Fabrication, and Test of a 5-kWh/100-kW Flywheel Energy Storage Utilizing a High-Temperature Superconducting Bearing,” *IEEE Transactions On Applied Superconductivity,* vol. 17, no. 2, pp. 2133-2137, June 2007.

[67] C. Zhang and K. J. Tseng, “A Novel Flywheel Energy Storage System With Partially-Self-Bearing Flywheel-Rotor,” *IEEE Transactions On Energy Conversion,* vol. 22, no. 2, pp. 477-487, 2007.

[68] C. Zhang and K. J. Tseng, “Design and control of a novel flywheel energy storage system assisted by hybrid mechanical-magnetic bearings,” *Mechatronics,* vol. 23, pp. 297-309, 2013.

[69] D. Bender, “Recommended Practices for the Safe Design and Operation of Flywheels,” Sandia National Laboratories, Livermore, California, December 2015.

[70] “Beacon Power LCC,” Beacon Power's Operating Plant in Stephentown, New York, [Online]. Available: http://beaconpower.com/stephentown-new-york/ . [Accessed 10 December 2017].

[71] R. Elliman, C. Gould and M. Al-Tai, “Review of current and future electrical energy storage devices,” in *Power Engineering Conference (UPEC), 50th International Universities*, Stoke on Trent, UK, 1-4 September 2015.

[72] M. S. Whittingham, “History, Evolution, and Future Status of Energy Storage,” in *Proceedings of the IEEE :Special Centennial Issue*, 13 May 2012.

[73] S. Amodeo, H. Chiacchiarini, J. Solsona and C. Busada, “High-performance sensorless nonlinear power control of a flywheel energy storage system,” *ScienceDirect: Energy Conversion and Management,* vol. 50, p. 1722–1729, 2009.

[74] R. Okou, A. B. Sebitosi, A. Khan and P. Pillay, “The potential impact of small-scale flywheel energy storage technology on Uganda’s energy sector,” *Journal of Energy in Southern Africa,* vol. 20, no. 1, pp. 14-19, February 2009.

[75] Z. Jiancheng, H. Lipei, C. Zhiye and W. Su, “Research on Flywheel Energy Storage System for Power Quality,” in *2002 IEEE International Conference on Power System Technology*, Kunming, China, China, 13-17 October 2002.

[76] R. Arghandeh, M. Pipattanasomporn and S. Rahman, “Flywheel Energy Storage Systems for Ride-through Applications in a Facility Microgrid,” *IEEE Transactions on Smar Grid,* vol. 3, no. 4, pp. 1955-1962, December 2012.

[77] “US Department of Energy: Global Energy Storage Database,” Office of Electricity Delivery and Energy Reliability, [Online]. Available: http://www.energystorageexchange.org/projects. [Accessed 25 November 2017].

[78] “Kenya First Flywheel Energy Storage Technology to be set up in Marsabit,” [Online]. Available: https://kenyaenergyfuture.wordpress.com/tag/powerstore/. [Accessed 25 November 2017].

[79] “ABB Microgrid Solution to Boost Renewable Energy Use by Remote Community in Kenya,” ABB PowerStoreTM technology to stabilize power supply from wind/diesel hybrid plant in the city of Marsabit , 2 September 2015. [Online]. Available: http://www.abb.com/cawp/seitp202/118e562a8edb8d40c1257eb400446361.aspxglobal/seitp/seitp202.nsf. [Accessed 28 November 2017].

[80] A. Al-Diab and C. Sourkounis, “Unbalanced Voltage Drops Compensations Using Flywheel Energy Storage System,” in *2011 11th International Conference on Electrical Power Quality and Utilisation (EPQU)*, Lisbon, Portugal , 17-19 October 2011.

[81] P. Fairly, “Flywheels Keep the Grid in Tune,” *IEEE Spectrum,* vol. 48, no. 7, pp. 16-18, 2011.

[82] M. L. Lazarewicz and A. Rojas, “Grid Frequency Regulation by Recycling Electrical Energy In Flywheels,” in *IEEE Power Engineering Society General Meeting, 2004*, Denver, CO, USA, 6-10 June 2004.

[83] “EFDA JET Fusion Flywheel,” EUROFusion, [Online]. Available: https://www.euro-fusion.org/2010/01/jets-flywheels-2/. [Accessed 05 December 2017].

[84] B. Keen and P. Kupschus, “JET-Operation and Development: Pulsed Power Supplies for JET Coils,” JET Joint Undertaking Progress Report, Abingdon, UK, 1987.

[85] “Spot on JET Technology: Power Supply,” EUROFusion, 2016. [Online]. Available: https://www.euro-fusion.org/fusion/jet-tech/jets-flywheels/ . [Accessed 27 October 2017].

[86] B. Power, “20MW Flywheel Frequency Regulation Plant; Final Technology Performance Report,” Beacon Power, Tyngsboro, MA, USA, 2016.

[87] V. A. Boicea, “Energy Storage Technologies: The Past and the Present,” *Proceedings of IEEE ,* vol. 102, no. 11, pp. 1777-1794, November 2014.

[88] L. Zhou and Z. P. Qi, “Modeling and Simulation of Flywheel Energy Storage System with IPMSM for Voltage Sags in Distributed Power Network,” in *In Proceedings of the 2009 IEEE International Conference on Mechatronics and Automation*, Changchun, China, 9-12 August 2009.

[89] “Flywheel Energy Storage. An Alternative to Batteries for Uninterruptible Power Supply Systems,” US Department of Energy (DOE): Federal Energy Management Program (FEMP), Washington DC, USA, 2003.

[90] “EasyStreet Ramps Up Data Center Operations, Deploys Additional VYCON Flywheel Systems to Protect its Green Data Center,” VYCON, CLANETIX Technologies, 03 April 2013. [Online]. Available: https://www.calnetix.com/newsroom/press-release/easystreet-ramps-data-center-operations-deploys-additional-vycon-flywheel. [Accessed 02 November 2017].

[91] A. S. Munoz, M. Garcia and M. Gerlich, "*Overview of Storage Technologies",* Project SENSIBLE: A project funded by the European Unions Horizon 2020 research and innovation programme, January 2016.

[92] S. Faisas, P. Santos, J. Sousa and R. Castro, “An Overview on Short and Long-Term Response Energy Storage Devices for Power Systems Applications,” in *International Conference on Renewable Energy and Power Quality*, Santander, Spain, 11-14 March 2008.

[93] “Kinetic energy storage wins acceptance,” Railway Gazette, METRO, 01 April 2004. [Online]. Available: http://www.railwaygazette.com/news/single-view/view/kinetic-energy-storage-wins-acceptance.html. [Accessed 20 October 2017].

[94] “VYCON Technology Allows Los Angeles Metro to be First Transit Agency in U.S. Using Flywheels to Achieve Nearly 20 Percent in Rail Energy Savings,” VYCON, CALNETIX Technologies, 30 October 2014. [Online]. Available: https://www.calnetix.com/newsroom/press-release/vycon-technology-allows-los-angeles-metro-be-first-transit-agency-us-using. [Accessed 05 November 2017].

[95] O. Solis, D. Turner, F. Castro, L. Brian Ng, A. Dombek, L. Bukhin and G. Thompson, “LA Metro Red Line Wayside Energy Storage Substation Revenue Service Regenerative Energy Saving Results,” in *Proceedings of Joint Rail Conference (JRC)* , Colorado Springs CO, 2-4 April 2014.

[96] “Advanced Flywheel Energy Storage,” ESA, Williams Hybrid Power, [Online]. Available: http://www.esa-tec.eu/space-technologies/for-space/williams-hybrid-power-advanced-flywheel-energy-storage/. [Accessed 26 October 2017].

[97] A. Cotton, “Audi R18 (2014). Racecar Engineering,” 01 June 2014. [Online]. Available: http://www.racecar-engineering.com/cars/audi-lmp14/#. [Accessed 25 October 2017].

[98] “GKN develops electric flywheel hybrid system for buses,” SAE International, 12 February 2015. [Online]. Available: http://articles.sae.org/13905/. [Accessed 27 October 2017].

[99] L. Truong, F. Wolff and N. V. Dravid, “Simulation of Flywheel Electrical System for Aerospace Applications,” *In Proceedings of the 35th Intersociety Energy Conversion Engineering Conference and Exhibition*, Las Vegas, NV, USA, 24-28 July 2008.

[100] B. H. Kenny, P. E. Kascak, R. Jansen, T. Dever and W. Santiago, “Control of a High-Speed Flywheel System for Energy Storage in Space Applications,” *IEEE Transactions on Industry Applications,* vol. 41, no. 4, pp. 1029-1038, July/August 2005.

[101] P. Fairley, “Flywheels Get Their Spin Back,” *IEEE Spectrum: Grid Stabilisation Energizes Flywheel Pioneer Beacon Power and a Host of New Competitors,* vol. 51, no. 1, pp. 18-18, January 2015.

[102] D. Williams, “US Marine Corps utilising microgrid energy storage project,” Decentralized Energy, Quantum Energy Storage, 17 September 2015. [Online]. Available: http://www.decentralized-energy.com/articles/2015/09/us-marine-corp-utilising-microgrid-energy-storage-project.html. [Accessed 10 October 2017].

[103] CNESA, “Flywheel Energy Storage,” China Energy Storage Alliance, 21 October 2015. [Online]. Available: http://en.cnesa.org/latest-news/2015/10/21/flywheel-energy-storage-in-china. [Accessed 15 April 2019].

[104] C. Doetsch, B. Droste-Franke, G. Mulder and M. Perrin, “Electric Energy Storage - IEA ECES26 Future Energy Storage Demand,” January 2015.

[105] Spotlight, *Solving Challenges in Energy Storage,* Office of Technology Transitions, August 2018.

[106] “Europe's Largest Hybrid Flywheel Battery Project,” Off-Grid Energy Independence, 13 June 2017. [Online]. Available: https://www.offgridenergyindependence.com/articles/11161/europes-largest-hybrid-flywheel-battery-project. [Accessed 10 April 2019].

[107] “Global Flywheel Energy Storage Market 2016-2020,” Market Intelreports, January 2016.

[108] “Global Flywheel Energy Storage Forcast 2018-2026: Global Flywheel Energy Storage Market to Grow at 8.93% of CAGR by 2027,” MENAFN, February 2019.

[109] A. Kailasan, T. Dimond, P. Allaire and D. Sheffler, “Design and Analysis of a Unique Energy Storage Flywheel System - An Integrated Flywheel, Motor/Generator, and Magnetic Bearing Configuration,” *Journal of Engineering for Gas Turbines and Power,* vol. 37, DOI: 10.1115/1.4028575, pp. 1-10, April 2015.

[110] C. Tang, J. Yang, D. Han and H. Lei, “Rotor Dynamics Research of the Composite Flywheel Spin Test System: Modelling and Simulation,” *In Proceedings of the 2016 IEEE International Conference on Power and Renewable Energy (ICPRE)*, Shanghai, China, 21-23 October 2016.

[111] K. Zhang, X. Dai and X. Zhang, “Dynamic Analysis and Control of an Energy Storage Flywheel Rotor with Active Magnetic Bearings,” *In Proceedings of the 2010 International Conference on Digital Manufacturing and Automation (ICDMA)*, Changsha, China, 18-20 December 2010.

[112] C. Mao and C. Zhu, “Vibration Control for Active Magnetic Bearing Rotor System of High-speed Flywheel Energy Storage System in a Wide Range of Speed,” *In Proceedings of the 2016 IEEE Vehicle Power and Propulsion Conference (VPPC)*, Hangzhou, China, 17–20 October 2016.

[113] M. Subkhan and M. Komori, “New Concept for Flywheel Energy Storage System Using SMB and PMB,” *IEEE Transactions On Applied Superconductivity,* vol. 21, no. 03, pp. 1485-1488, June 2011.

[114] J. Zhao, Z. Gu, B. Li, X. Liu, X. Li and Z. Chen, “Research on the Torque and Back EMF Performance of a High Speed PMSM Used for Flywheel Energy Storage,” *Journal of Energies,* vol. 8, no. 4, pp. 2867-2887, 15 April 2015.

[115] W. Gengji and W. Ping, “Rotor Loss Analysis of PMSM in Flywheel Energy Storage System as Uninterruptable Power Supply,” *IEEE Transactions On Applied Superconductivity,* vol. 26, no. 07, pp. 1-5, October 2016.

[116] Y.-C. Chang, J.-C. Chen, J.-T. Chan and K.-H. Sun, “Space-vector Based Current Control of Permanent-Magnet Synchronous Motor/Generator Drive Applied to Flywheel Energy Storage System,” in *2013 IEEE 10th International Conference on Power Electronics and Drive Systems (PEDS)*, Kitakyushu, Japan , 22-25 April 2013.

[117] W. Su, T. Jin and S. Wang, “Modeling and Simulation of Short-term Energy Storage: Flywheel,” in *2010 International Conference on Advances in Energy Engineering*, Beijing, China , 19-20 June 2010 .

[118] A. S. Nagorny, N. V. Dravid, R. H. Jansen and B. H. Kenny, “Design Aspects of a High Speed Permanent Magnet Synchronous Motor/Generator for Flywheel Applications,” in *IEEE International Conference on Electric Machines and Drives, 2005*, San Antonio, TX, USA, 15-15 May 2005 .

[119] J. Pyrhonen, T. Jokinen and V. Hrabovcova, “Chapter 9: Heat transfer,” *Design of Rotating Electrical Machines*, West Sussex, United Kingdom, John Wiley & Sons, Ltd, 2008, pp. 477-482.

[120] H.-P. Liu, M. Werst and J. J. Hahne, “Prediction of Windage Losses of an Enclosed High Speed Composite Rotor in Low Air Pressure Environments,” *Proceedings of ASME Summer Heat Transfer Conference*, Austin, Texas, July 21-23, 2003.

[121] F. J. Thoolen, “Development of an advanced high speed flywheel energy storage system,” PhD Thesis, Eindhoven University of Technology, Eindhoven, 1993.

[122] R. A. Millikan, “Coefficient of slip in gases and the law of reflection of molecules from the surfaces of solids and liquids,” *Physical Review,* vol. 21, no. 23, pp. 217-237, 1923.

[123] J. W. Beck, “Bimodal Two-Stream Distribution and Compressible Couette Flow,” *Rarefied Gas Dynamics, Institute for Fluid Mechanics, Technical University of Munchen, Germany,* pp. 354-369, 1965.

[124] J. R. Dorfman, J. V. Sengers and C. F. McClure, “Kinetic theory of the drag force on objects in rarefied gas flows,” *Physica A: Statistical Mechanics and its Applications,* vol. 134, no. 2, pp. 283-322, January 1986.

[125] D. J. Alofs and G. S. Springer, “Rotating Cylinder Apparatus for Rarefied Gas Flow Studies,” *The Review of Scientific Instruments,* vol. 41, no. 08, pp. 1161-1163, 1970.

[126] L. Lees, “A Kinetic Theory Description of Rarefied Gas Flows,” *Hypersonic Research Project, Memorandum No. 51,* 15 December 1959.

[127] A. R. Kuhlthau, “Air Friction on Rapidly Moving Surfaces,” *Journal of Applied Physics,* vol. 20, no. 2, pp. 217-223, 1949.

[128] E. H. Kennard, Kinetic Theory of Gases with and Introduction to Statistical Mechanics, New York: McGraw-Hill, 1938.

[129] J. M. Bowyer and L. Talbot, *Engineering Projects Research Report HE-150-199,* Berkeley, California: University of California, 1956.

[130] M. E. Amiryar, K. R. Pullen, D. Nankoo, “Development of a High-Fidelity Model for an Electrically Driven Energy Storage Flywheel Suitable for Small Scale Residential Applications,” *Journal of Applied Sciences, MDPI,* vol. 8, no. 3, pp. 453-482, 2018.

[131] F. Wardle, Ultra-Precision Bearings, Cambridge, UK: Woodhead Publishing in Mechanical Engineering, 2015.

[132] A. Palmgren, Ball and Roller Bearing Engineering, 3rd Edition, Philadelphia, Burbank, 1959.

[133] (NSK), *Super Precision Bearings,* Newark, UK: NSK website , 2009.

[134] S. H. Shah, “The Design and Development of a High Speed Composite Flywheel for Hybrid Vehicles,” Imperial College London, London, UK, March 2006.

[135] “SKF Bearings,” [Online]. Available: http://www.skf.com/uk/products/index.html. [Accessed 15 December 2018].

[136] IRD balancing: Technical paper, *Balance Quality Requirements of Rigid Rotors: The practical application of ISO1940/1,* Chester, UK: IRD Balancing (www.irdbalancing.com), March 2009.

[137] F. Diaz-Gonzalez, A. Sumper and O. Gomis-Bellmunt, “Energy Storage Technologies,” in *Energy Storage in Power Systems*, West Sussex, United Kingdom, John Wiley & Sons Ltd, 2016, pp. 94-141.

[138] S. G. Venna, S. Vattikonda and S. Mandarapu, “Mathematical Modeling and Simulation of Permanent Magnet Synchronous Motor,” *International Journal of Advanced Research in Electrical, Electronics and Instrumentation Engineering,* vol. 2, no. 8, pp. 3720-3726, August 2013.

[139] K. Zhao, “The study of Improved PI Method for PMSM Vector Control System Based on SVPWM,” in *In Proceedings of the 2011 IEEE Industry Applications Society Annual Meeting, 9-13 October*, Orlando, Florida, USA, October 2011.

[140] Z. Zhang and J. Shu, “MATLAB-based Permanent Magnet Synchronous Motor Vector Control Simulation,” *In Proceedings of the 2010 3rd International Conference on Computer Science and Information Technology, 9-11 July, pp. 539-542*, Chengdu, China, 2010.

[141] T. Liu, Y. Tan, G. Wu and S. Wang, “Simulation of PMSM Vector Control System Based on Matlab/Simulink,” *In Proceedings of the 2009 International Conference on Measuring Technology and Mechatronics Automation, 11-12 April, pp. 343-346*, Zhangjiajie, China, 2009.

[142] H. M. Soliman and S. M. L-Hakim, “Simple Model and PI Controller to Improve the Performance Characteristics of PMSM under Field Oriented Control with Using SVPWM,” *International Journal of Advanced Engineering in Nano Technology,* vol. 2, pp. 5-13, 2015.

[143] S.-H. Kim, “Chapter 4: Modelling of Alternating Current Motors and Reference Frame Theory,” in *Electric Motor Control DC, AC, and BLDC Motors*, Oxford, United Kingdom, Joe Hayton, Elsevier, 2017, pp. 153-202.

[144] S.-H. Kim, “Chapter 5: Vector Control of Alternating Current Motors,” in *Electric Motor Control DC, AC, and BLDC Motors*, Oxford, United Kingdom, Elsevier, 2017, pp. 203-246.

[145] H. V. Doe and P. R. U. Shekokar, “A Review of Speed Control Techniques Using PMSM,” *International Journal of Innovations in Research Technologies,* vol. 1, pp. 247-253, 2014.

[146] P. Balazovic and R. Filka, “Sensorless PMSM Control for H-axis Washing Machine Drive,” *IEEE Annual Power Electronics Specialists Conference* , Czech Republic, 2008.

[147] L. A. Jose and K. Karthikeyan, “A Comparative Study of Sinusoidal PWM and Space Vector PWM of a Vector Controlled BLDC Motor,” *International Journal of Advanced Research in Electrical, Electronics and Instrumentation Engineering,* vol. 2, no. 6, pp. 2662-2668, 2013.

[148] R. P. Burgos, P. Kshirsagar, A. Lidozzi, F. Wang, D. Boroyevich and A. A. D. Frame, “Mathematical Model and Control Design for Sensorless Vector Control of Permanent Magnet Synchronous Machines,” in *In Proceedings of the 2006 IEEE COMPEL Workshop, Renselaer Polytechnic Institute, Troy, pp. 16-19 July*, New York, USA, 2006.

[149] N. Mohan, Electric Machines and Drives: A first course, Minneapolis, MN, USA: Wiley & Sons Inc., 2012.

[150] K. H. Ang and G. Chong, “PID Control System Analysis, Design, and Technology,” *IEEE Transactions on Control Systems Technology,* vol. 13, no. 4, pp. 559-576, July 2005.

[151] R. K. Sharma, V. Sanadhya, L. Behera and S. Bhattacharya, *Vector Control of a Permanent Magnet Synchronous Motor,* Kanpur, India: Control Instrumentation Division, Bhabha Atomic Research Centre, IEEE 2008.

[152] S. Talebi, B. Nikbakhtian and H. A. Toliyat, *A Novel Algorithm for Designing the PID Controllers of High-speedFlywheels for Traction Applications,* Texas, USA: Advanced Electric Machines & Power Electronics Laboratory, Department of Electrical & Computer Engineering, Texas A&M University, 2007.

[153] L. Wang, S. Chai, D. Yoo, L. Gan and K. Ng, “PID Control System Design for Electrical Drives and Power Converters,” *PID and Predictive Control of Electrical Drives and Power Converters using MATLAB®/Simulink®, First Edition*, Singapore, John Wiley & Sons, 2015, pp. 41-50.

[154] S. N. Vukosavic, “Chapter 21: Variable Frequency Synchronous Machines,” in *Electrical Machines*, New York, Springer, 2013, pp. 621-640.

[155] N. D. Muhamad, “Digital PI Controller Design for Power Inverter Using MATLAB-SIMULINK,” in *Modelling and Control of Power Converters and Drives*, Negara Malaysia, 2008, pp. 50-66.

[156] E. McKenna and M. Thomson, “Centre for Renewable Energy Systems Technology (CREST) Demand Model,” Loughborough University, [Online]. Available: https://www.lboro.ac.uk/research/crest/demand-model/. [Accessed 03 November 2018].

[157] “MATLAB for Deep Learning,” MathWorks, [Online]. Available: https://uk.mathworks.com/. [Accessed 03 November 2018].

[158] PV Array Block, “MathWorks,” [Online]. Available: https://uk.mathworks.com/search/site_search.html?suggestion=&c%5B%5D=entire_site&q=PV+array. [Accessed 10 October 2018].

[159] M. A. G. De Brito, L. P. Sampaio, L. G. Jr., G. A. Melo and C. A. Canesin, *Comparative Analysis of MPPT Techniques for PV Applications,* Sao Paolo, Brazil: Sao Paolo State University, 2011.

[160] V. K. Viswambarau, A. Ghani and E. Zhou, “Modelling and Simulation of Maximum Power Point Tracking Algorithm & Review of MPPT Techniques for PV Applications,” in *5th International Conference on Electronic Devices, Systems and Applications (ICEDSA)*, Ras Al Khaimah, United Arab Emirates , January 2017.

[161] A. K. Gupta and R. Saxena, “Review on Widely-used MPPT Techniques for PV Applications,” in *1st International Conference on Innovation and Challenges in Cyber Security*, Noida, India, 2016.

[162] J. Gershuny and O. Sulivan, “United Kingdom Time Use Survey, 2014-2015,” UK Data Service. SN: 8128, http://doi.org/10.5255/UKDA-SN-8128-1, [Online]. Available: https://beta.ukdataservice.ac.uk/datacatalogue/studies/study?id=8128. [Accessed 08 December 2018].

[163] E. McKenna and M. Thomson, “High-resolution Stochastic Integrated Thermal–electrical Domestic Demand Model,” *Applied Energy, Elsevier,* vol. 165, pp. 445-461, 2016.

[164] S. Sanders, M. Senesky, M. He and E. Chiao, “Low-Cost Flywheel Energy Storage Demonstration,” Energy Research and Development Division Final Project Report; Amber Kinetics, Inc., Union City, CA, USA, 2015.

[165] M. Romare and L. Dahllof, “The Life Cycle Energy Consumption and Greenhouse Gas. A Study with Focus on Current Technology and Batteries for Light-duty Vehicles,” IVL Swedish Environmental Research Institute Ltd, Stockholm, Sweden, 2017.

[166] H. Vikstrom, S. Davidsson and M. Hook, “Lithium Availability and Future Production Outlooks,” *ELSEVIER: Applied Energy,* vol. 110, pp. 252-266, 2013.

[167] T. Georgi-Maschler, B. Friedrich, R. Weyhe, H. Heegn and M. Rutz, “Development of a Recycling Process for Li-ion Batteries,” *ELSEVIER: Journal of Power Sources,* vol. 207, pp. 173-182, 2012.

[168] M. Madziga, A. Rahil and R. Mansoor, “Comparison between Three Off-Grid Hybrid Systems (Solar Photovoltaic, Diesel Generator and Battery Storage System) for Electrification for Gwakwani Village, South Africa,” *Environments,* vol. 5, no. 5, p. 21, May 2018.

[169] A. Oulis Rousis, D. Tzelepis, I. Konstantelos, C. Booth and G. Strbac, “Design of a Hybrid AC/DC Microgrid Using HOMER Pro: Case Study on an Islanded Residential Application,” *Inventions,* vol. 3, no. 3, p. 14, August 2018.

[170] S.-H. Kim, “Chapter 7: Pulse Width Modulation Inverters,” *AC, DC, and BLDC Electric Motors Control*, Oxford, UK, Joe Hayton, Elsevier, 2011, pp. 292-317.

[171] J. Singh, B. Singh, S. P. Singh and M. Naim, “Investigation of Performance Parameters of PMSM Drives using DTC-SVPWM Technique,” *2012 Students Conference on Engineering and Systems*, Allahabad, Uttar Pradesh, India, 12-18 March 2012.

[172] K. M. Remitha and A. Mathew, “MATLAB/SIMULINK Model of Field Oriented Control of PMSM Drive Using Space Vectors,” *International Journal of Advances in Engineering & Technology,* vol. 6, no. 3, pp. 1355-1364, July 2013.

[173] L. Suresh, K. Mahesh, M. Janaradha and M. Mahesh, “Simulation of Space Vector Pulse Width Modulation for Voltage Source Inverter using MATLAB/SIMULINK,” *Journal of Automation and Systems Engineering,* vol. 8, no. 3, pp. 133-140, 2014.

[174] L. Yu, C. Wang, H. Shi, R. Xin and L. Wang, “Simulation of PMSM Field-Oriented Control Based on SVPWM,” *29th Chinese Control And Decision Conference (CCDC), pp. 7407 - 7411*, Chongqing, China , May 2017.

This content has been removed for copyright protection reasons

Appendix A - pages 202-207
Appendix E - pages 220-222
Appendix E.2 pages 223-225

Appendix A Bearing specifications and catalogues

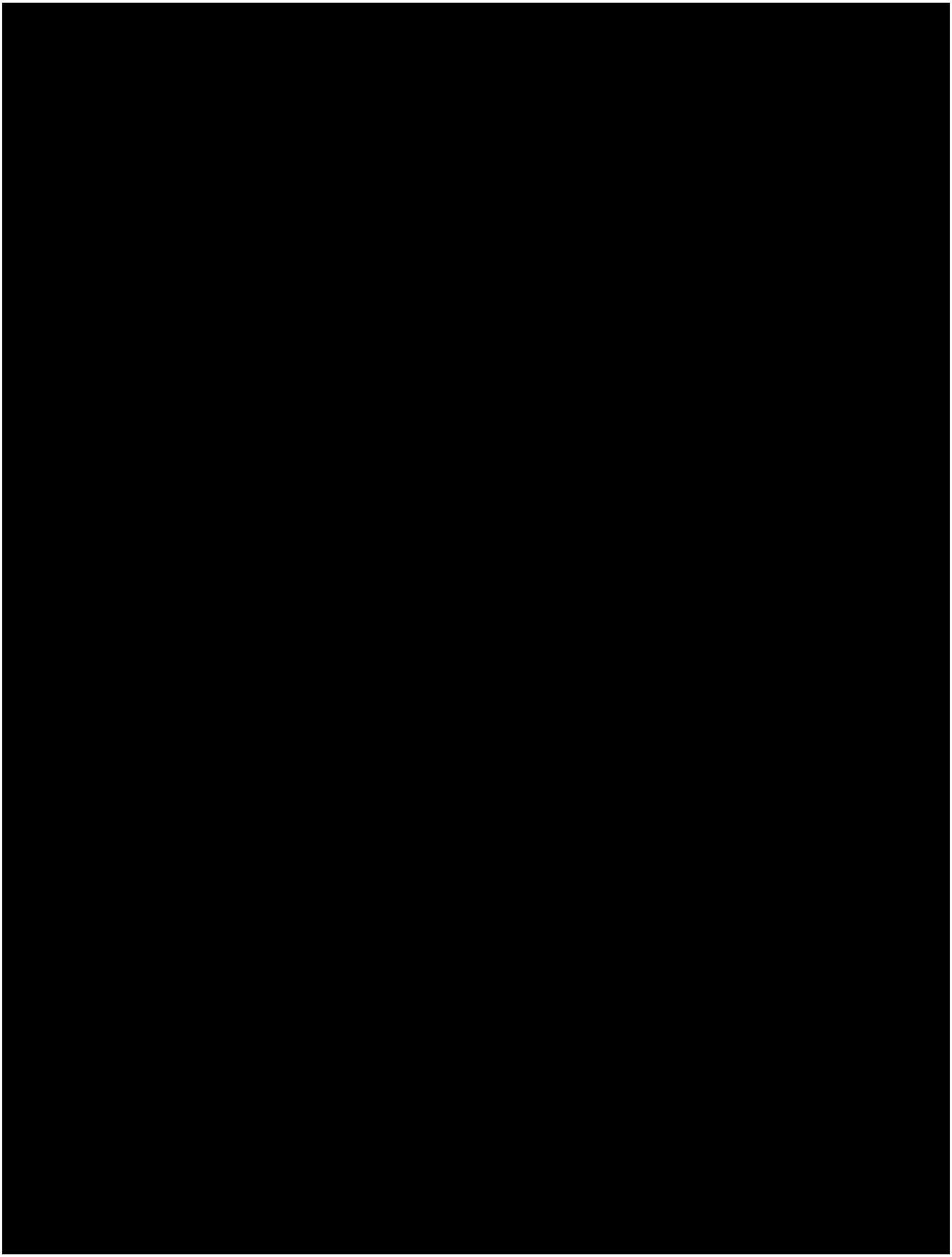

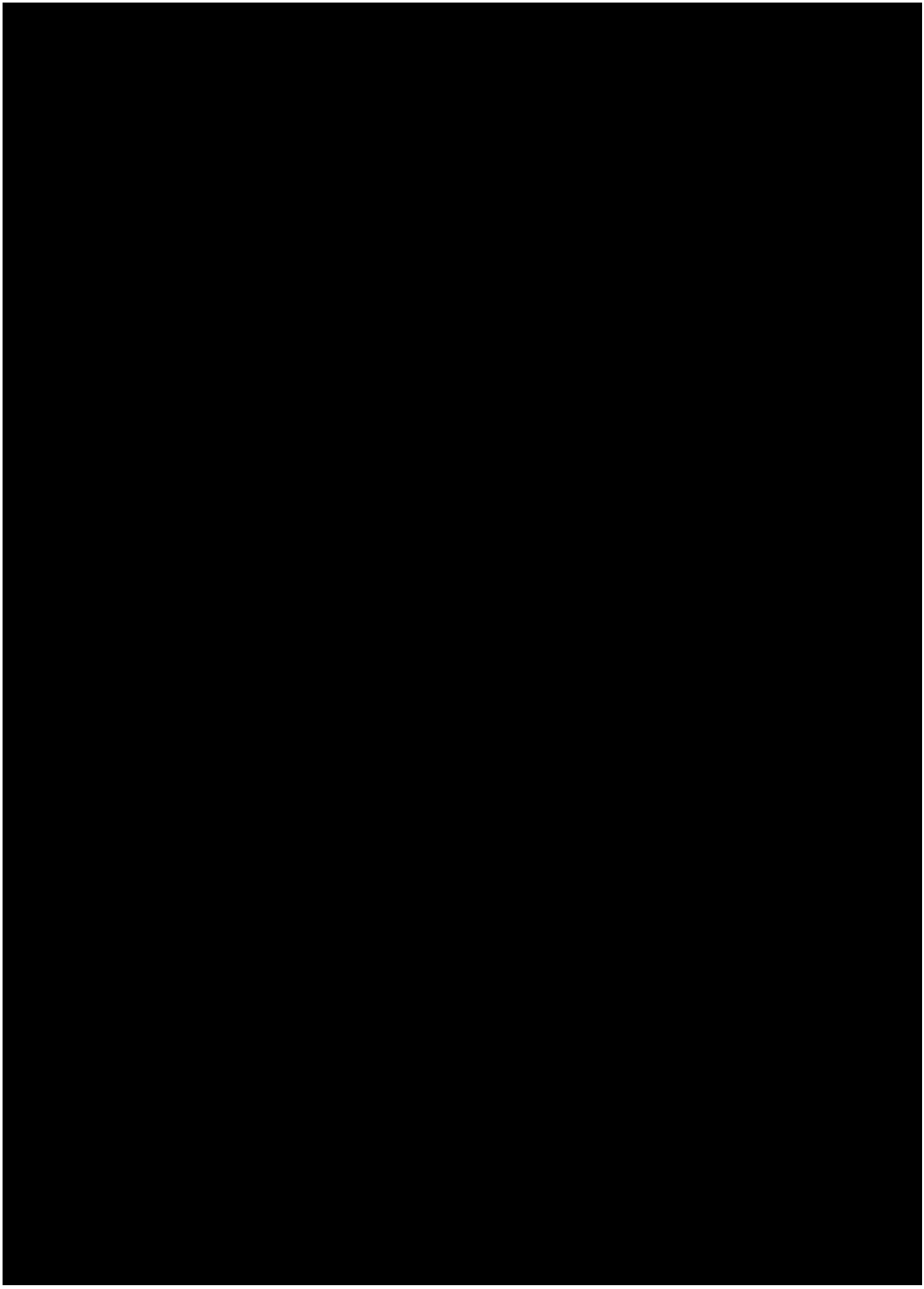

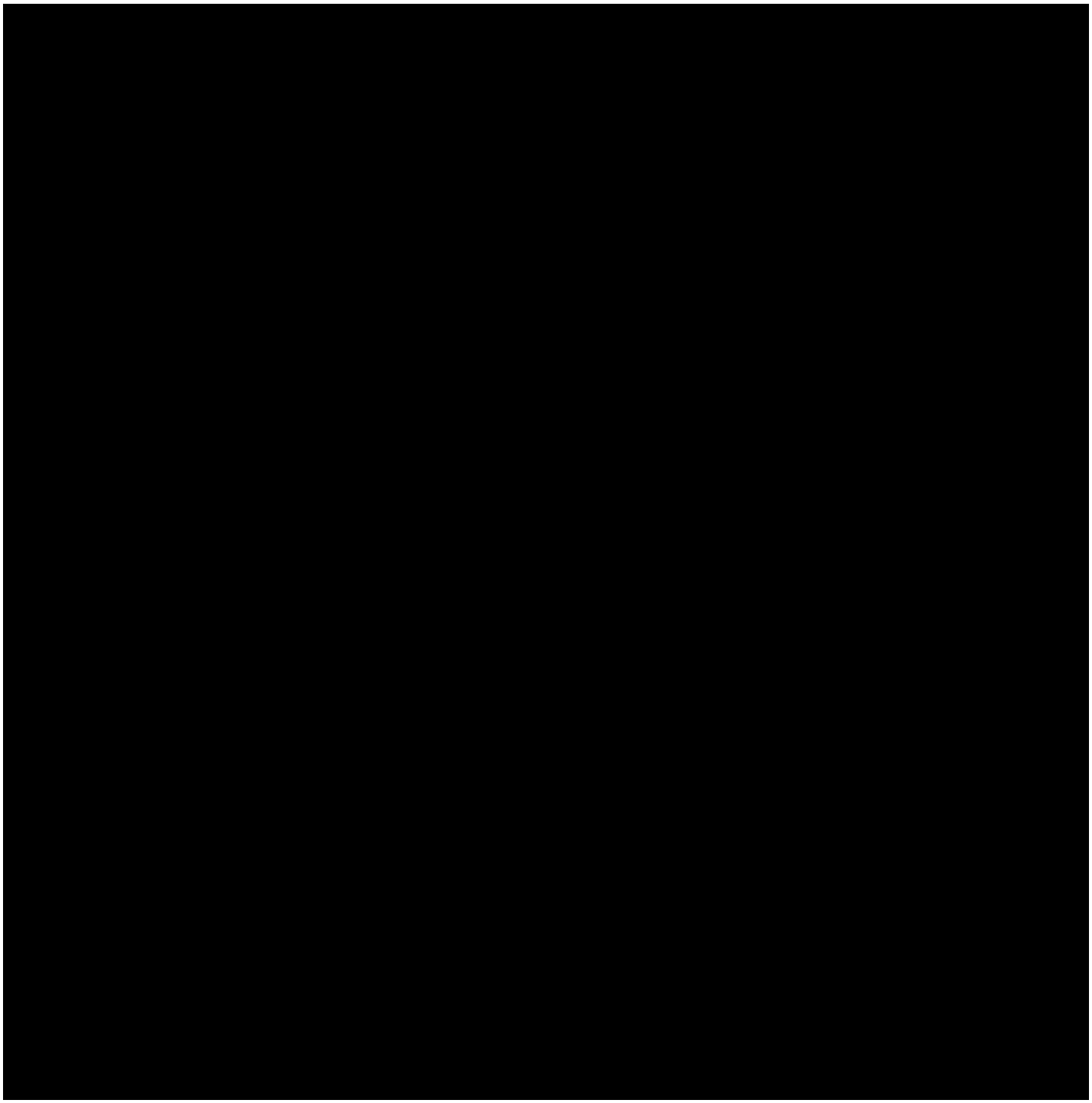

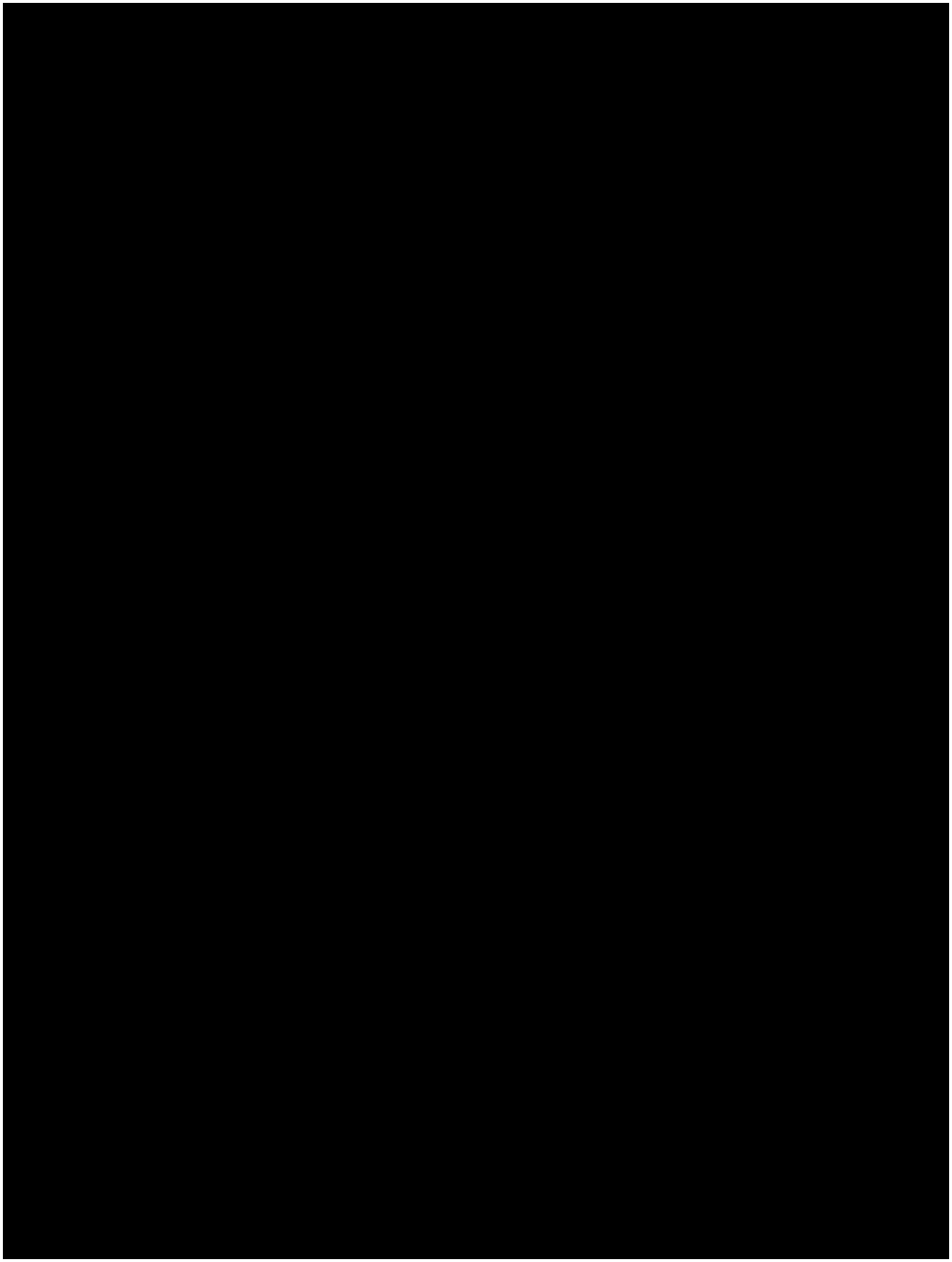

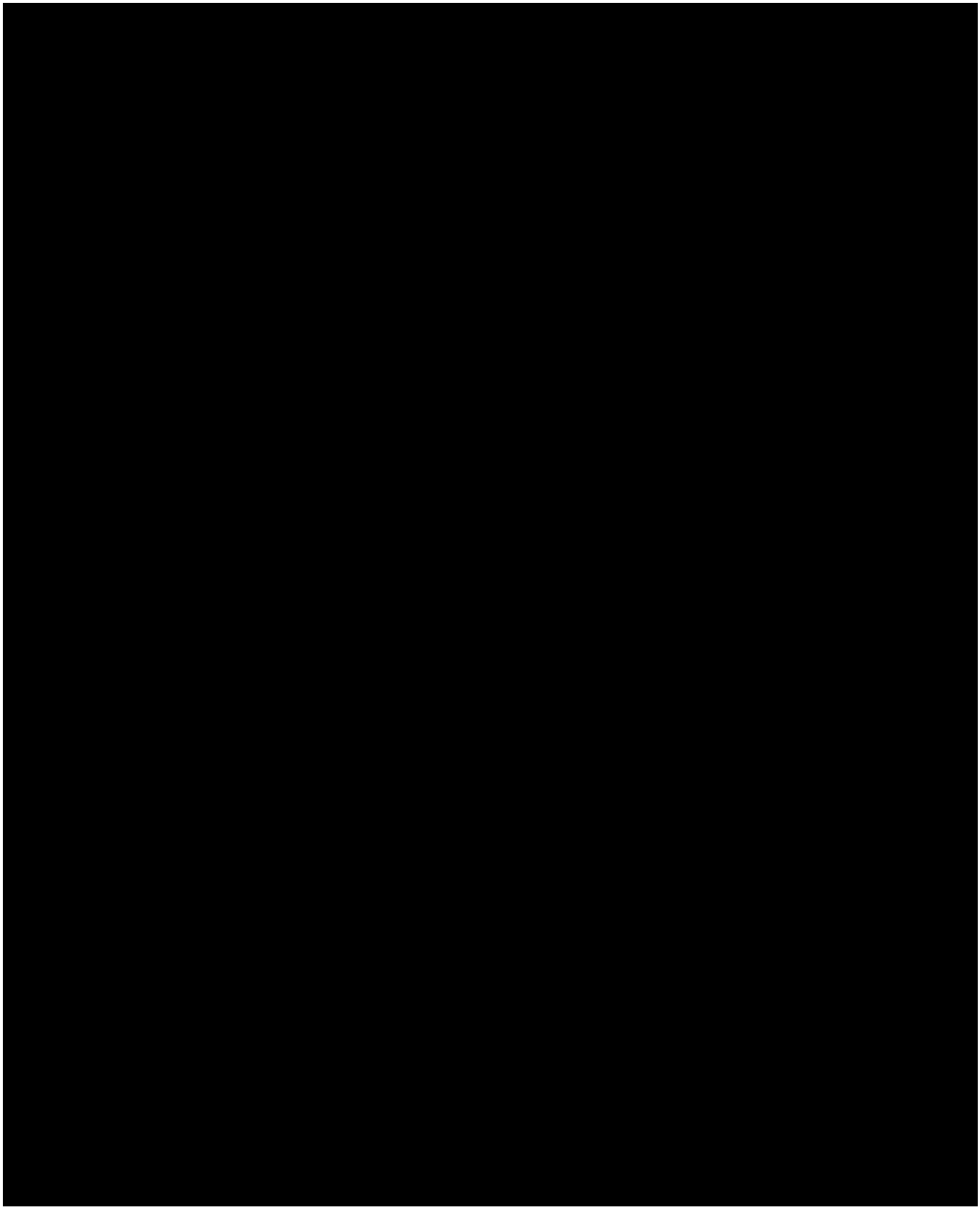

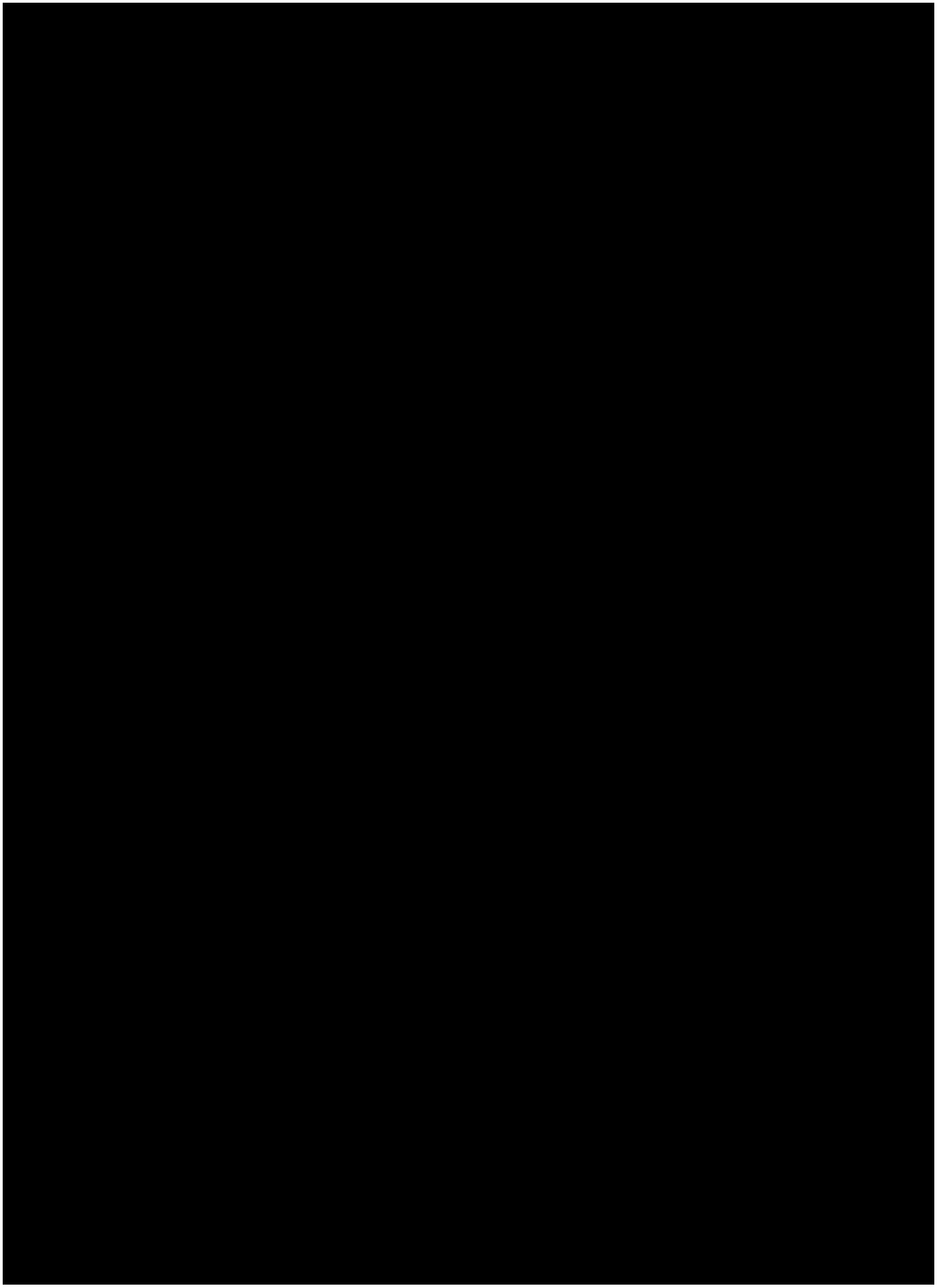

Appendix B Reference frame transformation

The reference frame transformation into rotating and stationary reference frames are known as Park's and Clark's transformation, respectively. In these transformations the three-phase system is transformed into an equivalent two-phase system as shown in *Figure B.1*.

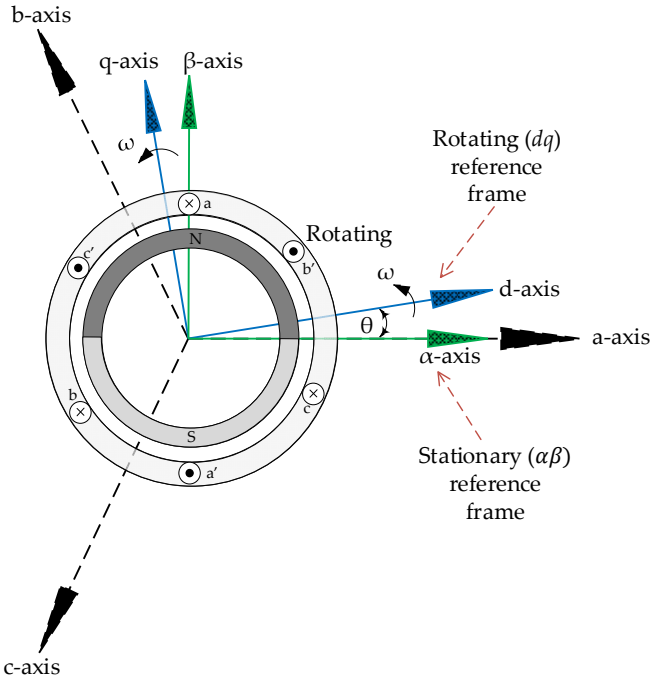

Figure B.1. Transformation of *abc* to *rotating reference frame* and *stationary reference frame* adapted from [143]

Transformation of three-phase *abc* variable to *dqn* variables is referred to as *rotating reference frame* transformation. This transformation is usually used in AC system and is known as *d-q* transformation. The direction of the *abc* variables that coincide with the direction of the magnetic axis is transformed to *d*, *q*, and *n* axes which are orthogonal to each other and are described as follows [143].

- Direct axis (*d*-axis): d-axis is often the reference axis in vector control of AC motors and is chosen along the direction of the magnetic flux. Therefore, *d*-axis indicates the direction of the flux producing component of the motor current.
- Quadrature axis (*q*-axis): q-axis is often orthogonal to *d*-axis and the back-EMF or torque producing component of the motor current is aligned along this axis.

- Neutral axis (*n*-axis): This axis is orthogonal to both d- and q-axes and is normally ignored in balanced three-phase systems. The n-axis is not related to the mechanical power of AC motors and must be considered in case of the presence of losses.

The *stationary reference frame* which is also known as $\alpha\beta$ or Clark transformation is not rotating and the α-axis is in phase with a-axis of the three-phase *abc* system. This is the reason it is also called *stator reference frame*. Similar to the *rotating reference frame*, the β-axis is orthogonal to α-axis (*Figure B.1*).

B.1 Clark Transformation

Using Clark Transformation, the three-phase motor voltages or currents are transformed from *abc* reference to $\alpha\beta$ quadrature reference quantities. The α-axis is along the a-axis and the β-axis is perpendicular to α-axis. This transforms the three-phase *abc* quantities to a co-planar two-phase quantities which are 90 degrees to each other as shown in *Figure B.1*.

The *abc* to *stationary reference frame* transformation matrix is represented as:

$$\begin{bmatrix} V_\alpha \\ V_\beta \\ V_o \end{bmatrix} = {}^{2}/_{3} \begin{bmatrix} 1 & Cos(120°) & Cos(120°) \\ 0 & -Sin(120°) & Sin(120°) \\ {}^{1}/_{2} & {}^{1}/_{2} & {}^{1}/_{2} \end{bmatrix} \begin{bmatrix} V_a \\ V_b \\ V_c \end{bmatrix} \qquad abc \rightarrow \alpha\beta o \qquad \text{(B.1)}$$

In equation (B.1), the zero-sequence voltage is represented as V_o which is zero for a balanced three-phase system.

To convert from the *stationary reference frame* to *abc* quantities, Inverse Clark Transformation is used. The transition matrix for $\alpha\beta$ to abc reference frame is as follows:

$$\begin{bmatrix} V_a \\ V_b \\ V_c \end{bmatrix} = \begin{bmatrix} 1 & 0 \\ -Cos(120°) & -Sin(120°) \\ -Cos(120°) & Sin(120°) \end{bmatrix} \begin{bmatrix} V_\alpha \\ V_\beta \end{bmatrix} \qquad \alpha\beta o \rightarrow abc \qquad \text{(B.2)}$$

B.2 Park Transformation

The Park transformation is used to transform the two-axis $\alpha\beta$ *stationary reference frame* into *rotating reference frame*. The transformation matrices are as follows:

$$\begin{bmatrix} V_d \\ V_q \end{bmatrix} = \begin{bmatrix} Cos(\theta) & Sin(\theta) \\ -sin(\theta) & Cos(\theta) \end{bmatrix} \begin{bmatrix} V_\alpha \\ V_\beta \end{bmatrix} \qquad \alpha\beta \rightarrow dq \qquad \text{(B.3)}$$

In equation (B.3), θ=ωt is the electrical angle. This means that the previous *abc* or $\alpha\beta$ stationary axis are rotated at a frequency ω and therefore, the voltages, currents, or flux are converted to constant values.

The Inverse Park Transformation matrix is represented as:

$$\begin{bmatrix} V_\alpha \\ V_\beta \end{bmatrix} = \begin{bmatrix} Cos(\theta) & -Sin(\theta) \\ sin(\theta) & Cos(\theta) \end{bmatrix} \begin{bmatrix} V_d \\ V_q \end{bmatrix} \qquad dq \rightarrow \alpha\beta \qquad \text{(B.4)}$$

B.3 Three-Phase (*abc*) to Rotary (*dq*) Transformation

Based on the relationships between the two common transformations (Clark and Park), other conversion matrices can be obtained to convert directly from *abc* to *dq* and vice versa. This is obtained from the following:

$$\begin{bmatrix} V_d \\ V_q \\ V_o \end{bmatrix} = {}^{2}/_{3} \begin{bmatrix} Cos(\theta) & Cos(\theta - 120°) & Cos(\theta + 120°) \\ Sin(\theta) & Sin(\theta - 120°) & Sin(\theta + 120°) \\ {}^{1}/_{2} & {}^{1}/_{2} & {}^{1}/_{2} \end{bmatrix} \begin{bmatrix} V_a \\ V_b \\ V_c \end{bmatrix} \qquad abc \rightarrow dqo \qquad \text{(B.5)}$$

$$\begin{bmatrix} V_a \\ V_b \\ V_c \end{bmatrix} = \begin{bmatrix} Cos(\theta) & Sin(\theta) & 1 \\ Cos(\theta - 120°) & Sin(\theta - 120°) & 1 \\ Cos(\theta + 120°) & Sin(\theta + 120°) & 1 \end{bmatrix} \begin{bmatrix} V_d \\ V_q \\ V_o \end{bmatrix} \qquad dqo \rightarrow abc \qquad \text{(B.6)}$$

A detailed description of reference frame transformations is addressed in references [143, 154].

Appendix C Space Vector Pulse Width Modulation Principle

Space vector pulse width modulation technique is used to produce output voltages from a voltage source inverter (VSI) to give less harmonic distortion currents, lower torque ripples and reduced switching losses [170]. The circuit diagram of a SVPWM controlled VSI connected to the terminals of a three-phase PMSM is shown in *Figure C.1*. The inverter consists of six switches (S1-S6) which are controlled by switching signals. The output voltages V_a, V_b and V_c are produced by turning the power transistor switches on and off in a particular pattern such that the two switches on the same arm are never turned on simultaneously [171].

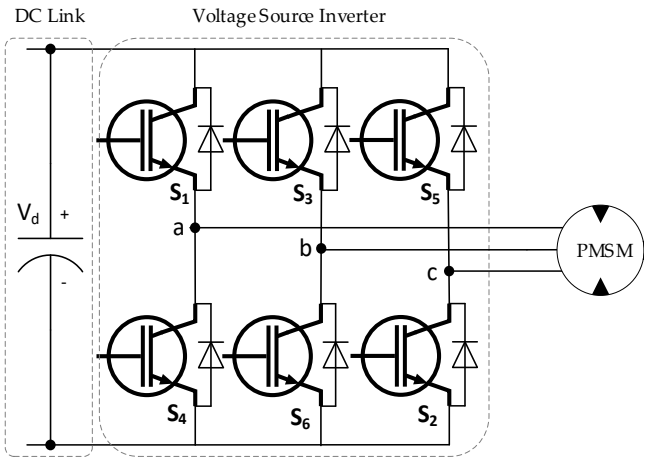

Figure C.1. Three-phase VSI circuit

When an upper switch is turned on, the corresponding lower switch of the same arm is turned off, and vice versa. This creates eight switching states as follows: (000), (100), (110), (010), (011), (001), (101), and (111), where '0' is for OFF and '1' is represents ON state. The first and the last states do not cause current flow to the motor and, therefore, are called zero (null) states. The remaining six states, called active states, generate a current flow and thus produce a voltage at the stator winding terminals of the motor. The six active switching states are represented by six vectors which form six vertices of a hexagon. The active vectors are 60 degrees apart and the null vectors are at the origin as shown in *Figure C.2*.

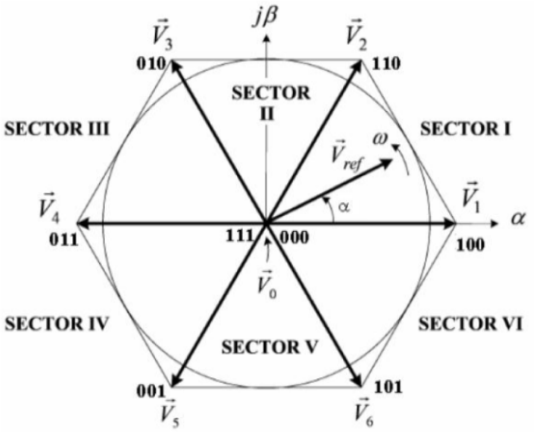

Figure C.2. Space vector switching in sectors [142]

The voltage V_{ref} is the reference voltage generated by active and null vectors in the sector it is positioned. The V_{ref} is rotated in the six-sector space of the hexagon with an angular frequency of ω. When V_{ref} completes one revolution in the space, the inverter outputs one cycle of sinusoidal voltage [172-174]. To determine the time duration of the operation of the switches to be turned ON or OFF, a sampling period T_s needs to be set in order to control the position of V_{ref} and corresponding active and null vectors in each sector [172].

C.1 SVPWM Algorithm and Calculations

SVPWM is implemented in the following steps:

1. Calculate V_α , V_β , V_{ref}, and the angel (α)
2. Determine time durations T_1, T_2, T_0
3. Determine the switching time of the switches

Step 1: Calculating V_α , V_β , V_{ref}, and the angel (α)

Space vector representing all three phasors is defined as:

$$V_s = \frac{2}{3}(V_a + \bar{a}V_b + \bar{a}^2 V_c) \tag{C.1}$$

Where

$$\bar{a} = e^{-j2\pi/3} \tag{C.2}$$

Since V_{ref} is a function of V_α and V_β, these are calculated as:

$$\begin{bmatrix} V\alpha \\ V\beta \end{bmatrix} = \begin{bmatrix} 1 & -1/2 & -1/2 \\ 0 & \sqrt{3}/2 & -\sqrt{3}/2 \end{bmatrix} \begin{bmatrix} Va \\ Vb \\ Vc \end{bmatrix} \quad \text{(C.3)}$$

Where

$$V_{ref} = \sqrt{V\alpha^2 + V\beta^2} \quad \text{(C.4)}$$

and

$$\alpha = \tan^{-1} \frac{V\alpha}{V\beta} \quad \text{(C.5)}$$

Step 2: Calculation of the time durations T_1, T_2, T_0

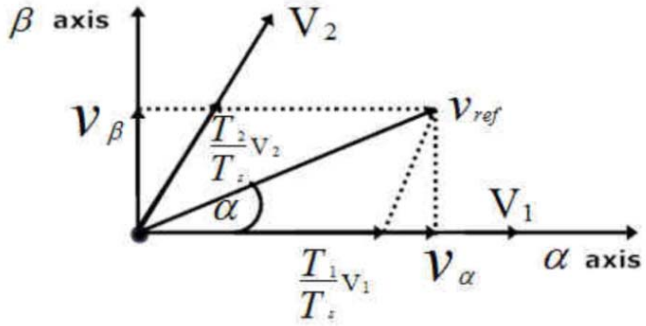

Figure C.3. Space vector representation in sector 1 [142]

To determine the time of operation of active vectors, the position of the V_{ref} is considered in sector 1 as shown in *Figure C.3*.

$$\frac{T_1 V_1}{T_s} = V_{ref} Cos(\alpha) \quad \text{(C.6)}$$

and

$$\frac{T_2 V_2}{T_s} = V_{ref} Sin(\frac{\pi}{3} - \alpha) \quad \text{(C.7)}$$

Generally:

$$\frac{T_1 V_1}{T_s} = V_{ref} Sin(n\frac{\pi}{3} - \alpha) \quad \text{(C.8)}$$

where 'n' shows the sector number

Since

$$V_{ref,max} = V_d Cos\left(\frac{60}{2}\right) = \frac{\sqrt{3}}{2} V_d \quad \text{(C.9)}$$

The time duration of each active vector can be calculated with equations (C.10) - (C.12):

$$T_1 = \sqrt{3}\,\frac{V_{ref}}{V_d} T_s\, Sin(\frac{n\pi}{3} - \alpha) \quad \text{(C.10)}$$

$$T_2 = \sqrt{3}\,\frac{V_{ref}}{V_d} T_s\, Sin(\alpha - \frac{(n-1)\pi}{3}) \quad \text{(C.11)}$$

$$T_0 = T_s - T_1 - T_2 \quad \text{(C.12)}$$

Step 3: Calculation of the switching times

Switching time calculation of each sector (S1-S6) of the inverter switches determined by SVPWM technique [173].

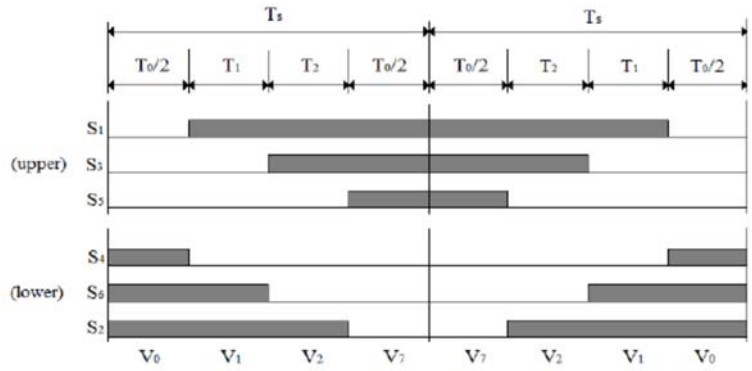

(a) Sector 1

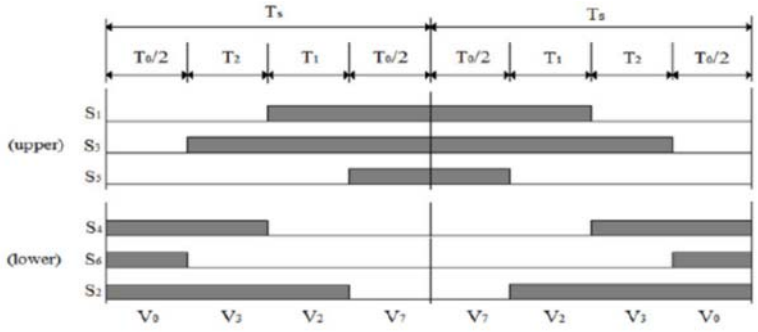

(b) Sector 2

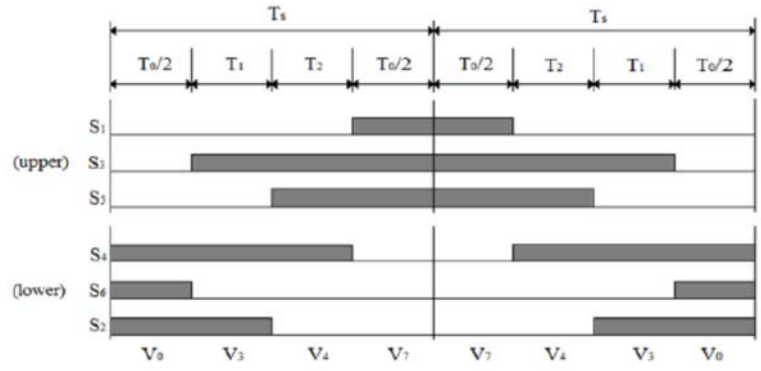

(c) Sector 3

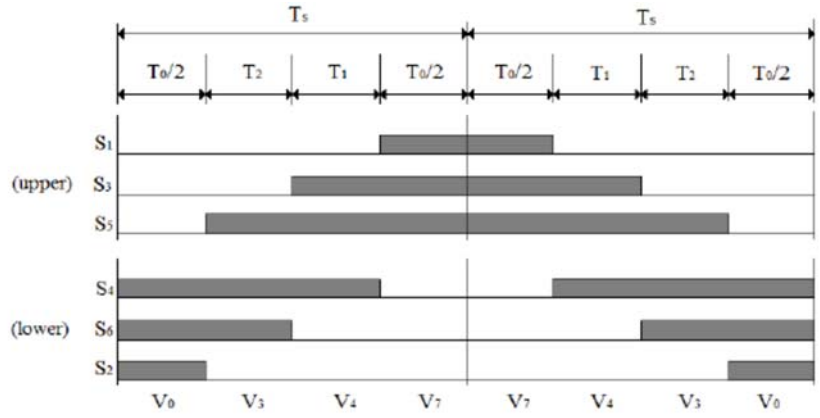

(d) Sector 4

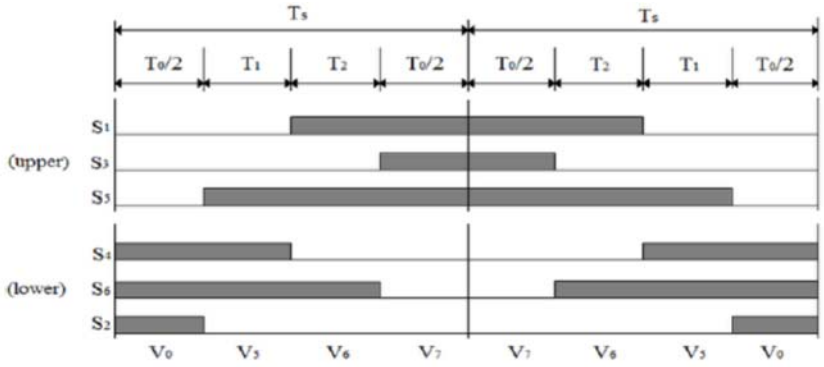

(e) Sector 5

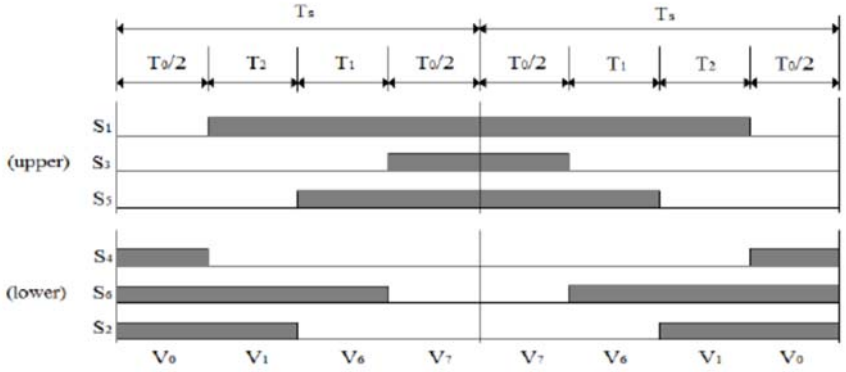

(f) Sector 6

Figure C.4: Switching time of sectors (S1-S6) [173]

Table C1. *Summary of switch time calculations [173]*

Sector	Upper Switches (S1, S3, S5)	Lower Switches (S2, S4, S6)
1	S1=T1+T2+T0/2 S3=T2+T0/2 S5=T0/2	S4=T0/2 S6=T1+T0/2 S2= T1+T2+T0/2
2	S1=T1+T0/2 S3=T1+T2+T0/2 S5=T0/2	S4=T2+T0/2 S6=T0/2 S2=T1+T2+T0/2
3	S1=T0/2 S3=T1+T2+T0/2 S5=T2+T0/2	S4= T1+T2+T0/2 S6=T0/2 S2=T1+T0/2
4	S1=T0/2 S3=T1+T0/2 S5=T1+T2+T0/2	S4= T1+T2+T0/2 S6=T2+T0/2 S2=T0/2
5	S1=T2+T0/2 S3=T0/2 S5=T1+T2+T0/2	S4=T1+T0/2 S6= T1+T2+T0/2 S2=T0/2
6	S1=T1+T2+T0/2 S3=T0/2 S5=T1+T0/2	S4=T0/2 S6=T1+T2+T0/2 S2=T2+T0/2

Table C2. *Output voltage vectors corresponding to switch states [170]*

Switch States			Phase Voltages			Space Voltage Vector
S_a	S_b	S_c	v_{as}	v_{bs}	v_{cs}	$V_n(n=1-7)$
0	0	0	0	0	0	$V_0 = 0\angle 0^\circ$
1	0	0	$\frac{2}{3}V_{dc}$	$-\frac{1}{3}V_{dc}$	$-\frac{1}{3}V_{dc}$	$V_1 = \frac{2}{3}V_{dc}\angle 0^\circ$
1	1	0	$\frac{1}{3}V_{dc}$	$\frac{1}{3}V_{dc}$	$-\frac{2}{3}V_{dc}$	$V_2 = \frac{2}{3}V_{dc}\angle 60^\circ$
0	1	0	$-\frac{1}{3}V_{dc}$	$\frac{2}{3}V_{dc}$	$-\frac{1}{3}V_{dc}$	$V_3 = \frac{2}{3}V_{dc}\angle 120^\circ$
0	1	1	$-\frac{2}{3}V_{dc}$	$\frac{1}{3}V_{dc}$	$\frac{1}{3}V_{dc}$	$V_4 = \frac{2}{3}V_{dc}\angle 180^\circ$
0	0	1	$-\frac{1}{3}V_{dc}$	$-\frac{1}{3}V_{dc}$	$\frac{2}{3}V_{dc}$	$V_5 = \frac{2}{3}V_{dc}\angle 240^\circ$
1	0	1	$\frac{1}{3}V_{dc}$	$-\frac{2}{3}V_{dc}$	$\frac{1}{3}V_{dc}$	$V_6 = \frac{2}{3}V_{dc}\angle 300^\circ$
1	1	1	0	0	0	$V_7 = 0\angle 0^\circ$

Appendix D Calculation of the PI controller gains

D.1 Current controller gains

The open-loop transfer function of the current as derived in section 5.3.1 is given by:

$$TF_{OL,I} = \left(\frac{K_{pi}\mathrm{s} + K_{ii}}{s}\right)\left(\frac{V_{DC}}{V_{tri}}\right)\left(\frac{1}{R_s + \mathrm{s}L_q}\right) \tag{D.1}$$

Then closed-loop transfer function of the current can be stated as:

$$G_{(S),I} = \frac{\frac{K_{pi}}{L}\mathrm{s} + \frac{K_{ii}}{L}}{s^2 + \left(\frac{K_{pi} + R}{L}\right)s + \frac{K_{ii}}{L}} \tag{D.2}$$

The PI controller introduces a zero to the closed-loop transfer function for commanded changes and is located at $\left(-\frac{K_{ii}}{L}\right)$. The zero is cancelled by introducing a zero cancellation block in the feedforward path as follows:

$$G_{(S),I} = \frac{\frac{K_{ii}}{K_{pi}}}{\left(s + \frac{K_{ii}}{K_{pi}}\right)} \frac{\frac{K_{pi}}{L}\mathrm{s} + \frac{K_{ii}}{L}}{\left(s^2 + \left(\frac{K_{pi} + R}{L}\right)s + \frac{K_{ii}}{L}\right)} \tag{D.3}$$

However, the zero cancellation block must have a unity gain and $\left(s + \frac{K_{ii}}{K_{pi}}\right)$ with $s = 0$ can be considered. Hence Equation (D.3) can be simplified to:

$$G_{(S),I} = \frac{\frac{K_{ii}}{L}}{\left(s^2 + \left(\frac{K_{pi} + R}{L}\right)s + \frac{K_{ii}}{L}\right)} \tag{D.4}$$

The standard second-order system is given by:

$$G_{W(S)} = \frac{\omega^2}{(s^2 + 2\zeta\omega s + \omega^2)} \tag{D.5}$$

The following gain values for PI current controller can be determined by comparing $G_{(S),I}$ with the standard second-order system (Equation D.5):

$$K_{pi} = 2\zeta\omega L - R$$

$$K_{ii} = L\omega^2$$

D.2 Speed controller gains

The open-loop transfer function of the speed as derived in section 5.3.2 is given by:

$$TF_{OL,\omega} = (\frac{K_{p\omega}s + K_{i\omega}}{s})(\frac{K_T}{Js}) \tag{D.6}$$

The closed-loop transfer function of the speed can be presented as:

$$G_{(S),\omega} = \frac{(\frac{K_{i\omega}}{s} + K_{p\omega})(\frac{K_T}{Js})}{1 + (\frac{K_{i\omega}}{s} + K_{p\omega})(\frac{K_T}{Js})} \tag{D.7}$$

and

$$G_{(S),\omega} = \frac{(K_{p\omega}K_T s + K_{i\omega}K_T)}{Js^2 + K_{p\omega}K_T s + K_{i\omega}K_T} \tag{D.8}$$

A zero cancellation block is introduced in the feedforward path to cancel the zero as follows:

$$G_{(S),\omega} = \frac{\frac{K_{i\omega}}{K_{p\omega}}}{(s + \frac{K_{i\omega}}{K_{p\omega}})} \frac{(K_{p\omega}K_T s + K_{i\omega}K_T)}{Js^2 + K_{p\omega}K_T s + K_{i\omega}K_T} \tag{D.9}$$

Considering a unity gain for zero cancellation block with $s = 0$ and dividing by J to get the s^2 term:

$$G_{(S),\omega} = \frac{\frac{K_{i\omega}}{K_{p\omega}}/J}{(s^2 + \frac{K_{p\omega}K_T}{J}s + \frac{K_{i\omega}K_T}{J}} \tag{D.10}$$

Comparing $G_{(S),\omega}$ with the standard second-order system (Equation D.5), the gain values for PI speed controller can be determined as follows:

$$K_{p\omega} = \frac{2J\zeta\omega}{K_T}$$

$$K_{i\omega} = \frac{J\omega^2}{K_T}$$

D.3 Voltage controller gains

The open-loop transfer function of the voltage as derived in section 5.3.3 is given by

$$TF_{OL,V} = (\frac{K_{pv}\mathrm{s} + K_{iv}}{s})(\frac{\frac{1}{R}}{1 + \frac{C}{R}\mathrm{s}}) \tag{D.11}$$

The closed-loop transfer function of the voltage can be simplified as

$$G_{(S),V} = \frac{\frac{K_{pv}}{R} + \frac{K_{iv}}{R\mathrm{s}}}{1 + \frac{C}{R}\mathrm{s} + \frac{K_{pv}}{R} + \frac{K_{iv}}{R\mathrm{s}}} \tag{D.12}$$

Multiplying by $\frac{R}{C}\mathrm{s}$ to get the s^2 term, Equation D.12 can be simplified as

$$G_{(S),V} = \frac{\frac{K_{pv}}{C}\mathrm{s} + \frac{K_{iv}}{C}}{(s^2 + \left(\frac{K_{pv} + R}{C}\right)s + \frac{K_{iv}}{C})} \tag{D.13}$$

Similar to the previous cases for current and speed PI controllers, a zero cancellation block is introduced in the feedforward path to cancel the zero as follows:

$$G_{(S),V} = \frac{\frac{K_{iv}}{K_{pv}}}{(s + \frac{K_{iv}}{K_{pv}})} \frac{\frac{K_{pv}}{C}\mathrm{s} + \frac{K_{iv}}{C}}{(s^2 + \left(\frac{K_{pv} + R}{C}\right)s + \frac{K_{iv}}{C})} \tag{D.14}$$

However, the zero cancellation block must have a unity gain and $(s + \frac{K_{iv}}{K_{pv}})$ with $s = 0$ can be assumed and Equation D.14 can be simplified as:

$$G_{(S),V} = \frac{\frac{K_{iv}}{K_{pv}}}{(s^2 + \left(\frac{K_{pv} + R}{C}\right)s + \frac{K_{iv}}{C})} \tag{D.15}$$

The gain values for PI voltage controller can be determined by comparing $G_{(S),V}$ with the standard second-order system (Equation D.5)

$$K_{pv} = 2\zeta\omega C - R$$

$$K_{iv} = C\omega^2$$

Appendix F Diesel Engine Specifications

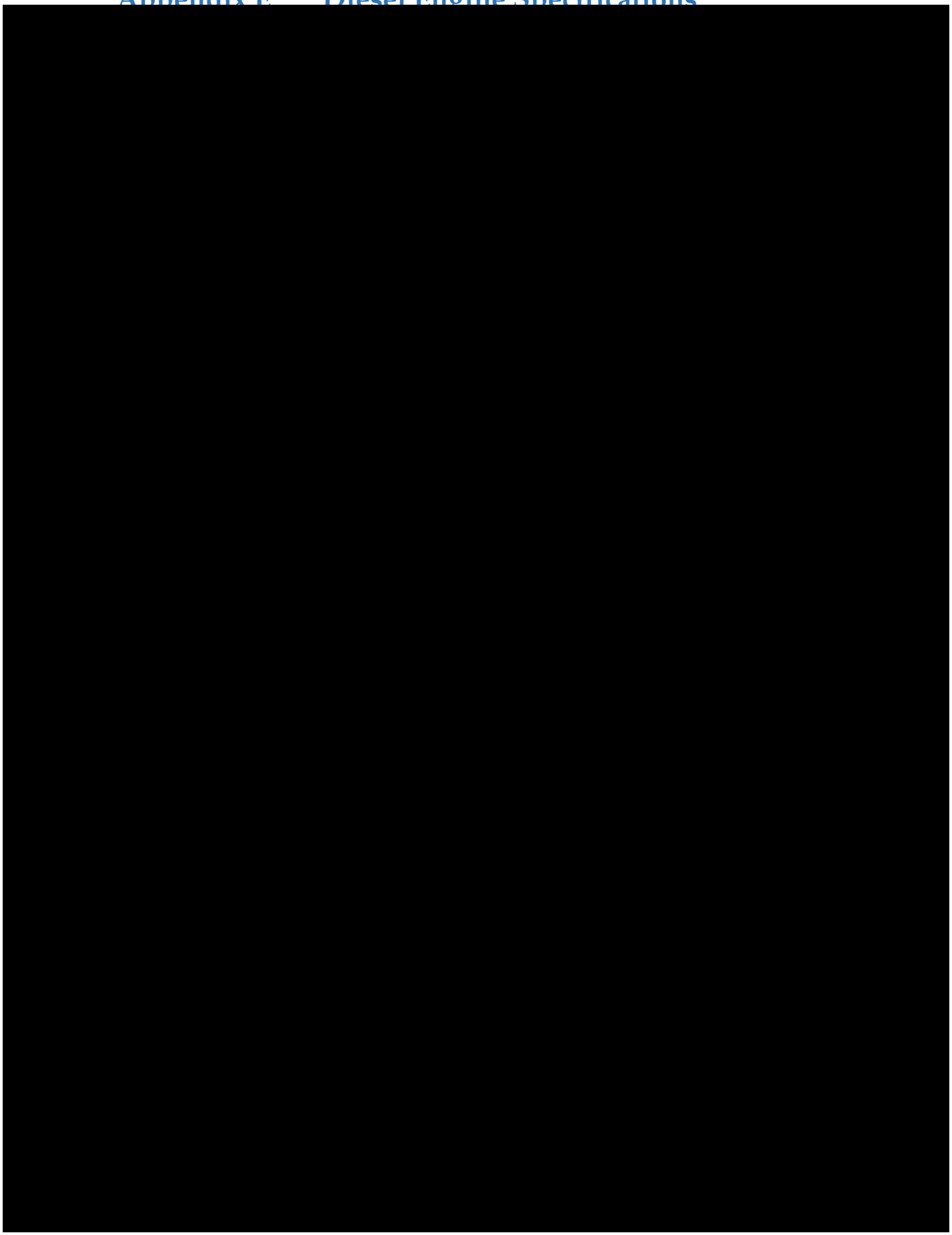

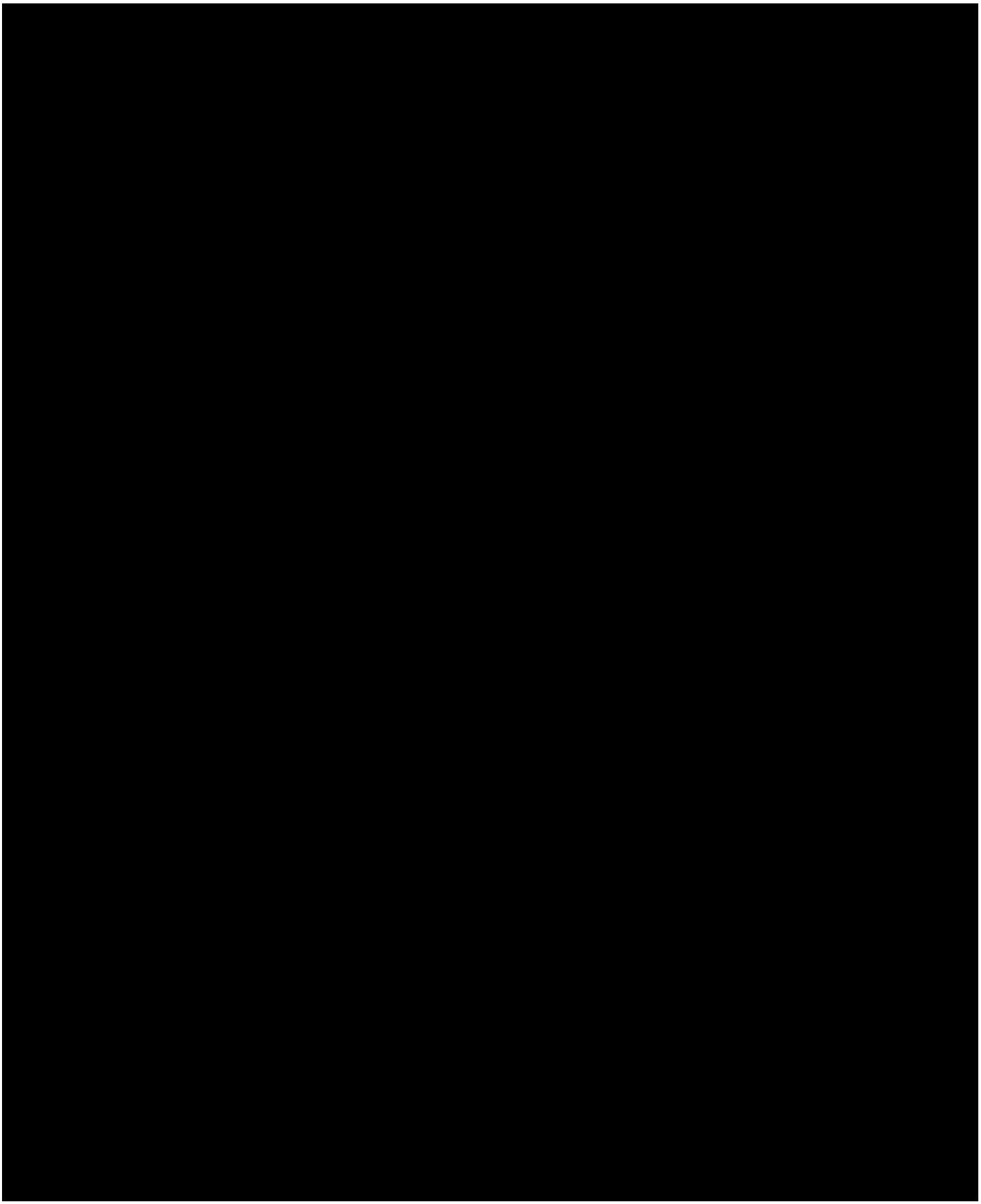

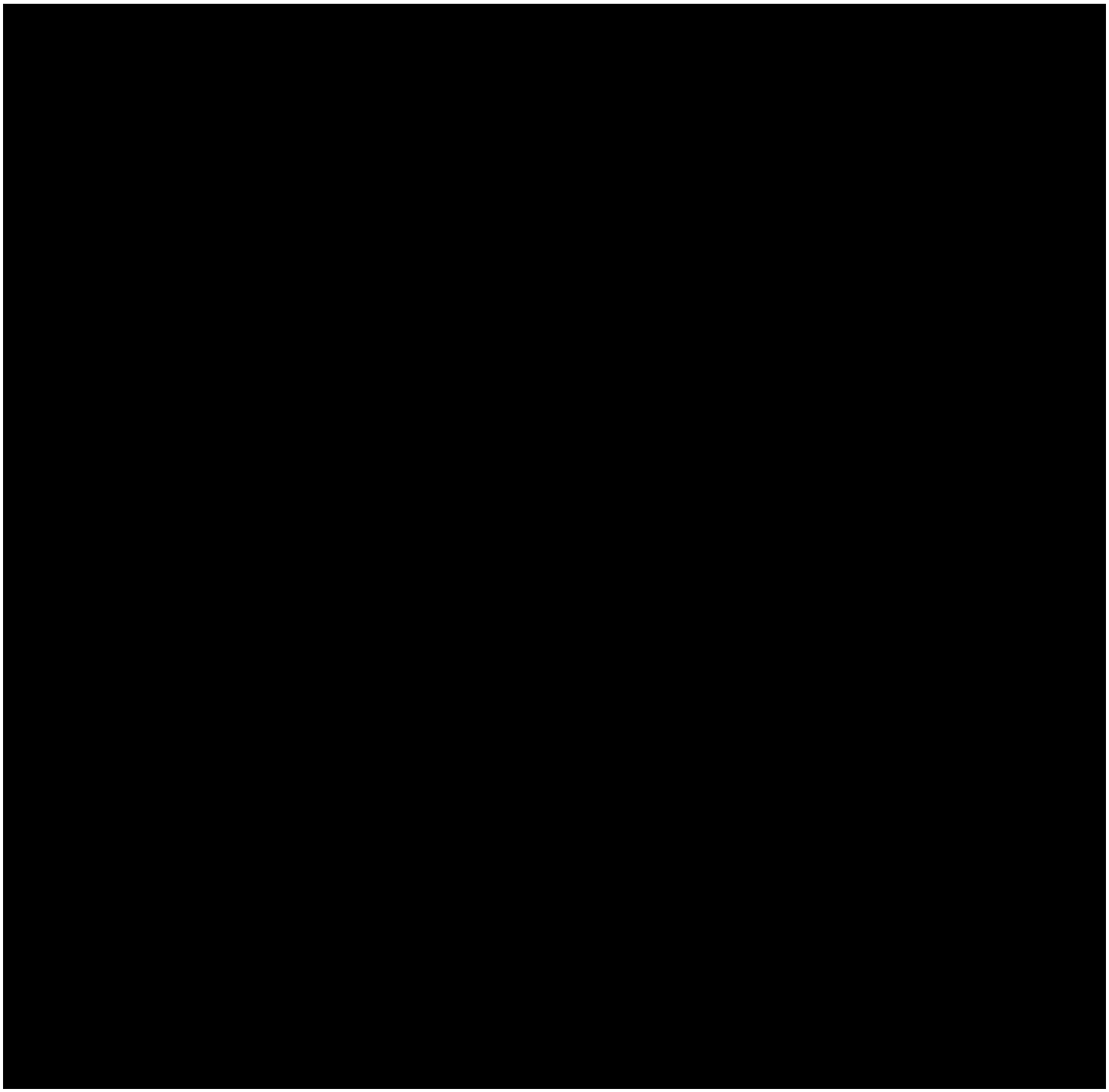

E.2 PERKINS Generator specifications